NEURONAL CORRELATES OF DIACRITICS AND AN OPTIMIZATION ALGORITHM FOR BRAIN MAPPING AND DETECTING BRAIN FUNCTION BY WAY OF FUNCTIONAL MAGNETIC RESONANCE IMAGING

A Dissertation Presented
By

Ali Khaled Bourisly

Submitted to the Faculty
of the

WORCESTER POLYTECHNIC INSTITUTE

in partial fulfillment of the requirements for the degree of

DOCTOR OF PHILOSOPHY

in

BIOMEDICAL ENGINEERING
14 March 2011

Approved:

_____	_____
Christopher H. Sotak, Ph.D. (Advisor and Committee Chair) Professor of Biomedical Engineering Professor of Chemistry and Biochemistry Biomedical Engineering Department Worcester Polytechnic Institute	Charles W. Haynes , EdD, CCC-SLP (Committee Member) Associate Professor Department of Communication Sciences and Disorders School of Rehabilitation Sciences MGH Institute of Health Professions
_____	_____
Jean King, Ph.D. (Committee Member) Professor of Psychiatry Vice Chair of Research Director Center for Comparative NeuroImaging University of Massachusetts Medical School	Matthew Gounis, Ph.D. (Committee Member) Assistant Professor Department of Radiology Director New England Center for Stroke Research University of Massachusetts Medical School
_____	_____
Blaise Frederick, Ph.D. (Committee Member) Assistant Professor of Psychiatry Harvard Medical School Director Technical and Instrumentation Core Brain Imaging Center McLean Hospital	Maria Mody, Ph.D., CCC-SLP (Committee Member) Assistant Professor of Radiology Harvard Medical School Massachusetts General Hospital

“Even if there is only one possible unified theory, it is just a set of rules and equations. What is it that breathes fire into the equations and makes a universe for them to describe?”
- Stephen William Hawking

"He is the Originator of the heavens and the earth."
(The Holy Qur'an; 6:101)

"And it is We who have constructed the heaven with might, and verily, it is We who are steadily expanding it."
(The Holy Qur'an; 51:47)

"Do not the Unbelievers see that the heavens and the earth were joined together (as one unit of creation), before We clove them asunder, and We made from water every living thing. Will they not then believe?" (The Holy Qur'an; 21:30)

"It is He Who created the night and the day, and the sun and the moon. They swim along, each in an orbit. "
(The Holy Qur'an; 21:33)

"And the sun runs to its resting place. That is the decree of the Almighty, the All-Knowing."
(The Holy Qur'an; 36:38)

To my parents Khaled & Fawzia;
Who have given me what I cannot repay in a lifetime
& To my wife Abrar

Acknowledgments

It is my pleasure to thank the following people for their support towards my work in this thesis.

I would like to extend my deepest gratitude to my mentor and advisor Dr. Christopher Sotak (WPI), and to my mentors Dr. Maria Mody (MGH/HST/Harvard/MIT Martinos Center), and Dr. Charles Haynes (MGH-IHP). Their inspiration, love for research, and enthusiasm made my graduate school experience the more enriching and fun. Despite their very busy schedules, they still found time to provide me with a one-on-one learning experience. This, and the fact that they are very well respected in their respective research fields, is the more humbling to me, and will indeed be a cherished experience.

I would also like to thank all my siblings (Fawaz, Mohammed and Nibal) and my nephew Yousif and niece Sarah for their support back home, and special thanks to my only sister Nibal and her son Yousif for their extended support. Thanks also to Maher, my brother-in-law, for his suggestions based on his passed experience in earning a PhD.

My gratitude also extends to all those who I worked with in the Advanced MRI Center and the Center for Comparative Neuroimaging at University of Massachusetts Medical School. I had the great pleasure of meeting, working with, and learning from the following people: Dr. Salman Shazeeb, Paul Reddy, Philip Alvarez, Dr. John Chetley Ford, Dr. Birgul Bastan, Dr. Gina Vincent, Austin Reno, Dr. Ronn Walvick, Joey Mansour, Dr. Wei Huang, Dr. Nanyin Zhang, Dr. Jean King, Dr. Gregory DiGirolamo, Dr. Joseph Difranza, Dr. Carl Fulwiler,

Dr. David Kennedy, Dr. Matthew Gounis, Dr. Lee, Dr. Jin, Linxi, Terence, Jill, Ella, Kim, and Rubie.

I would like also to extend my gratitude to my research committee for their remarks and helpful guidance towards my thesis: Dr. Blaise Frederick (Harvard), Dr. Charles Haynes (MGH-IHP), Dr. Christopher Sotak (WPI), Dr. Jean King (UMass Medical School), Dr. Maria Mody (MGH/HST/Harvard/MIT Martinos Center), and Dr. Matthew Gounis (UMass Medical School).

Thanks to all the participants who participated in any of the fMRI experiments I worked on as part of my PhD work.

Lastly, but most importantly, I dedicate this thesis to my loving parents, Khaled and Fawzia, who bore me, raised me, taught me, and supported me throughout my life, and to my lovely wife Abrar.

Table of Contents

Abstract

The purpose of this thesis is threefold: 1) A behavioral examination of the role of diacritics in Arabic, 2) A functional magnetic resonance imaging (fMRI) investigative study of diacritics in Arabic, and 3) An optimization algorithm for brain mapping and detecting brain function.

Firstly, the role of diacritics in Arabic was examined behaviorally. The stimulus was a lexical decision task (LDT) that constituted of low, mid, and high frequency words and nonwords; with and without diacritics. Results showed that the presence of vowel diacritics slowed reaction time but did not affect word recognition accuracy. The longer reaction times for words with diacritics versus without diacritics suggest that the diacritics may contribute to differences in word recognition strategies.

Secondly, an Event-related fMRI experiment of lexical decisions associated with real words with versus without diacritics in Arabic readers was done. Real words with no diacritics yielded shorter response times and stronger activation than with real words with diacritics in the hippocampus and middle temporal gyrus possibly reflecting a search from among multiple meanings associated with these words in a semantic store. In contrast, real words with diacritics had longer response times than real words without diacritics and activated the insula and frontal areas suggestive of phonological and semantic mediation in lexical retrieval. Both the behavioral and fMRI results in this study appear to support a role for diacritics in reading in Arabic .

The third research work in this thesis is an optimization algorithm for fMRI data analysis. Current data-driven approaches for fMRI data analysis, such as independent component analysis (ICA), rely on algorithms that may have low computational expense, but are much more prone to suboptimal results. In this work, a genetic algorithm (GA) based on a clustering technique was designed, developed, and implemented for fMRI ICA data analysis. Results for the algorithm, GAICA, showed that although it might be computationally expensive; it provides global optimum convergence and results. Therefore, GAICA can be used as a complimentary or supplementary technique for brain mapping and detecting brain function by way of fMRI.

Chapter 1:From Nuclear Magnetic Resonance to Magnetic Resonance Imaging

1.1 A Historical Introduction

One cannot provide an accurate and complete consecutive historical perspective of Magnetic Resonance Imaging (MRI) or functional Magnetic Resonance Imaging (fMRI), without mentioning Pauli's conjecture and his contribution to Magnetic Resonance Imaging (MRI). In 1924, the Austrian physicist Wolgang Pauli postulated the theory that atomic nuclei have both spin and magnetic moment and that these two properties could only take discrete values (quanta). However this theory was not tested until Otto Stern and Walther Gerlach devised their molecular beam that proved Pauli's theory. Moreover, in 1933 Isidor Rabi modified the Stern-Gerlach technique to realize that when the frequency of an oscillating magnetic field is matched with the atomic nucleus's spin frequency, the nucleus absorbs energy from the magnetic field. This concept came to be known as magnetic resonance (the MR in MRI).

In the mid 1940s, after World War II, both Felix Bloch and Edward Purcell independently detected magnetic resonance effects in a pure water sample. This nuclear magnetic resonance (NMR) phenomena forms the basis of all modern-day MRI. By the 1960s NMR measurements provided a contrast between water molecules in biological specimen and those outside. This led Raymond Damadian to hypothesize that similar differences might be observed between cancerous and non-cancerous cells using NMR. Nonetheless, modern day MRI systems would not have been possible without the 1970s work of Paul Lauterbur

on magnetic field gradients and Peter Mansfield's work on rapid acquisition of images.

Mansfield's method of rapid image acquisition, or what was coined as echo-planar imaging (EPI), made fMRI possible. In that, it has the ability to detect an endogenous blood contrast that would provide inference of brain activity. The effects of blood oxygenation on this contrast (T2*) was first shown by Keith Thulborn in 1982. However, it was not until 1990 that Seiji Ogawa discovered the blood oxygen level dependent (BOLD) contrast. Then, the first fMRI studies using BOLD contrast were published in 1992 and 1993. Ever since; engineering, physics, and scientific advancements progressed to lead to our modern-day fMRI capabilities.

1.2 Operation of MRI

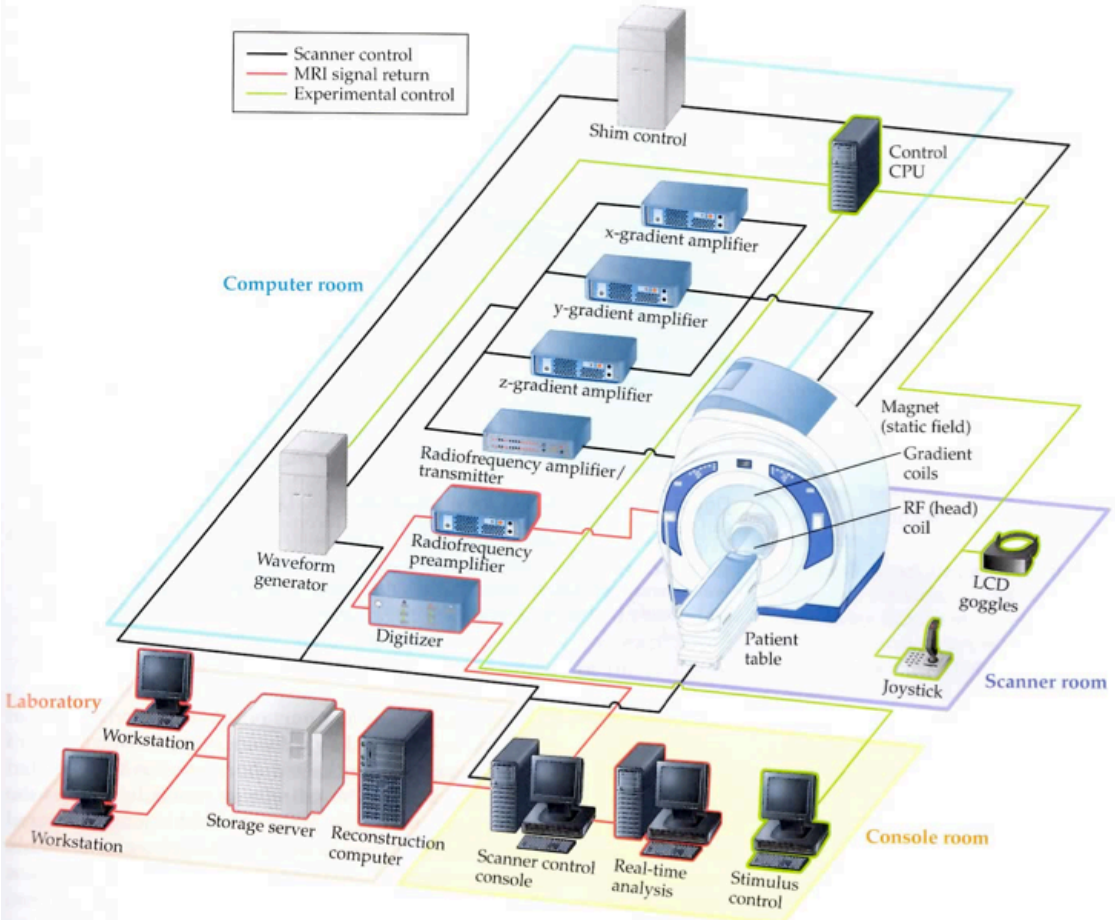

Figure 1-1 [1] A simplified organization diagram of an MRI and computer systems. The console room in the lower right is the control center where the MRI scanning is conducted, protocols are setup, pulse sequences are designed and implemented, and stimulus delivery system is situated. The laboratory (lower left) holds the reconstruction computer, workstation and storage server. The upper right shows the scanner room where the Static field is along with required coils, plus response systems (i.e. joy stick, goggles). The top left is what is often called the computer room where all the amplifiers and transmitters that create and deliver the pulse sequences and gradients. The lines show representational connections between different parts of the MRI setup (*Reprinted with permission from publisher*).

A modern-day MRI system with fMRI capabilities is an integration of many software and hardware components Figure 1-1. The console room holds the computer from which the scanning protocols are designed, setup and

implemented. Usually from the same computer pulse sequences are designed and implemented. These pulse sequences are the deriving force behind image creation in MRI using changing magnetic field gradients and electromagnetic fields. Also, sometimes on the same computer or a separate one, real-time fMRI data analysis is available, plus a separate stimulus delivery computer where the fMRI stimuli is designed and delivered. The data acquired using the consoles may be sent over to a laboratory setting that would reconstruct the data, store the data, and have a workstation for data viewing and analysis. This laboratory setup can also be in the console area.

What is frequently called the computer room (see Figure 1-1) holds the hardware and software that makes the physics possible to get the required data (i.e. image). In that, it contains amplifiers and transmitters that provide rapidly changing magnetic field gradients and oscillating electromagnetic fields allowing for image creation. This setup is connected directly to the scanner room where the static magnetic field is situated (also see Figure 1-1). The scanner room is copper shielded so that no electromagnetic signal from the outside environment affects the MRI signal. In the same apparatus where the static magnet is, the gradient coils are also situated. Also, a separate radio frequency (RF) coil (Figure 1-2) is usually needed to provide a perpendicular field to that of the static magnetic field. Moreover, the scanner room may also hold fMRI stimuli delivery and response systems such as video goggles and response measuring joysticks.

Figure 1-2 The left image shows an 8-channel SENSE RF coil, and the right image is of the MRI apparatus that contains the gradient and static magnetic field coils. These images are from The Advanced MRI Center at the University of Massachusetts Medical School (*Printed with permission from University of Massachusetts Medical School*).

Outside the scanner room, displays of safety warning signs are placed (Figure 1-3). These signs warn of the strong magnetic field inside the room that have the potential of aggressive and swift pulling of ferromagnetic objects towards the bore of the MRI scanner (donut shaped hole in Figure 1-2). This projectile effect on ferromagnetic objects can cause damage to the scanner, and can lead to human or animal injury or fatality. Examples of objects that may be ferromagnetic are pens, knives, aneurysm clips, and head bands. There are also a plethora of other ferromagnetic objects. That is why there is usually a strict screening protocol administered on people or animals before taking them inside the MRI scanner room.

Figure 1-3 An example of a warning sign displayed outside the scanner room.

1.3 Principles of Magnetic Resonance

Although he did not name it as such, Wolgang Pauli was the first to introduce the concept of spin. If we consider the single proton on a hydrogen atom under normal conditions; thermal energy causes the proton to spin about itself (Figure 1-4). In that, protons behave like spinning magnets; when they are placed in a magnetic field they exert a torque which is called magnetic moment (*u*). The magnetic moment is the tendency of an object possessing magnetic properties (i.e. proton) to align with the main magnetic field (i.e. static magnet in MRI). Also, the spinning of the proton on its rotational axis results in spin angular momentum. The angular momentum (J) is a measure resulting by the multiplication of the mass (*m*) of a spinning body by its angular velocity (*v*) equation 1-1. See Figure 1-5 for a depiction of angular momentum and magnetic moment.

$J = mv$ **Equation 1-1**

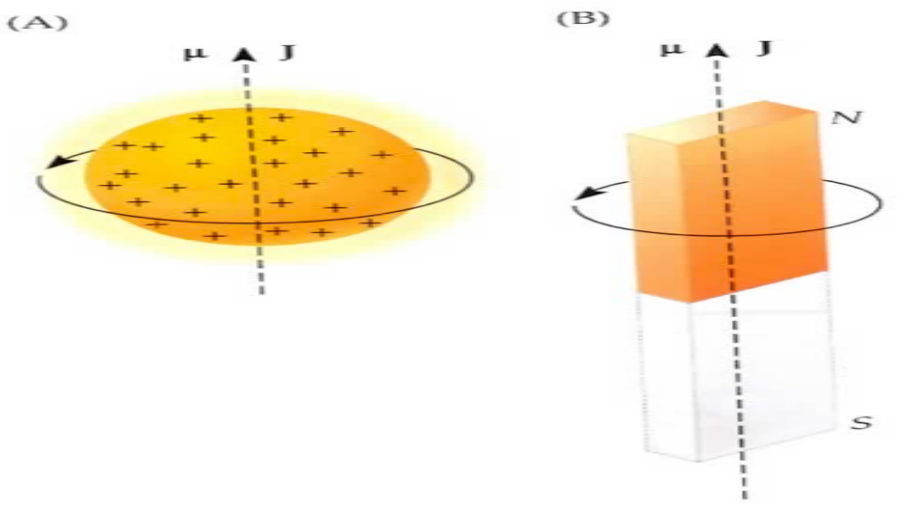

Figure 1-4 [1] The similarity between a spinning proton (A) and a spinning magnet (B). Both posses angular momentum (J) and magnetic moment (*u*) (*Reprinted with permission from publisher*).

In order for MRI to detect any given nucleus, the nucleus must posses both properties; magnetic moment and angular momentum. When a nucleus holds these two properties it is then called a spin in NMR or MRI terminology. A few commonly used spins in MRI are $^{13}C, ^{19}F, ^{31}P, ^{23}Na, ^{1}H$.

Hydrogen nuclei is by far the spin that is mostly used in human MRI, because of its abundance in the human body. Also, since we are interested in it with regards to the human brain, our discussion will focus on it. On average, water constitutes two thirds of a persons weight and , thus, the hydrogen protons from these water molecules are approximately 6.7×10^{27} in number for a person who weighs 200 lbs. (~90 kg). Each of these protons is freely rotating on its own, and since the protons are rotating at random directions they cancel each other out (Figure 1-5A). In other words, in the absence of a magnetic field, these protons have a net magnetization of zero. The net magnetization, which is the

sum of all magnetic moments from spins in a system, becomes positive in the presence of a magnetic field (Figure1-5B).

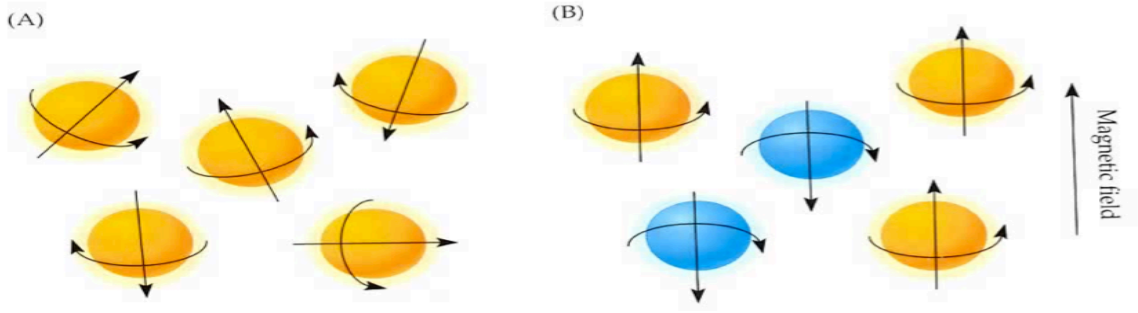

Figure 1-5 [1] Protons rotating in free space with no magnetic field in A. In B, Protons orient either with or against the applied magnetic field (*Reprinted with permission from publisher*).

In MRI, the main or static magnetic field is referred to as B_0 (B zero). When the hydrogen nuclei protons in a human body are subject to the B_0 field, they will line up either with or against B_0, and precess in a gyroscopic motion around B_0 (Figure 1-6). The protons precessing parallel to the applied magnetic field B_0 are in a lower energy state, while protons precessing in the anti-parallel state have higher energy levels (Figure 1-5b,Figure 1-6). Note that there are always more protons precessing in the former state than the latter one. The difference between these two states is what is called the net magnetization (M), which MRI measures.

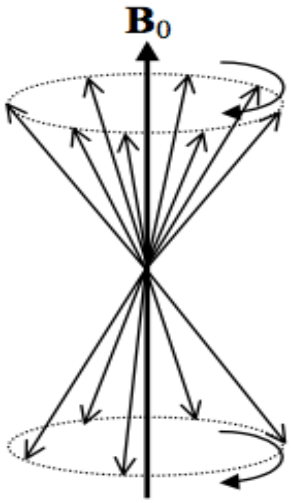

Figure 1-6 [2] Each arrow represents a precessing proton around the precession axis B_0 (*Reprinted with permission from publisher*).

It is worth noting that the strict parallel and anti-parallel states of the protons are idealized for explanation purposes. A more random orientation is actually present that results in the net magnetization. Moreover, the precession of protons occurs at an angular frequency that is proportional to the magnetic field B_0. This relationship is described by the Larmor equation :

$\omega_0 = \gamma B_0$ **Equation 1-2**

Here (Equation 1-2) the gyromagnetic ratio, γ, relates the main magnetic field B_0 to the angular frequency ω_0. The gyromagnetic ratio (or magnetogyric ratio) is an element specific ratio of the magnetic dipole moment to the angular momentum of that specific element, and is measured in radians per second per tesla ($s^{-1}T^{-1}$). Table 1-1 provides a list of MRI-detectable nuclei each with its corresponding gyromagnetic ratio. Moreover, the gyromagnetic ratio relates linear frequency f_0 to the main magnetic field B_0 by:

$$f_0 = \frac{\gamma}{2\pi} B_0$$ **Equation 1-3**

$$w = 2\pi f$$ **Equation 1-4**

Nucleus	$\frac{\gamma}{2\pi}$**(MHz/Tesla)**
^{1}H	42.58
^{13}C	10.7
^{17}O	5.8
^{19}F	40.0
^{23}Na	11.3
^{31}P	17.2

Table 1-1 Gyromagnetic ratio for some MRI-detectable nuclei

In general, frequency is always proportional to energy. In this case, the linear frequency f_0 is proportional to the energy separation ΔE between the lower energy state and the higher energy state. The ΔE can be seen in Figure 1-7 as the gap between the protons at the lower energy state (orange) and the protons at the higher energy state (blue). When the protons are in a magnetic field (i.e. B_0) an abundance of the protons assume either of these two states, separated by ΔE, and more assume the lower energy state (Figure 1-7A). When the right amount of energy is transmitted into such a system, some spins (i.e. protons of hydrogen) will absorb the energy and bounce to the higher energy state (Figure 1-7B). This phenomena is called excitation. However, when the source of energy is turned off, the spins go back to their lower energy state, and by doing that transmit the absorbed energy (Figure 1-7C). This phenomena is the basis of what is called relaxation in MRI.

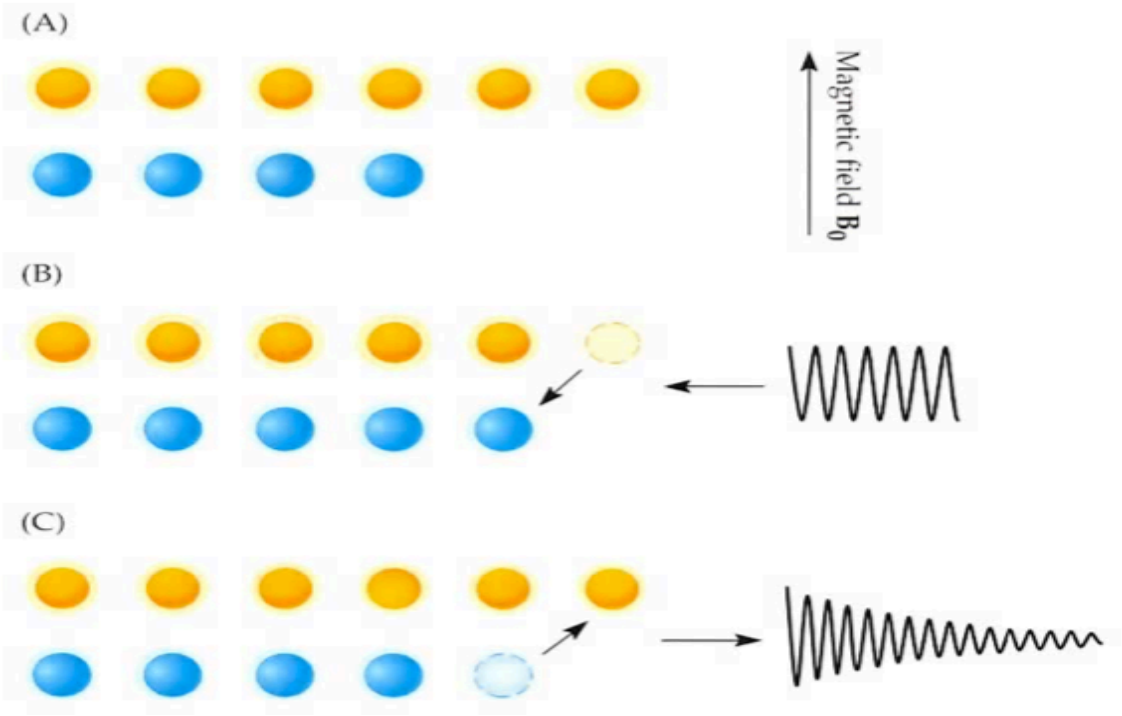

Figure 1-7 [1] Depiction of spins at lower energy states (orange) and higher energy states (blue). (A) shows the spins under only a magnetic field. (B) shows spins response to energy transmitted into such a system (excitation).(C) shows the relaxation of spins back to the lower energy state once the energy sources is off and enough time is passed (*Reprinted with permission from publisher*).

The excitation of spins in this case is made possible by a radio frequency (RF) pulse. This energy source (RF pulse) is also known as the B1 field, and is usually transmitted using an extra RF coil (i.e. Figure 1-2). In order for such an excitation to occur, the Larmor frequency (Equation 1-2) needs to precisely match the precessional frequency of the protons in a given system. Furthermore, it is the Larmor frequency that defines the frequency of the RF pulse needed during excitation to make spins jump to the high energy state, as well as the frequency discharged by spins when they return to the low energy state.

In bulk matter, such as the human brain, the RF pulse excitation does not occur on a single nuclei level. Instead, the RF pulse excites the bulk of nuclei's

(i.e. hydrogen protons) net magnetization. When a bulk matter such as the brain is subjected to the static magnetic field of the MRI system, the net magnetization of the protons initially points along the main static magnetic field. Its precission angle is 0 degrees at equilibrium (Figure 1-8A). At this time point (before t=0) and before any RF pulse, the motion of the net magnetization (*M*) can be described by the following scalar equations with respect to the x,y, and z planes:

$$\frac{dM_x}{dt} = \gamma M_y B_0$$ **Equation 1-5**

$$\frac{dM_y}{dt} = -\gamma M_x B_0$$ **Equation 1-6**

$$\frac{dM_z}{dt} = 0$$ **Equation 1-7**

Solving the set of differential equations (Equations 1-5,1-6, and 1-7) given the initial conditions before time zero gives:

$$M(t) = \left(M_{x0}\cos(wt) + M_{y0}\sin(wt)\right)x + \left(M_{y0}\cos(wt) - M_{x0}\sin(wt)\right)y + M_{z0}z$$

Equation 1-8

This equation (Equation 1-8) summarizes how the net magnetization precesses around the main B_0 magnetic field at time zero before any RF pulse is transmitted into the system (i.e. brain).

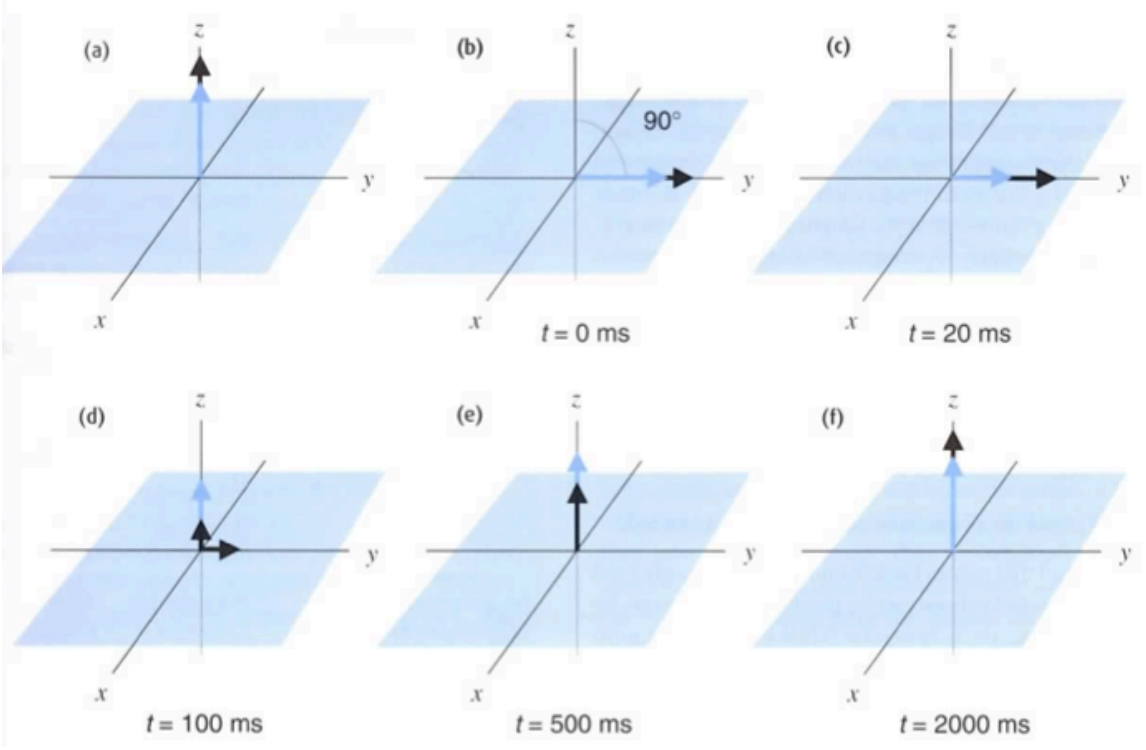

Figure 1-8 [3] Net magnetization before and after RF pulse excitation. The black and blue arrows resemble the magnetization for two different tissue types (i.e. white matter and gray matter in the brain). The length of the arrow resembles proton density (A) Before any RF pulse, at t=0, net magnetization is along the z axis (M_0). (B) A $90°$ RF pulse excites the spins and knocks both magnetizations onto the *xy* plane. (C-E) Relaxation takes place at different rates for the two different tissue types. (F) eventually both tissues will relax back to the initial equilibrium state (M_0)(*Reprinted with permission from publisher*).

In order to measure the magnetization of a spin system, we have to provide a perturbation to the system. This perturbation causes the spin system to move away from equilibrium (M_0) on the z axis, and then the response of the system is measured from the emitted energy as the magnetization grows back to equilibrium (Figure 1-8B - F). As mention earlier, such an excitation is caused by the application of an RF pulse. Since the magnetization is rapidly oscillating around the main magnetic field (64 million times/second in a 1.5 T magnet), it is almost impossible to perturb or knock down the magnetization with a single RF

pulse. Instead, RF pulse energy is applied at a given frequency (Larmor frequency) in a RF coil that creates a perpendicular field (B_1) to the main magnetic field (B_0).

$$B_1 = B_1 x \cos(wt) - B_1 y \sin(wt) \qquad \textbf{Equation 1-9}$$

Since both the spins and excitation pulse are rotating at the same Larmor frequency, we can adopt a rotating frame of reference (Figure 1-9A) that rotates at the Larmor frequency. This is aside from the normal frame of reference that is aligned with the B_0 field (Figure 1-9B).

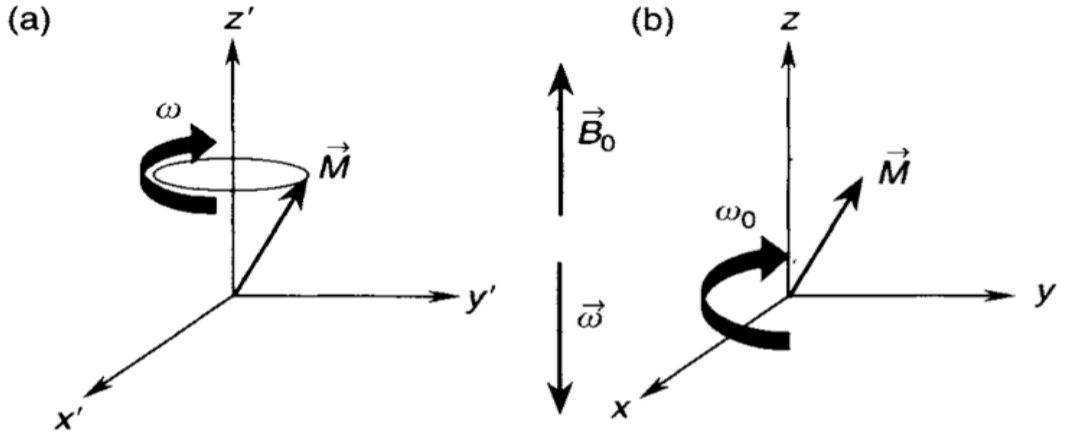

Figure 1-9[2] Spin precession view from (a) laboratory frame of reference, and (b) rotating frame of reference (*Reprinted with permission from publisher*).

The rotating frame of reference is adopted to provide a depiction of the mathematical descriptions to follow. Since the rotating frame rotates with the Larmor frequency, it appears as stationary. In the transverse plane, the unit vectors of the rotating frame are represented by *x* and *y*, and are related to the unit vectors of the laboratory frame by:

$$x = x'\cos(wt) - y'\sin(wt) \qquad \textbf{Equation 1-10}$$

$$y = x'\sin(wt) + y'\cos(wt)$$ **Equation 1-11**

Because within the rotating frame both spins and RF excitation pulse become stationary, we can write the net magnetization (*M*) and the B_1 as :

$$M = M_0 z$$ **Equation 1-12**

$$B_1 = B_1 x'$$ **Equation 1-13**

Therefore the rate of change of *M*, with respect to magnetization across all planes (M_x, M_y, M_z), in the rotating frame of reference is:

$$\frac{dM}{dt} = \frac{xM_x + yM_y + zM_z}{dt} = M_x\frac{dx}{dt} + M_y\frac{dy}{dt} + x\frac{dM_x}{dt} + y\frac{dM_y}{dt} + z\frac{dM_z}{dt}$$ **Equation 1-14**

Although this equation (Equation1-14) determines the rate of change of *M*, the time it takes for the net magnetization to get back to equilibrium is partly determined by the flip angle. The flip angle determines the change in the precession angle of the magnetization following an RF pulse excitation. Common flip angles are 90 degrees and 180 degrees, though a variety of smaller flip angles are also frequently used. If the flip angle is greater than zero, there will always be a net magnetization that is the sum of z-plane and xy-plane magnetizations (M_z, M_{xy} respectively).

If we consider a 90 degree RF pulse excitation delivered to a spin system, two relaxation phenomena take place. The first one is longitudinal relaxation

(Figure1-10A) and the second one is transverse relaxation (Figure1-10B). The former is also given the name spin-lattice relaxation or T1 relaxation, and the

latter can also be referred to as spin-spin relaxation or T2 relaxation. Therefore the amount of longitudinal magnetization, M_z, present at time *t* following an RF pulse is given by

$$M_z = M_0(1 - e^{\frac{-t}{T_1}}) \quad \textbf{Equation 1-15}$$

and the transverse signal loss or dephasing due to T2 relaxation (a.k.a T2 decay) is given by:

$$M_{xy} = M_0 e^{\frac{-t}{T_2}} \quad \textbf{Equation 1-16}$$

However, T2 is an idealized decay rate that assumes no extrinsic effects. However in a real-world situation there exists extrinsic effects, such as phase differences and magnetic field inhomogeneities. This lead to a new coined term; T2* (T2 star) which takes into account these effects. T2* is always shorter than T2 and, as we will see later, and it is by far the most used contrast for fMRI.

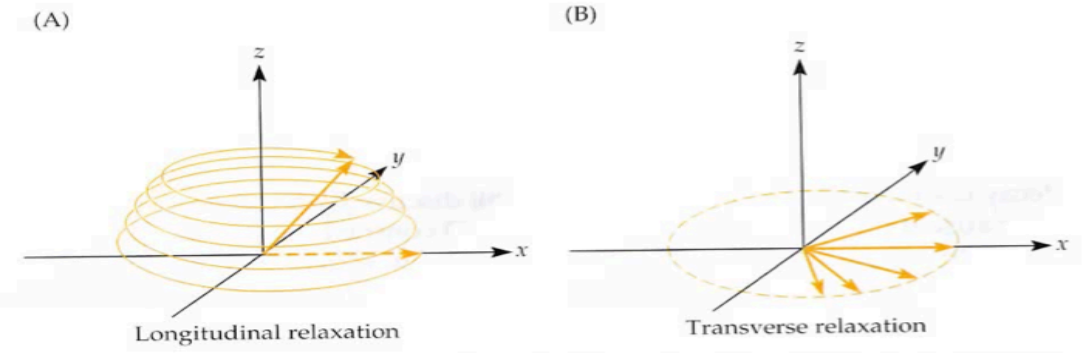

Figure 1-10 [1] (a) T1 or spin-lattice relaxation , (b) T2 or spin-spin relaxation. It is worth noting that the longitudinal magnetization in fact grows back onto the z axis (*Reprinted with permission from publisher*).

An all-combining equation that describes the above phenomena and equations that describes how the net magnetization of a spin system changes as a function of time in the presence of a time-varying magnetic field is the Bloch equation:

$$\frac{dM}{dt} = \gamma MB + \frac{1}{T_1}(M_0 - M_z) - \frac{1}{T_2}(M_x + M_y) \qquad \textbf{Equation 1-17}$$

1.4 Relaxation Mechanisms and Tissue Contrasts

The Bloch equation (Equation 1-17) determines the change in magnetization $\frac{dM}{dt}$ by the summation of the precession term (γMB),the T1 term ($\frac{1}{T_1}(M_0 - M_z)$),and the T2 term ($\frac{-1}{T_2}(M_x + M_y)$).From this we note that the T_1 term only reflects the magnetization on the z-axis, while the T_2 term reflects magnetization in both the *x* and *y* axes. If we consider the axis separately from the Bloch equation, we get:

$$\frac{dM_x}{dt} = \gamma M_y B - \frac{M_x}{T_2} \qquad \textbf{Equation 1-18}$$

$$\frac{dM_y}{dt} = -\gamma M_x B - \frac{M_y}{T_2} \qquad \textbf{Equation 1-19}$$

$$\frac{dM_z}{dt} = -\frac{(M_z - M_0)}{T_1} \qquad \textbf{Equation 1-20}$$

The T1 (spin-lattice) relaxation is only dependent on the longitudinal magnetization. Therefore, it is only dependent on Equation 1-20 which is a first order differential equation and its solution is an exponential recovery function given by:

$$M_z = M_0(1 - e^{\frac{-t}{T_1}})$$ **Equation 1-21**

A depiction of T1 relaxation is provided in Figure 1-11.

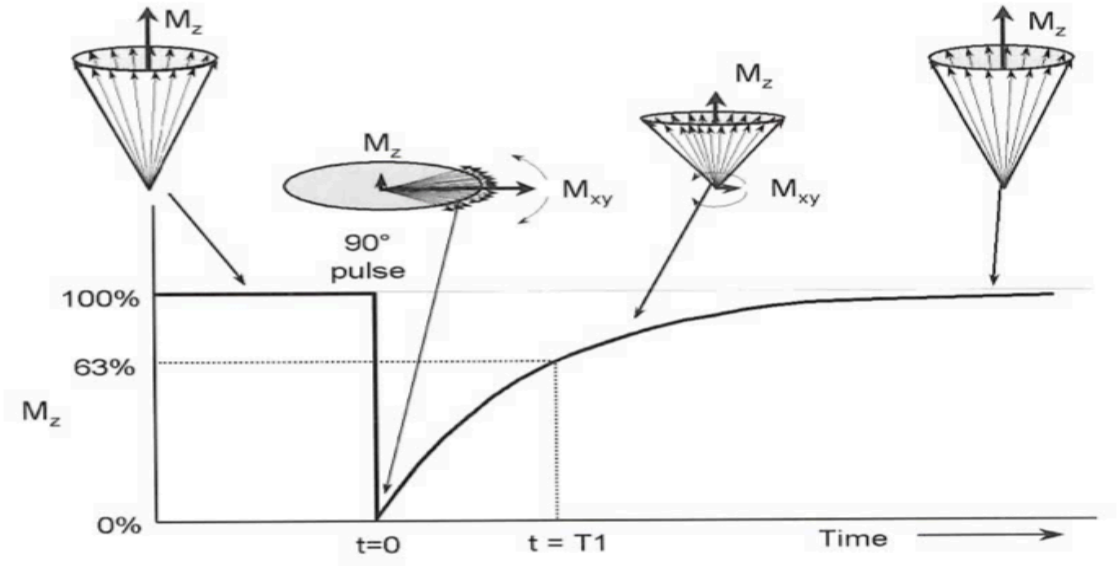

Figure 1-11[4] The change of the T1 relaxation overtime after applying a 90 degree RF pulse (*Reprinted with permission from publisher*).

Figure 1-11 illustrates the longitudinal relaxation of M_z (T1 relaxation). At t=0, a 90 degree RF pulse tips over the longitudinal magnetization M_z to the x-y plane. Therefore at t=0 M_z is zero. As time progresses longitudinal magnetization relaxation takes place and the 63% point of such a relaxation is the T1 constant for a specific tissue. Eventually all of the magnetization will recover back to the z axis, and at that time point the system does not dissipate any signal. Therefore, in order to acquire what is called a T1 weighted image in MRI, the signal has to be acquired at a time point before full relaxation (magnetization is back to the z axis).

Another MRI contrast mechanism is the T2 weighted contrast (Figure 1-12a). The T2 contrast is concerned with the dephasing of spins that occurs in the

x-y plane. It can be derived by solving the Bloch equation which will ultimately give $M_{xy} = M_{xy0} e^{\frac{-t}{T_2}} e^{-iwt}$ where accumulated change in angle (phase) is a factor. This is true after a 90 degree pulse tips over the magnetization into the x-y plane and the spins go through a process called fanning or dephasing. This dephasing phenomena, as illustrated in Figure 1-12A, occurs exponentially and is caused by spin-spin interactions in the tissues. Over time, M_{xy} will go from a maximum at t=0 (point at which RF pulse is administered) to zero. The rate governing this decay of signal is tissue specific and the T2 decay constant for a tissue is at the 37% mark of the signal. However, the T2 decay does not account for extrinsic magnetic field variations and inhomogeneities. Therefore a T2* contrast mechanism has been coined to account for such extrinsic factors Figure 1-12B. Because of these factors, the T2* decay is always shorter than the T2 exponential decay. It remains that in order to acquire a T2 or T2* weighted MRI image, there has to be enough dephasing of the spins; thus, such an image is optimally acquired at a time point between 100% and 0% in Figure 1-12A,B.

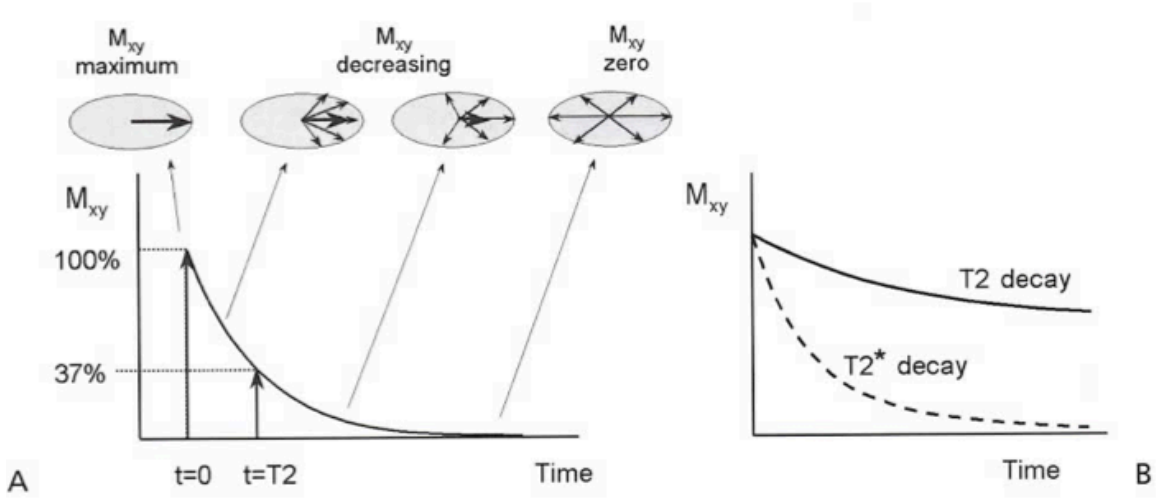

Figure 1-12 [4] (A) The dephasing of spins and T2 relaxation overtime after applying a 90 degree RF pulse. (B) T2 and T2* exponential decay overtime (*Reprinted with permission from publisher*).

A third, less used, MRI contrast worth mentioning is proton density (PD). As the name implies, this contrast provides an image based on the number of protons within a specified region in any given tissue. In order to acquire a PD weighted image, both T1 and T2 contrast must be at a minimum. With regards to T1 minimization, a time point is selected after most, if not all, longitudinal relaxation is recovered; while T2 minimization is accomplished by selection of a time point closer to the beginning of the decay before any or minimal dephasing occurs.

As can be inferred from the above MRI contrast mechanisms, time is a major factor that governs MR images. There are special coined terms that relate these specific time points that are set by the user to acquire an MR image according to a pre-determined contrast. These time factors are: repetition time (TR), and time to echo (TE). The former is the time interval between successive RF pulses and is often expressed in seconds, while the latter refers to the time

between the RF excitation pulse and acquisition of the MR signal (echo) and is expressed in milliseconds.

In order to illustrate TR and TE with regards to acquiring a PD weighted MR image, as discussed above, we provide Figure 1-13. Here the TR and TE have been selected in order to optimize a PD weighted MR image. The TR is the time point that affects the T1 contrast, whilst the TE is used to control the T2 contrast contribution.

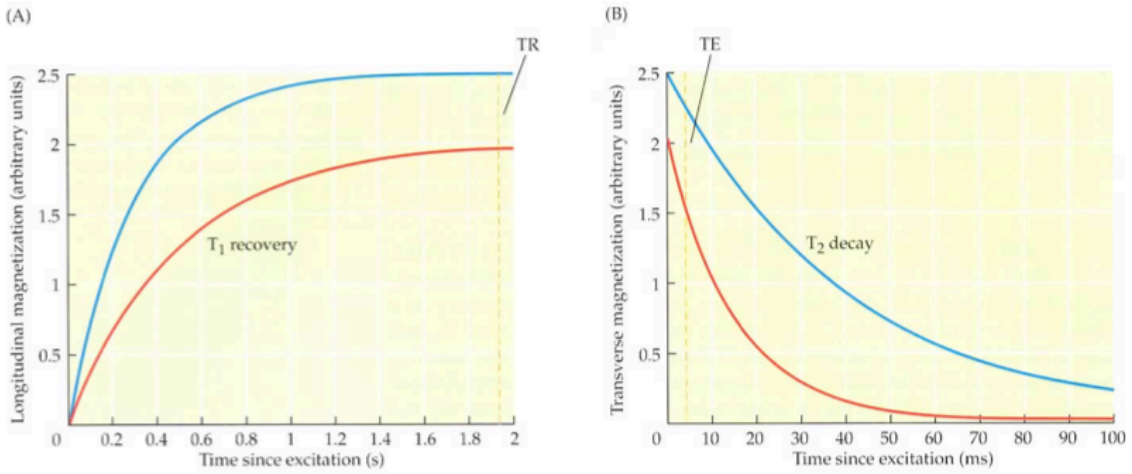

Figure 1-13 [1] The blue and red lines represent two different tissue types with different relaxation properties. (A) is the T1 recovery or relaxation of the tissue types, with TR (dashed yellow line) is selected so that to minimize T1 contribution to the MR signal. (B) is the T2 decay or relaxation of both tissue types, with TE (dashed yellow line) selected so that to minimize T2 effects on the acquired signal (*Reprinted with permission from publisher*).

An equation that relates the contrast of two tissue types based on T1 and T2 relativities is:

$$C_{AB} = M_{0A}(1 - e^{\frac{-TR}{T_{1A}}})e^{\frac{-TE}{T_{2A}}} - M_{0B}(1 - e^{\frac{-TR}{T_{1B}}})e^{\frac{-TE}{T_{2B}}};$$

$$A: Tissue\ A \qquad \textbf{Equation 1-22}$$

$$B: Tissue\ B$$

1.5 Image Formation

Most RF coils are transmit-receive coils. In that, they are able to both transmit the RF pulses and detect or receive the MR signal for image reconstruction. In a typical MRI setting, the MR signal from an imaged bulk matter is the sum of the transverse magnetizations of all voxels. A voxel is a three dimensional volume which can be seen as corresponding to a pixel in a two dimensional space. Each voxel in an imaging volume is excited when an RF pulse is delivered, and the total MRI signal measured combines the changes in net magnetization produced at all excited voxels. This can be represented by Equation 1-23 below, which gives the spatial summation of MR signal from all excited voxels.

$$S(t) = \int_x \int_y \int_z M_{xy}(x,y,z,t)dxdydz \qquad \textbf{Equation 1-23}$$

In the same apparatus that holds the B_0 field, there are also three other gradient (G) magnetic fields along the *x* , *y*, and *z* axis respectively. These gradient fields modulate the strength of the main static B_0 magnetic field. Therefore, it is possible to describe the total magnetic field, *B*, experienced by a spin system at a specific spatial location (*x, y, z*) and at a given time (*t*) by:

$$B(t) = B_0 + G_x(t)x + G_y(t)y + G_z(t)z \qquad \textbf{Equation 1-24}$$

This derived equation (Equation 1-25) explains the accumulated phase caused by both the B_0 and by the time varying gradient fields ($G_x(t),G_y(t),G_z(t)$).

Now, if we combine Equation 1-25 and Equation 1-23, we get the MR signal equation below (Equation 1-26) that describes the acquired MR signal as

a function of the NMR properties of the imaged objects under the ascribed magnetic fields.

$$S(t) = \int_x \int_y \int_z M_{xy0}(x,y,z) e^{\frac{-t}{T_2}} e^{-i\gamma B_0 t} e^{-i\gamma \int_0^t (G_x(t)x + G_y(t)y + G_z(t)z)dt} dxdydz$$ **Equation 1-26**

The MR signal equation (Equation 1-26) remains a 3-D formulation, because of the signal contribution from the three spatial gradients gradients ($G_x(t), G_y(t), G_z(t)$). In order to reduce such an equation to 2-D form, sections of the imaging volume (slices) are excited using one-dimensional RF excitation pulse, and the remaining two gradients are used for phase encoding and data acquisition (frequency encoding) respectively. The data from the three gradients are acquired on what is termed as k-space. This space is used as a notation scheme used to describe MRI data before it is transformed to the image-space. The process that k-space is transformed into image-space is by inverse fourier transform (IFT). See Figure 1-14.

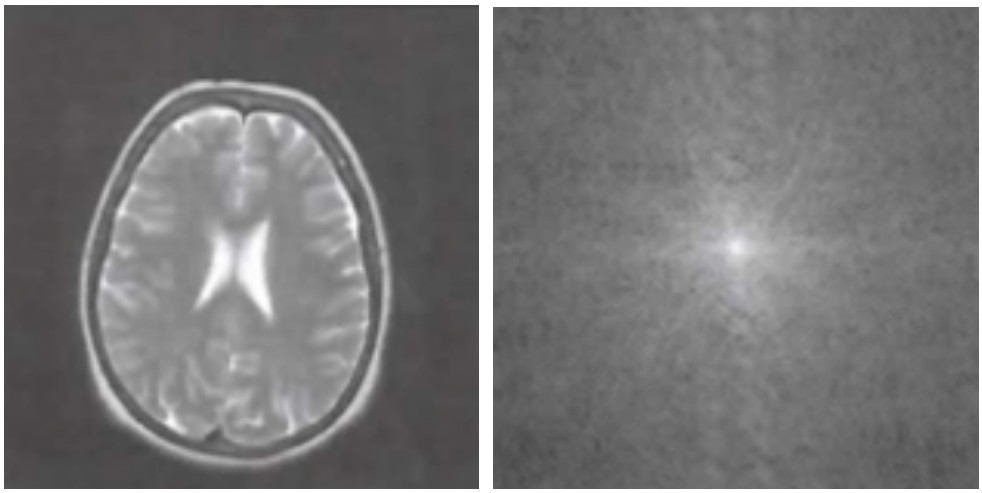

Figure 1-14 Inverse fourier transform is used to obtain the image space (left image) from the k-space (right image). Therefore, clearly, fourier transform can be used to go in the other direction (from image space to k-space). Note that low frequency spatial information is encoded in the middle of k-space, while high frequency spatial components are encoded in the peripheries of k-space.

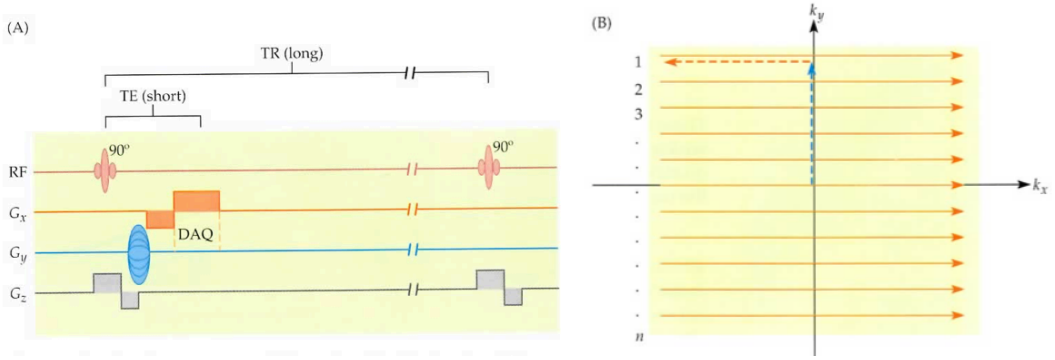

Figure 1-15[1] (A) is a timing diagram for an MRI pulse sequence (gradient echo pulse sequence). (B) k-space trajectory according to the pulse sequence in (A) (*Reprinted with permission from publisher*).

The k-space is filled through specific k-space trajectories that are administered by an MRI pulse sequence (Figure 1-15). A pulse sequence is what allows image acquisition in MRI. It is a series of variable gradient magnetic fields and RF pulse(s) that determine how k-space is acquired.

Figure 1-15A depicts an example of a sub-category of pulse sequences called gradient-echo (GE). Here the GE pulse sequence begins with a 90 degree pulse accompanied by, at the same time, a slice selection gradient (G_z). Multiple slices are acquired to cover the whole imaging volume in such a 2D MRI acquisition. Then the trajectory and acquisition of the k-space lines are controlled by the remaining two gradients (in this example: G_x,G_y). The G_y is the phase encoding gradient. It allows for spatial variation of the phase of magnetization, therefore allowing for incremental acquisition of k-space lines (blue dashed line trajectory in Figure 1-15B). On the other hand, the frequency encoding gradient (G_x) is turned on at TE during data acquisition so that the MRI signal is spatially encoded by assigning a specific precession frequency, such as the Larmor frequency, to spins precessing at the same frequency. This assignment is done at unique spatial locations along the frequency gradient direction. Therefore allowing for single/multiple line acquisition in k-space (solid yellow line trajectory in Figure 1-15B). In order to acquire all k-space lines in this pulse sequence (Figure 1-15A), these steps are repeated every TR to allow full k-space acquisition.

Slice selection

Slice selection is achieved by combined use of an RF pulse to excite spins with in a slab of the imaging volume and the use of a magnetic field gradient. The bulk magnetization in a given location (*x,y*) within a slice of thickness Δz can be described by

$$M(x,y) = \int_{z_0-\frac{\Delta z}{2}}^{z_0+\frac{\Delta z}{2}} M_{xy0}(x,y,z)dz \quad \textbf{Equation 1-27}$$

This Equation 1-27 shows that *M* is only dependent on x and y, which simplifies the 3-D MR signal equation (Equation 1-26) to the following 2-D form

$$S(t) = \int_x \int_y M(x,y) e^{-i\gamma \int_0^t (G_x(\tau)x + G_y(\tau)y)d\tau} dxdy \quad \textbf{Equation 1-28}$$

which describes that the slice's signal is dependent upon the net magnetization at every (*x,y*) location in a slice and the phase at that location is dependent on the gradient field strength at (*x,y*). Moreover, the role of the gradient in localization and thickness of the slice is provided in Figure 1-16.

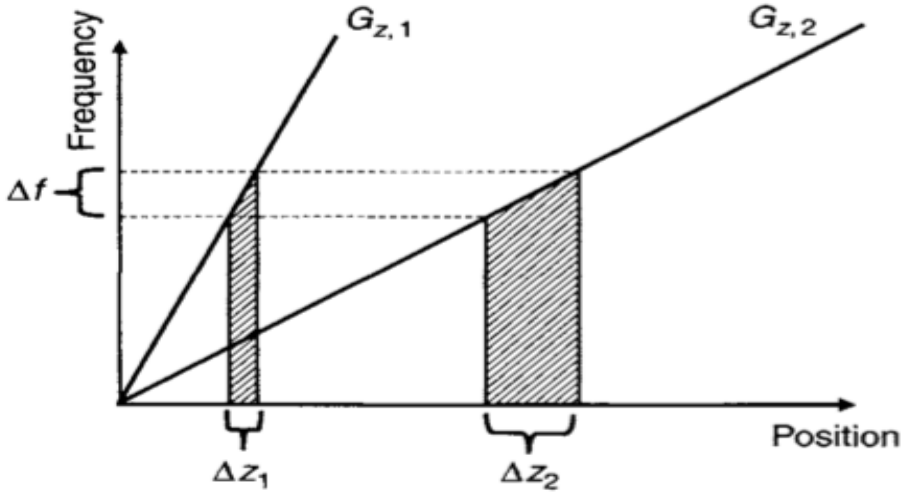

Figure 1-16[2] The effect of RF pulse frequency (Δf) and the strength (slope) of slice gradient (G_z) on slice position and thickness (Δz)(*Reprinted with permission from publisher*).

Figure 1-16 illustrates how the slice gradient can be used to specify slice location and thickness. By changing the slope (strength) of the slice selection gradient

(i.e $G_{z,1} \rightarrow G_{z,2}, G_{z,2} \rightarrow G_{z,1}$) the slice thickness can be changed (Δz) and so can the slice's position. This can also be achieved adjusting the bandwidth (Δf) or central frequency f of the RF pulse sequence. Therefore slice position is given by

$$z = \frac{f_1 - f_0}{\gamma G_z} \qquad \textbf{Equation 1-29}$$

and slice thickness can be attained and calculated by

$$Slice\ Thickness = \frac{RF\ \ bandwidth}{\gamma G_z} \qquad \textbf{Equation 1-30}$$

frequency encoding

Frequency encoding is a common spatial encoding mechanism used in MRI pulse sequences. It utilizes a variable magnetic field gradient to acquire time-domain MR signals consisting of a range of frequencies, which correspond to different spatial locations. A frequency encoding gradient does that by noting distinct spatial positions along the direction of the gradient, and assigning unique precession frequency (i.e. larmor frequency) to each group of spins spinning at the same frequency. Since each frequency is linearly related to the corresponding spatial location along the gradient direction (G_x) it encodes the k-space lines in that direction (Figure 1-17). The signal from a frequency encoding gradient can be written as

$$S(t) = p(x) e^{(\frac{-t}{T2^*})} e^{(i\gamma x G_x t)} dx \quad ;\ p(x) \text{ is proton density} \qquad \textbf{Equation 1-31}$$

and can be depicted in Figure 1-17 where each frequency encoded line of k-space is acquired every TR according to a GE pulse sequence as that provided in Figure 1-15 above.

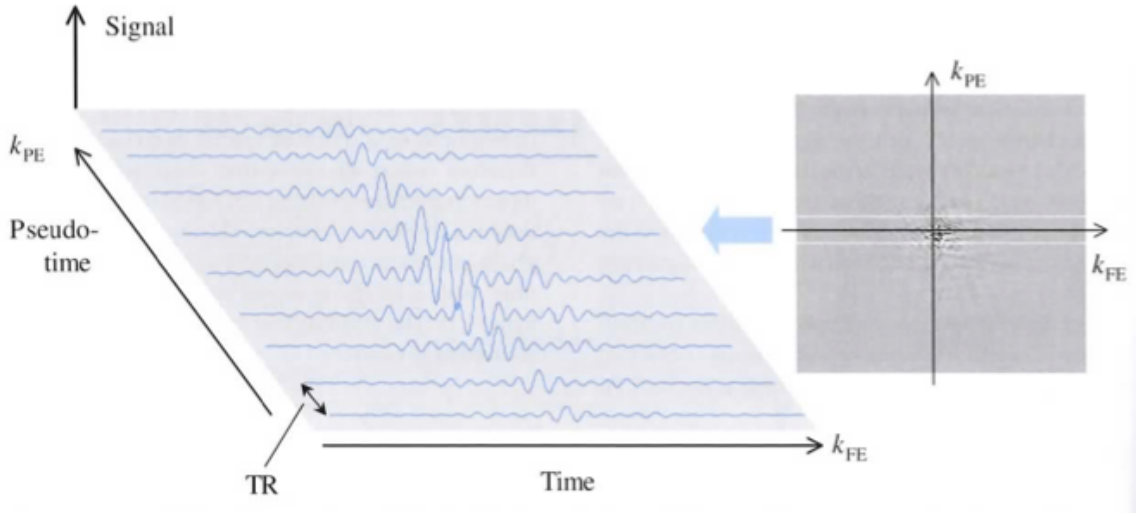

Figure 1-17[3] Illustration of frequency encoding direction of k-space, where each line in frequency encoding direction is acquired every TR according some pulse sequences (*Reprinted with permission from publisher*).

Phase encoding

To put it simply; phase encoding is used to jump from line to line to allow for frequency encoding acquisition on k-space. This is because spatial localization in MR employs both phase and frequency encoding to acquire k-space. In phase encoding, a gradient is applied during the time when the magnetization is in the transverse (x-y) plane before data acquisition. The idea behind phase encoding is to create a linear spatial variation of the phase of magnetization (Figure 1-18). In that, it allows for spatial encoding of information orthogonal to the frequency encoding direction (blue line in Figure 1-15B).

Moreover the incrementation of k-space lines due to phase accumulation in a basic GE pulse sequence can be characterized by:

$$G_y(n) = \Delta G n \quad for\ n = \frac{-N}{2} to \frac{N}{2} - 1;$$
$$N : number\ of\ TR\ repetitions$$

Equation 1-32

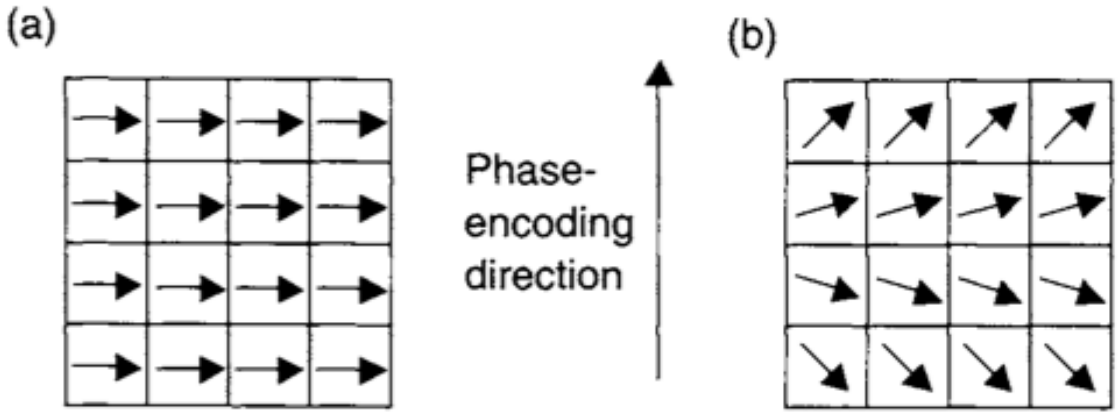

Figure 1-18 [2] The arrows represent the transverse magnetization at a given location *(x,y)*. (a)At the end of an RF pulse all the magnetization at the different locations have the same phase. (b) After a phase-encoding gradient is applied, the phase of the transverse magnetization varies according to the location from the phase-encoding gradient. Therefore providing a perturbation that allows for measurement of signal along the gradient (*Reprinted with permission from publisher*).

1.6 Pulse sequences

We already provided a brief overview of an example of a pulse sequence called gradient echo (GE) pulse sequence in Figure 1-15A. A pulse sequence allows for the tailoring of timing, polarity, order, and repetition frequency of the magnetic field gradients and RF pulse(s) to provide MR contrast (i.e. T1, T2,T2*). There are two main and broad categories of pulse sequences that encompass

most MRI pulse sequences. These are spin echo (SE) pulse sequence and gradient echo (GE) pulse sequence.

In a spin echo (SE) pulse sequence a 90 degree RF pulse is applied to tip the magnetization in the x-y plane , and then followed by a second RF pulse (180 degree) to produce an echo for data acquisition. Figure 1-19 illustrates the timing of RF pulses and associated magnetization to get an echo. It starts with a 90 degree RF pulse which tips over the magnetization into the x-y plane. The spins at the x-y plane go through a process of dephasing or fanning and the emitted signal is a free induction decay (FID) with a decay rate called T2*. As time progresses, the dephasing increases and FID approaches zero. At TE/2 a 180 degree RF plus inverts the spins to re-establish phase coherence. This causes a cancelation of inhomogeneities in the magnetic fields and the peak amplitude of the echo comes at TE during which data acquisition is administered.

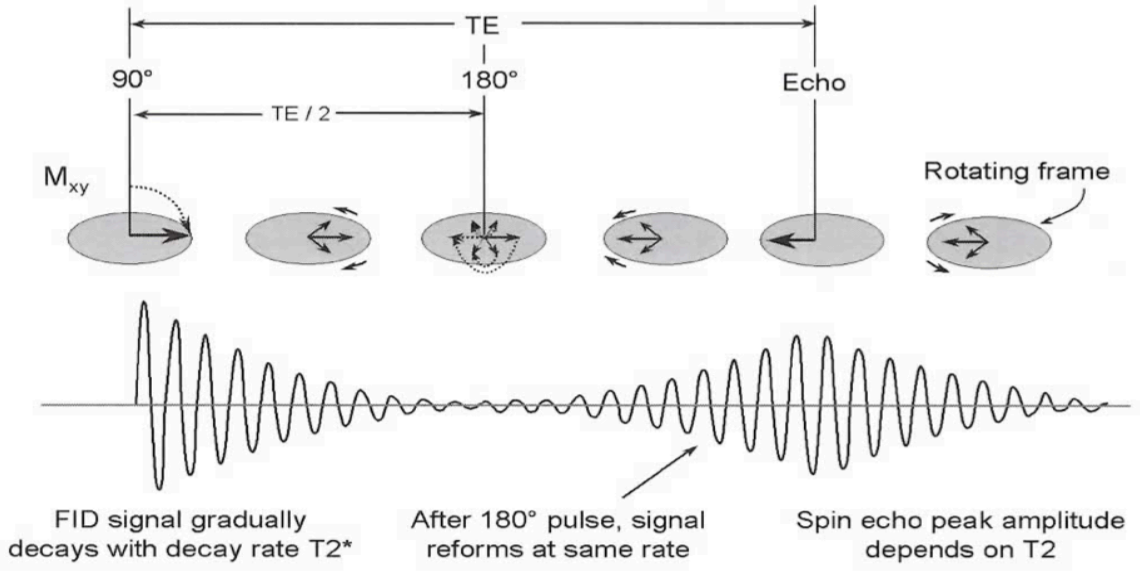

Figure 1-19 [4] RF pulse timing, M_{xy} dephasing, and echo generation for a spin echo pulse sequence (*Reprinted with permission from publisher*).

The advantage of a SE pulse sequence is in its ability to acquire specific contrast weighting (i.e. T1, T2, Proton Density) by using specific TR and TE values. Also, because of the 180 degree RF pulse, off-resonance effects (i.e. first 90 degree RF pulse not on exact resonance frequency) are cancelled. Therefore resulting in less image artifacts.

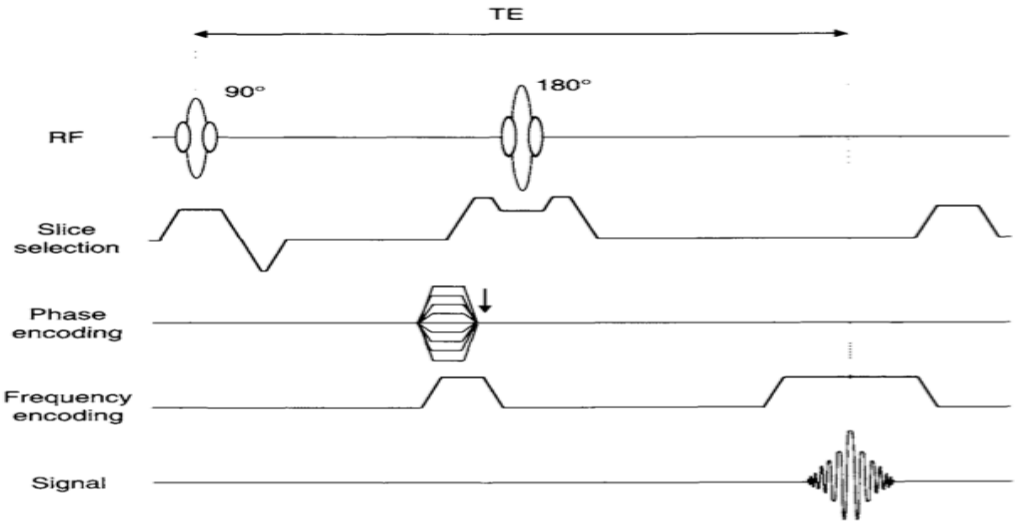

Figure 1-20[2] Timing diagram of a spin echo pulse sequence (*Reprinted with permission from publisher*).

The first line of Figure 1-20 illustrates the timing of the 90 degree pulse and the 180 degree pulse at time zero (t=0) and TE/2 respectively. The second line is the slice selection gradient by which the first gradient lobe selects the slice, the second gradient lobe is a crusher gradient used to preserve the desired signal pathways and eliminates undesired ones. Then a spoiler gradient (third lobe on the second line) is applied at the end of the waveform to get rid of any residual transverse magnetization before the next TR begins. The third line in Figure 1-20 depicts the phase encoding gradient lobe that allows for k-space trajectory to acquire subsequent k-space lines, and the arrow is the direction of

the change in gradient to allow for such k-space acquisition. In the frequency encoding waveform (fourth line in Figure 1-20) a balancing gradient lobe is applied before frequency encoding to acquire details of the respective k-space line at the time of echo (signal line). This is repeated in increments of TR until all of the k-space is acquired.

The other category of pulse sequences is gradient echo (GE). The main difference between GE and SE pulse sequences, is that GE do not have a second refocusing RF pulse as in SE pulse sequences. Moreover, in GE, smaller (<90 degrees) flip angles are sometimes administered depending on the imaging task. This allows for shorter time period for T1 recovery, because the longitudinal magnetization is not fully inverted onto the x-y plane. Therefore, faster image acquisition can be achieved using GE pulse sequences.

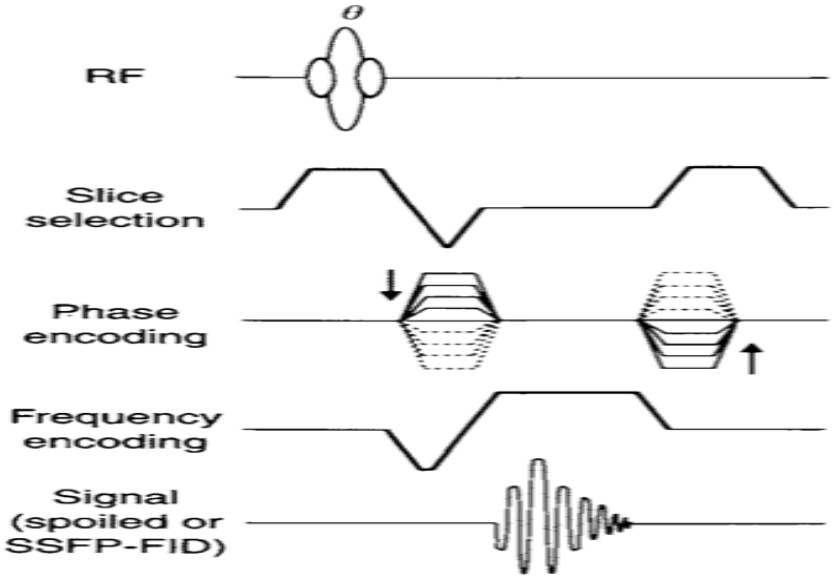

Figure 1-21 [2] Timing diagram of a gradient echo pulse sequence (*Reprinted with permission from publisher*).

Figure 1-21 provides an outline of the timing sequence of a basic gradient echo (GE) pulse sequence with spoiling. This pulse sequence starts out with an

RF pulse at prescribed angle and a slice selection gradient. The phase encoding and frequency encoding gradients in this case work similarly to the SE pulse sequence explained earlier. The phase encoding allows for trajectory of k-space line acquisitions every TR, and frequency encoding allows for data acquisition at TE. This example of a GE pulse sequence is called a spoiled GE pulse sequence, because a spoiling gradient is allocated at the end of the slice selection waveform. Therefore, eliminating any excess transverse magnetization before the next TR.

Though GE pulse sequences gained use in MRI because of their speed when compared to SE pulse sequences, they also have other unique advantages too. GE pulse sequences can be used for dynamic scans and can be used to provide blood flow quantization. GE sequences can also provide susceptibility-weighted images, because they don't have the second refocusing pulse as in the case of SE sequences. Moreover, in GE sequences the phase of the spins in the transverse plane can continue to accumulate during the entire echo time. Consequently providing images that are contrast weighted by T2* instead of T2. Although excessive T2* can cause signal-loss in MRI, a moderate amount of T2* weighting in GE pulse sequences allows for measuring brain activity in fMRI.

$$\frac{1}{T2*} = \frac{1}{T2} + \frac{1}{T2'}; \qquad \textbf{Equation 1-33}$$

$T2' \sim \frac{1}{\gamma \Delta B}$ in each imaging voxel

$T2$: is the intrinsic property of the tissue

Although GE sequences are faster than SE sequences in general, the acquisition of each k-space line (i.e. through phase encoding gradient) every TR is slow for certain imaging requirements (i.e fMRI). Therefore a pulse sequence was developed for even more rapid image acquisition. Such a pulse sequence was first developed by Peter Mansfield and called Echo-Planar Imaging (EPI). EPI allows for the acquisition of all of k-space (i.e. entire 2D image) by rapidly interchanging spatial gradients following a single RF pulse.

Unlike other fast pulse sequences that can be configured by software and pulse sequence design, EPI requires high performance gradients. These gradients come standard in most MRI systems today, and allow for rapid on/off switching. This is because k-space needs to be filled out in one shot (single-shot EPI) or in multiple shots (multi-shot EPI) by using multiple excitation pulses. Both of these EPI techniques permit substantial reduction in scan time over conventional imaging protocols and at the same time maintain good image quality.

In fMRI, single-shot GE-EPI are used because of their sensitivity to T2* contrast and for their speed (We will see later how T2* allows for fMRI and brain activation measurements). The fast speed of GE-EPI is primarily due to the blipping of the phase-encoding gradient and the fast interchange of the frequency encoding gradient between polarities (Figure 1-22). The blipping effect allows for acquisition of all of k-space in one TR. The blips (G_y Figure 1-22) allows for jumping from one k-space line to the next, while the frequency encoding gradient is switching polarity for signal acquisition.

For a triangular blipped phase encoding, as that of in Figure 1-22, the amplitude of the blip, G_{bp}, is related to the amplitude of a constant phase encoding gradient (continuous plateau with no blips) by direct relation between echo spacing, ES, and the blip's effective application time (unit area), $\frac{t_{bp}}{2}$, giving:

$$G_{bp} = \frac{2G_y ES}{t_{bp}} = \frac{2}{\gamma FOV_y t_{bp}}; \qquad \textbf{Equation 1-34}$$

FOV_y: field-of-view in the phase encoding gradient direction

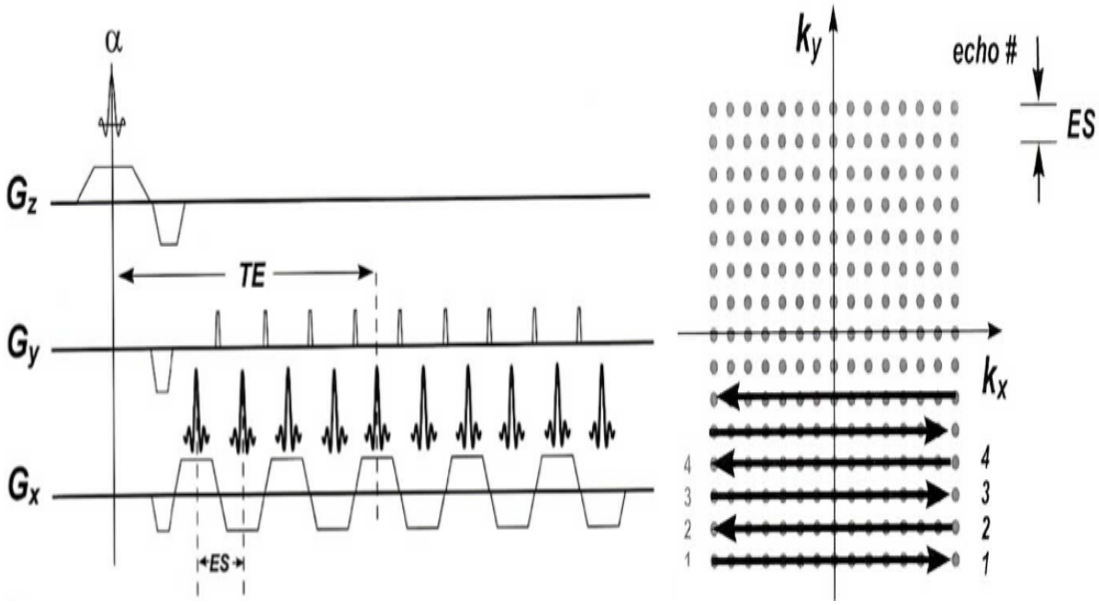

Figure 1-22 [2] (left)Timing diagram of GE-EPI. (right) k-space trajectory due to blipping of phase-encoding gradient; ES is echo spacing (*Reprinted with permission from publisher*).

In a single-shot GE-EPI (gradient-echo echo planar imaging) pulse sequence the scan time for a single slice is limited by T2* decay (on the order of 100 msec). This is due to the fact that a single RF excitation pulse is used to acquire the data for each slice. Moreover, the time required for a single-shot GE-EPI (*T*) sequence is related to the echo sampling period (time between two

successive echoes), *ESP*, the number of k-space lines, N_y, and the number of excitations (*NEX*) by:

$$T = (ESP)(N_y)(NEX)$$ **Equation 1-35**

Although EPI based pulse sequences may have some drawbacks that include, potential phase error, increased potential of tissue heating due to the rapid on/off switching of gradients, and diamagnetic susceptibility effects which may result in increasing phase error, it has many advantages. These advantages include less than 100 msec in scan time can be achieved using EPI sequences, cardiac and respiratory motion are diminished, and allows for study of organ function (i.e. brain) rather just mere anatomy.

1.7 References

[1] A. W. S. Scott A. Huettel, Gregory McCarthy, *Functional Magnetic Resonance Imaging*. Sunderland: Sinauer Associates, 2004.

[2] M. A. Bernstein*, et al.*, *Handbook of MRI Pulse Sequences*. Burlington,MA: Elsevier Academic Press, 2004.

[3] D. McRobbie*, et al.*, *MRI: From Picture to Proton*. Cambridge,UK: Cambridge University Press, 2005.

[4] J. T. Bushberg*, et al.*, *The Essential Physics of Medical Imaging*. Philadelphia,PA: Lippincott Williams & Wilkins, 2002.

[5] J. Detre and J. Wang, "Technical aspects and utility of fMRI using BOLD and ASL.," *Clin Neurophysiol,* vol. 113, pp. 621-34, May 2002.

[6] D. J. Heeger and D. Ress, "What does fMRI tell us about neuronal activity?," *Nature Reviews Neuroscience,* vol. 3, pp. 142-151, 2002.

[7] R. H. Hashemi*, et al.*, *MRI: The Basics*. Philadelphia, PA: Lippincott Williams & Wilkins, 2004.

[8] A. Dale and R. Buckner, "Selective averaging of individual trials using fMRI," *Human Brain Mapping,* vol. 5, pp. 329-340, 1997.

[9] L. Davachi, "FMRI Experimental Design."

[10] E. J. Amaro and G. Barker, "Study design in fMRI: basic principles.," *Brain Cogn,* vol. 60, pp. 220-32, Apr 2006.

[11] M. McKeown*, et al.*, "Deterministic and stochastic features of fMRI data: implications for analysis of event-related experiments.," *J Neurosci Methods,* vol. 118, pp. 103-13, Aug 2002.

[12] J. Mattson and M. Simon, *The Pioneers of NMR and Magnetic Resonance in Medicine: The Story of MRI*. New York: Dean Books, 1996.

[13] R. Damadian, "Tumor detection by nuclear magnetic resonance.," *Science,* vol. 171, pp. 1151-3, Mar 1971.

[14] S. Ogawa and T. Lee, "Magnetic resonance imaging of blood vessels at high fields: in vivo and in vitro measurements and image simulation.," *Magn Reson Med,* vol. 16, pp. 9-18, Oct 1990.

[15] S. Ogawa*, et al.*, "Brain magnetic resonance imaging with contrast dependent on blood oxygenation.," *Proc Natl Acad Sci U S A,* vol. 87, pp. 9868-72, Dec 1990.

[16] S. Ogawa*, et al.*, "Functional brain mapping by blood oxygenation level-dependent contrast magnetic resonance imaging. A comparison of signal characteristics with a biophysical model.," *Biophys J,* vol. 64, pp. 803-12, Mar 1993.

[17] K. Kwong*, et al.*, "Dynamic magnetic resonance imaging of human brain activity during primary sensory stimulation.," *Proc Natl Acad Sci U S A,* vol. 89, pp. 5675-9, Jun 1992.

[18] P. Bandettini*, et al.*, "Time course EPI of human brain function during task activation.," *Magn Reson Med,* vol. 25, pp. 390-7, Jun 1992.

[19] R. Buxton, *Introduction to Functional Magnetic Resonance Imaging: Principles and Techniques*. Cambridge, UK: Cambridge University Press, 2002.
[20] E. M. Haacke*, et al.*, *Magnetic Resonance Imaging: Physical Principles and Sequence Design*. Canada: John Wiley & Sons, Inc., 1999.
[21] R. N. Bracewell, *The Fourier Transform and its Applications*. London: McGraw Hill, 1986.
[22] A. Schmitt*, et al.*, *Echo-Planar Imaging: Theory, Technique and Application*. New York: Springer-Verlag Berlin Hiedelberg, 1998.
[23] W. Edelstein*, et al.*, "Spin warp NMR imaging and applications to human whole-body imaging.," *Phys Med Biol,* vol. 25, pp. 751-6, Jul 1980.
[24] P. Mansfield and F. Ranallo, "Medical Imaging by NMR," *Br J Radiol,* vol. 50, pp. 188-194, 1977.
[25] P. Mansfield, "Mutli-planar image formation using NMR spin echoes," *J Phys,* vol. C10, pp. L55-L58, 1977.
[26] D. Twieg, "The k-trajectory formulation of the NMR imaging process with applications in analysis and synthesis of imaging methods.," *Med Phys,* vol. 10, pp. 610-21, 1983 Sep-Oct 1983.
[27] D. Malonek and A. Grinvald, "Interactions between electrical activity and cortical microcirculation revealed by imaging spectroscopy: implications for functional brain mapping.," *Science,* vol. 272, pp. 551-4, Apr 1996.
[28] P. Magistretti*, et al.*, "Energy on demand.," *Science,* vol. 283, pp. 496-7, Jan 1999.
[29] D. Chawla*, et al.*, "The physiological basis of attentional modulation in extrastriate visual areas," *Nature Neuroscience,* vol. 2, pp. 671-676, 1999.
[30] D. Donaldson*, et al.*, "Dissociating state and item components of recognition memory using fMRI.," *Neuroimage,* vol. 13, pp. 129-42, Jan 2001.
[31] R. Savoy, "Experimental design in brain activation MRI: cautionary tales.," *Brain Res Bull,* vol. 67, pp. 361-7, Nov 2005.
[32] J. T. A. Karl J. Friston, Stefan J. Kiebel, Thomas E. Nichols, William D. Penny, *Statistical Parametric Mapping: The Analysis of Functional Brain Images*. London: Academic Press, 2007.
[33] I. Vanzetta and A. Grinvald, "Increased cortical oxidative metabolism due to sensory stimulation: implications for functional brain imaging.," *Science,* vol. 286, pp. 1555-8, Nov 1999.

Chapter 2: Introduction to Functional Magnetic Resonance Imaging

2.1 Biophysics of Brain Activation

Brain function or activation can be measured and studied through direct or indirect techniques that allow for assessment and measurement of electrical, magnetic, metabolic, and hemodynamic changes that are temporally and spatially associated with neuronal activity. With regards to the brain, activation is when membrane polarity changes are experienced by a single or a group of neurons in the brain. In such an activity, noticeable increase in neuronal metabolism occurs due to energy requirement and neurotransmitter synthesis by the neuron(s). These variations have accompanied changes in blood volume, blood flow, and blood oxygenation.

In 1936, the Nobel laureate Linus Pauling and his student Charles Coryell discovered that the magnetic susceptibility of hemoglobin differed depending upon whether or not it was bound to oxygen. They showed that oxygenated hemoglobin is diamagnetic; that is, it has zero magnetic moment and no unpaired electrons, while deoxygenated hemoglobin has more significant magnetic moment due to the unpaired electrons, and thus, is paramagnetic. Moreover, the difference in susceptibility between 100% oxygenated hemoglobin and 0% oxygenated hemoglobin (100% deoxygenated hemoglobin) is 0.18×10^{-6} . As it turns out, this difference is enough to detect brain activity in fMRI.

As can be inferred from our previous discussion, an introduction of a magnetic susceptible matter into a magnetic field causes faster spin dephasing. Therefore, in the case of fMRI, this results in a faster T2*/T2 decay of the

transverse magnetization. Because of the magnetic susceptibility of deoxygenated hemoglobin, MRI pulse sequences sensitive to T2* (i.e. single shot GE-EPI) are used to detect the contrast between oxygenated and deoxygenated blood. Such a pulse sequence would measure more MR signal where blood is highly oxygenated and less MR signal where blood is less oxygenated (more deoxygenated). It is also worth noting that T1 relaxation is not affected by blood oxygenation levels (see Figure 2-1).

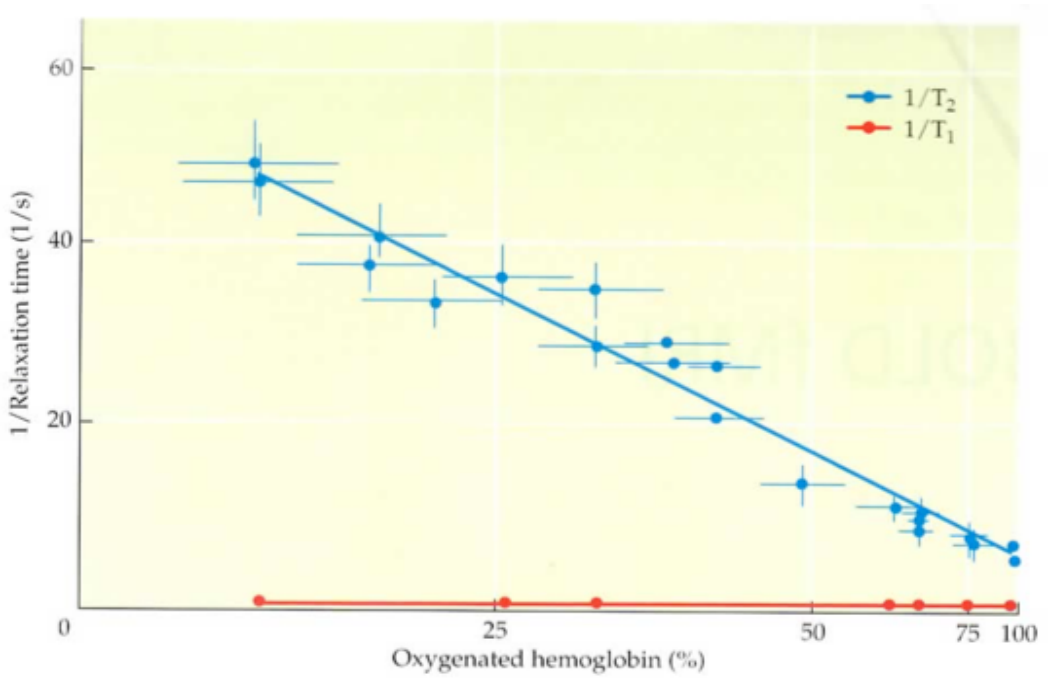

Figure 2-1[1] Effects of blood oxygenation levels on relaxation constants (blue: 1/T2, red: 1/T1). Note that as the percent of oxygenated level (x-axis) increases, 1/T2 and therefore 1/T2* decreases, and 1/T1 is not affected by blood oxygenation (*Reprinted with permission from publisher*).

It was not until the 1990s, however, when brain blood oxygenation level effects on MRI signal was shown. In 1990, Seiji Ogawa, a research scientist at Bell Laboratories, and his colleagues hypothesized that manipulation of blood oxygenation levels would affect the manifestation of blood vessels in a T2*-weighted MRI image.

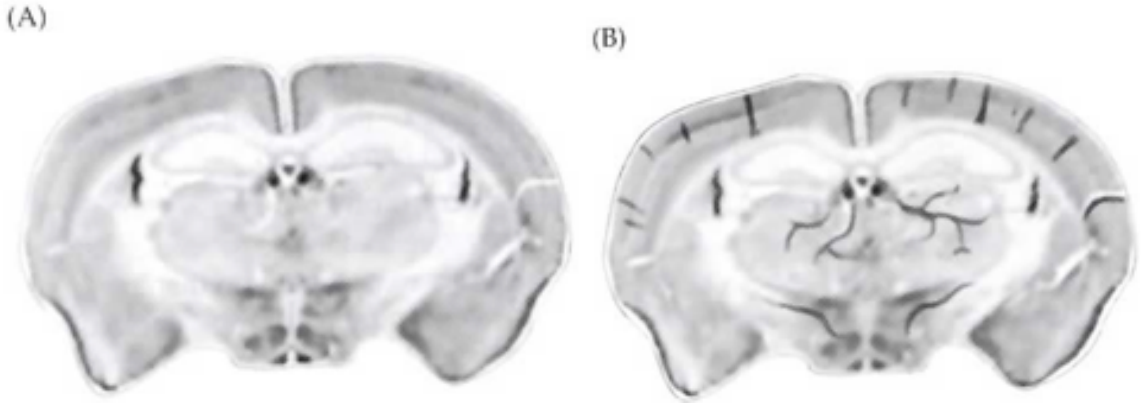

Figure 2-2[1] A schematic illustration of blood oxygenation level dependent (BOLD) contrast in a rat's brain. (A) T2* image during which the rat breathed pure oxygen, which shows uniformity across the brain. (B) more lines representing signal loss in this T2* image; representing signal loss. These lines indicated areas of higher levels of deoxygenated (paramagnetic) hemoglobin (*Reprinted with permission from publisher*).

To test their hypothesis, Ogawa and colleagues scanned anesthetized rats and varied the oxygen that the animals breathed in (Figure 2-2). When the rats breathed in 100% oxygen or 100% carbon monoxide, T2* sensitive GE sequences provided images of brains that showed anatomical contrast but very few blood vessels (Figure 2-2A). On the other hand, when these rodents breathed normal air which contains 21% oxygen, dark lines emerged in the T2* image of the brain (Figure 2-2B). Furthermore, when the oxygen content was further dropped to 0%, these lines became more prominent. Therefore, Ogawa and his colleagues concluded in this pioneering work that these thin lines were a result of local magnetic field distortions on GE images due to the presence of paramagnetic deoxygenated hemoglobin in blood vessels, and thus, provide a measure and representation of magnetic susceptibility effects generated by

deoxygenated hemoglobin. This phenomena came to be called blood oxygenation level dependent (BOLD) contrast, and could enable measurement of functional changes in the brain.

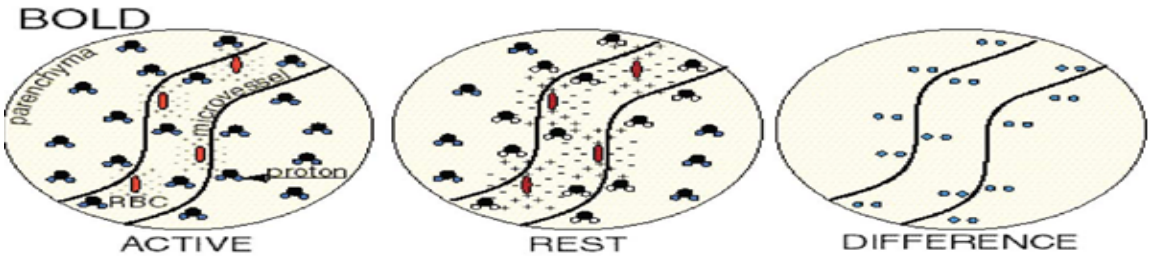

Figure 2-3[2] BOLD contrast as it pertains to the brain. Each circle is a schematic that contains parenchyma, red blood cells in a micro-vessel, and protons in the distributed hydrogen atoms from water. (Active) is a depiction of the active state of a given region in the brain; where there is more oxygenated hemoglobin than deoxygenated hemoglobin. (Rest) is when that same brain region is in a rest state, thus, abundance of paramagnetic deoxygenated blood is present. The (Difference) is the contrast that allows for detection of brain activity (*Reprinted with permission from publisher*).

Figure 2-3 illustrates the fundamental BOLD signal used in fMRI. In a magnetic field, these hydrogen atoms absorb energy that is applied at the characteristic frequency (i.e. larmor frequency). The hydrogen atoms then emit energy until they gradually return (or grow back) to the equilibrium state. This energy in the form of T2* decay varies from the active state and the rest state (Figure 2-3). Because of the abundance of diamagnetic oxygenated hemoglobin in red blood cells transported to the functioning brain region, image intensity is not severely affected. On the other hand, paramagnetic deoxygenated hemoglobin during the rest state severely decreases the image intensity. This difference (Figure 2-3) is what allows for the study of neuronal activity in the brain.

The hemodynamic response model posits that neuronal activity or stimulation causes an initial increase in oxygen consumption due to increased metabolic demand. This, in turn, increases the concentration of deoxygenated hemoglobin in red blood cells, while decreasing the concentration of red blood cells containing oxygenated hemoglobin. The neuronal activity also triggers, after a ~2s delay, a significant increase of blood flow containing oxygenated-hemoglobin red blood cells. This increase in blood flow is proportional to an increase in glucose consumption at the site of neuronal activity. However, neuronal activity results in oversupply of oxygenated blood that is delivered to the activity site. Moreover, the increase in blood flow results in vasodilatation of the veins and venules resulting in and increase of venous blood volume which is mostly deoxygnetated hemoglobin. In fact, the BOLD contrast is related to cerebral blood volume (CBV), and cerebral blood flow (CBF) by

$$\frac{\Delta BOLD}{BOLD_0} \cong M\left(1-\left(\frac{CBV}{CBV_0}\right)\left(\frac{CBF}{CBF_0}\right)^{-\beta}\right);$$

$$\beta: 1 \le \beta \le 2 \ (empirically\ set\ at\ 1.5)$$

$$M = TE \bullet R_2^* |_{dHb_0};$$

$$TE: echo\ time$$

$$R_2^* |_{dHb_0}: transverse\ relaxation\ rate\ with\ zero\ hemoglobin$$

Equation 2-1

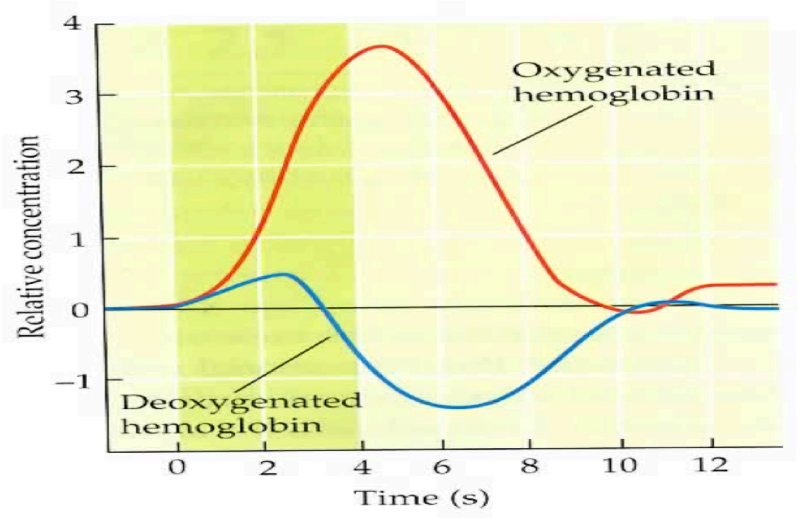

Figure 2-4[1] Illustration of relative concentration fluctuations and duration of oxygenated and deoxygenated hemoglobin following neuronal activity (*Reprinted with permission from publisher*).

At the onset of neuronal activity deoxygenated hemoglobin concentration rapidly increases and peaks at ~2s (Figure 2-4). Then it declines to a minimum value at ~6s. This is while oxygenated hemoglobin relative concentration starts to increase soon after the onset of activity and peaks around 6 seconds with a slow decline to ~10s (Figure 2-4). This hemodynamic model has been based on repeated empirical tests that relied on separate measurements of blood flow, volume, and oxygenation. Of particular importance has been what is termed the initial dip, which is a dip in the relative concentration of oxygenated hemoglobin during the increase of relative concentration of deoxygenated hemoglobin. However, the initial dip is still highly controversial in fMRI, because it has not always been detected.

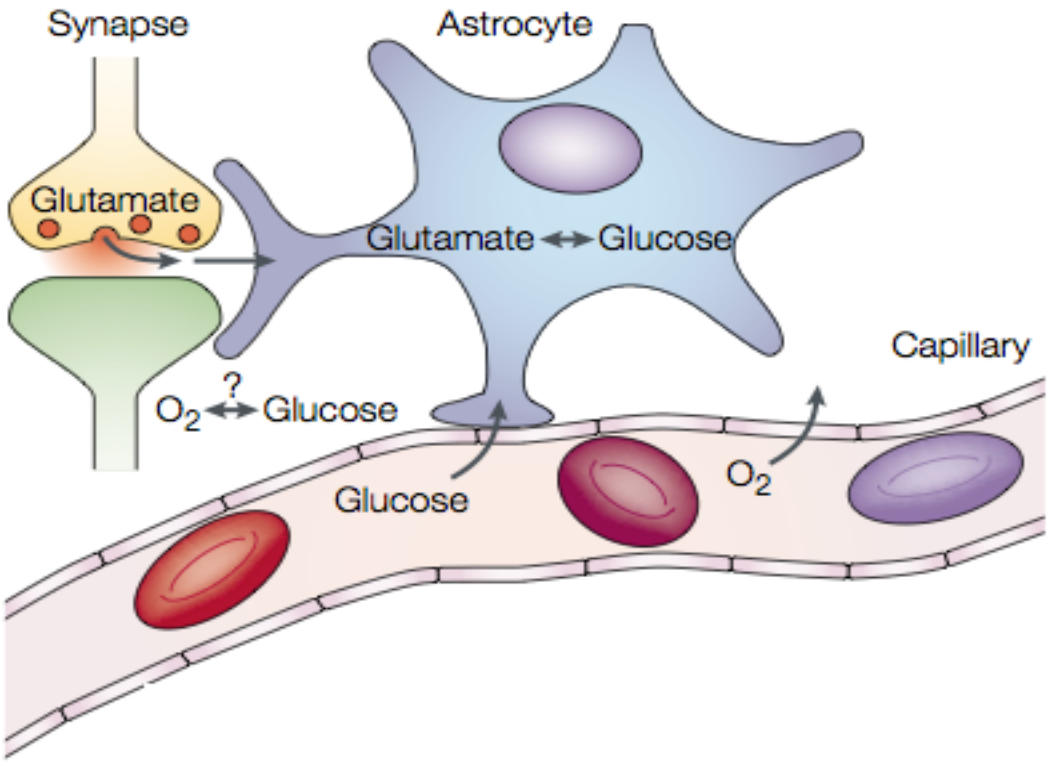

Figure 2-5[3] Depiction of two theories of cerebral metabolism; The first one entails anaerobic glycolysis (non-oxidative glucose metabolism) in the astrocyte, while the second theory posits increased blood flow is to supply neurons with required oxygen (aerobic metabolism), and any anaerobic metabolism in the astrocyte requires non-substantial energy and is not the primary reason for increased blood flow to region of neuronal activity (*Reprinted with permission from publisher*).

Two research groups (Magistretti, Pellerin et. al. and Shulman, Rothman et al.) independently posited that stimulated neurons are in close cooperation with anaerobic glycolysis (non-oxidative glucose metabolism) in the neighboring astrocyte. Astrocytes, which are glial cells, wrap around neurons and capillaries, and among other tasks, form a chemical communication link between blood vessels and neurons. Among other tasks, astrocytes help maintain homeostasis, and according to this model is the site where anaerobic metabolism takes place that leads to increased blood flow to the site of neuronal activity.

The anaerobic metabolism model postulates that when glutamate is released from the synapse, following a change in neuronal membrane voltage (neuronal activity), it is then swiftly transported into an adjacent astrocyte (Figure 2-5). Blood flow is then increased by the neuronal activity to supply glucose which is used to recycle the glutamate to glutamine in the astrocyte. The glucose that is attained from fresh oxygenated capillary blood goes through the process of anaerobic glycolysis which produces adenosine triphosphate (ATP) and lactate. The ATP is used to convert glutamate to glutamine, and the glutamine is then recycled back into the neuron(s). This is while lactate is released in the extracellular space. In this model, the increase in blood flow carrying fresh oxygenated hemoglobin has been proposed to deliver the amount of glucose needed by the astrocyte(s) with no regards to blood oxygenation. This explains the mismatch between cerebral metabolic rate of glucose (CMR_{glu}), cerebral metabolic rate of oxygen ($CMRO_2$), and cerebral blood flow (*CBF*). This is whereby $CMR_{glu} >> CMRO_2$ when *CBF* is increased, and thus, excessive amounts of oxygenated hemoglobin remains in the capillaries even after adjacent neuronal activity.

An alternative view to the anaerobic model posits that the response of increased CBF serves to deliver the level of oxygen required by the neurons (Figure 2-5). According to this view the mismatch between oxygen consumption (i.e. $CMRO_2$) and CBF is due to diffusion properties. Because of oxygen extraction from blood (via passive diffusion) is less efficient at higher levels of flow rate, a disproportionally considerable increase in blood flow is required for a

small change in oxygen metabolism (aerobic metabolism). Moreover, this model conceives that oxygen consumption increases with neuronal activity, though to a much lesser extent than does blood flow, and that most of the energy is used by the neurons and the energy usage is highly dependent on neuronal activity (i.e. firing rate); whereas only a small percentage of energy is used for neurotransmitter recycling (i.e. glutamate) by the astrocytes. Finally, this model assumes that in-built stores of glycogen is used to provide the required energy for astrocytes during neuronal activity. Therefore this posits that there is no need for increased glucose delivery during increased blood flow, which provides an oversupply of oxygenated hemoglobin to the site of neuronal activity.

2.2 Temporal and Spatial Association of Brain Activation

Neuronal activity associated with brain function (i.e. cognition, motor, and visual processes) occurs in both space and time. Therefore in-order to investigate such brain processes, both spatial and temporal aspects must be considered; specifically: spatial and temporal resolution. In fMRI, spatial resolution is given by voxel dimensions that allow for distinguishing variability in the image across space. On the other hand, temporal resolution allows for detecting variability in a given spatial resolution across time.

The spatial resolution of an fMRI experiment is dependent on three parameters that all affect the voxel size: field of view (FOV), matrix size and slice thickness. The FOV and matrix size determine the in-plane or within slice resolution, while the slice thickness provides the third dimension (through-plane) resolution. The FOV describes the size of the imaging volume in a given slice

and is expressed in centimeters. The matrix size determines how many voxels are in a given FOV. Figure 2-6 illustrates the relation ship between FOV and matrix size. Matrices used in

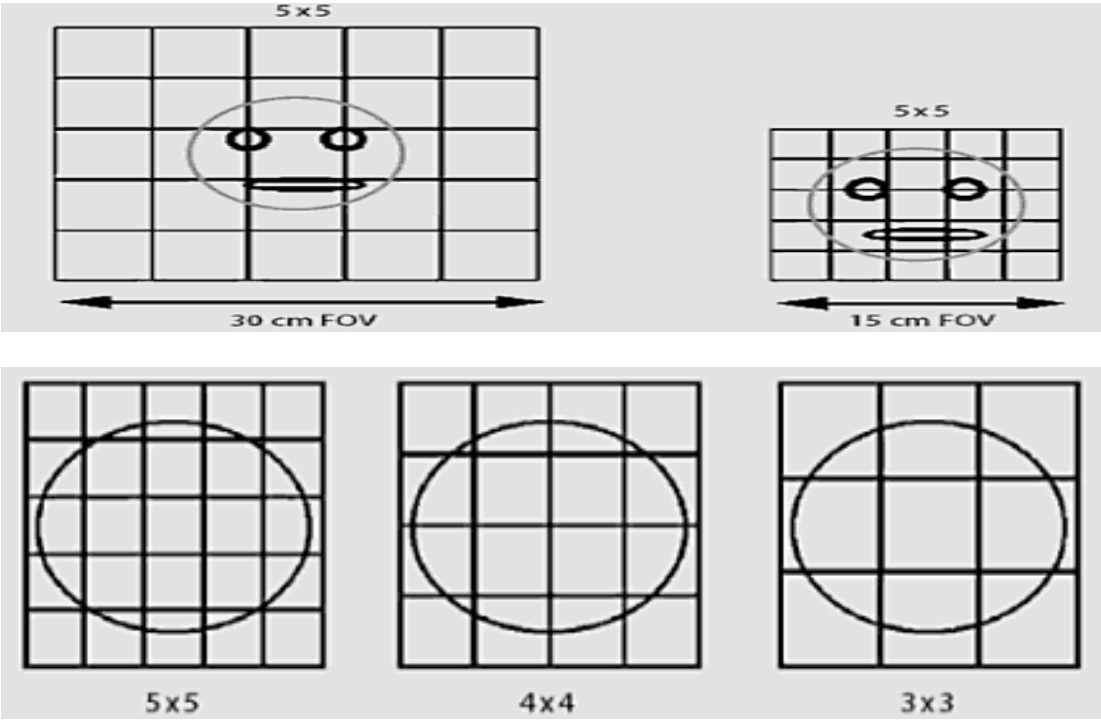

Figure 2-6 [4] The top row is an illustration where FOV is changed while the matrix size is held constant. The bottom row shows the effect of holding the FOV constant while changing the matrix size (*Reprinted with permission from publisher*).

fMRI are generally either 64, 128, or 256, which provide good resolution. On the other hand, slice thickness is generally the same or larger than the in-plane voxel size. It is when slice thickness is equal to the in-plane resolution, the voxels are cubic and are called isotropic.

Given this relationship between voxel size and resolution, it would almost sound intuitive: that the smaller the voxel size; the better the images. However, this postulation is not always true in MRI, especially in fMRI. There are two

primary challenges for such a postulation: Decreasing voxel size would lead to 1) reduced signal to noise ratio (SNR), and 2) increased acquisition time.

With regards to the first challenge, SNR and voxel size are linearly related. So if the voxels' size is reduced so is SNR. Likewise, if the voxel size increases so will the signal, and thus, SNR. The noise will not matter at this point because it is white noise, which covers a spectrum of frequencies and is uncorrelated from different measurements. To the contrary, the scanning time and voxel size are inversely related. In that, decreasing either the in-plane resolution and/or the through-plane resolution will increase scanning time. For instance, doubling the size of the matrix in a gradient echo (GE) sequence can double or even quadruple acquisition time. Such an increase in time may often affect temporal resolution and therefore detecting brain activity, because the BOLD response may occur at a faster rate. Therefore, in optimizing an fMRI imaging protocol, the researcher must consider such an inverse relationship between spatial and temporal resolution.

Recalling from our previous discussion; the fMRI BOLD hemodynamic response has a period ~10-15s. This is though the duration of neuronal activity is on the order of milliseconds. Therefore, BOLD fMRI is an indirect measure of neuronal activity that is dependent on changes in the vascular system. Furthermore, lowering TR provides a better estimate of the neuronal activity, which in turn improves inferences of regional or global brain activity. Because the BOLD response evolves over ~10-15s, a sampling rate of the BOLD signal 1-3s is sufficient resolution in general for many fMRI experiments. Although shorter

TRs may provide improved temporal resolution, they also have disadvantages. In that, very short TRs may not allow enough magnetization relaxation (less MR signal), and short repetition times (TR) affect spatial coverage (less slices). Moreover, temporal resolution can be improved by optimizing the experimental design of the stimuli that is often specific to the experimental question.

2.3 Experimental Design

As with other experiments, fMRI experiments manipulate one or more variables, then measure and evaluate any dependent outcomes or variables. For that, a strict organization for the experiment must be designed, developed, and implemented; This is what is termed experimental design. A well designed experiment will ultimately answer a proposed question, rule out alternative explanations for the data, and minimize any associated costs. Although a plethora of books and research articles have been written on fMRI experimental design, we provide a brief overview of some of the basic concepts and methods in fMRI experimental design.

A crucial part of fMRI experimental design is optimization of the fMRI stimuli. There are three broad categories of fMRI stimuli design; blocked design, event-related design, and mixed design. There are inter- and intra-design optimization schemes that depend on the question asked for a given fMRI experiment.

Block Design

This design was the first fMRI stimuli design introduced after the discovery of fMRI in the 1990s. During the early 1990s, the magnitude of the BOLD change

as a result of neuronal activity was still little understood. Therefore, researchers adopted block intervals of stimuli in an attempt to evoke enough BOLD response for measurement. It is by far the simplest design, and is still used to this day to answer fMRI experimental questions. An fMRI blocked design constitutes of partitioning the stimuli into blocks, whereby each condition is presented for an extended time period (Figure 2-7).

Figure 2-7 The top row illustrates a simple block design, where the fMRI experiment has two tasks (A and B). Note that each stimuli block (i.e. TaskA and TaskB) contains multiple individual stimuli of the same task/category. A rest condition can be inserted between the stimuli (bottom row) so to provide a baseline for BOLD response and/or provide activity that is independent of the fMRI task or stimuli.

Blocked design (Figure 2-7) is powerful in detecting significant BOLD activity within a voxel. The longer the block length (i.e. ~20-40s), the larger the BOLD contrast between stimuli and baseline. Therefore providing maximal variability between different blocks in the stimuli. In contrast, sufficiently short blocks (i.e <10s) will reduce the amplification of BOLD response because the hemodynamic response does not fully recover to baseline (recall that the hemodynamic response takes ~10-15s). Furthermore, there should be as many as possible repetitions of all blocks within the stimuli paradigm. This is in order to provide enough transitions to minimize any task-frequency noise.

Although block designs are very good at detecting brain activity within a given voxel, they are relatively insensitive to the hemodynamic response and

measuring the pattern of change over time in any given voxel. This drawback can be understood by superposition of the hemodynamic response (Figure 2-8). Since in each stimuli block more than one trial of the same task is presented, the hemodynamic response for these trials sum up across the whole block.

Figure 2-8 illustrates a simple example with three trials. In that, it is evident that with three trials, block design is unable to estimate what the hemodynamic response looks like.

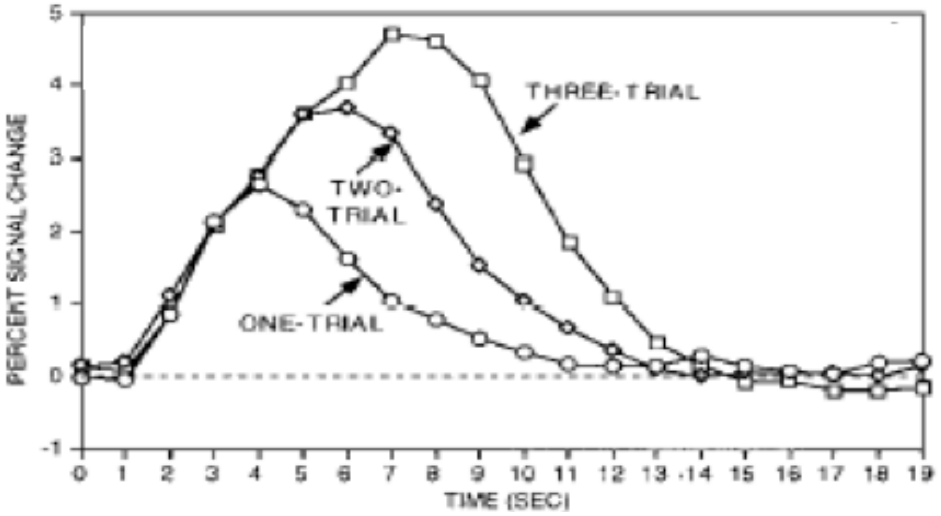

Figure 2-8 [5] Illustration of insensitivity of block design to hemodynamic response (*Reprinted with permission from publisher*).

In summary, although block design has poor estimation and is insensitive to the shape of the hemodynamic response, it non-the-less has excellent detection power and is very useful for examination and testing of BOLD state changes (Figure 2-9).

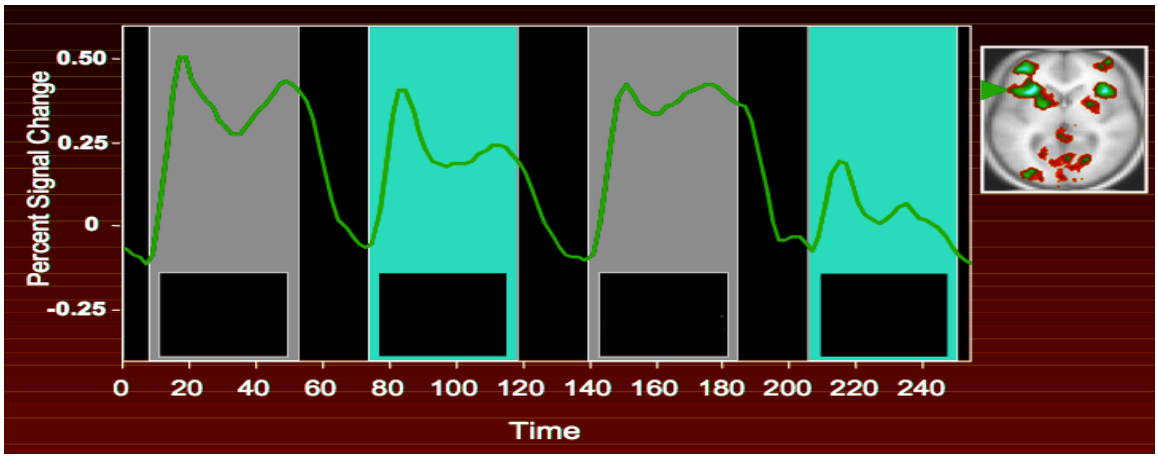

Figure 2-9 Illustration of block design and associated brain activity. The gray and yellow columns represent two different tasks, and the red line time series is the BOLD signal. This BOLD response was evident in the activated voxels in the brain; provided in the top right corner of the figure (*Derived from L. Davachi's lecture notes* [6]*)*.

Event-Related Design

The second major class of fMRI experimental designs is the event-related designs. In an event-related design (ERD); the presentation of discrete stimuli trials occurs for a short duration whereby the order and timing of these trials may be randomized. These, often, randomized tasks are separated by time intervals called inter-stimulus intervals. The inter-stimulus interval, or ISI, generally range from ~2s - 20s. This is different from blocked design in that trials from the same task or category are not presented in a consecutive manner. Furthermore, unlike block design, the stimuli trials are presented in a random order and not bounded by blocks of the same stimuli task (Figure 2-10).

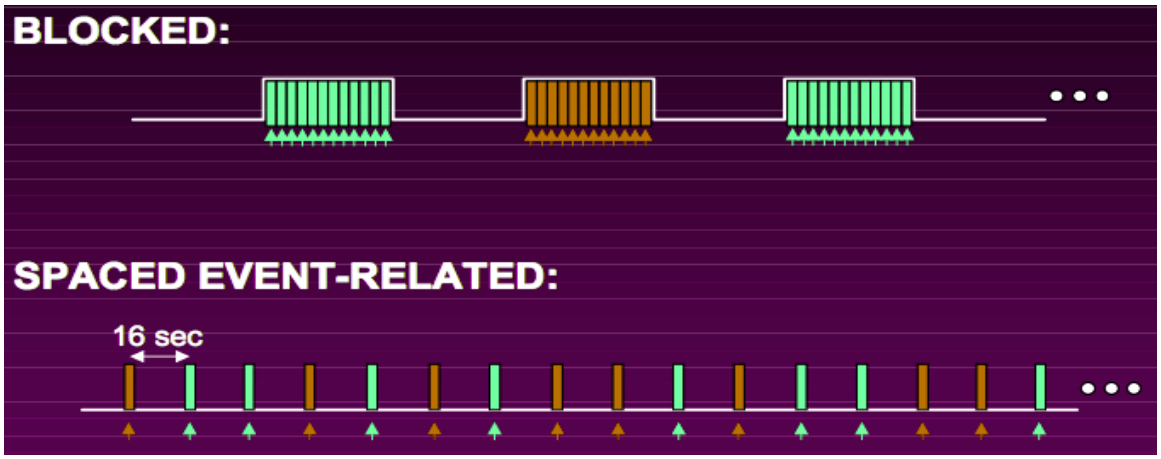

Figure 2-10 Comparison between blocked design (top row) and event-related design. The yellow and red columns represent two different tasks; whereby each column is a single presentation trial of the respective task. For event-related design, the inter-stimulus interval in this case is 16 seconds (*Derived from L. Davachi's lecture notes* [6]*)*.

In comparison to block design, ERD has reduced detection power and is sensitive to errors associated with hemodynamic response. However, HDR is very good for measuring any pattern of change over time in a given voxel, or estimation. ERD also provides a better estimate of the hemodynamic response (Figure 2-11) due to the presence of ISI.

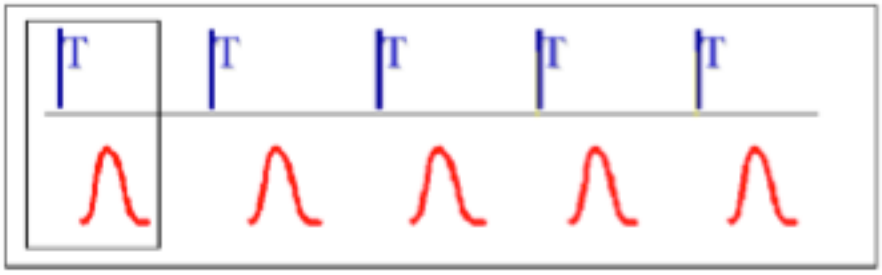

Figure 2-11[7] Event-related design stimuli (top row) and associated hemodynamic response. Note that each task's (T) hemodynamic response is detected (*Reprinted with permission from publisher*).

Mixed Design

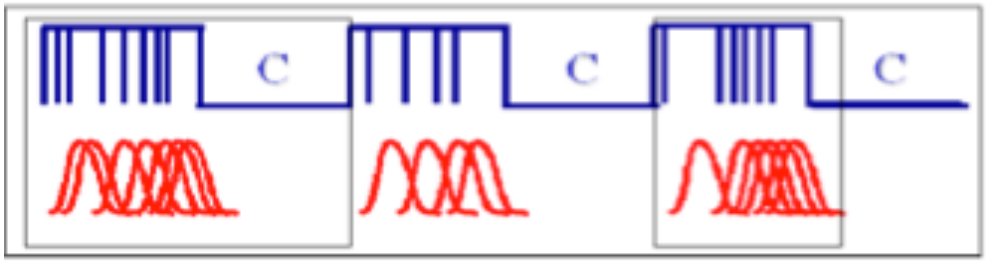

Figure 2-12 [7] Mixed Design stimuli (top row) and associated hemodynamic response (bottom row). Note that such design contains both block and event-related design (*Reprinted with permission from publisher*).

The third major group of fMRI experimental design is mixed design (Figure 2-12). As may be inferred from the name, mixed design combines both block and event-related design. Therefore, though it relies more on linearity assumptions, it non-the-less provides the best combination of detection and estimation and is capable of distinguishing transient and sustained components of brain activity. As with all designs its power is dependent on the fMRI experiment question.

2.4 FMRI Statistical Data Analysis

There are quite-a-few fMRI data analysis methods, yet there are two main approaches that are readily used. The first is a hypothesis-driven analysis method and the second is a data-driven analysis (a.k.a. exploratory) method. The former assumes an experimental stimuli paradigm and tests for a null hypothesis. A commonly used hypothesis-driven analysis method is the general linear model (GLM). On the other hand, an exploratory data analysis method does not assume any stimuli paradigm and finds time series by exploring the data; an example of such a method is independent component analysis (ICA). In this section we will

focus on the former analysis method (GLM) and the latter (ICA) will be discussed later.

The general linear model (GLM) characterizes the relationship between the experimental stimuli paradigm and the observed fMRI data. It allows for answering question such as: Is brain activity in a region of interest (ROI) different between old and young people? What brain regions are used for a specific linguistic task? To answer such questions GLM postulates that following with regards to fMRI.

$$Y = X\beta + \varepsilon; \qquad \textbf{Equation 2-2}$$

Y: is the BOLD signals (observations) and is a matrix of time points x voxels

X: is the design matrix, which is a specification of how the BOLD signal changes overtime and is often based on the stimuli paradigm design.

β: is an unknown experimental parameter that defines the contribution of each component of the design matrix to Y in order to minimize the error, ε.

ε: is the error or the difference between the observed fMRI data, *Y*, and the design matrix, *X*.

In matrix form, the GLM equation (Equation 2-2) would be:

$$\begin{pmatrix} Y_1 \\ \vdots \\ Y_j \\ \vdots \\ Y_J \end{pmatrix} = \begin{pmatrix} x_{11} \cdots x_{1l} \cdots x_{1L} \\ \vdots \ \ddots \ \vdots \ \ddots \vdots \\ x_{j1} \cdots x_{jl} \cdots x_{jL} \\ \vdots \ \ddots \ \vdots \ \ddots \vdots \\ x_{J1} \cdots x_{Jl} \cdots x_{JL} \end{pmatrix} \begin{pmatrix} \beta_1 \\ \vdots \\ \beta_l \\ \vdots \\ \beta_L \end{pmatrix} + \begin{pmatrix} \varepsilon_1 \\ \vdots \\ \varepsilon_j \\ \vdots \\ \varepsilon_J \end{pmatrix} \qquad \textbf{Equation 2-3}$$

Also, as part of the GLM data analysis, the BOLD time series are temporally filtered (i.e. whitened). Moreover, since there are more observations (*J* in Equation 2-3) than *L* parameters, residual sum-of-squares (a.k.a least-squares

errors) is employed to provide a best estimate of the data. The residual sum-of-squares is the sum of square differences between the fitted and actual data:

$$S = \sum_{j=1}^{J} \left(Y_j - x_{j1} \tilde{\beta}_1 - \cdots - x_{jL} \tilde{\beta}_L \right)^2;$$

$$\tilde{\beta} = \left[\tilde{\beta}_1, \cdots, \tilde{\beta}_L \right]^T$$

$Furthermore\ solving\ for\ \hat{\beta}:$

$\because$

$$\tilde{Y} = \left[\tilde{Y}_1, \ldots, \tilde{Y}_J \right]^T = X \tilde{\beta}$$

$$S = \sum_{j=1}^{J} e_j^{\,2} = e^T e = (Y - X\beta)^T (Y - X\beta)$$

$\therefore$ **Equation 2-4**

$$X^T Y = (X^T X)\beta$$

$\because$

$X^T X\ is\ invertable$

$X\ is\ full\ rank$

$\therefore$

$$\hat{\beta} = (X^T X)^{-1} X^T Y$$

In summary, the GLM allows for finding the β parameters which provide the best fit of the fMRI data. GLM does that by assuming a design matrix which includes the stimuli paradigm design, and treats the data as a linear summation of a number of separable factors. Therefore, GLM allows for testing a hypothesis against the fMRI data in classical parametric approach.

2.5 References

[1] A. W. S. Scott A. Huettel, Gregory McCarthy, *Functional Magnetic Resonance Imaging*. Sunderland: Sinauer Associates, 2004.

[2] J. Detre and J. Wang, "Technical aspects and utility of fMRI using BOLD and ASL.," *Clin Neurophysiol,* vol. 113, pp. 621-34, May 2002.

[3] D. J. Heeger and D. Ress, "What does fMRI tell us about neuronal activity?," *Nature Reviews Neuroscience,* vol. 3, pp. 142-151, 2002.

[4] R. H. Hashemi*, et al.*, *MRI: The Basics*. Philadelphia, PA: Lippincott Williams & Wilkins, 2004.

[5] A. Dale and R. Buckner, "Selective averaging of individual trials using fMRI," *Human Brain Mapping,* vol. 5, pp. 329-340, 1997.

[6] L. Davachi, "FMRI Experimental Design."

[7] E. J. Amaro and G. Barker, "Study design in fMRI: basic principles.," *Brain Cogn,* vol. 60, pp. 220-32, Apr 2006.

[8] M. McKeown*, et al.*, "Deterministic and stochastic features of fMRI data: implications for analysis of event-related experiments.," *J Neurosci Methods,* vol. 118, pp. 103-13, Aug 2002.

[9] J. Mattson and M. Simon, *The Pioneers of NMR and Magnetic Resonance in Medicine: The Story of MRI*. New York: Dean Books, 1996.

[10] D. McRobbie*, et al.*, *MRI: From Picture to Proton*. Cambridge,UK: Cambridge University Press, 2005.

[11] R. Damadian, "Tumor detection by nuclear magnetic resonance.," *Science,* vol. 171, pp. 1151-3, Mar 1971.

[12] S. Ogawa and T. Lee, "Magnetic resonance imaging of blood vessels at high fields: in vivo and in vitro measurements and image simulation.," *Magn Reson Med,* vol. 16, pp. 9-18, Oct 1990.

[13] S. Ogawa*, et al.*, "Brain magnetic resonance imaging with contrast dependent on blood oxygenation.," *Proc Natl Acad Sci U S A,* vol. 87, pp. 9868-72, Dec 1990.

[14] S. Ogawa*, et al.*, "Functional brain mapping by blood oxygenation level-dependent contrast magnetic resonance imaging. A comparison of signal characteristics with a biophysical model.," *Biophys J,* vol. 64, pp. 803-12, Mar 1993.

[15] K. Kwong*, et al.*, "Dynamic magnetic resonance imaging of human brain activity during primary sensory stimulation.," *Proc Natl Acad Sci U S A,* vol. 89, pp. 5675-9, Jun 1992.

[16] P. Bandettini*, et al.*, "Time course EPI of human brain function during task activation.," *Magn Reson Med,* vol. 25, pp. 390-7, Jun 1992.

[17] R. Buxton, *Introduction to Functional Magnetic Resonance Imaging: Principles and Techniques*. Cambridge, UK: Cambridge University Press, 2002.

[18] J. T. Bushberg*, et al.*, *The Essential Physics of Medical Imaging*. Philadelphia,PA: Lippincott Williams & Wilkins, 2002.

[19] M. A. Bernstein*, et al.*, *Handbook of MRI Pulse Sequences*. Burlington,MA: Elsevier Academic Press, 2004.

[20] E. M. Haacke*, et al.*, *Magnetic Resonance Imaging: Physical Principles and Sequence Design*. Canada: John Wiley & Sons, Inc., 1999.
[21] R. N. Bracewell, *The Fourier Transform and its Applications*. London: McGraw Hill, 1986.
[22] A. Schmitt*, et al.*, *Echo-Planar Imaging: Theory, Technique and Application*. New York: Springer-Verlag Berlin Hiedelberg, 1998.
[23] W. Edelstein*, et al.*, "Spin warp NMR imaging and applications to human whole-body imaging.," *Phys Med Biol,* vol. 25, pp. 751-6, Jul 1980.
[24] P. Mansfield and F. Ranallo, "Medical Imaging by NMR," *Br J Radiol,* vol. 50, pp. 188-194, 1977.
[25] P. Mansfield, "Mutli-planar image formation using NMR spin echoes," *J Phys,* vol. C10, pp. L55-L58, 1977.
[26] D. Twieg, "The k-trajectory formulation of the NMR imaging process with applications in analysis and synthesis of imaging methods.," *Med Phys,* vol. 10, pp. 610-21, 1983 Sep-Oct 1983.
[27] D. Malonek and A. Grinvald, "Interactions between electrical activity and cortical microcirculation revealed by imaging spectroscopy: implications for functional brain mapping.," *Science,* vol. 272, pp. 551-4, Apr 1996.
[28] P. Magistretti*, et al.*, "Energy on demand.," *Science,* vol. 283, pp. 496-7, Jan 1999.
[29] D. Chawla*, et al.*, "The physiological basis of attentional modulation in extrastriate visual areas," *Nature Neuroscience,* vol. 2, pp. 671-676, 1999.
[30] D. Donaldson*, et al.*, "Dissociating state and item components of recognition memory using fMRI.," *Neuroimage,* vol. 13, pp. 129-42, Jan 2001.
[31] R. Savoy, "Experimental design in brain activation MRI: cautionary tales.," *Brain Res Bull,* vol. 67, pp. 361-7, Nov 2005.
[32] J. T. A. Karl J. Friston, Stefan J. Kiebel, Thomas E. Nichols, William D. Penny, *Statistical Parametric Mapping: The Analysis of Functional Brain Images*. London: Academic Press, 2007.
[33] I. Vanzetta and A. Grinvald, "Increased cortical oxidative metabolism due to sensory stimulation: implications for functional brain imaging.," *Science,* vol. 286, pp. 1555-8, Nov 1999.

Chapter 3: Particulars of Semitic Languages: Hebrew and Arabic

3.1 Reading in Hebrew Orthography

There is a general consensus that Hebrew Orthography is alphabetical, having a typical phoneme-grapheme relationship between phonemes and letters. Its, nonetheless, a mainly consonantal orthography which reflects its fundamental Semitic roots [1] [2]. As such, modern Hebrew employs two variants of the same orthography; vowelized and non-vowelized. The vowelized version, which represents both vowel diacritics and consonants, is considered shallow and transparent. As such, this variant of orthography provides precise phonological information about the respective Hebrew word. The five vowels (a,e,i,o,u) are represented by 9 diacritical marks. Each modern Hebrew vowel has at least two, and in some cases three corresponding written signs. Diacritical marks are also used to distinguish between stop and spirant forms of the letters B, K, and P [2, 3].

The other variant of orthographic representation in Hebrew is one without diacritics (no vowelization). This version of orthography represents all consonantal letters with no nikud (vowel diacritical marks). Non-vowelized orthography may be referred to as “unpointed orthography” or orthography without diacritical marks. Both terms suggest an orthography with no disambiguating marks (i.e. nikud). Unpointed Hebrew text is considered to be deep and opaque orthography. In fact, unpointed Hebrew looses a significant part of the graphemic information necessary for efficient grapheme-to-phoneme

conversion. As such, unvowelized text may represent a particular burden for readers with insufficient internalized phonological knowledge [2, 4, 5].

Despite the phonological under-representation of nonvowelized Hebrew (no nikud), it is the default version of written Hebrew used across literacy activities, even in school texts beyond 4th grade [2, 6]. Diacritics, including vowel diacritics, are in fact gradually removed from textbooks in school beginning at the second grade level, and are completely omitted beyond 4th Grade. Due to this, researchers have become increasingly interested in the role that diacritics play and their functional status in reading Hebrew[7] and other semitic texts.

Some studies on the effectiveness of diacritics have shown that reading pointed (i.e. with diacritics/vowelized) single words is faster than reading unpointed (i.e. no diacritics/non-vowelized) words; however, if such words are presented in context, the effectiveness of diacritics diminishes [2, 8, 9]. Additional studies conducted with competent Hebrew readers and children at different stages of schooling have provided significant proof that participants' processing of Hebrew words is influenced by the presence or absence of diacritics [7]. Moreover, there is evidence that pointed Hebrew results in quantitative and qualitative enhancement in isolated word recognition [7, 10-12].

Ravid (1996) performed experiments on reading with nikud marks in children, adolescents and adults [13]. The subject pool consisted of 75 Hebrew speaking first graders, fourth graders and college students. This study showed that adult readers had mastery of the orthographic system in the presence or absence of nikud (diacritical marks). First graders read vowelized words more

accurately and with more self-repair than fourth graders. These results indicate that

novice readers pay close attention to the diacritical marks and are incapable of accessing lexical semantics through addressed reading (direct orthographic retrieval of phonological forms) [2, 13]. These results were further supported in a 2001 study by Ravid and Shlesinger [3], where it was shown that adult and experienced readers can elicit phonological information from diacritical marks unlike grade schoolers who cannot elicit this information [14, 15].

Although there are many studies that show diacritics play a major role in word recognition, there is also evidence that indicates otherwise. Using lexical and categorical decision paradigms, some researchers have found that the presence or absence of diacritics has no impact on word processing [7, 16-19]. The minimal effects of diacritics found on word recognition are pronounced in low-frequency words [20, 21]. Moreover, the enhancing effect of diacritics in Hebrew exhibited when reading text aloud disappears when in silent reading tasks [7, 22-25].

Given that Miller (2004) [7] concludes that even though omission of vowel diacritics significantly diminishes the amount of a word's phonological information, in fact it may not have detrimental effects on reading comprehension in Hebrew [7]. Moreover, literate Hebrew users discard nikud in many cases and they are averse to using them, and that nikud may be an essential tool for novice readers, but interfere with normal processing of Hebrew words at late, more advanced, stages of Hebrew text reading [2, 4, 13, 14].

Evidence for diacritic vowelization playing a facilitative role for word recognition does exist [26, 27]. This role has also been shown to be dependent on learning stage and age [24]. These results as well as others[28, 29] provide further evidence that the role and effects of diacritics still remain inconclusive.

3.2 Reading in Arabic Orthography

The Arabic alphabet has 28 letters, all of which are consonants with three long vowels. Letters are divided according to the basic letter shapes, with dots differentiating those of the same shapes, i.e. : ب-b , ت-t, ث-th; 15 letters have dots; 10 of which have one dot, three with two dots and two have three dots. Also, Arabic letters have more than one written form, depending on the letter's location in a word. Nevertheless, the essential shape of the letter is maintained [28, 30].

In addition, Arabic orthography has diacritical marks that contribute to reading of Arabic. They can be seen as short vowels: ـَ /a, ـِ /e, ـُ /u, and ـ٥ (sukoon) to indicate silent sounds, and ـّ (shadda) to indicate stressed syllables.

Only beginning readers and poor readers are provided with vowelized texts; mainly for teaching purposes. Skilled and adult readers are expected to read texts without short vowels. In daily reading, such as newspapers and most texts from third grade level on, the diacritics that denote short vowels and stressed syllables are omitted; these latter texts are said to be "unvowelized.". Vowelized Arabic is a shallow orthography, having highly regular sound-symbol

relationships, whereas unvowelized Arabic is considered a deep orthography, due to the opaque relationship between the letters and the phonemes and morphemes they represent. Reading accuracy in unvowelized Arabic requires accessing the underlying vowelized form of the word according to the grammatical role of the word within sentence, therefore, reading of unvowelized text requires great reliance on the context to attribute accurate semantic meaning to each word[28].

Arabic Language Developmental Awareness

A phoneme is the smallest speech sound unit in a language that often influences meaning [31]. Phonemic awareness (PA) is the ability to reflect on and manipulate the speech sounds of one's language. As such, PA is a key ability that supports phonics skills development. Furthermore, PA skill plays a crucial role in the development of word recognition skills. General phonological awareness for rhyme, word boundaries and syllables is usually gained in the preschool years and serves as a good predictor of basic word recognition skills in school. Kindergarten and first grade awareness of phonemes per se has been shown to be highly predictive of second and third grade word decoding accuracy and fluency[32].

Phonemic awareness is often taught to children at early stages of learning to read. In phonemic awareness instruction, children are introduced to the unique sounds of the letters in alphabetic languages (i.e. English, Arabic) with no emphasis on the syllables. For example, although the word "smart" has only one syllable, it has five unique characters each with a unique sound; /s/ /m/ /a/ /r/ /t/.

In English, it has been shown that students who acquire such skills at early stages of schooling (i.e. Kindergarten) become better readers and are more likely to be successful in school [33].

Robust phonemic awareness skills give rise to correct grapheme-phoneme decoding of words in isolation and in discourse. In other words phonemic awareness provides the ability to provide correct correspondence between the fundamental linguistic unit (grapheme) and phoneme. Such an ability is crucial to proper language reading ability development in most alphabetic orthographies [33, 34]. In fact several research studies [35-37] studies have demonstrated that word-level reading deficits are highly correlated with deficits in phonemic awareness [38].

Another important ability that is crucial for proper reading abilities is morpheme awareness. Morpheme awareness is the capacity to attribute semantic meaning to the smallest linguistic units that hold such meaning (e.g., root words, affixes, infixes). Since languages such as Arabic and English represent both phonology and morphology, awareness of both these levels of language structure is necessary for successful reading and spelling. There is evidence that some children and adolescents with spelling and reading problems show a deficit in morpheme awareness while showing normal results for phonemic awareness tasks. Furthermore, morpheme awareness has been shown to be imperative for successful reading and spelling in children and adolescents [38].

The relationships between phonemes and graphemes and their orthographic counterparts are introduced in early grade school in all languages. In European languages like English, the representations for phonemes and morphemes remain orthographically stable from early grade school through adulthood. This is not true for Semitic languages such as Arabic.

What sets Arabic (and Hebrew) apart from other languages (i.e. English) is what may be called “diacritics awareness.” Children gain morpheme and phonemic awareness using diacritics. In early stages of Arabic language acquisition, children are taught how to read and write using diacritics. However, as the children grow up, the diacritics are not provided in most texts, and reading and writing is expected to be done without diacritics. Adults and good readers are expected to assign correct diacritics while reading non-vowelized texts, according to context. Also, writing is done with no diacritics. It is up to the adult reader-writer to assign these un-ambiguating marks, diacritics, to attain accurate semantic meaning of the words and sentences.

3.3 References

[1] F. Coulmas, *The writing systems of the world*. Oxford,UK: Blackwell, 1989.

[2] D. Ravid, "Hebrew Orthography and Literacy," in *Handbook of Orthography and Literacy*, R. Joshi and P. Aaraon, Eds., Mahwah, New Jersey: Lawrence Erlbaum Associates, Inc., 2006, pp. 339-364.

[3] D. Ravid and Y. Shlesinger, "Vowel reduction in Modern Hebrew:Traces of the past and current variation," *Folia Linguistica,* vol. 35, pp. 371-397, 2001.

[4] D. Ravid, "Internal structure on new-word formation devices in Modern Hebrew," *Folia Linguistica,* vol. 24, pp. 289-346, 1990.

[5] O. R. Schwarzwald and D. Cohen-Gross, "The frequent nominal patterns in Hebrew," in *Contemporary Journalistic Hebrew*, M. Horwitz, Ed., Tel Aviv: Mofet Institute, Reches, 2000.

[6] D. L. Share and I. Levin, "Learning to read and write in Hebrew," in *Learning to read and write*, M. Harris and G. Hatano, Eds., Cambridge, U.K.: Cambridge University Press, 1999, pp. 89-111.

[7] P. Miller, "The importance of vowel diacritics for reading in Hebrew: What can be learned from readers with prelingual deafness?," *Reading and Writing: An Interdisciplinary Journal,* 2004.

[8] A. Koriat, "Reading without vowels: Lexical access in Hebrew," in *Reading without vowels: Lexical access in Hebrew*. vol. 10, H. Bouma and D. G. Bouwhuis, Eds., Hillsdale,NJ: Lawrence Erlbaum Associates, 1985, pp. 227-242.

[9] D. Navon and Y. Shimron, "Reading Hebrew: How necessary is the graphemic representation of vowels ?," in *Orthographies and reading: Perspectives from cognitive psychology, neuropsychology, and linguistics*, L. Henderson, Ed., London: Lawrence Erlbaum Associates, 1984.

[10] D. Navon and J. Shimron, "Does word naming involve grapheme-to-phoneme translation?," *Journal of Verbal Learning and Verbal Behavior,* vol. 20, 1981.

[11] A. Koriat, "Reading without vowels: Lexical access in Hebrew," in *Attention and performance X: Control of Language processes (pp. 227-242)*, H. Bauma and D. G. Bouwhius, Eds., Hillsdale, NJ: Earlbaum, 1984, pp. 227-242.

[12] R. Frost, "Prelexical and postlexical strategies in reading: Evidence from a deep and a shallow orthography," *Journal of Experimental Psychology: Learning, Memory and Cognition,* vol. 20, pp. 116-129, 1994.

[13] D. Ravid, "Accessing the mental lexicon: Evidence from incompatibility between representation of spoken and written morphology," *Linguistics,* vol. 34, pp. 1219-1249, 1996.

[14] D. Ravid and E. Kubi, "What is a spelling error? The discrepancy between perception and reality," *The dynamics of scripts: A multidisciplinary approach,* vol. 22, pp. 87-98, 2003.

[15] D. Ravid, "A developmental perspective on root perception in Hebrew and Palestinian Arabic," in *The processing and acquisition of root-based morphology*, Y. Shimron, Ed., Amsterdam: Benjamins, 2003, pp. 293-319.
[16] D. Navon and J. Shimron, "Source and function of phonological code in processing written Hebrew," in *Final Report to the U.S.-Israeli Binational Foundation*, Haifa: University of Haifa, 1985.
[17] A. Koriat, "Laterlization effects in reading pointed and unpointed hebrew," *British Journal of Psychology,* vol. 76, pp. 161-173, 1985a.
[18] R. Frost, "Phonological computation and missing vowels: Mapping lexical involvement in reading," *Journal of Experimental Psychology: Learning, Memory, and Cognition,* vol. 21, pp. 398-408, 1995.
[19] P. Miller, "Communication mode and the processing of printed words: Evidence from readers with prelingually acquired deafness," *Journal of Deaf Studies and Deaf Education,* vol. 7, pp. 312-329, 2002.
[20] A. Koriat, "Lexical access for low- and high-frequency words in Hebrew," *Memory & Cognition,* vol. 13, pp. 37-44, 1985b.
[21] R. Frost, "Prelexical and postlexical strategies in reading: evidence from a deep and a shallow orthography.," *J Exp Psychol Learn Mem Cogn,* vol. 20, pp. 116-29, Jan 1994.
[22] R. Even, "Phonological computation and missing vowels: Mapping lexical involvement in reading," *Journal of Experimental Psychology: Learning, Memory, and Cognition,* vol. 21, pp. 398-408, 1995.
[23] J. Shimron and T. Sivan, "Reading proficiency and orthography: Evidence from Hebrew and English," *Language and Learning,* vol. 44, pp. 5-27, 1994.
[24] J. Shimron, "The role of vowel signs in Hebrew: Beyond word recognition," *Reading and Writing: An Interdisciplinary Journal,* vol. 11, pp. 301-319, 1999.
[25] A. Nachmani-Ronen, "The contribution of diacritics to Hebrew reading comprehension among beginning readers," Unpublished MA thesis, University of Haifa, 2000.
[26] R. Frost and S. Bentin, "Reading consonants and guessing vowels: Visual word recognition in Hebrew orthography," in *Orthography, phonology, morphology, and meaning. Advances in psychology*. vol. 94, R. F. &*, et al.*, Eds., Amsterdam,Netherlands: North- Holland, 1992, pp. 27-44.
[27] S. Bentin and R. Frost, "Processing lexical ambiguity and visual word recognition in adeep orthography," *Memory and Cognition,* vol. 15, pp. 13-23, 1987.
[28] S. Abu-Rabia, "The role of vowels in reading Semitic scripts: Data from Arabic and Hebrew," vol. 14: Reading and Writing: An Interdisciplinary Journal, 2001.
[29] S. Abu-Rabia, "The role of morphology and short vowelization in reading Arabic among normal and dyslexic readers in grades 3, 6, 9, and 12.," *J Psycholinguist Res,* vol. 36, pp. 89-106, Mar 2007.
[30] F. M. A. El-Minem, "Elm Al Sarf (Arabic)." Jerusalem: Al-Taufik Press, 1987.

[31] S. International. (2010). *SIL International*. Available: http://www.sil.org/linguistics/GlossaryOfLinguisticTerms/WhatIsAPhoneme.htm

[32] M. Myrna, "Helping Children Learn "Phonemic" and "Graphemic" Awarness.," in *The Riggs Institute*, 2000.

[33] M. J. Snowling, "The development of grapheme-phoneme correspondence in normal and dyslexic readers," *Journal of Experimental Child Psychology,* vol. 29, pp. 294-305, 1980.

[34] S. Liddell and R. Johnson, "American Sign Language: The Phonological Base," *Sign Language Studies,* vol. 64, pp. 195-277, 1989.

[35] R. K. Wagner and J. K. Torgesen, "The nature of phonological processing and its causal role in the acquisition of reading skills," *Psychological Bulletin,* vol. 101, pp. 192-212, 1987.

[36] K. Stanovich and D. Bauer, "Experiments on the spelling-to-sound regularity effect in word recognition," *Memory & Cognition,* vol. 6, pp. 410-415, 1978.

[37] S. A. Brady and D. P. Shankweiler, Eds., *The role of working memory in reading disability* (Cross-age consistency in phonological processing. Hillsdale,NJ: Lawrence Erlbaum Associates, 1991.

[38] L. B. Feldman, *Morphological Aspects of Language Processing*. New Jersey: Lawrence Earlbaum Associates, Inc., 1995.

Chapter 4: Language and the Brain

4.1 Neuronal Correlates of Language

In the last century, understanding of how the human brain analyzes and produces language has been shaped by aphasiology. Aphasiology is the study of language impairment stemming from brain damage. Research in this field has helped to define basic neural correlates and cerebral regions associated with language. Two loosely defined and fairly large areas, Broca's and Wernicke's, play major roles in language production and comprehension [1].

However, recent developments in functional neuroimaging have provided researchers further insight into specific language processing regions [2]. Through functional neuroimaging methods and neurolinguistic paradigms, researchers have been able to examine these brain regions of interest that are involved in language. A bulk of such research has gone into investigating neural correlates of phonological and semantic processing in both normal and impaired human subjects[1, 3].

One of the main neuronal correlates of language and reading is the region where the brain processes phonology. "Phonology" refers the sound system used in a given language. The ability to associate sounds with letters (decoding) is based on phonological processing in the brain. There is overwhelming evidence that phonological awareness is a fundamental and significant cognitive capacity required for decoding [4]. Phonological processing has been studied with paradigms that require normal or impaired human subjects to perceive and evaluate the sound structure of words and letters. Such paradigms most often

rely on rhyme judgments, in which participants have to indicate if two words rhyme or not, for example *weigh* and *way*. This methodology is a standard method for investigating the neural basis of phonological processing. Using this method, research has shown activation of similar brain regions, specifically the left Broca's area [5], the angular gyrus (BA 39) [6], and Wernick's area [5, 7, 8] Figure 4-1 .

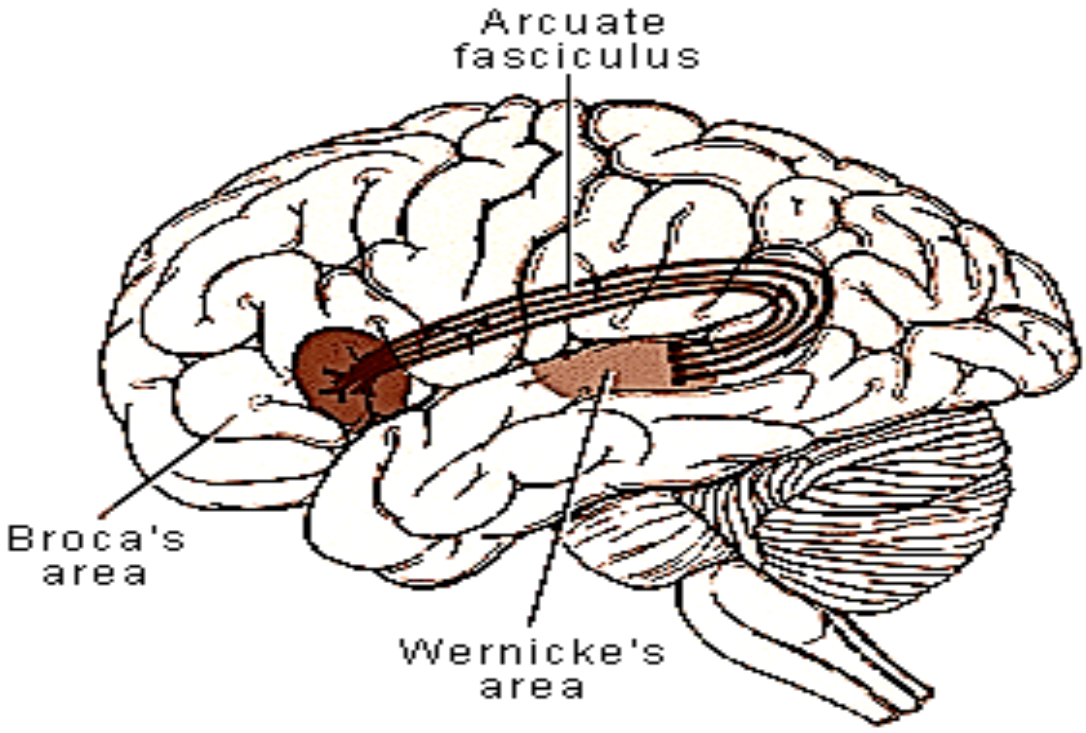

Figure 4-1 Language areas: Broca's and Wernicke's areas connected through the arcuate fasciculus axonal fibers.

Another aspect of language processing concerns semantics. Semantic processing engages brain regions responsible for deriving conceptual knowledge about the referents of words and their associated concepts [9]. Investigators of semantic processing have often used judgment paradigms, in which subjects are

asked to decide whether or not a written word is a part of a given semantic category; for example, vehicle or food ? [8-10]. Such categorization semantic tasks have been associated with activations in the left medial frontal gyrus (LMFG) [11], right and left superior [8, 9, 11], middle [8, 9], and inferior [8, 9, 12] [11] temporal gyri as well as the left inferior frontal lobe [9, 11].

Semantic processing has two categories: explicit and implicit. Explicit semantic processing involves the semantic processing of clear statements and/or readily observable objects. Explicit semantic processing allows for meaning retrieval for explicitly written words or sentences. For example fluent reading of an English newspaper in which functional attributes of letters and words, and in which semantic relatedness of nouns and verbs are explicit, requires explicit semantic processing. Through the use of explicit semantic paradigms and functional neuroimaging, researchers have consistently shown that activation of the left inferior frontal gyrus is associated with explicit semantic tasks [11].

On the other hand, implicit semantic processing is by definition the semantic processing of objects, words, or statements that are not plainly expressed. Implicit semantic processing occurs when subjects are required to make a decision on the lexical status of a word based on its context and the semantics of other words in a statement or sentence [13]. Such implicit tasks have shown activation in the right and left superior temporal gyri (STG) and left inferior temporal gyrus (LITG) [11, 14, 15].

Some functional neuroimaging research with healthy monolinguals [2] and bilinguals has addressed the question of whether languages vary in terms of their

brain activation patterns based on similarities vs. differences between the linguistic structure. While some neuroimaging research studies provide evidence for common regions [16-18], others have shown different cortical activations for different languages [7, 19, 20]. The bulk of neuroimaging research has been done with languages related to Latin, for example French and English, with a few studies exploring Japanese and Chinese. On the other hand, there appears to be no published functional neuroimaging work that has investigated the neuronal correlates of elements of word-level reading in Arabic.

4.2 Neuronal Correlates and Orthographic Depth

The Orthographic Depth Hypothesis (ODH) is the basic claim that word recognition processes are influenced by the depth of the orthography. Orthographic depth and its effects on reading strategies has been a controversial topic for the past two decades [21-23]. The controversy has surrounded whether or not differences in orthographic depth lead to differences in the processing of printed words. In fact, it is theorized that processing is subconsciously affected by the orthography and not obvious to the reader. It is worth noting that the ODH is not a developmental theory, rather it was developed to account for inter-language and intra-language skilled reading [22, 24].

The ODH is mainly concerned with the phonological process required for reading a word or group of words. In a shallow orthography, readers have the complete information needed to decode, or determine grapheme-phoneme pronunciation. Therefore, the phonological configuration or form can be prelexically determined. In contrast, the more ambiguous relation of subwords,

subword components, segments and phonemes in deep orthographies prevents the prelexical determination of the phonological form of a word. In this case the reader is required to have swift access to the mental lexicon to determine the phonological form of the word. Therefore, in deep orthography, phonology is determined lexically, as opposed to prelexical determination [22]. Furthermore, studies have investigated the psychological requirements of orthographic depth and its influences on word recognition and found that in general the phonology of shallow orthography is generated directly from print and therefore precedes lexical recognition [22, 23].

As mentioned earlier, shallow and deep orthography invoke implicit processing that is subconsciously determined during the reading process. It is known that languages such as Italian and Spanish have shallow orthographies, while English and French are considered to have deep orthographic characteristics. Therefore mappings between grapheme, phoneme, and word sounds are more opaque in English and French than, for example, in Italian and Spanish [25].

Research on the effects of culture on the brain [17, 25] have investigated the neuronal correlates of shallow and deep European orthographies. It was found that for the deeper orthographies greater activation was evident in the left posterior inferior temporal region and in the anterior inferior frontal gyrus, this was more particular when reading non-words. Also, the same study showed that when reading both words and non-words, readers of the shallow orthography

showed greater activations at the junction between the left superior temporal gyrus and the inferior cortex (planum temporale) [25].

4.3 References

[1] M. Vigneau*, et al.*, "Meta-analyzing left hemisphere language areas: phonology, semantics, and sentence processing.," *Neuroimage,* vol. 30, pp. 1414-32, May 2006.

[2] H. Chen*, et al.*, "Optical imaging of phonological processing in two distinct orthographies.," *Exp Brain Res,* vol. 184, pp. 427-33, Jan 2008.

[3] S. Petersen*, et al.*, "Positron emission tomographic studies of the cortical anatomy of single-word processing.," *Nature,* vol. 331, pp. 585-9, Feb 1988.

[4] S. Abu-Rabia, "The role of morphology and short vowelization in reading Arabic among normal and dyslexic readers in grades 3, 6, 9, and 12.," *J Psycholinguist Res,* vol. 36, pp. 89-106, Mar 2007.

[5] A. Herbster*, et al.*, "Regional cerebral blood flow during word and nonword reading.," *Hum Brain Mapp,* vol. 5, pp. 84-92, 1997.

[6] J. Démonet*, et al.*, "Differential activation of right and left posterior sylvian regions by semantic and phonological tasks: a positron-emission tomography study in normal human subjects.," *Neurosci Lett,* vol. 182, pp. 25-8, Nov 1994.

[7] W. Tham*, et al.*, "Phonological processing in Chinese-English bilingual biscriptals: an fMRI study.," *Neuroimage,* vol. 28, pp. 579-87, Nov 2005.

[8] J. Démonet*, et al.*, "The anatomy of phonological and semantic processing in normal subjects.," *Brain,* vol. 115 (Pt 6), pp. 1753-68, Dec 1992.

[9] J. Joseph*, et al.*, "The neurobiological basis of reading.," *J Learn Disabil,* vol. 34, pp. 566-79, 2001 Nov-Dec 2001.

[10] S. Kapur*, et al.*, "The role of the left prefrontal cortex in verbal processing: semantic processing or willed action?," *Neuroreport,* vol. 5, pp. 2193-6, Oct 1994.

[11] I. Ruff*, et al.*, "Recruitment of anterior and posterior structures in lexical-semantic processing: An fMRI study comparing implicit and explicit tasks.," *Brain Lang,* vol. 105, pp. 41-9, Apr 2008.

[12] K. Pugh*, et al.*, "Cerebral organization of component processes in reading.," *Brain,* vol. 119 (Pt 4), pp. 1221-38, Aug 1996.

[13] D. Thuy*, et al.*, "Implicit and explicit processing of kanji and kana words and non-words studied with fMRI.," *Neuroimage,* vol. 23, pp. 878-89, Nov 2004.

[14] C. Price*, et al.*, "Demonstrating the implicit processing of visually presented words and pseudowords.," *Cereb Cortex,* vol. 6, pp. 62-70, 1996 Jan-Feb 1996.

[15] N. Brunswick*, et al.*, "Explicit and implicit processing of words and pseudowords by adult developmental dyslexics: A search for Wernicke's Wortschatz?," *Brain,* vol. 122 (Pt 10), pp. 1901-17, Oct 1999.

[16] M. Chee*, et al.*, "Processing of visually presented sentences in Mandarin and English studied with fMRI.," *Neuron,* vol. 23, pp. 127-37, May 1999.

[17] E. Paulesu*, et al.*, "Dyslexia: cultural diversity and biological unity.," *Science,* vol. 291, pp. 2165-7, 2001 Mar 2001.

[18] J. Illes*, et al.*, "Convergent cortical representation of semantic processing in bilinguals.," *Brain Lang,* vol. 70, pp. 347-63, Dec 1999.
[19] S. Dehaene*, et al.*, "Anatomical variability in the cortical representation of first and second language.," *Neuroreport,* vol. 8, pp. 3809-15, Dec 1997.
[20] O. Yetkin*, et al.*, "Use of functional MR to map language in multilingual volunteers.," *AJNR Am J Neuroradiol,* vol. 17, pp. 473-7, Mar 1996.
[21] D. Besner*, et al.*, "Basic processes in reading: computation of abstract letter identities.," *Can J Psychol,* vol. 38, pp. 126-34, Mar 1984.
[22] R. Frost, "Prelexical and postlexical strategies in reading: evidence from a deep and a shallow orthography.," *J Exp Psychol Learn Mem Cogn,* vol. 20, pp. 116-29, Jan 1994.
[23] R. Frost*, et al.*, "Strategies for visual word recognition and orthographical depth: a multilingual comparison.," *J Exp Psychol Hum Percept Perform,* vol. 13, pp. 104-15, Feb 1987.
[24] M. Caravolas. (2009, 11 January). *Orthographic Depth Hypothesis*. Available: http://www.childrenofthecode.org/interviews/caravolas.htm#The_Orthographic_Depth_Hypothesis
[25] E. Paulesu*, et al.*, "A cultural effect on brain function.," *Nat Neurosci,* vol. 3, pp. 91-6, Jan 2000.

Chapter 5: Vowel Diacritics and Single Word Recognition in Adult Readers of Arabic

5.1 Motivation and Background

Research on literacy in English is disproportionate relative to other major world languages [1]. Arabic literacy, in particular, has been grossly under-researched compared to English, despite the presence of more than two hundred million native speakers of Arabic in the world. Studies of major features of the Arabic writing system, such as vowel diacritics, are needed to provide a more complete understanding of processes involved in Arabic reading.

There are two main types of written Arabic: Classical, and Modern Standard Arabic (MSA). Classical Arabic is present in Qur'anic texts and early classical literature, while MSA is universal to Arabic media, newspapers, lectures, and non-archaic literature. Classical Arabic and MSA use the same consonantal orthography, or *abjad,* and, with the exception of the Qur-an, vowel diacritics are absent from most texts encountered in everyday reading including contemporary literature, newspapers, books, and articles [2, 3].

The Arabic alphabet comprises 28 letters, most of which are consonants. The long vowels /a/, /e/, and /u/ are represented by the letters *'alif*, *ya'*, and '*waw',* while short vowels /a/, / ʊ / and / ɛ / are represented by the diacritics "ً ", "ٍ ", and "ٌ" (refered to as "vowelization'). Vowelized Arabic is a transparent, or shallow, orthography, having almost perfect one-to-one correspondence between grapheme and phoneme. Vowelization provides primary-level readers with additional phonological information to detect the correct meaning and pronunciation of words. Whereas diacritics are present in all educational texts

throughout Kindergarten and early elementary school, they are removed from educational texts at around Grade 3, when basic decoding skills have typically been mastered. The resulting devowelization represents a transition from a shallow, transparent orthography to one that is deep and opaque [4-7], requiring the reader to rely more heavily on the surrounding syntactic and discourse context for attributing accurate meaning and pronunciation of words [7].

Arabic is not alone with regards to the use of diacritics for vowelization. Hebrew, another Semitic language, also has a consonantal orthography that employs diacritics to denote vowels. Like in Arabic, diacritics are gradually removed from textbooks in the early to mid elementary levels. Thereafter, children and adults are expected to read Hebrew text without diacritics [8]. Text without diacritics, however, loses a significant part of the graphemic information necessary for efficient grapheme-to-phoneme conversion. Therefore, as with Arabic, devowelization may represent a burden for readers with insufficient internalized phonological knowledge [9-11].

The orthographic shift from transparency to opacity raises questions regarding the role that diacritics may play in word recognition in both mature and beginning readers. In a study of Hebrew, Ravid (1996) examined the role of diacritics in groups of Hebrew speaking first graders, fourth graders and college students. Out of the three groups, the college-level readers read with the highest accuracy and with the fewest self-corrections in both conditions (with and without diacritical marks); fourth graders' showed similar reading accuracy across the two conditions, whereas first graders read text with diacritics more accurately

than did the fourth graders. Based on these findings, Ravid concluded that beginning readers are more dependent on diacritics for accurate reading and hence pay close attention to diacritics. Consequently, they are less able to access lexical semantics when reading vowelized words [12].

Koriat (1984), too, investigated the role of diacritics in Hebrew, examining lexical decision latencies for letter strings with and without diacritics in adult Hebrew readers. The presence of diacritics resulted in no significant difference in lexical decision latencies compared to letter strings without diacritics. However, in a follow-up study , Koriat (1985b) found that diacritics facilitated adult readers' word recognition of low frequency words more than of high frequency words. Additionally, low-frequency words with no diacritics elicited more errors and required longer processing times for a correct response than did high frequency words with no diacritics [13].

Navon and Shimron (1981) employed three experiments to examine whether or not grapheme-to-phoneme rules for diacritics are applied automatically when a word pattern is encoded. Their first experiment included 36 native Hebrew-speaking adults. The stimuli consisted of 50 Hebrew words presented in isolation. Half of the words were correctly vowelized, and in the other half, diacritics were either a) absent, or b) graphemically distorted, but phonemically intact, or c) phonemically and graphemically distorted. Participants were instructed to read as quickly as possible while ignoring vowel diacritics, while latency (RT for voice onset) and accuracy were recorded by the experimenter. Participants' performance indicated that the effect of wrong

vowelization (wrong diacritical marks) was not accounted for by the absence of correct vowelization (correct diacritical marks). The participants' performance also showed that the effect of vowelization was ,also, not accounted for by the identification of a word given such absence of correct vowelization, nor did it account for the degree of difficulty of word identification [14].

In the second experiment, Navon and Shimron employed the same vowelization and misvowelization paradigm from Experiment 1 with twenty-one adults, all of whom were native Hebrew speakers. Participants were required to sort cards with letraset symbols into two categories. The first sorting task involved discrimination between vowel signs that if interchanged would produce a phonemic distortion. The second sorting task involved discrimination between vowel signs whose interchange would produce a graphemic distortion. Results showed that signs signifying the same phoneme are not more visually similar to each other than signs that signify different phonemes.

Navon and Shimron's third experiment in order to examine whether the results of experiment 1 were due to selective attention instructions. Twenty-four new adult participants who met the inclusion criteria for Experiment 1 were included. The tasks in experiment 1 were repeated but with no instructions to ignore the vowel signs. Results showed that participants were indeed disregarding the vowel signs when asked to do so. The results of the three experiments support the view that vowel signs (diacritics) facilitate word recognition, at least for isolated words [14].

Frost (1994) examined the validity of the orthographic depth hypothesis (ODH) for skilled Hebrew readers using Hebrew text in which diacritics were present (shallow orthography) or absent (deep orthography). According to the ODH, the degree by which prelexical phonologic processing is active is a function of the depth of the orthography; the prelexical processing is more active for shallow orthographies. According to the ODH, for shallow orthographies (i.e. text with diacritics) phonology plays a greater role in lexical access and retrieval than for deep orthographies (i.e. text without diacritics).

In Experiment 1, Frost (1994) compared lexical decision and naming performance for print with and without diacritics. The goal of the experiment was to examine the effects of lexical factors on naming performance in relation to lexical decision in both deep and shallow Hebrew. Native Hebrew–speaking adult participants were required to provide yes-no lexical decision on stimuli that included 40 high-frequency words, 40 low-frequency words, and 80 nonwords. Results showed that larger frequency effects were exhibited for words without diacritics compared to words with diacritics. High frequency words without diacritics showed significantly shorter RTs than low frequency words without diacritics. The results suggested that the lexical status of the stimuli affected both lexical decision and naming in words without diacritics compared to words with diacritics [15].

In another experiment in the same study, Frost investigated the ODH claim that unless processing costs are too high (i.e. in deep orthographies), the default cognitive strategy is not to access phonology from the lexicon following

visual access, but rather assemble a phonologic code for lexical access. To examine this, Frost designed stimuli where processing demands were manipulated by delaying the presentation of the diacritics relative to the presentation of the consonant letters. The participants (96 native Hebrew-speaking adults), were shown consonant letter strings first and diacritics were superimposed on the letters at different time intervals ranging from 0 ms to 300 ms from the onset of the initial letter strings. The stimuli consisted of 40 high-frequency words, 40 low-frequency words, and 80 nonwords, and the participants keyed in their response as in the first experiment. Results of this experiment suggested that adult readers were inclined to wait for the vowel marks to appear although the respective words can be named clearly using lexical phonology alone. Frost concluded that prelexical phonology is the default method for skilled readers in shallow orthography and this provides strong support for the ODH [15].

Given the results from these studies of the influence of diacritics on reading in consonantal orthographies in general, and in Arabic in particular, it is unclear how the orthographic depth hypothesis (ODH) applies to Arabic or how the presence or absence of diacritics influences speed and accuracy of Arabic word recognition. A systematic examination of the influence of diacritics in word-level reading of Arabic would provide a prerequisite step towards better understanding the role of diacritics within discourse contexts and at different reading age levels. The present study employs a lexical decision to examine adult reader's recognition of single words and orthographically matched

nonwords, both with and without diacritics, and at varying levels of word frequency.

5.2 Materials and Methods

Participants

Participants consisted of twenty undergraduate college students at Kuwait University, between 20 to 23 years of age (M= 21.7; S.D. = 0.9), with Arabic as their first language (L1). All participants were right-handed based on the Edinburgh Handedness Inventory [16], with normal hearing, normal or corrected-to-normal vision and no frank neurological or psychological problems. Additionally, all participants were screened for language, reading, and/or attention deficits based on a self-report questionnaire. Data for two of the participants had to be excluded due to technical problems during stimulus presentation,. the remaining 18 participants (10 male, 8 female) making up the final sample.

Stimuli and Experimental Design

A lexical decision task (LDT) was used for this study, which included both vowelized (diacritics present) and devowelized (diacritics absent) real word stimuli from Aralex , a lexical database for Modern Standard Arabic [17], as well as nonwords with and without diacritics. The stimuli consisted of 45 high-, 45 mid-, and 45- low frequency nouns. The frequency ranges per million words for the stimuli were: high = 215.47 – 772.33, mid = 81.73 – 200.12, and low = 1.18 – 68.58. Each real word with diacritics and its corresponding real word form without diacritics were tightly matched for frequency and length. The nonwords were

created by switching the order of consonants for each respective real word stimulus, while retaining a phonotactically plausible string sharing the same orthographic constituents (including diacritics for pairs involving vowelized forms). (See Table 5-1). Nonwords without diacritics were examined carefully to rule out any consonant string that could be inferred to be a word. A total of 540 stimuli (45 stimuli/per category for 12 stimulus categories) were randomly presented on a laptop PC using presentation software (Neurobehavioral Systems, Inc, CA). Table 5-1 below provides the stimulus categories and sample stimuli.

Stimuli subcategories	**Sample Arabic Stimuli**	**English translation**
REAL WORDS WITH DIACRITICS (RWD)		
HIGH FREQUENCY REAL WORDS WITH DIACRITICS (HFRWD)	إِنْسان	human
MID FREQUENCY REAL WORDS WITH DIACRITICS (MFRWD)	شاعِر	poet
LOW FREQUENCY REALWORDS WITH DIACRITICS (LFRWD)	كِساء	clothing
REAL WORDS WITH NO DIACRITICS (RWND)		
HIGH FREQUENCY REALWORDS NO DIACRITICS (HFRWND)	إنسان	human
MID FREQUENCY REALWORDS NO DIACRITICS (MFRWND)	شاعر	poet
LOW FREQUENCY REALWORDS NO DIACRITICS (LFRWND)	كساء	clothing
NONWORDS WITH DIACRITICS (NWD)		
HIGH FREQUENCY NONWORDS WITH	سِأنان	

DIACRITICS (HFNWD)		
MID FREQUENCY NONWORDS WITH DIACRITICS (MFNWD)	رَاشِع	
LOW FREQUENCY NONWORDS WITH DIACRITICS (LFNWD)	أَكَاس	
NONWORDS WITH NO DIACRITICS (NWND)		
HIGH FREQUENCY NONWORDS NO DIACRITICS (HFNWND)	سأنان	
MID FREQUENCY NONWORDS NO DIACRITICS (MFNWND)	راشع	
LOW FREQUENCY NONWORDS NO DIACRITICS (LFNWND)	أكاس	

Table 5-1 A list of the stimulus categories used in the study. The acronym for each stimulus category is in parentheses. The English translation of words with no diacritics is based upon the corresponding frequency matched word with diacritics.

Orthographic similarity measure (OSM) formulas (Equation 5-1, Equation 5-2) were developed based on Van Orden (1987) OSM, but with Arabic specific design and parameters. The purpose of these formulas is to measure the degree of orthographic similarity across frequency ranges (Equation 5-1) and between words and nonwords (Equation 5-2) of the same stimuli category. Since there is no standard orthographic similarity measure for Arabic, we developed one for such a purpose. Below are the formulation and quantization according to the orthographic similarity measures across frequency levels and across words and nonwords.

Stimuli words were selected and structured as follows:

1) 45 non-abstract nouns (real words) with diacritics (NWD) in each frequency range (high, mid, and low)

2) 45 non-abstract nouns (real-words) with-out diacritics (NWND) in each frequency range (high, mid, and low) that are identical to the NWD in number 1 above, but have no diacritics.
3) Both NWND and NWD have been frequency matched so that it can be argued that both the respective NWND and NWD word has the same meaning.
4) The frequency ranges are:
    a. High : 215.47 – 772.33 / million
    b. Mid : 81.73 – 200.12 / million
    c. Low : 1.18 – 68.58 /million
5) The frequency gap between high and mid frequency levels is 14.1/million
6) The frequency gap between mid and low frequency levels is 13.15/million
7) The log difference between the lowest frequency word in the high frequency range and the highest frequency word in the mid frequency range is : log(215.47) – log(200.12) = 0.032.
8) The log difference between the lowest frequency word in the mid frequency level and the highest frequency word in the lowest frequency level is : log(81.73) – log(68.58) = 0.0761
9) The log difference between the lowest frequency word in the high frequency level and the highest frequency word in the lowest frequency level is : log(200.12) – log(68.58) = 0.465
10) All NWD and NWND have been exactly matched across frequency levels except for 11 words in each frequency level. Therefore giving an

orthographic similarity measure (OSM) of 0.17. According to Equation 5-1, the OSM provides a 0 – 1 range; 0 = exact orthographic composition and 1 = extreme orthographic dissimilarity between a group of words.

$$L = \left(\frac{\begin{array}{l}[A_{1,1}(B_{1,1}+B_{1,2}+B_{1,3})+A_{1,2}(B_{1,4}+B_{1,5}+B_{1,6})+A_{1,3}(B_{1,7}+B_{1,8}+B_{1,9})]+ \\ [A_{2,1}(B_{2,1}+B_{2,2}+B_{2,3})+A_{2,2}(B_{2,4}+B_{2,5}+B_{2,6})+A_{2,3}(B_{2,7}+B_{2,8}+B_{2,9})]+\ldots[A_{i,k}(B_{i,k}+B_{i,k}+B_{i,k})+A_{i,k}(B_{i,k}+B_{i,k}+B_{i,k})+A_{i,k}(B_{i,k}+B_{i,k}+B_{i,k})]\end{array}}{(3(3(3+3+3)))(S)} \right)(0.5)+\left(\frac{S}{T}\right)(0.5)$$

Equation 5-1

Orthographic similarity measure for words across frequency (OSMWAF)

OSMWAF variables:

L = orthographic similarity measure for words across frequency levels (high, mid, low)

A = the number of categories (number of letters, number of syllables, number of diacritics) that are different of the given two words across frequency levels.

B = the difference between a given category across two words in different frequency levels. For i.e. if we take the first word from the table above and look at the high-mid level frequency cell , the difference between the number of letters would be $B_{1,1}$ and the difference between number of

syllables is $B_{1,2}$, and the difference between the number of diacritics across the respective two words in the respective two categories is $B_{1,3}$.

S = number of words that are different across frequency levels (in this case S = 11).

T = total number of words in each frequency level (In this case T = 45)

(3(3(3+3+3))) was set as the maximum allowable difference between words. Therefore, words that differ in more than three categories and differ by 3 in all the three categories (number of letters, number of syllables, and number of diacritics) are disregarded and not used in the stimuli. This is because they exceed such a set threshold.

11) The nonwords were created by switching around the consonants in the real words. For example “ganoon” is a real word, the nonword derived from this word is “nagoon”. The nonwords were check for “non-existence” in Arabic through the use of “Mokhtar ilsihaah” dictionary and Aralex. This methodology was used for all nonwords except for three words (one in each frequency level) where all possible sequence of consonants/letters resulted in a real word. Therefore an “E” vowel was added to these words to create a nonword, such a change was made to 1 word in each frequency level. This gave an OSM of .001 for orthographic similarity between all words and nonwords (See Equation 5-2).

    a. OSM for high frequency: 0.0007
    b. OSM for mid frequency: 0.002
    c. OSM for low frequency: 0.0007

Orthographic similarity measure for words and nonwords (OSMWNW):

$$V = \left(\frac{|N-R|}{N+R}\right)(0.2) + \left(\frac{|D-W|}{D+W}\right)(0.2) + (S)(0.2) + (L)(0.2) + \left(\frac{|Q-E|}{Q+E}\right)(0.2)$$

Equation 5-2

OSMWNW Variables :

V = Orthographic similarity measure each respective word and nonword combination. Note: Each word and nonword combination has a V value.

N = number of letters in the nonword

R = number of letters in the real word

D = number of diacritics in the nonword

W = number of diacritics in the real word

S = 1 or 0 ; 1 if sequence of vowels and consonants of words and nonwords are exactly the same, 0 otherwise

L = 1 or 0 ; 1 if sequence of the diacritics in the words and nonwords are exactly the same, 0 otherwise

Q = number of syllables in the real words

E = number of syllables in the nonwords

$$P = \frac{\sum V_i}{T}$$

P = Orthographic similarity measure

T = total number of words in the stimuli

Parameters used for measuring degree of orthographic similarity:

1) Number of letters
2) Number of diacritics
3) Number of syllables

Not Exactly Matched Word #	high - Mid	high - low	mid - low	sum of the rows
1	(0) (000)	(1) (010)	(1) (010)	2
2	(2) (101)	(2) (011)	(2) (110)	12
3	(1) (010)	(1) (010)	(0) (000)	2
4	(0) (000)	(1) (002)	(1) (002)	4
5	(0) (000)	(2) (101)	(2) (101)	8
6	(2) (110)	(0) (000)	(2) (110)	8
7	(0) (000)	(3) (111)	(3) (111)	18
8	(2) (011)	(0) (000)	(2) (011)	8
9	(1) (010)	(0) (000)	(1) (010)	2
10	(1) (001)	(2) (210)	(2) (211)	15
11	(2) (110)	(2) (110)	(0) (000)	8
Total				87

Table 5-2 The first column is the index number for the words that are not exactly matched across frequency levels. In the second columns, the first number in parenthesis is the number of categories that are different (i.e # of letters, # of syllables, # of diacritics) and the three numbers represent the difference between the respective levels (i.e. high, mid, low) at each respective category. The last row is the sum of the categories times the number of different categories for each respective word (i.e. equation for word # 1 : 0*(0+0+0) + 1*(0+1+0) + 1*(0+1+0) = 2). The total is the sum of all the "sum of rows."

Experimental Procedure

Prior to starting the study, participants were instructed about the experimental procedure, and then a practice run the sample stimuli not included in the test runs.. The participants were instructed to respond as quickly and as accurately as possible, pressing the letter key "K " for words and "S" for non-words. The stimuli were presented in six runs of 90 randomized word- and nonword stimuli, with each run separated by 3.5 minute break. Each stimulus was displayed for a maximum of 4 seconds, and moved to the next stimulus as

soon as the subject responded or on timing out if the subject did not respond within the time limit.

5.3 Results

Table 5-3 presents the means and standard deviations for both accuracy (number of correct responses) and reaction time (RT) across all stimulus categories.

Accuracy: A Frequency (high, mid, low) X Diacritics (present, absent) ANOVA for real words yielded a main effect for Frequency ($F=48.88$, $p=.00$). Post-hoc t-tests revealed significantly higher accuracy for both high and mid frequency words compared to low frequency words ($p<.001$). There was no main effect for Diacritics or Frequency X Diacritics interaction.

A Frequency x Diacritics ANOVA yielded neither main nor interaction effects for nonword accuracy.

Response Time (RT): Mean lexical decision times were calculated for the different stimulus categories. A Frequency (high, mid, low) x Diacritics (present, absent) ANOVA for real words revealed main effects for both Frequency ($F=4.32$, $p=.02$)and Diacritics ($f=15.31$, $p=.00$) but no interaction between them. Post-hoc t-tests found low frequency words with significantly longer lexical decision times than high and mid-frequency words ($p < .001$).

A Frequency x Diacritics ANOVA yielded no main or interaction effects for nonwords.

Letter string	Frequency	Diacritics (with/without)	Mean (RT)	SD (RT)	Mean (Accuracy)	SD (Accuracy)
Words	High Frequency	Diacritics	1.13	0.21	43.72	1.36
		No Diacritics	0.99	0.17	44.06	1.16
	Mid Frequency	Diacritics	1.17	0.22	44.11	0.96
		No Diacritics	0.96	0.15	44.61	0.50
	Low Frequency	Diacritics	1.22	0.22	40.78	2.18
		No Diacritics	1.14	0.17	41.11	2.45
Non-words	High Frequency	Diacritics	1.43	0.28	42.78	2.13
		No Diacritics	1.34	0.29	43.28	1.71
	Mid Frequency	Diacritics	1.41	0.30	42.17	2.23
		No Diacritics	1.31	0.23	42.22	1.52
	Low Frequency	Diacritics	1.44	0.26	42.33	1.28
		No Diacritics	1.36	0.26	42.50	2.55

Table 5-3 Mean reaction times and accuracy with standard deviations (SD) for all stimulus categories

5.4 Discussion and Conclusions

To date, studies of diacritics in Arabic have primarily examined the effects of vowelization in sentence or discourse-level contexts with no systematic efforts to examine vowelization in words versus nonwords, or in isolated words of varying frequencies. In addition, only a limited number of studies have examined the effect of diacritics on speed of lexical decisions. Given the paucity of research in these areas, the present study examines the role of diacritics at the single word level. Findings of the current study reveal that both frequency and diacritics play significant roles in single word recognition in adult readers. Lexical decision times were significantly faster for high frequency words and mid frequency words than for low frequency words. Additionally, real words with diacritics (RWD) took longer to recognize than real words with no diacritics (RWND). We suspect greater processing demands associated with the role of diacritics word in single word recognition in Arabic. There were, however, no frequency effects for words with vs. without diacritics.

Results from past studies of the effects of diacritics on visual word recognition have been mixed. Whereas some studies have shown that diacritics facilitate word recognition [14, 15], others have found no facilitative effects [18-20]; yet others suggest that the role of diacritics may vary as a function of reading experience, as with the fourth graders read text with diacritical marks less accurately than did first graders [21, 22]. Abu-Rabia and colleagues, too, have found diacritics to be critical in reading accuracy across a spectrum of poor and skilled readers in Arabic [3, 5, 23-25]. In the present study, however, we found a

main effect for frequency but not for diacritics in real word accuracy. Taken together with the absence of any frequency effect for words with vs without diacritics the results do not support a facilitative role of diacritics in real word recognition in this study.

Our findings suggest that, although diacritics provide for explicit grapheme-to-phoneme conversion, they slow the rate of single word recognition in Arabic. The adult reader of Arabic is accustomed to daily reading without diacritics even on the single word level; the novelty of reading single real words with diacritics may have resulted in slower word recognition. The close orthographic similarity across several of our stimulus conditions may have further added to the participants' processing load. An alternative explanation for the slowing effect of diacritics is that they may invoke grapheme-to-phoneme translation via a phonological recoding route, while recognition of words without diacritics may rely on a rough phonological representation, based simply on consonantal information, that allows for rapid initial access to multiple lexical entries and hence shorter lexical decision times. Thus, despite the phonological under-representation of real words with no diacritics, devowelization is the default version for written Arabic for adult readers, making for efficient processing of text across common literacy activities.

In conclusion, the current study provides no evidence of a facilitative role for diacritics in speed or accuracy of single word recognition in Arabic.This, study lays a foundation for future studies to provide a more complete developmental theory of the function of diacritics in Arabic reading. As stated earlier, exposure to

diacritics is limited to beginning stages of learning to read Arabic, and therefore, future studies should investigate the role of diacritics at earlier stages of reading skill development and within varying levels of linguistic context, including phrase, sentence and discourse environments. This would ultimately help us to develop a more complete understanding of reading in Arabic.

5.5 References

[1] D. L. Share, "On the Anglocentricities of current reading research and practice: the perils of overreliance on an "outlier" orthography.," *Psychol Bull,* vol. 134, pp. 584-615, Jul 2008.

[2] S. Abu-Rabia, "The role of vowels in reading Semitic scripts: Data from Arabic and Hebrew," vol. 14: Reading and Writing: An Interdisciplinary Journal, 2001.

[3] S. Abu-Rabia, "The role of morphology and short vowelization in reading Arabic among normal and dyslexic readers in grades 3, 6, 9, and 12.," *J Psycholinguist Res,* vol. 36, pp. 89-106, Mar 2007.

[4] S. Abu-Rabia, "Effects of exposure to literary Arabic on reading comprehension in a diglossic situation. ," *Reading and Writing: An Interdisciplinary Journal,* vol. 13, pp. 147-157. , 2000.

[5] S. Abu-Rabia and L. Siegel, "Reading, syntactic, orthographic, and working memory skills of bilingual Arabic-English speaking Canadian children.," *J Psycholinguist Res,* vol. 31, pp. 661-78, Nov 2002.

[6] S. Abu-Rabia and L. S. Siegel, "Reading skills in three orthographies: The case of trilingual Arabic-Hebrew-English-speaking Arab children. ," *Reading and Writing: An Interdisciplinary Journal,,* vol. 16,, pp. 611-634. , 2003.

[7] N. J. Taibah and C. W. Haynes, "Contributions of phonological processing skills to reading skills in Arabic speaking children," *Reading and Writing: An Interdisciplinary Journal,* vol. Online First, 2010.

[8] P. Miller, "The importance of vowel diacritics for reading in Hebrew: What can be learned from readers with prelingual deafness?," *Reading and Writing: An Interdisciplinary Journal,* 2004.

[9] D. Ravid, "Hebrew Orthography and Literacy," in *Handbook of Orthography and Literacy*, R. Joshi and P. Aaraon, Eds., Mahwah, New Jersey: Lawrence Erlbaum Associates, Inc., 2006, pp. 339-364.

[10] D. Ravid, "Internal structure on new-word formation devices in Modern Hebrew," *Folia Linguistica,* vol. 24, pp. 289-346, 1990.

[11] O. R. Schwarzwald and D. Cohen-Gross, "The frequent nominal patterns in Hebrew," in *Contemporary Journalistic Hebrew*, M. Horwitz, Ed., Tel Aviv: Mofet Institute, Reches, 2000.

[12] D. Ravid, "Accessing the mental lexicon: Evidence from incompatibility between representation of spoken and written morphology," *Linguistics,* vol. 34, pp. 1219-1249, 1996.

[13] A. Koriat, "Lexical access for low- and high-frequency words in Hebrew," *Memory & Cognition,* vol. 13, pp. 37-44, 1985b.

[14] D. Navon and J. Shimron, "Does word naming involve grapheme-to-phoneme translation?," *Journal of Verbal Learning and Verbal Behavior,* vol. 20, 1981.

[15] R. Frost, "Prelexical and postlexical strategies in reading: Evidence from a deep and a shallow orthography," *Journal of Experimental Psychology: Learning, Memory and Cognition,* vol. 20, pp. 116-129, 1994.

[16] R. C. Oldfield, "The assessment and analysis of handedness: The Edinburgh inventory. Neuropsychologia," *Neuropsychologia,* vol. 9, pp. 97-113, 1971.

[17] S. Boudelaa and Marslen-Wilson, "Aralex: A Lexical Database for Modern Standard Arabic," *Behaviour Research Methods,* 2009.

[18] R. Frost, "Phonological computation and missing vowels: Mapping lexical involvement in reading," *Journal of Experimental Psychology: Learning, Memory, and Cognition,* vol. 21, pp. 398-408, 1995.

[19] A. Koriat, "Laterlization effects in reading pointed and unpointed hebrew," *British Journal of Psychology,* vol. 76, pp. 161-173, 1985a.

[20] P. Miller, "Communication mode and the processing of printed words: Evidence from readers with prelingually acquired deafness," *Journal of Deaf Studies and Deaf Education,* vol. 7, pp. 312-329, 2002.

[21] D. Ravid, "A developmental perspective on root perception in Hebrew and Palestinian Arabic," in *The processing and acquisition of root-based morphology*, Y. Shimron, Ed., Amsterdam: Benjamins, 2003, pp. 293-319.

[22] D. Ravid and E. Kubi, "What is a spelling error? The discrepancy between perception and reality," *The dynamics of scripts: A multidisciplinary approach,* vol. 22, pp. 87-98, 2003.

[23] S. Abu-Rabia, "Reading in Arabic orthography: the effect of vowels and context on reading accuracy of poor and skilled native Arabic readers in reading paragraphs, sentences, and isolated words.," *J Psycholinguist Res,* vol. 26, pp. 465-82, Jul 1997.

[24] S. Abu-Rabia, "The effect of Arabic vowels on the reading comprehension of second- and sixth-grade native Arab children.," *J Psycholinguist Res,* vol. 28, pp. 93-101, Jan 1999.

[25] S. Abu-Rabia, "Reading in Arabic Orthography: Characteristics, Research Findings, and Assessment," in *Handbook of Orthography and Literacy*, R. M. Joshi and P. G. Aaron, Eds., Mahwah,New Jersey: Lawrence Erlbaum Associates, 2006.

Chapter 6: Neuronal Correlates of Diacritics in Arabic: An fMRI Study

6.1 Motivation and Background

In Arabic orthography, diacritical marks ("diacritics") are employed to represent (a) the short vowels, as in ◌َ/a/,◌ُ/u/, ◌ِ /ɛ/, (b) silent sounds, as in ◌ْ/sukoon/and (c) stressed syllables, as in ◌ّ/shadda/. However, in everyday reading materials, including newspapers and most books, the short vowels and stressed syllables are not indicated. This is because only beginning readers and poor readers require vowelized texts, which are used mainly for teaching purposes. Vowelized Arabic is a shallow, transparent orthography: sound-symbol relationships are highly predictable; in contrast, devowelized Arabic is a deep, opaque orthography. To the extent that meaningful reading in Arabic requires the retrieval of vowelized forms of words from one's lexical store, devowelized Arabic relies on context for accurate word recognition and semantic retrieval [1, 2]. In some studies, diacritics, too, have been shown to facilitate word recognition and comprehension in both good and poor Arabic readers [1, 3]. These findings raise interesting questions about the role of diacritics in Arabic reading.

In Arabic, diacritics are primarily used in teaching with introductory level learners. However, they are also included, to varying degrees, in educational texts throughout primary school, and can be found in pre-college education in grammar, language rules, and/or principles of composition courses. For the most part, the use of diacritics in all educational texts (i.e. short stories and historical texts) is limited to primary school, and for whatever length of time deemed

sufficient to learn to read without them, typically until around third grade. Thereafter, students are expected to be able to read texts without diacritics. After diacritics are dropped, readers must employ syntax, vocabulary and sometimes world knowledge in order to recognize words and to attribute correct semantic meaning to devowelized text [3-5].

In languages such as English, however, both phonemic and morphemic awareness are gained through letters only. There are no symbols employed in written English to help beginning readers to decode, that are then removed at more advanced stages of reading. This unique feature of Arabic and related Semitic orthographies such as Hebrew and Syriac sets them apart from other languages, such as English, insofar as their orthographies can change at different levels of language learning and usage. Thus, the beginning Arabic reader must master the special diacritics that are part of the orthography of the language in order to be successful in later years, as an adult reader, when faced with devowelized text.

A number of researchers have investigated the effects of diacritics in Hebrew and Arabic. Koriat (1984) examined lexical decision latencies for letter strings with and without diacritic vowelization in adult Hebrew readers. He found that there was no significant difference in lexical decision latencies for letter strings containing diacritic vowels versus letter strings with no diacritic vowels. However, in a follow-up study, he found that diacritic vowelization was more beneficial for processing of low frequency than high frequency words [6]. Other studies in Hebrew, too, have shown a facilitative effect of diacritic vowelization in

word recognition [7, 8]. In a study comparing reading with versus without diacritics in Hebrew first graders, fourth graders and college students, Ravid (1996) found that the college-level readers read with the highest accuracy and with the fewest self-corrections in both conditions (with and without diacritical marks); fourth graders' reading accuracy did not differ across the two conditions, whereas first graders read text with diacritics more accurately than the fourth graders. Ravid concluded that perhaps beginning readers pay more attention to diacritics and are less able to access lexical semantics when reading vowelized words. Research with Arabic has yielded similar findings. Abu Rabia found that vowelization through diacritics significantly facilitated word recognition among both poor and skilled Arabic readers [3], and across different age groups [9]. More recently, he has shown that diacritics also have a significant effect on comprehension in good and poor Arabic readers [2, 5], though this effect appears to be dependent on the learning stage and age of the reader [10]. Thus, the role of diacritics in reading in Arabic remains an empirical question.

Orthographic Depth and Diacritics

Orthographic depth refers to the degree to which the orthography of a language deviates from simple one-to-one sound-symbol correspondences. In Hebrew and Arabic, vowelized text using diacritics is considered a shallow orthography whereas text with no diacritics is considered to be deep orthography [1, 2, 7, 11, 12]. According to the orthographic depth hypothesis (ODH)[11, 13], the ease of word recognition is dependent on the depth of the orthography. The

ODH predicts that children learning to read a shallow orthography in which sound–symbol mappings are transparent (i.e., regular and consistent) should learn to read aloud and to spell faster than those learning a deep orthography where the pronunciation code is more opaque. Accordingly, the process of reading is affected by the orthography in ways that are not obvious to the reader. However, the ODH does not provide a developmental theory of reading; rather, it was generated to account for differences in reading skill within and between languages.[12, 14].

Insofar as diacritics are an integral part of the beginning Arabic reader's orthography, which the mature reader must then learn to do without, the role of diacritics in Arabic in relation to orthographic depth theories of the language has been a topic of interest for over a decade [5, 12, 13, 15] and is the focus of the present study.

Orthographic Depth and Neuroimaging

Neuroimaging studies comparing shallow and deep orthographies have shown differences in neural activation patterns between them [16, 17]. Specifically, for deep orthographies such as English, greater activation has been found in the left inferior temporal and inferior frontal areas, implicating both orthographic and phonological processing. This effect was most evident when participants were reading non-words. In contrast, readers of a shallow orthography (e.g., Italian) show greater activation at the junction between the left superior temporal gyrus, and the planum temporale in Wernicke's area, when

reading both words and nonwords [16], reflecting the more transparent grapheme-to-phoneme correspondences in shallow orthographies.

To the extent that word recognition involves semantic processing, studies have also shown increased involvement of inferior frontal and anterior temporal areas in word processing tasks [18-20]. Prefrontal brain areas, too, have been implicated in language tasks depending on the cognitive demands of the task [21, 22]. Fiebach and colleagues found that contrasting words with pseudowords in a lexical decision task resulted in significant bilateral activity in occipito-temporal brain areas as well as posterior left middle temporal areas (Fiebach et al, 2002). The authors also showed that the left IFG, caudate nucleus and anterior insula are involved in grapheme-to-phoneme conversion. Other studies of lexical decision have implicated similar brain areas associated with lexical retrieval and word recognition (Carreiras et al., 2007; Madden et al, 2002; Nobre et al, 1994)

A majority of the early studies in visual word recognition were carried out in English. However, English does not provide a full account of the processes involved in word recognition given the unique features of the world's different languages. The particulars of the linguistic environment and writing system must be considered. In Arabic, words without diacritics is part of the everday encounters of the average reader. Given the paucity of research with the Arabic language, especially empirical data on the effects of diacritics on both speed and accuracy of word recognition in Arabic, we aimed to investigate this question using a lexical decision task (LDT). Previous studies have examined the role of

diacritics in sentence, paragraph and discourse contexts in Arabic [1, 2]. Here, we focus on diacritics at the single-word level and use functional magnetic resonance imaging (fMRI) to better understand their role in reading in Arabic. The stimuli were specifically designed to allow direct comparisons between real words with and without diacritics in order to be able to infer the involvement , if any, of the phonological lexicon in single word recognition in Arabic, and thereby, the role of diacritics in the process. The task involved reading words and orthographically-matched non-words, with and without diacritics and incorporated both high and low frequency words to help tease out the contribution of diacritics to lexical processing and visual word recognition in Arabic. To provide a solid basis for direct comparisons, words and nonwords with and without diacritics were tightly matched orthographically. Insofar as there is ample evidence that diacritics are disambiguating marks that affect orthographic depth, as cited above, we predicted that in keeping with the Orthographic Depth Hypothesis, words with diacritics would be processed as shallow orthography and activate posterior temporal areas. In contrast, words without diacritics would activate deep orthography-related processing areas like the inferior frontal and temporal areas.

6.2 Materials and Methods

Participants

Participants consisted of eleven males, native Arabic speakers, ranging in age from 23 - 35 years (mean age = 28 yrs). All participants had completed their primary and secondary education in countries where Arabic is the primary

language. Based on the Edinburgh Handedness Inventory [23], ten of the participants were right handed, and one was ambidextrous. All the participants had normal hearing, normal or corrected-to-normal vision, and no frank neurological or psychological problems. Additionally, all participants were screened for language, reading, and attention deficits. The University of Massachusetts Medical School Institutional Review Board (IRB) approved the protocol, and informed consent was obtained from all participants.

Stimuli and Experimental Design

Stimuli consisted of real words and nonwords, both with and without diacritics (see Table 6-1). The real words were made up of an equal number of high and low frequency concrete nouns drawn from Aralex, a lexical database for Modern Standard Arabic [24]. Aralex is the only large-scale corpus currently available for Modern Standard Arabic. In the Aralex corpus only the stem words are provided with diacritics. (A stem word refers to the residual form after removing clitics and affixes). Additionally, in Arabic, the frequency of a non-diacriticized word is affected by the addition of diacritics. That is, the same word with and without diacritics may have different frequencies. Given these factors, all concrete nouns (with and without diacritics) used as stimuli were selected from the stem words, and the diacriticized and non-diacriticized forms were tightly matched for frequency. The selected word stimuli were piloted in a lexical decision task with 20 undergraduate students from Kuwait University and only those high frequency (200-700/per million) and low frequency (1-93/per million)

words with and without diacritics that were correctly recognized with at least 80% accuracy were used in the imaging study.

The non-words with and without diacritics were derived from the real words and constructed to be orthographically similar to them. An orthographic similarity measure (OSM) modeled after that of Van Orden (1987) but with Arabic specific design parameters was specifically developed to match the orthographic characteristics of the words across the two frequency levels, as well as with their nonword counterparts. As such, the OSM value can range from 0 (exactly same orthographic composition) to 1 (extreme orthographic dissimilarity; that is, no orthographic overlap). The mean OSM value in this study was below 0.17 (see Chapter 5 for formulas).

Word and nonwords were presented in a randomized order for lexical judgment. There were 46 stimuli in each of the 8 stimulus categories: High Frequency Real Words with Diacritics (HFRWD), High Frequency Real Words with no Diacritics (HFRWND), Low Frequency Real Words with Diacritics (LFRWD), Low Frequency Real Words with no Diacritics (LFRWND), High Frequency Nonwords with Diacritics (HFNWD), High Frequency Nonwords with no Diacritics (HFNWND), Low Frequency Nonwords with Diacritics (LFNWD), Low Frequency Nonwords with no Diacritics (LFNWND). Table 6-1 provides a list of the stimulus categories and sample stimuli for each category.

Full Category Name	Sample Arabic Stimuli	English translation
REAL WORDS WITH DIACRITICS (RWD)		
HIGH FREQUENCY REAL WORDS WITH DIACRITICS (HFRWD)	إِنْسان	human
LOW FREQUENCY REALWORDS WITH DIACRITICS (LFRWD)	كِساء	clothing
REAL WORDS WITH NO DIACRITICS (RWND)		
HIGH FREQUENCY REALWORDS NO DIACRITICS (HFRWND)	إنسان	human
LOW FREQUENCY REALWORDS NO DIACRITICS (LFRWND)	كساء	clothing
NONWORDS WITH DIACRITICS (NWD)		
HIGH FREQUENCY NONWORDS WITH DIACRITICS (HFNWD)	سِأْنان	
LOW FREQUENCY NONWORDS WITH DIACRITICS (LFNWD)	أَكَاس	
NONWORDS WITH NO DIACRITICS (NWND)		
HIGH FREQUENCY NONWORDS NO DIACRITICS (HFNWND)	سأنان	
LOW FREQUENCY NONWORDS NO DIACRITICS (LFNWND)	أكاس	

Table 6-1 A list of all stimulus categories (abbreviated form in parentheses) and sample stimuli. Note that the English translation for a word with no diacritics is based on the corresponding frequency matched word with diacritics.

Experimental procedure

Functional Imaging: Prior to scanning, subjects were given verbal and written instructions on the task, along with a few practice trials. Each participant was provided with a two-button response pad, and verbally instructed to press the right button if the displayed letter string on the screen was a word, and the left one if the letter string was a non-word, and to respond as quickly and as accurately as possible. During scanning, the stimuli were projected on a screen at the back of the scanner bore, which participants could see in a mirror mounted on the head coil. A total of 368 stimuli (46 stimuli/per category for 8 stimulus categories) were presented using a laptop PC running the Presentation software (Neurobehavioral Systems, Inc, CA). The stimuli were presented in 5 runs, using an event related paradigm with a fixation cross between consecutive stimuli jittered at 6 +/- 2 seconds, and participants were asked to fixate on the cross. The order of presentation of the stimuli was identical for each participant, with each stimulus (word/non-word) displayed for a maximum of 3 seconds and moving on to the next if the subject failed to make a button-press response. Each run had a maximum duration of 10 minutes (depending of the participant's reaction times), the session lasting about 50 minutes to an hour.

MRI acquisition: Data were acquired on a Philips Achieva 3T whole body MRI System with an 8-channel head SENSE radio frequency (RF) coil. Following a localizer Survey scan, high resolution structural images were obtained using a 3D T1-weighted scan (TR = 7.4 ms, TE=3.4 ms, flip angle= 8 degrees, FOV= 250 x 250 mm, matrix = 256 x 256 mm, slice thickness 0.6 mm, voxel size =

1.1x1.1x0.6). The 3D brain image served as a high-resolution anatomic reference frame for subsequent overlay of functional activation maps. Functional imaging was done using gradient-echo echo planar imaging (GE-EPI; TR = 3000 ms, TE = 35 ms, flip angle = 90 degrees, FOV = 230 x 230 mm^2, matrix = 128 x 128 mm, voxel size = 2 x 2 x 3 mm, 27 slices, 3 mm slice thickness with 1 mm gap). Five dummy GE-EPI scans were collected at the start of each run to allow for longitudinal equilibrium of the signal. The start of the stimuli was triggered automatically after the dummy scans. During the structural scans, subjects were allowed to close their eyes and relax but instructed not to move.

FMRI Data Analysis

The fMRI data was analyzed using a general linear model with FSL (FMRIB, Oxford, UK) [25, 26]. Only correct responses were included in the analysis. The acquired 3D anatomical images were segmented and extracted for only the brain using FSL brain extraction tool (BET)[27]. The functional data was then motion corrected, spatially smoothed using a 9 mm FWHM, and then high pass filtered to remove low frequency artifacts. Signal intensity was averaged for each condition across runs in each subject and across the group. The fMRI images were co-registered with the participants' high resolution 3D anatomical image with 7 degrees of freedom and then registered to the MNI brain template (MNI152) in standard space with 12 degrees of freedom. The group data were submitted to a mixed effects analysis [28] to allow for population inference of the resulting statistical parametric maps (SPMs). Each effect was tested by applying the appropriate linear contrast, and significant hemodynamic changes for each

contrast were assessed. We report activations below a set threshold of P < 0.001. Of particular interest were the activation differences between real words with and without diacritics.

6.3 Results

Behavioral

Accuracy: A Frequency (high vs. low) x Diacritics (present vs. absent) ANOVA for real words yielded a main effect for Frequency ($F=10.53$, $p = 0.002$): Participants were more accurate on high frequency real words (HFRW)(98.8%) than low frequency real words (LFRW) (94.7%). There was no main effect of Diacritics or a Frequency x Diacritics interaction. Subjects were equally accurate on words with vs. without diacritics regardless of frequency. A Frequency x Diacritics ANOVA for the nonwords yielded neither main nor interaction effects for the same comparisons (Figure 6-1).

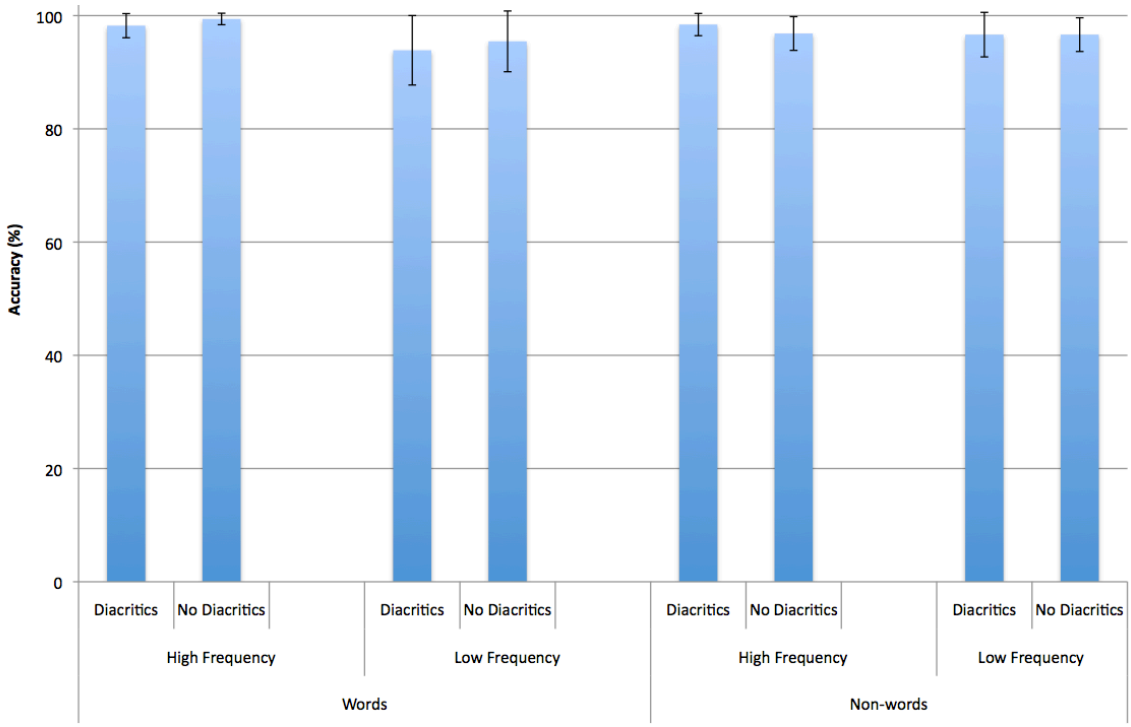

Figure 6-1 Mean percent correct for all stimulus categories. Error bars represent standard deviation of the mean.

Response Time (RT): Mean lexical decision times were calculated for the different stimulus categories. A Frequency (high vs. low) x Diacritics (present vs. absent) ANOVA for real words yielded a main effect of Diacritics ($F=8.110$, $p = 0.007$): real words with diacritics (RWD) had longer lexical decision times (1.03 s) than real words with no diacritics (RWND) (.89 s). There was no main effect of Frequency or Frequency x Diacritics interaction. The ANOVA for non-words yielded no main or interaction effects for the same comparisons (Figure 6-2).

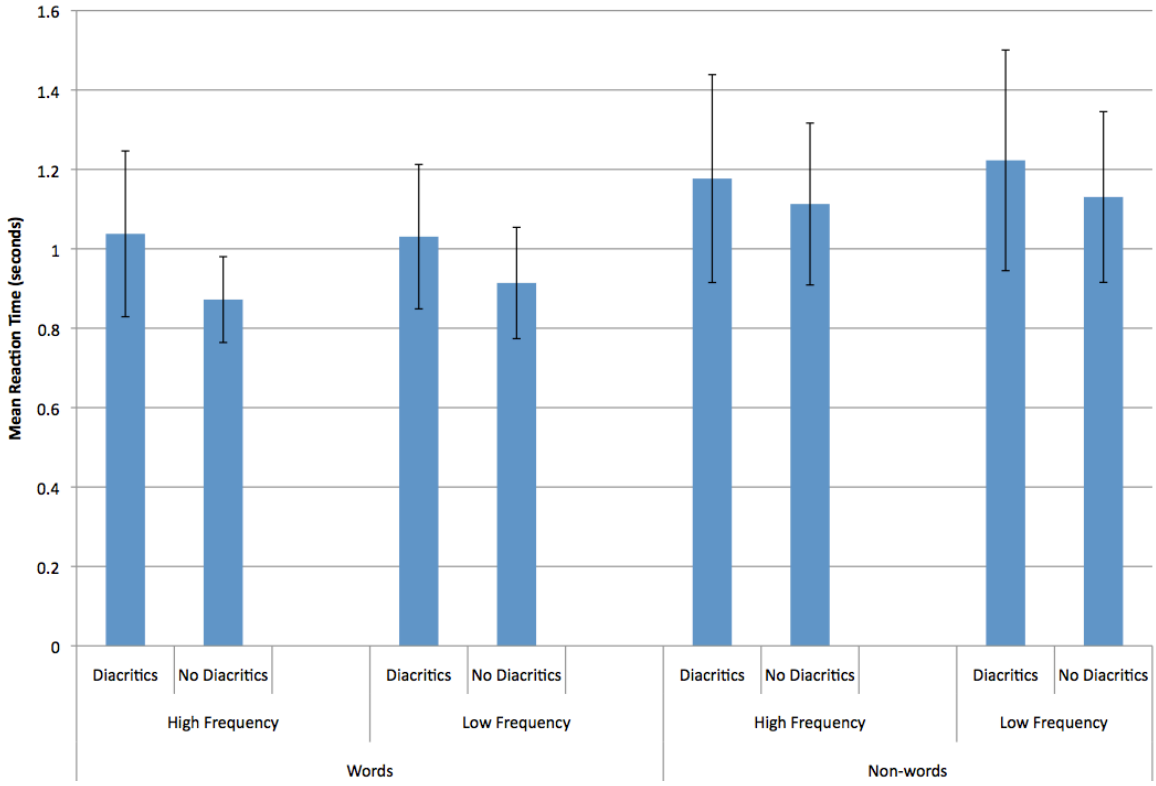

Figure 6-2 Mean lexical decision times (in seconds) for all stimulus categories. Error bars represent standard deviation of the mean.

FMRI

A summary of the activation findings in the study are presented in Table 6-2 below.

RWD > RWND

Brain Region	**Z – value**	**X,Y,Z**
Right insular cortex	2.99	32,26,2
Right insular cortex	2.9	32,24,-2

RWND > RWD

Brain Region	**Z – value**	**X,Y,Z**
Right parahippocampal gyrus (including Brodmann area 36)	3.88	26,-30,-14

Right parahippocampal gyrus	3.6	26,-32,-12
Right parahippocampal gyrus (including Brodmann area 36)	3.33	20,-30,-12
Right middle temporal lobe	2.78	40,-8,-12
Right parahippocampal gyrus	2.67	34,-4,-12
Right Hippocampus	2.6	32,-36,0
Left parahippocampal gyrus (including Brodmann area 36)	2.45	-24,-34,-12

RWD > NWD

Brain Region	**Z – value**	**X,Y,Z**
Right cerebellum	2.48	8,-56,-14

NWD > RWD

Brain Region	**Z – value**	**X,Y,Z**
Right parahippocampal gyrus (Brodmann area 28)	2.79	20,-12,-12
Right brainstem	2.6	16,-10,-12
Right brainstem	2.3	14,-8,-8
Right parahippocampal gyrus (Brodmann area 35)	2.53	26,-26,-14
Left anterior cingulate	2.51	0,26,-6
Left anterior cingulated (Brodmann area 25)	2.34	-2,18,-8

NWD > NWND

Brain Region	**Z – value**	**X,Y,Z**
Left cerebellum	2.27	-4,-80,-16

NWND > NWD

Brain Region	**Z – value**	**X,Y,Z**
Left caudate	2.68	-18,22,0
Right cerebellum	2.32	14,-52,-12
Right cerebellum	2.32	8,-56,-8
Left insular cortex	2.31	-42,4,-2

(including Brodmann area 13)		
Left insular cortex	2.23	-42,4,-4

HFRWD > LFRWD

Brain Region	**Z – value**	**X,Y,Z**
Left frontal lobe	3	-38,44,2
Right insular cortex (Brodmann area 13)	2.92	48,16,0
Right inferior frontal gyrus (including Brodmann area 47)	2.88	48,14,-4

LFRWD > HFRWD

Brain Region	**Z – value**	**X,Y,Z**
Left parahippocampal gyrus	2.54	-26,-44,-14

HFRWND > LFRWND

Brain Region	**Z – value**	**X,Y,Z**
Right putamen	2.83	24,18,-4
Left frontal lobe (including inferior frontal gyrus)	2.66	-30,40,-4
Right putamen	2.4	24,14,-6
Right anterior cingulate (Brodmann area 32)	2.4	14,46,4
Left insular cortex (Brodmann area 13)	2.4	-50,10,2
Right superior temporal gyrus (including Brodmann area 38)	2.4	56,8,-10
Right parahippocampal gyrus (Brodmann area 35)	2.3	24,-16,-12

LFRWND > HFRWND

Left cerebellum	2.3	-4,-62,-8

HFRWD > HFRWND

Brain Region	**Z – value**	**X,Y,Z**
Left insular cortex	2.54	-30,24,-2

Right insular cortex	2.39	36,28,0
Right inferior frontal gyrus (including Brodmann area 47)	2.3	40,24,-4

HFRWND > HFRWD

Brain Region	**Z – value**	**X,Y,Z**
Right parahippocampal gyrus	3.27	24,-30,-14
Right anterior cingulate cortex	3.07	12,42,-6
Right putamen	2.59	20,18,-6
Left anterior cingulate cortex	2.48	-8,38,-2

LFRWD > LFRWND

Brain Region	**Z – value**	**X,Y,Z**
Right insular cortex	2.61	30,26,-6

LFRWND > LFRWD

Brain Region	**Z – value**	**X,Y,Z**
Left cerebellum	2.9	-10,-62,-12
Right parahippocampal gyrus (including Brodmann area 36)	2.78	30,-34,-14
Right inferior temporal gyrus (including Brodmann area 21)	2.63	60,-10,-14
Right insula	2.59	-42,-14,2
Left middle frontal gyrus (including Brodmann area 10)	2.58	-22,60,6
Right putamen	2.44	34,-4,-6

Table 6-2 Stereotactic MNI coordinate(x,y,z) locations of clusters with z > 2.2 and associated brain region for each comparison

Of particular relevance are the activation differences related to the effects of diacritics. Real words with no diacritics (RWND) showed significant activation

compared to real words with diacritics (RWD) in areas including Brodmann area (BA) 36, the hippocampus and middle temporal gyrus (Figure 6-3). In contrast, significant activation was evident for real words with diacritics (RWD) compared to real words without diacritics (RWND) in the insula. A closer examination also revealed greater activation of the inferior frontal region for real words with versus without diacritics for both high and low frequency words (i.e., HFRWD>HFRWND, LFRWD>LFRWND). Additional probing of the real words with diacritics revealed that in comparison with nonwords with diacritics, RWD>NWD in the right cerebellum, but NWD> RWD in the left anterior cingulate (ACC) (BA 25) as well as in right parahippocampal gyrus (including BA 28 and 35) (Figure 6-4).

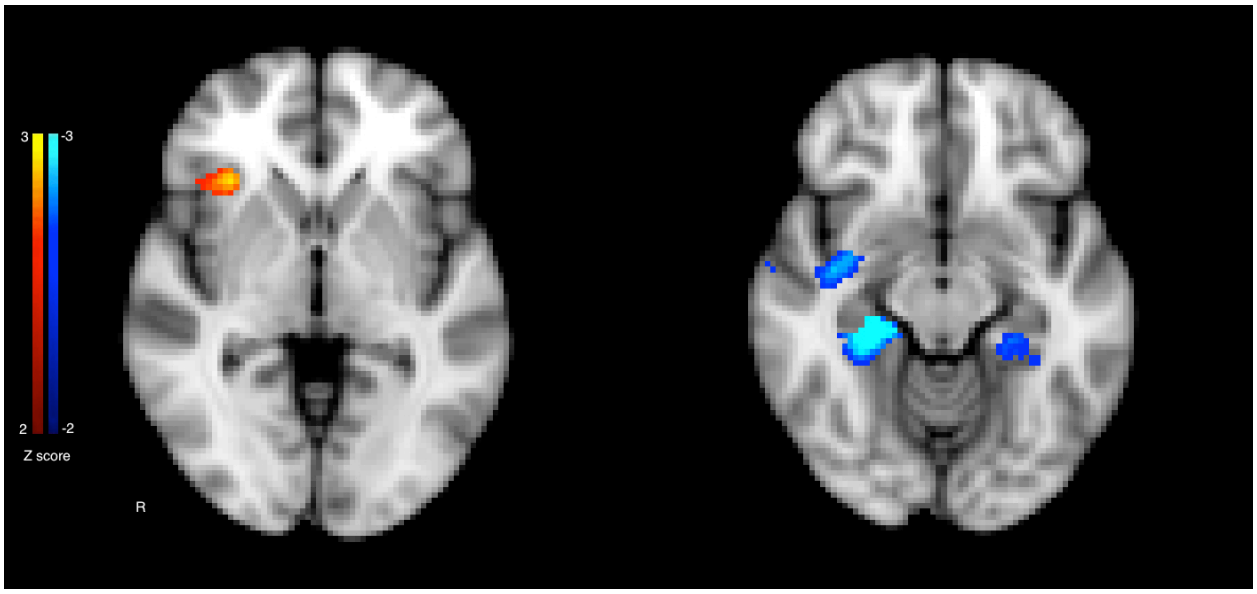

Figure 6-3 Statistical parametric activation map for brain regions associated with RWD > RWND (red, yellow), and RWND > RWD (light blue, blue).

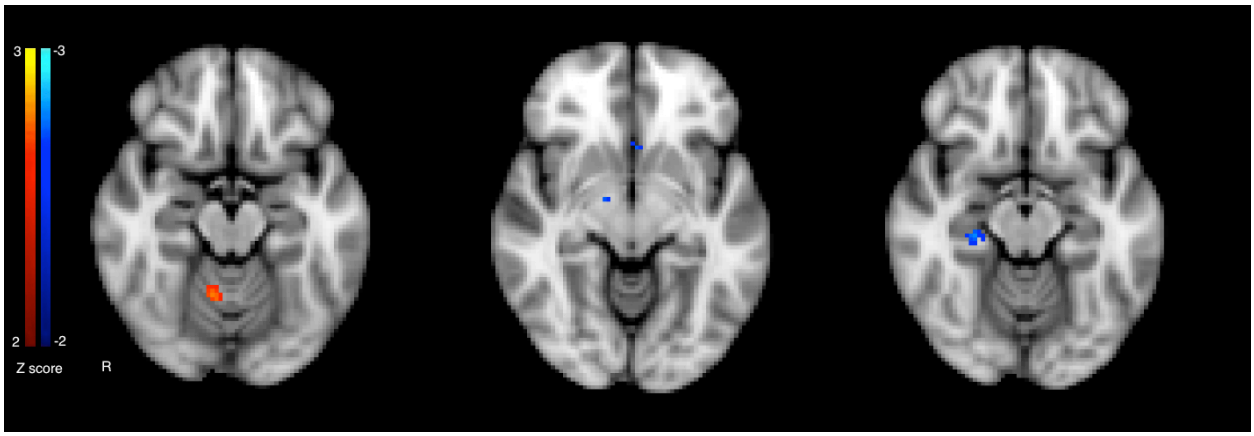

Figure 6-4 Statistical parametric activation map for brain regions associated with RWD > NWD (red, yellow), and NWD > RWD (light blue, blue).

6.4 Discussion and Conclusions

The purpose of the present study was to investigate the role of diacritics in visual word identification in Arabic in relation to the orthographic depth hypotheses about the language. We used a lexical decision task with words of varying frequency and orthographically-matched nonwords, each set with and without diacritics, to examine the effects of diacritics on single word recognition in Arabic. Of particular interest were the activation differences between real words with and without diacritics and the effects of frequency on this difference. The accuracy data yielded a main effect for Frequency for real words. (nonwords are meaningless letter strings and were therefore not expected to show a Frequency effect). Accuracy was predictably higher for high frequency real words than low frequency real words. However, there was no main effect of Diacritics nor any interaction of Frequency with Diacritics. This suggests that the adult Arabic reader did equally well in recognizing words with and without diacritics. In contrast, response times yielded a significant effect for Diacritics: real words with diacritics (RWD) required longer lexical decision times than real words with no

diacritics (RWND) regardless of frequency. There was no corresponding effect of diacritics for the nonwords designed to orthographically match the real words with and without diacritics. The observed difference at a word level may reflect the role of diacritics in lexical recognition. In summary, frequency appeared to affect word accuracy, whereas diacritics affected lexical decision times.

We found that real words (both high and low frequency) with no diacritics (RWND) had significant parahippocampal activation when compared to real words with diacritics (RWD). The parahippocampus is part of the medial temporal lobe which is known to be implicated in memory. Insofar as Arabic words stripped of their diacritic markings and presented in isolation may lend themselves to more than one meaning, the increased parahippocampal activation may reflect a search among these alternative meanings in making a lexical decision. However, care was taken to match the frequencies of the word pairs with and without diacritics in designing our stimuli, with any potential concerns regarding the ambiguity of the latter being secondary for purposes of this task. The availability of multiple meanings for a RWND may, however, have facilitated lexical decision making and contributed to the quicker response times for these words compared to RWD. In contrast, a real word with diacritics is associated with a specific lexical entry and a defined phonological form that would need to be retrieved in order to make a lexical decision. This may explain why RWD yielded longer response times, and greater activation than RWND in the insula and inferior frontal areas which are known to be actively engaged in verbal processes (Ardilla, 1999). The difference in lexical decision times for RWD vs. RWND may

also reflect the reading experience of the participants. Specifically, real words with diacritics may be less familiar than real words without diacritics for adult Arabic readers for whom reading devowelized text has become a natural and automated process, resulting in shorter lexical decision times for words without diacritics.

The greater activation of the anterior cingulate cortex (ACC) in NWD compared to RWD presents as an interesting observation(see Table 2). The ACC is typically engaged in effortful decision-making tasks that require error monitoring (Carter et al., 1998; Kaneda & Osaka, 2008). Perhaps the visuo-orthographic similarity between the words and nonwords may have made the process of lexical decision making more challenging. As such, the increased demand for error monitoring may have contributed to the enhanced activation of the left ACC in the NWD > RWD finding (Chan et al., 2004). On a related note, the increased activation of the cerebellum for RWD compared to NWD is in keeping with the involvement of this area in lexical-semantic processes during reading (Fulbright et al, 1999).

A striking observation in the fMRI results was the significant activation of the insula in most of the diacritic-related comparisons. The insular cortex has been shown to be implicated in phonological working memory and in semantic retrieval [29] Ardilla, 1999; Chan et al. 2004). Chan and colleagues (2004) compared ambiguous and unambiguous words in a related-word generation task, and found that semantically precise words were associated with significant insular activation. In the present study, real words with diacritics (RWD) showed

increased insular and frontal activation compared to RWND possibly reflecting the contribution of diacritics to enhanced phonological and semantic specification at a word level. In keeping with the literature, the diacritics may have served as disambiguating marks that affected orthographic depth. The results, though, run counter to predictions based on an orthographic depth view of vowelized Arabic: they suggest that that the presence of diacritics on real words mediates phonological and semantic processing in visual word recognition in Arabic.. On the other hand, the results may resemble those of Frost, Katz & Bentin (1987) in which the authors found that vowels did not play a facilitative role in word naming in Hebrew. Rather, pronunciation was achieved through retrieving the word's phonological form from lexical memory. It may well be that Arabic readers are sensitive to the phonological structure of a word, but a lexical decision about the letter string may be based on the consonantal structure without requiring detailed phonological analysis as in the case of RWND. The high degree of visuo-orthographic similarity of the words and nonwords may have heightened the participants' awareness of and attention to diacritics, contributing to the longer reaction times and enhanced phonological activation related to processing of RWD relative to RWND.

The Behavioral and Cortical Effects of Diacritics

In summary, the neural evidence appears to support a role for diacritics in visual word recognition in Arabic. The results suggest that diacritics provide phonological and semantic information about a word that may be used in a

lexical decision task . This would account for the enhanced activation of the insula and inferior frontal areas for words with diacritics compared to words without diacritics. Diacritics had a main effect on real word recognition evident in the longer reaction times for RWD than RWND. Insofar as real words without diacritics may be associated with more than one meaning (though we tightly matched the frequency of word pairs with and without diacritics), this may have facilitated the lexical decision process and resulted in shorter response times to these words. This shorter reaction times may also relate to the greater familiarity with and hence easier processing of words without diacritics by the adult Arabic reader. On a related note, our participants were experienced readers; their lexical decisions may have been based on recognizing the orthographic letter string or abstract roots and may not involve specific access to the phonological lexicon as suggested by the RWND findings. Conversely, the presence of diacritics while providing greater phonological and semantic specification may have added to the lexical processing time for words with diacritics.

As mentioned earlier, the evidence of a role for diacritics in single word processing has been mixed [2, 5-7, 30, 31]. However, the behavioral and brain data from the present study appear to suggest that diacritics provide phonological and semantic information about a word that may be used in visual word recognition by the experienced Arabic reader. While the study has paved the way for further neuroimaging investigations of reading in Arabic, there remain several outstanding issues that need to be addressed. It would be important to replicate these findings with a larger number of subjects. The subject selection

criteria made it difficult to find a larger number of qualified subjects. Future studies should examine the effects of diacritics across a wide age span, including readers at different stages of reading mastery in order to understand the developmental influences. Additionally, follow-up studies should include both typically developing Arabic readers and Arabic readers with dyslexia and other learning disabilities. Studies will also need to systematically examine the effects of diacritics in phrase, sentence, and discourse-level contexts. These are a few directions that would contribute to the development of a more complete theory about the role of diacritics in Arabic reading.

6.5 References

[1] S. Abu-Rabia, "The role of vowels in reading Semitic scripts: Data from Arabic and Hebrew," vol. 14: Reading and Writing: An Interdisciplinary Journal, 2001.

[2] S. Abu-Rabia, "The role of morphology and short vowelization in reading Arabic among normal and dyslexic readers in grades 3, 6, 9, and 12.," *J Psycholinguist Res,* vol. 36, pp. 89-106, Mar 2007.

[3] S. Abu-Rabia, "Reading in Arabic orthography: the effect of vowels and context on reading accuracy of poor and skilled native Arabic readers in reading paragraphs, sentences, and isolated words.," *J Psycholinguist Res,* vol. 26, pp. 465-82, Jul 1997.

[4] S. Abu-Rabia, "The learning of Hebrew by Israeli Arab students in Israel.," *J Soc Psychol,* vol. 138, pp. 331-41, Jun 1998.

[5] S. Abu-Rabia, "Reading in Arabic Orthography: Characteristics, Research Findings, and Assessment," in *Handbook of Orthography and Literacy*, R. M. Joshi and P. G. Aaron, Eds., Mahwah,New Jersey: Lawrence Erlbaum Associates, 2006.

[6] A. Koriat, "Lexical access for low- and high-frequency words in Hebrew," *Memory & Cognition,* vol. 13, pp. 37-44, 1985b.

[7] R. Frost and S. Bentin, "Reading consonants and guessing vowels: Visual word recognition in Hebrew orthography," in *Orthography, phonology, morphology, and meaning. Advances in psychology*. vol. 94, R. F. a. L. Katz, Ed., Amsterdam,Netherlands: North- Holland, 1992, pp. 27-44.

[8] S. Bentin and R. Frost, "Processing lexical ambiguity and visual word recognition in adeep orthography," *Memory and Cognition,* vol. 15, pp. 13-23, 1987.

[9] S. Abu-Rabia, "The effect of Arabic vowels on the reading comprehension of second- and sixth-grade native Arab children.," *J Psycholinguist Res,* vol. 28, pp. 93-101, Jan 1999.

[10] J. Shimron, "The role of vowel signs in Hebrew: Beyond word recognition," *Reading and Writing: An Interdisciplinary Journal,* vol. 11, pp. 301-319, 1999.

[11] L. Katz and R. Frost, "The reading process is different for different orthographies: the orthographic depth hypothesis," in *Haskins Laboratories Status Report on Speech Research*, Moscow: Haskins Laboratories, 1992, pp. 147-160.

[12] R. Frost, "Prelexical and postlexical strategies in reading: evidence from a deep and a shallow orthography.," *J Exp Psychol Learn Mem Cogn,* vol. 20, pp. 116-29, Jan 1994.

[13] D. Besner*, et al.*, "Basic processes in reading: computation of abstract letter identities.," *Can J Psychol,* vol. 38, pp. 126-34, Mar 1984.

[14] M. Caravolas. (2009, 11 January). *Orthographic Depth Hypothesis*. Available: http://www.childrenofthecode.org/interviews/caravolas.htm#The_Orthographic_Depth_Hypothesis

[15] R. Frost*, et al.*, "Strategies for visual word recognition and orthographical depth: a multilingual comparison.," *J Exp Psychol Hum Percept Perform,* vol. 13, pp. 104-15, Feb 1987.
[16] E. Paulesu*, et al.*, "A cultural effect on brain function.," *Nat Neurosci,* vol. 3, pp. 91-6, Jan 2000.
[17] E. Paulesu*, et al.*, "Dyslexia: cultural diversity and biological unity.," *Science,* vol. 291, pp. 2165-7, 2001 Mar 2001.
[18] P. Fletcher*, et al.*, ""Sculpting the response space"--an account of left prefrontal activation at encoding.," *Neuroimage,* vol. 12, pp. 404-17, Oct 2000.
[19] B. T. Gold and R. L. Buckner, "Common prefrontal regions coactivate with dissociable posterior regions during controlled semantic and phonological tasks.," *Neuron,* vol. 35, pp. 803-12, Aug 2002.
[20] D. T. Wehner*, et al.*, "The influence of semantic processing on phonological decisions in children and adults: a magnetoencephalography (MEG) study.," *J Speech Lang Hear Res,* vol. 50, pp. 716-31, Jun 2007.
[21] A. Rubens, "Transcortical motor aphasia," in *Studies in neurolinguistics*. vol. 28, W. H, Ed., New York: Academic, 1976, pp. 293–306.
[22] J. Binder*, et al.*, "Human brain language areas identified by functional magnetic resonance imaging.," *J Neurosci,* vol. 17, pp. 353-62, Jan 1997.
[23] R. C. Oldfield, "The assessment and analysis of handedness: The Edinburgh inventory. Neuropsychologia," *Neuropsychologia,* vol. 9, pp. 97-113, 1971.
[24] S. Boudelaa and Marslen-Wislon, "Aralex: A Lexical Database for Modern Standard Arabic," *Behaviour Research Methods,* 2009.
[25] M. Woolrich*, et al.*, "Bayesian analysis of neuroimaging data in FSL.," *Neuroimage,* vol. 45, pp. S173-86, Mar 2009.
[26] S. Smith*, et al.*, "Advances in functional and structural MR image analysis and implementation as FSL.," *Neuroimage,* vol. 23 Suppl 1, pp. S208-19, 2004.
[27] S. Smith, "Fast robust automated brain extraction.," *Hum Brain Mapp,* vol. 17, pp. 143-55, Nov 2002.
[28] K. J. Worsley, "Statistical analysis of activation images," in *Functional MRI: An Introduction to Methods*, P. Jezzard*, et al.*, Eds.: OUP, 2001.
[29] A. Chan*, et al.*, "Neural systems for word meaning modulated by semantic ambiguity.," *Neuroimage,* vol. 22, pp. 1128-33, Jul 2004.
[30] A. Koriat, "Reading without vowels: Lexical access in Hebrew," in *Attention and performance X: Control of Language processes (pp. 227-242)*, H. Bauma and D. G. Bouwhius, Eds., Hillsdale, NJ: Earlbaum, 1984, pp. 227-242.
[31] A. Koriat, "Laterlization effects in reading pointed and unpointed hebrew," *British Journal of Psychology,* vol. 76, pp. 161-173, 1985a.

Chapter 7: Independent Component Analysis and FMRI

7.1 Independent Component Analysis

Independent Component Analysis (ICA) is a type of blind source separation method. ICA is a method for separating components of a mixed signal with no, or very minimal, prior information. Independent component analysis recovers independent signals provided only sensor inputs that have an unknown linear mixture of the unobserved independent source signals [1]. It is worth noting that the decomposition of ICA is not equivalent to the decorrelation done in principle component analysis (PCA) for nongaussian random vectors. While PCA finds the projections by maximizing variance between the data, ICA finds the projections that increases non-gaussianity and independence (i.e. $E\{h(y_1)h(y_2)\} = E\{h(y_1)\}E\{h(y_2)\}$). Therefore ICA is able to "blindly" (i.e. with no or very limited information outside non-gausanity of source signals) separate nongaussian source signals from their linear mixtures. Moreover, ICA can be used to extract features from sound, images and other sources by minimizing the redundancy between the elements of the output layer (redundancy reduction principle), which has its roots in biomedical signals and neuroscience[1-3].

An illustration to provide a simplified depiction of how ICA works, would include 3 microphones and 3 different sound sources. Lets imagine that the first sound source is from construction work, the second sound is from a violinist on the street, and the third sound is from a person talking on her mobile phone. We setup three microphones to acquire these sounds. The microphones will detect

all these sounds. In this case, the output of these microphones will be a mixture of all three sounds. From all these three mixtures (from each microphone) ICA can recover all three original sounds or source signals (independent components) and separate them. Now, it can be easily be seen that if we are only interested in one signal and the rest is considered noise. ICA can do such a decomposition and source signal retrieval.

ICA assumes the relationship and linear mixing provided by Equation 7-1 and Equation 7-2.

X=AS ; **Equation 7-1**

X: Observed signal
A: Mixing matrix
S : Original signal

or

$$X_1 = a_{11}S_1 + a_{12}S_2 + \ldots + a_{1p}S_p \quad \textbf{Equation 7-2}$$
$$X_2 = a_{21}S_1 + a_{22}S_2 + \ldots + a_{2p}S_p$$
$$\vdots$$
$$X_p = a_{p1}S_1 + a_{p2}S_2 + \ldots + a_{pp}S_p$$

X is the observed signal collected from the sensors, and ICA assumes that the original signal of interest *S* is linearly mixed in a mixing matrix *A* . Therefore, the task for ICA is to retrieve the original signals *S* without knowing the mixing matrix *A*.

ICA retrieves the original signal of interest by defining an unmixing matrix *W* (Equation 7-3). The reason for an unmixing matrix (*W*) is that we do not know the mixing matrix (*A* in Equation 7-1) in order to recover the original signals of interest. Therefore, *Z* in Equation 7-3 is an estimate of *S* in the sense that each component *S* appears in any component *Z* with a scalar factor. See Figure 7-1

and Figure 7-2 for a clear illustration of how ICA takes a mixed input and outputs all the independent components.

Z = WX; **Equation 7-3**

Z: Independent components (recovered signals) ($Z = [Z_1,...,Z_N]$)
W: Unmixing matrix
X: source signal

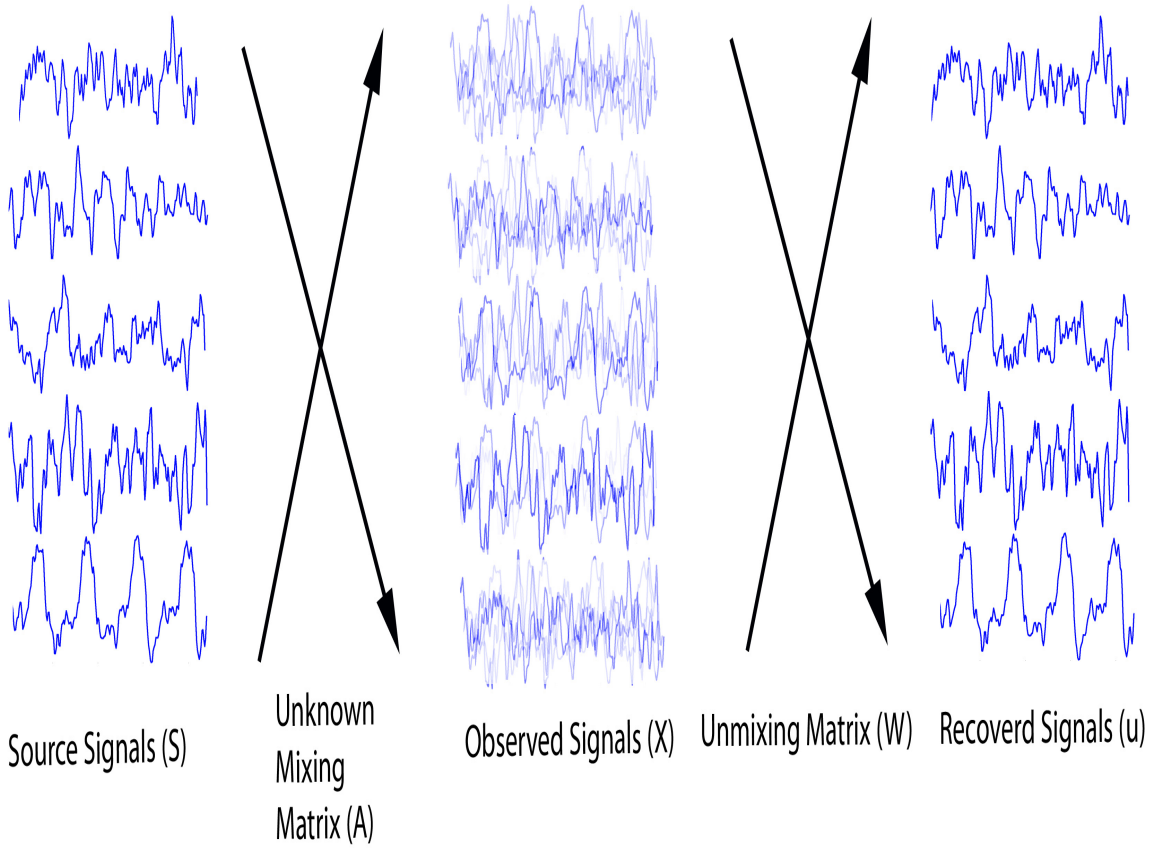

Figure 7-1 An example illustration of the basic theory of ICA in retrieving the original source signals. Observables (X) are the outputted signals from the signal sources (S) mixed with an unknown mixing matrix (A). An un-mixing matrix (W) is then used to un-mix the signals, and recover the independent signal sources (u).

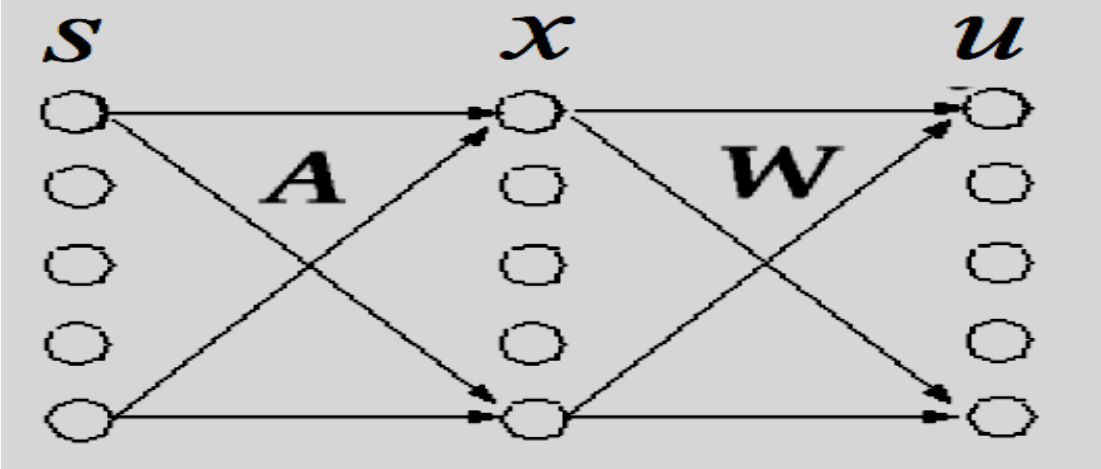

Figure 7-2 An illustration of how the source signals (*S*) are assumed to be mixed by an unknown mixing matrix *A*, and then ICA uses an unmixing matrix *W* to recover the original signals (*u*).

Again, unlike PCA where 2nd order statistics are used, ICA uses higher order statistics to recover the independent signals. It is worth noting that such a recovery is obviously not possible using PCA, since PCA uses lower order statistics to maximize variance. Furthermore, there are different algorithms that ICA uses to optimize the maximum independence between the data. Among these algorithms are: Infomax[4], blind deconvolution[5], maximum likelihood [6],non-linear PCA[7], and maximum negentropy[1]. Although these algorithms differ in their optimization in finding the solution in ICA, they all draw upon higher order statistics (i.e. kurtosis).

Kurtosis is the measure of the "peakedness" of a given distribution relative to a normal distribution. Data sets with low kurtosis values would have a lower peak than a normal distribution and a flatter top near the mean. On the other hand, data sets with high kurtosis values will have a more distinct peak near the mean and heavy tails. Kurtosis can be calculated using Equation 7-4 [8].

$$Kurtosis = \frac{\sum_{i=1}^{N}(Y_i - \bar{Y})^4}{(N-1)s^4} \; ; \qquad \textbf{Equation 7-4}$$

$Y_i = Y_1, Y_2, ..., Y_N$ (data)

$\bar{Y} = \frac{1}{N}\sum_{i=1}^{N} Y_i$; N = number of data points

$s = \sigma = \sqrt{E[(X-u)^2]}$

Kurtosis of a normal distribution, as defined by Equation 7-4, is 3. Another form of calculating kurtosis is to add (-3) to the Equation 7-4 above; such a definition is used so that a normal distribution would have a kurtosis value of zero. A distribution that is more “peaked” than a normal distribution and therefore has a higher kurtosis value, is called supergaussian or leptokurtic. On the other hand, if a distribution has a lower kurtosis value than that of a normal distribution and its distribution is less “peaked” and more flat, it is called a subgaussian or platykurtic distribution. Mesokurtic is the same as normal or Gaussian distribution. See Figure 7-3 for more details.

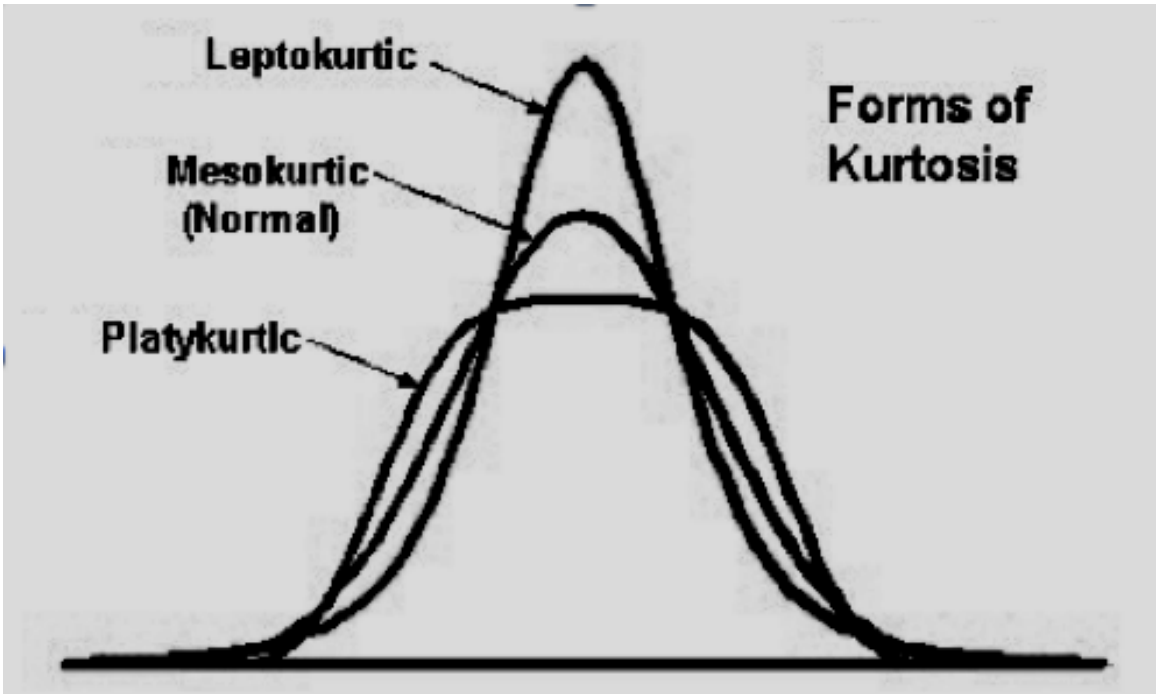

Figure 7-3 Distributions with different "peakedness" and kurtosis values.

An example of how ICA uses kurtosis can be seen with what is called FastICA as illustrated in Figure 7-4 and Figure 7-5 [9]. If we take the signals and their input densities provided in Figure 7-4 and allow FastICA to iterate, we will be able to separate and recover the two original source signals Figure 7-5. Therefore, showing the power of ICA in recovering the original source signals with no , or very limited, apriori set information.

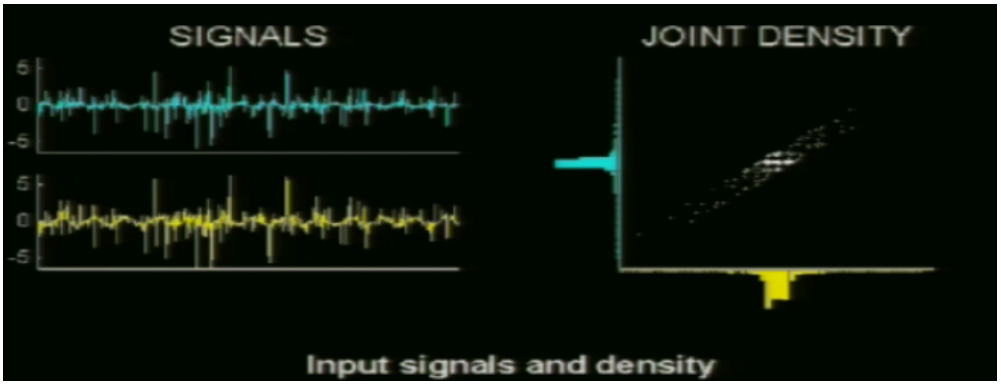

Figure 7-4 On the left are the mixed input signals, on the right is the respective joint density for the signals. This is before any iteration of FastICA (*Reprinted with permission from publisher*).

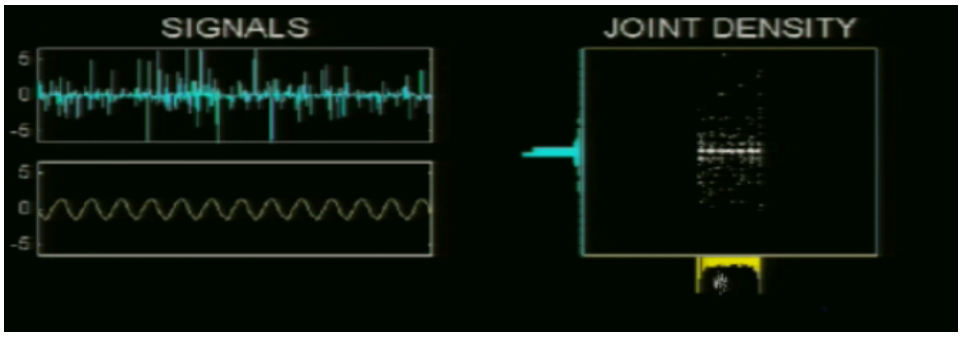

Figure 7-5 On the left are the recovered separate signals after iterationof FastICA. On the right are their joint densities respectively with clear depiction of the non-gaussanity of the yellow signal(*Reprinted with permission from publisher*).

7.2 Independent Component Analysis in fMRI

Independent Component Analysis (ICA) gained more popularity in the past decade among the fMRI research community. This is primarily due to its data-driven or exploratory analyses approach. In that, it provided a complimentary, and at times supplementary, approach to hypothesis-driven analysis (i.e. general linear model) for analyzing fMRI data. Its appeal to fMRI is the fact that it is a model-free analysis method, because it does not assume an experimental design matrix and does not depend on any estimates of the hemodynamic response. ICA assumes that the data can be modeled by finding voxels or cluster of voxels whose activity varies in sync with each other and that are maximally different from activity in other voxels or clusters [10-12].

In the first application of ICA to fMRI data analysis, McKeown[13] utilized infomax [4] ICA algorithm and was successful in separating fMRI data into task-related, transiently task-related, and motion related [14]. This is very beneficial for fMRI data analysis; where signals of interest are grouped together and signals that are considered noise or non-stimuli task related are grouped together.

Signals that may be not of interest in fMRI experiments may include, scanner noise, scanner drift, physiological noise, and motion noise. Therefore, such grouping achieved by ICA is very advantageous to single out fMRI signals of interest.

Spatial and Temporal ICA

ICA achieves the groupings or independent components (ICs) with respect to fMRI either through spatial ICA (sICA) or temporal ICA (tICA). The temporal distribution of task-related brain activation is often considered bimodal, and the components are assumed to be spatially independent and add linearly[14]. Moreover, ICA is used in fMRI to understand spatio-temporal characteristics of the signal, and thus spatial and/or temporal independent components. Most applications use the former rather than the latter[15].

The choice between sICA and tICA still remains controversial. However, McKewon et al. [13] argued that sICA was fitting for the distributed nature of brain activation across space. Moreover, because fMRI confounds are also sparse and localized (i.e. vascular pulsation, breathing-induced motion), Bell-Sejnowski[4] method is very well fit for such spatial analysis[16] which has also been used for tICA[17]. Other work[18, 19] proposed methods that combine both spatial and temporal ICA for fMRI data analysis. Therefore, choosing between spatial independency as in the case of sICA or temporal independency as in the case of tICA becomes merely a choice of two different modeling assumptions [15].

An ICA Model Framework for FMRI Data Analysis

The model in Figure 7-6 provides a generalized analysis model for ICA for blind source separation of independent components (ICs). The first block is unknown where the source signals $(S_1,...,S_n)$ are mixed together using an unknown mixing matrix *A*. What we observe is *X*, which is shown in the second block. The mixed observed signals $(X_1,...,X_m)$ are then inserted into an iterative ICA algorithm which uses an optimization feedback mechanism to recover the original source signals as independent components $(Y_1,...,Y_n)$.

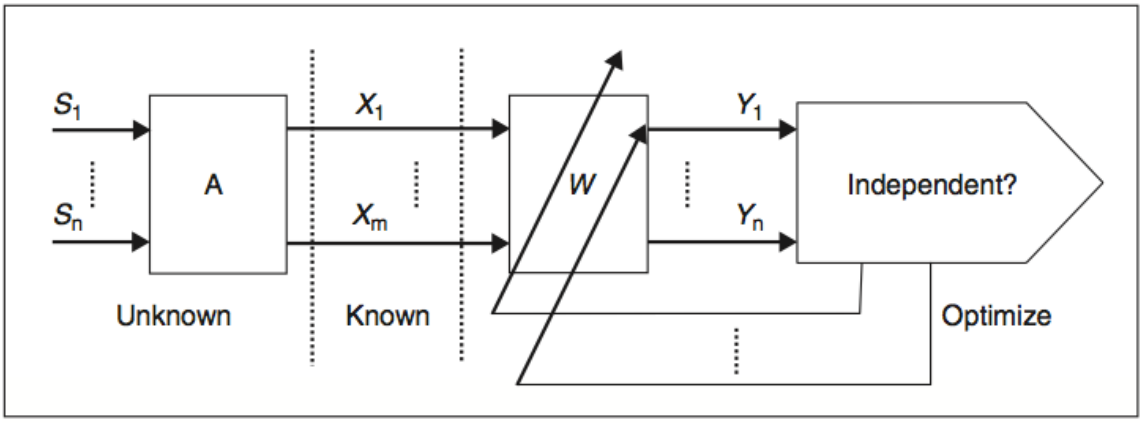

Figure 7-6 A general ICA model for blind source separation[15] (*Reprinted with permission from publisher*)

A more detailed model of the ICA model for fMRI is provided in Figure 7-7 [15, 20]. It provides a framework to understand how ICA is applied to fMRI data analysis. Although the model assumes sICA it can be easily applied to tICA with minor modifications. In that, the data generation phase includes the statistically independent hemodynamic source location in the brain $S_i(v)$ for the location at *v* for the *i*th source. These sources reflect the magnetic properties of tissue. In fMRI these are often changes reflected by T_2* contrast, which measures

changes in oxygenation levels in the brain due to changes in brain activity. The source signals $S_i(v)$ are assumed to be mixed by an unknown mixing matrix *A*. The second block (*B*) represent MR parameters (i.e. TR, TE, FOV,slice thickness, and pulse sequence).

Then the observed data $(Y_1(i),...,Y_k(i))$ goes to the second phase (data processing). The first block in this analysis phase the transformation *T* phase, where preprocessing steps such as motion correction, slice phase correction, smoothing and spatial normalization takes place. The second block (C) is usually done as a data reduction step using PCA. Then an unmixing matrix *A* is used to recover the independent fMRI source signals $(\hat{S}_1(j),...,\hat{S}_N(j))$ [15].

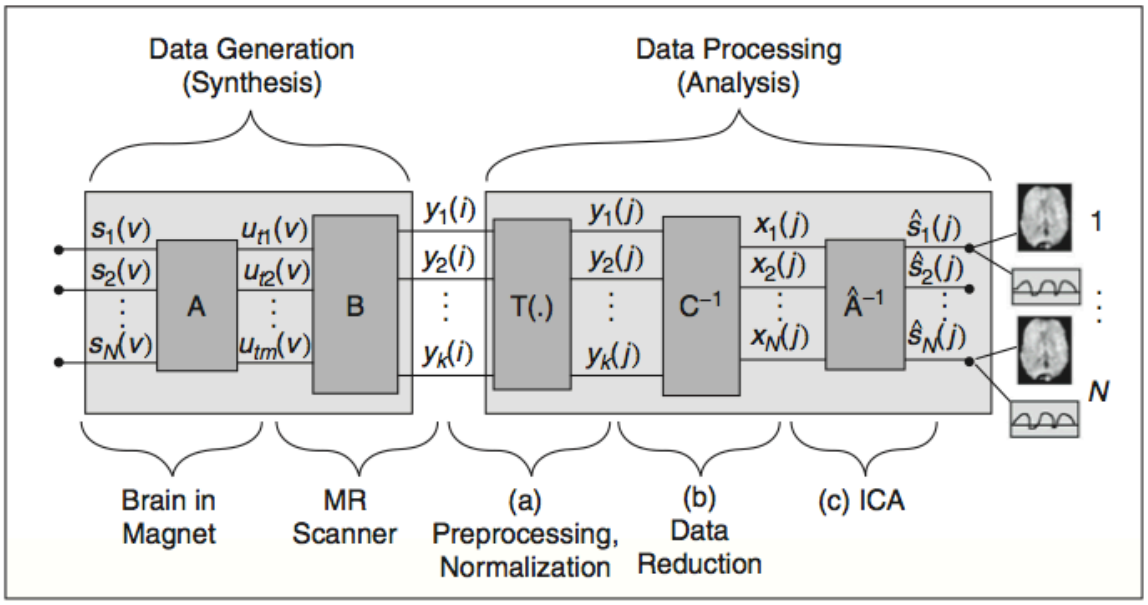

Figure 7-7 ICA model for fMRI data analysis [15, 20] (*Reprinted with permission from publisher*).

With regards to ICA and brain activity, a study by Calhoun et al.[11] examined the neural correlates of visual perceptual processing using both the general linear model (hypothesis-driven approach) and ICA which is a data-driven approach. They found that both detected similar, but not identical brain regions. The general linear model (GLM) was more sensitive to the primary visual cortex and the cerebellum , while ICA detected superior parietal and prefrontal cortical regions that displayed extended brain activation for the stimuli paradigm. In addition, ICA was able to detect motor components that was not detected via GLM. See Figure 7-8 and Figure 7-9 for a depiction of activated brain regions associated with the visual perceptual task.

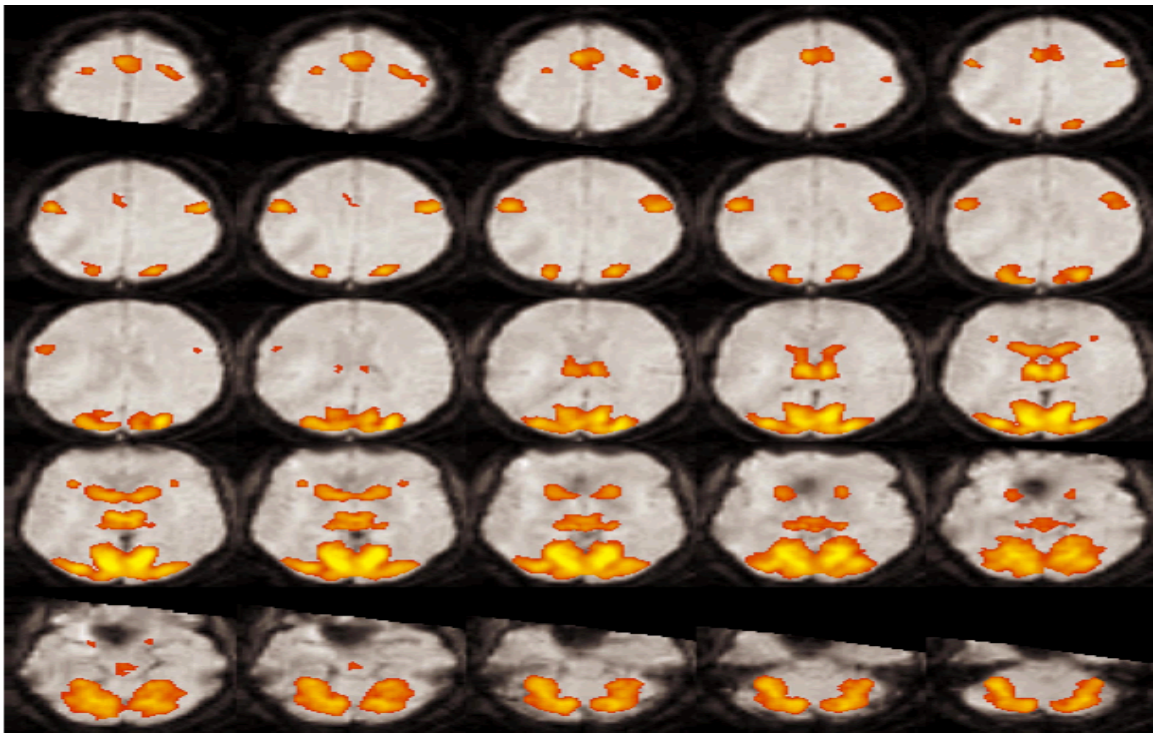

Figure 7-8 [11]Brain activation as detected by the general linear model (hypothesis- driven method). (*Reprinted with permission from publisher*).

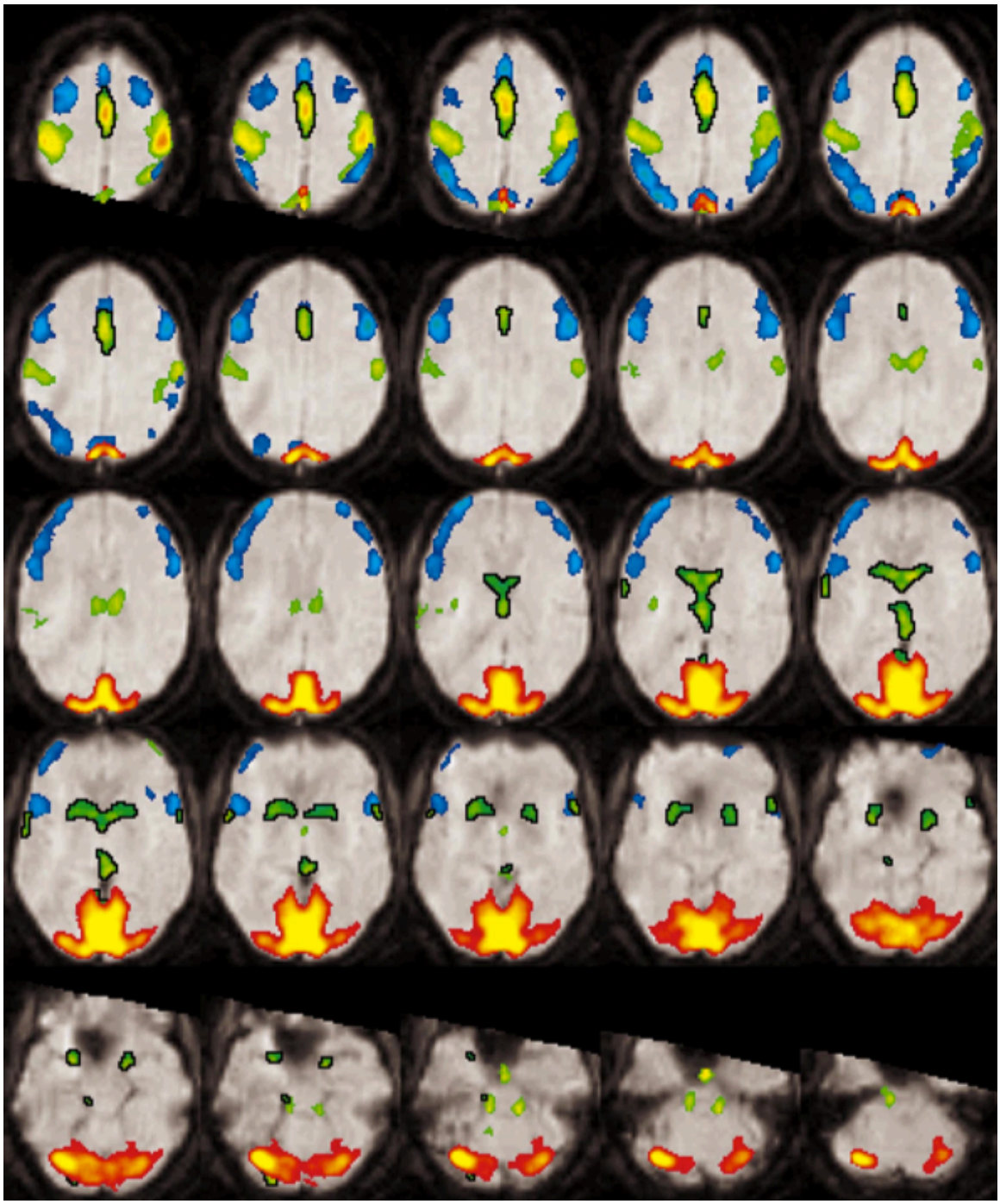

Figure 7-9 [11]Brain activation as detected by ICA (data-driven/exploratory method). (*Reprinted with permission from publisher*)

7.3 References

[1] P. Comon, "Independent Component Analysis, a new concept ?," *Signal Proces,* vol. 36, pp. 287-314, 1994.

[2] A. Hyvarinen, "Fast and robust fixed-point algorithms for independent component analysis," *Neural Networks, IEEE Transactions on,* vol. 10, pp. 626-634, 1999.

[3] J. V. Stone, *Independent Component Analysis: A Tutorial Introduction*. Cambridge, Massachusetts: The MIT Press, 2004.

[4] A. Bell and T. Sejnowski, "An information-maximization approach to blind separation and blind deconvolution.," *Neural Comput,* vol. 7, pp. 1129-59, Nov 1995.

[5] R. H. Lambert, "A New Method for Source Seperation," in *Proceedings of IEEE Intemational Conference on. Acoustics, Speech and Signal Processing*, Detroit, MI, 1995, pp. 2116-2119.

[6] B. Pearlmutter, "A Context-Sensitive Generalization of ICA," in *International Conference on Neural Information Processing*, Hong Kong, 1996.

[7] E. Oja, "The nonlinear PCA learning rule in independent component analysis," *Neurocomputing,* vol. 17, pp. 25-45, 1997.

[8] *N. S. e.-H. o. S. Methods*, *Engineering Statistics Handbook*: National Institute of Standards and Technology, 2003.

[9] V. Calhoun, "Independent Component Analysis," unpublished.

[10] M. J. McKeown and T. J. Sejnowski, "Independent component analysis of fMRI data: Examining the assumptions," *Hum. Brain Map.,* vol. 6, pp. 368-372, 1998.

[11] V. Calhoun*, et al.*, "fMRI activation in a visual-perception task: network of areas detected using the general linear model and independent components analysis.," *Neuroimage,* vol. 14, pp. 1080-8, Nov 2001.

[12] A. W. S. Scott A. Huettel, Gregory McCarthy, *Functional Magnetic Resonance Imaging*. Sunderland: Sinauer Associates, 2004.

[13] M. J. McKeown*, et al.*, "Analysis of fMRI data by blind separation into independent spatial components," *Hum. Brain Map.,* vol. 6, pp. 160-188, 1998.

[14] V. Calhoun*, et al.*, "ICA of Functional MRI Data: An Overview," presented at the International Symposium on Independent Component Analysis and Blind Signal Seperation, Nara, Japan, 2003.

[15] V. Calhoun and T. Adali. (2008) Unmixing fMRI with Independent Component Analysis: Using ICA to characterize high dimensional fMRI Data in a Concise Manner. *IEEE Engineering in Medicine and Biology*.

[16] K. Petersen*, et al.*, "On the independent components of functional neuroimages," in *Proceedings of ICA*, Finland, 2000.

[17] V. Calhoun*, et al.*, "Spatial and temporal independent component analysis of functional MRI data containing a pair of task-related waveforms.," *Hum Brain Mapp,* vol. 13, pp. 43-53, May 2001.

[18] J. V. Stone*, et al.*, "Spatial, temporal, and spatiotemporal independent component analysis of fMRI data," in *Proceeding Leeds Statistical Research Workshop*, Leeds, England, 1999.

[19] E. Seifritz*, et al.*, "Spatiotemporal pattern of neural processing in the human auditory cortex.," *Science,* vol. 297, pp. 1706-8, Sep 2002.

[20] V. D. Calhoun*, et al.*, "Independent component analysis applied to fMRI data: A generative model for validating results," *J. VLSI Signal Process. Syst,* vol. 37, pp. 281-291, 2004.

Chapter 8: Genetic Algorithms

8.1 Introduction and History of Genetic Algorithms

A Genetic Algorithm (GA) is an iterative, search and optimization algorithm inspired by the idea of natural selection, genetics and evolution. It starts with an initial pool of candidate solutions, called *parents (parent chromosomes)*, that are randomly generated. During each iteration step, called a *generation*, each parent is evaluated by a *fitness function* [1]. The objective of the *fitness function* is to identify good and bad *parents* or candidate solutions. Good *parents* thrive and more of their information, called *chromosomes,* is passed on to the next generation by *crossover. Crossover* is a genetic operator that combines or *mates* two parents to produce a new set of *chromosomes* (*offspring*). Also to maintain genetic diversity along different generations and avoid local minima or maxima, a *mutation* rate is introduced into the GA. The *mutation* will randomly alter the sequence of *chromosomes* in a randomly chosen fit *parent*. This will allow inference if a particular chromosome will be modified or not, and avoid local optima [2].

Genetic Algorithms were invented in the early 1960s by John Holland and were later developed by his students and collaborators. GAs were first developed as an abstraction of biological evolution which gave a theoretical bases for adaptation in GAs. Holland devised GAs as a method for iterating through generations using an initial population of chromosomes that go through a “natural selection” process that was inspired by genetics; such as crossover or mating,

mutation, selection. This process “survival of the fittest” is governed by the fitness or survival criteria set in the GA[2].

8.2 Components of Genetic Algorithms

Parents

Parents (parent chromosomes) derive their name from parent chromosomes in biology. Each chromosome represents a potential solution in the algorithm. The chromosomes are made up of genes. In most instances these genes are represented in binary, real numbers, integers or letters. Genuinely, chromosomes can be given any representation that gives a finite number of genes that enables a solution [3, 4]. Figure 8-1 illustrates two parent chromosomes represented by binary genes; each chromosome with its respective sequence of genes represents a potential solution.

Chromosome 1
1 0 1 1 0 1 1
Chromosome 2
1 0 0 0 1 0 1

Figure 8-1 Depiction of 2 Chromosomes (Chromosome 1 and Chromosome 2) with their binary genes (1/0)

Fitness

The fitness, which is often encoded as a fitness function, is the “natural selection” criteria that allows for survival of the fittest. It defines the probability of a given chromosome or set of chromosomes being able to live and reproduce. As the GA iterates through an increasing number of generations, the individual fitness of each chromosome and of the population as a whole will increase, eventually leading to a global optimum solution [2, 5].

Selection

After encrypting a fitness function, a selection criteria has to be encoded in the GA. A selection criteria determines how to choose individuals in a given population that will go on to create offspring for proceeding generations, and how each offspring will be created [2, 6]. Therefore, the purpose is to select the fittest individuals to create new offspring for the new generation.

Crossover

One of the main differentiating characteristics of GAs as an optimization method is crossover. After a pair or more of chromosomes have been selected, these chromosomes mate to produce the next offspring, and the mating is governed by a crossover criteria. The most common forms of the criteria are the following:

Single-point Crossover

Note: " | " indicates the randomly chosen splicing/crossover point (one point).

The exchange of the genes that creates the new offspring occurs at a single splicing location. Consider the following chromosomes;

Parent Chromosome 1: 101|1011

Parent Chromosome 2: 1000|101

After these parents mate and crossover across the randomly selected point, the offspring chromosomes will be as follows:

Offspring Chromosome 1: 1010101

Offspring Chromosome 2: 1000011

As can be inferred from the offspring, Offspring Chromosome 1 obtained the remaining genes (binary digits) after the crossover point from Parent Chromosome 2, while in the case of Offspring Chromosome 2, the remaining genes (binary digits) after the crossover point were obtained from Parent Chromosome 1.

Two-point Crossover

Two Point crossover is similar to One Point crossover technique. However in the Two Point technique there are two instead of one crossover points. Again considering an example :

Parent Chromosome 1: 101|1|011

Parent Chromosome 2: 100|0|101

After these parents mate and the crossover across at the randomly selected point, the offspring chromosomes will be as follows:

Offspring Chromosome 1: 1010011

Offspring Chromosome 2: 1001101

As can be inferred from the offspring; Offspring Chromosome 1 obtained the genes (binary digits) after the first crossover point from Parent Chromosome 2, and from Parent Chromosome 1 after the second crossover point. In the case of Offspring Chromosome 2 the genes (binary digits) after the crossover point were obtained from Parent Chromosome 1 and from Parent Chromosome 2 after the second crossover point.

Arithmetic Crossover

In Arithmetic crossover, a mathematical function is used for each parent. In that, a function is set for each parent that determines how many genes, which genes, and/or in what sequence of genes to crossover and create the new offspring. We may consider the following formulation:

Parent 1: (7)(10)(0.3)

Parent 2: (5)(11)(12.1)

And the offspring formulation criteria is given by :

Offspring 1: Parent1*b + (3+b)*Parent2

Offspring 2: Parent1*(b*3) + (Parent2+b)

If the above parents mated or performed a crossover where b = 0.5, the following will be the results for each offspring (according to the formulas of Offspring1 and Offspring2)

Offspring1: (21)(43.5)(42.5)

Offspring2: (16)(26.5)(13.05)

Uniform Crossover

This is a probabilistic crossover that determines the crossover rate based on an apriori set mixing ratio. We may consider the following parent chromosomes with a mixing ratio of 0.5, which will result in the proceeding offspring.

Parent Chromosome 1: 11111111

Parent Chromosome 2: 00000000

Resulting Offspring:

Offspring Chromosome 1: 10110001

Offspring Chromosome 2: 00011010

Due to the 0.5 (50%) crossover rate, each of the resulting offspring contains 50% of its genes from one parent and the other 50% of the genes from the other parent. The genes are randomly sequenced for each offspring.

Heuristic Crossover

Another crossover type in GAs is heuristic crossover. It is an analytical crossover in which the search direction is determined by an operator that makes use of fitness values of the two parent chromosomes. An illustration of this is:

Offspring1 = (most fit parent) – (least fit parent) *0.175

Offspring 2 = (most fit parent) * 3

8.3 Optimization with Genetic Algorithms

Genetic Algorithms (GA) are iterative, parallel optimizers that have been successfully designed, developed and applied for a plethora of optimization problems[7].Though GAs might be computationally expensive in different occasions, they are well suited for global optimization convergence. GAs are less hindered by local optimum convergence as opposed to many other optimization algorithms and techniques[2, 8]. This characteristic has been attributed to the mutation rate in GAs and the stochastic approach[9, 10] it uses to converge[1, 11].

Convergence in GAs is retrieved from the provided candidate solutions. These candidate solutions or GA’s search space are provided with a notion of the

distance between each candidate solution. The GA searches the “search space” to choose candidate solutions to test against a fitness function or criteria. In most cases the next candidate solutions to be tested depends on previous fitness. The uniqueness of GA’s lies in that GAs assume best parents (i.e. best solution(s)) from different regions in the search space can be manipulated through crossover to produce fit and high quality offspring candidate solutions. The crossover and mutation are ways of moving a given set of population around on a landscape set by a fitness function. Therefore they can be less adapted to local peaks or optimums, and converge to global optimums[2, 12].

In Figure 8-2 below the effect of mutation on global optimum convergence is portrayed. It can be observed from the figure that the GA is not ensured to reach a global optimum without mutation. Moreover, extreme mutation rates tend to slow down GAs. In that, there is hardly any mutation applied at very low mutation rates, whilst high mutation rates the strings change at very fast rates that the algorithm does not have time to exploit more of the search space. It is also suggested that the mutation rate is the integral parameter that manipulates the performance of GAs[11].

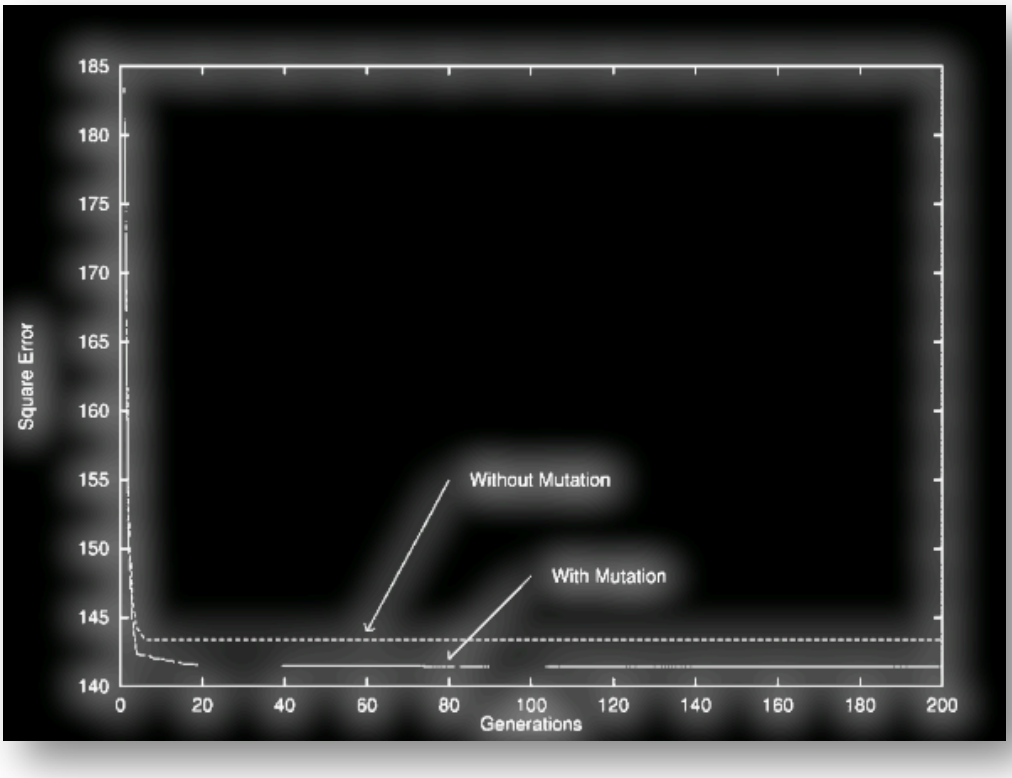

Figure 8-2 Shows a GA with and without distance-based mutation; Square Error across Generations.

8.4 References

[1] J. H. Holland, *Adaptation in Natural and Artificial Systems*. Ann Arbor, 1975.

[2] M. Mitchell, *An Introduction to Genetic Algorithms*. Cambridge,MA: MIT Press, 1996.

[3] Y.-C. Chiou and L. W. Lan, "Genetic clustering algorithms," *European Journal of Operational Research,* vol. 135, pp. 413-427, 2001.

[4] M. D. Vose, "The Simple Genetic Algorithm: Foundation and Theory." Cambridge,MA: MIT Press, 1999.

[5] Y. Zhou, "Study on Genetic Algorithm Improvement and Application," Mechanical Engineering, Worcester Polytechnic Institute, Worcester, 2006.

[6] A. Fanni*, et al.*, "A greedy genetic algorithm for continuous variables electromagnetic optimization problems," *Magnetics, IEEE Transactions on,* vol. 33, pp. 1900-1903, 1997.

[7] M. L. Raymer*, et al.*, "Dimensionality reduction using genetic algorithms," *Evolutionary Computation, IEEE Transactions on,* vol. 4, pp. 164-171, 2000.

[8] L. J. Eshelman, "The chc adaptive search algorithm: How to have safe search when engaging in nontraditional genetic recombination," in *Foundations of Genetic Algorithms-1*: Morgan Kauffman, 1991, pp. 265-283.

[9] D. R. Jones and M. A. Beltramo, "Solving partitioning problems with genetic algorithms," in *Proc. 4th Int. Conf. Genetic Algorithms*, San Mateo, CA, 1991.

[10] S. Z. Selim and K. Alsultan, "A simulated annealing algorithm for the clustering problem," *Pattern Recognition,* vol. 24, pp. 1003-1008, 1991.

[11] K. Krishna and M. Murty, "Genetic k-means algorithm," *IEEE Trans. on Systems, Man and Cyber.,* vol. 29, 1999.

[12] A. H. Wright, "Genetic algorithms for real parameter optimization," in *Foundations of Genetic Algorithms* vol. G. Rawlins, ed.: Morgan Kaufmann, 1991.

Chapter 9: Genetic Algorithm Clustering Technique for fMRI Data Analysis: A New FMRI ICA Algorithm

9.1 Motivation and Background

In recent years, a number of methodologies have been developed and implemented for analysis of group fMRI data. Among these methodologies is independent component analysis (ICA). Since ICA is a data driven analysis method, and because of its minimal assumptions, it has proven to be a very powerful data analysis methodology for single participant and group fMRI data[1]. Current group ICA analysis methods rely on hierarchical, K-means, and/or fuzzy logic approaches[2]. Such methods are known to be affected by local optimums and are more prone to converging to local optimum results, and thus often may provide suboptimal solutions [3]. On the other hand, genetic algorithms are well suited for converging to the global optimum(s) and are not hindered by local optimum(s) [4]. Also, with regards to group ICA analysis of fMRI data, a genetic algorithm (GA) will ultimately converge to a global optimum and can provide a deterministic partition or clustering of fMRI time series, leading to an optimum group activation map. Therefore we have designed and developed a genetic algorithm based clustering technique for group ICA fMRI data analysis we called GAICA.

9.2 Methods and Design

FMRI Data Acquisition , Stimulus Paradigm, and Participants

The fMRI data was obtained from the ICA GIFT project database, with permission from Medical Imaging Analysis Laboratory, University of New Mexico [5] [6]. The fMRI data was from three right-handed male participants with normal vision. The stimuli was a visuomotor paradigm (Figure 9-1). The visual paradigm consisted of an 8 Hz reversing checkerboard displayed for 15 seconds in the right visual hemifield. Then it was followed by an asterisk fixation of 5 seconds, followed by another 15 seconds of checkerboard, but presented to the left visual hemifield. Then another asterisk fixation for 20 seconds. These events were repeated four times for a total of 220 seconds, hence time points. The motor task had the participants, at a self-paced rate, sequentially touching their thumb to all four fingers, back and forth, using the hand on the same side where the visual stimulus is displayed [5, 6]. This fMRI data was acquired on a 1.5T Philips Medical Systems' MRI. An Echo planar sequence was used to acquire the functional images (64x64 matrix; flip angle = 90°; TR = 1000 ms; TE = 39 ms; FOV=24 cm; slice thickness, 5 mm; 18 slices) each with a 3 minute 40-s period for a total of 220 time points [5].

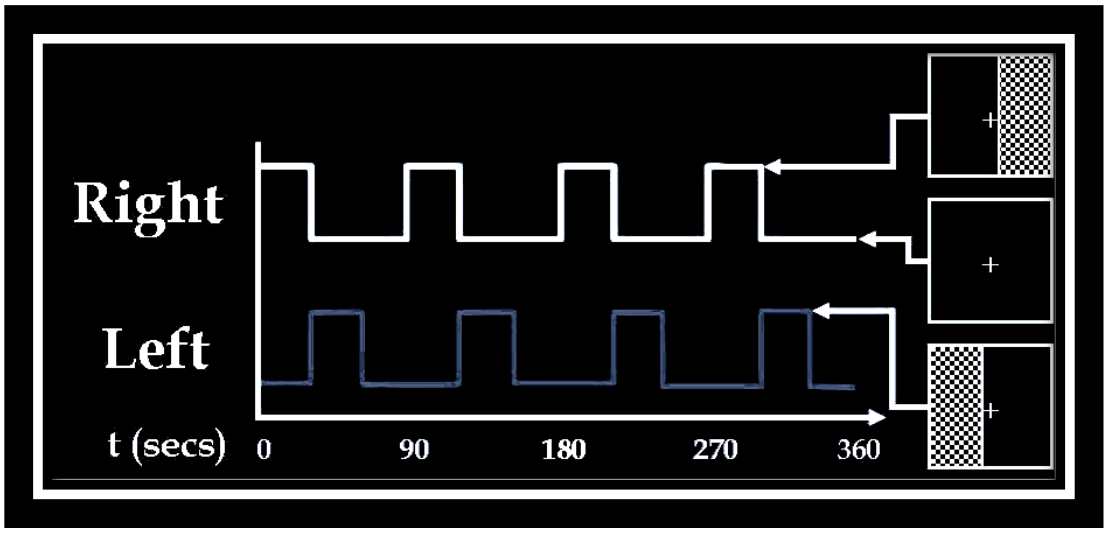

Figure 9-1 Visuomotor stimuli paradigm.

FMRI Data Preprocessing

Images were corrected for timing differences using Fourier interpolation. Then the data were motion corrected, spatially smoothed with a 6x6x10mm Gaussian kernel and spatially normalized into the standard Montreal Neurological Institute spaced, and converted to standard Talairach space [7] using SPM99 software package [6, 8].

Framework and Design of GAICA

The framework of the new clustering algorithm for fMRI ICs is provided in Figure 9-2. We will refer to this new algorithm as GAICA. The first phase of the framework constitutes fMRI data preprocessing of which steps were stated earlier. The preprocessing steps constitute spatial and temporal alignment, motion correction, normalization, and smoothing. Then the data is analyzed via GIFT algorithms [6] for data reduction using principle component analysis, and then for ICA.

The third phase is GAICA, as seen in Figure 9-2. This is where ICs of the participants are optimally partitioned. The initialization step generates the initial population of parents or candidate cluster solutions randomly. Then, the fMRI time series are participanted to a fitness function. The fit parents according to the fitness function are selected, and mate (crossover) to produce the next generation where the offspring will have come from the best parents. Therefore ultimately providing the best solution. The next step is a mutation operator where a number of parents are mutated. It is recommended that the mutation probability be low (~.005 - .05), because high values may sometimes lead to oscillating behavior of the genetic algorithm[9]. In the case of GAICA, the mutation acts at a .01 probability to randomly choose a parent(s) and randomly alter its genetic makeup to avoid local optimums. Then, if the end of generations are reached, the resultant most fit parent (global optimum fMRI ICs cluster) will be selected. Otherwise GAICA will continue to iterate until the last generation or apriori set convergence criteria is met.

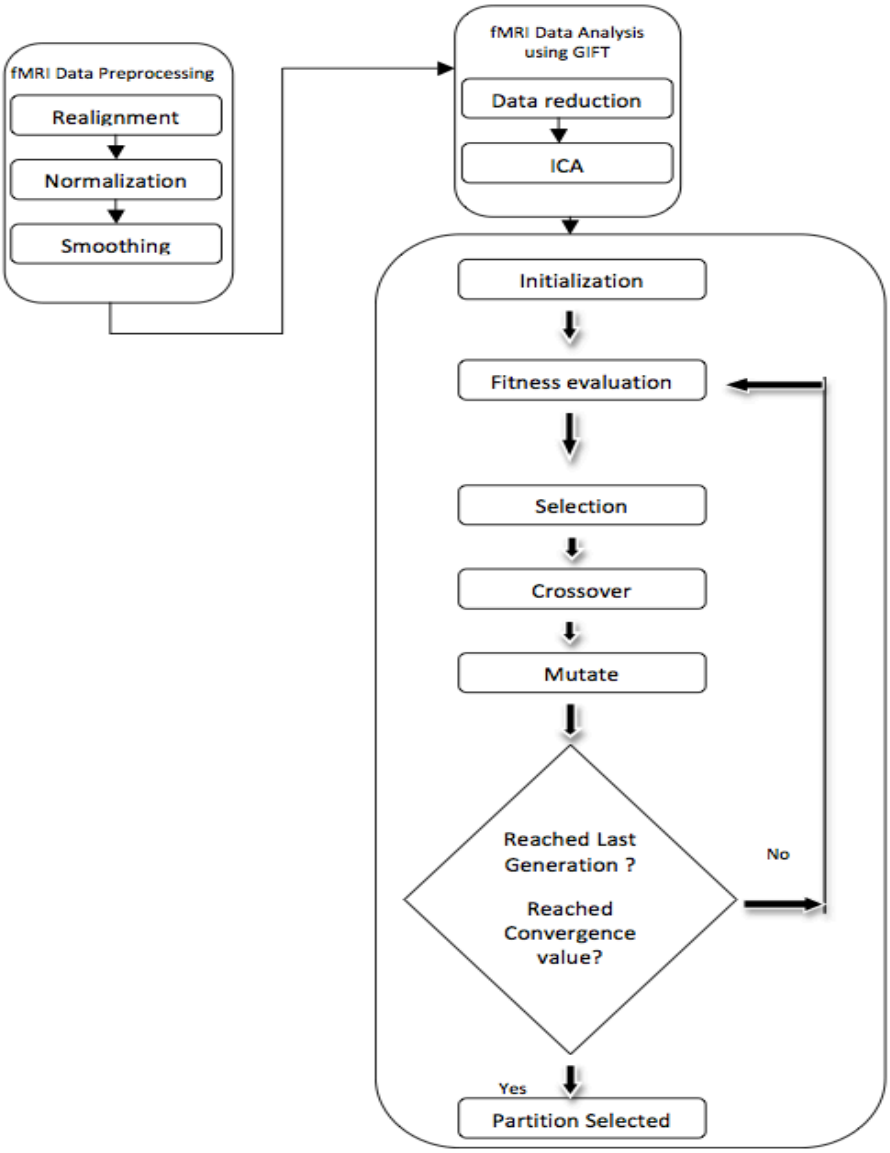

Figure 9-2 Framework (starting from the left) for fMRI data analysis using GAICA (third phase).

GAICA Encoding and steps of the algorithm design

We start out with an *N* number of fMRI independent components (ICs) time series. Each IC represents fMRI intensity values across different time points respectively. The goal of the GAICA is to output an optimum partition, so that the within cluster sums of squares is minimized. In that, GAICA starts out with an initial amount of parents and number of clusters. Each parent represents a

cluster solution through its chromosomes. The GAICA maintains a population of solutions (parents). Each parent is coded by a string of length *n* ($a_1,a_2,a_3,...,a_n$), where a_n takes a unique character that represents the cluster index to which a respective fMRI IC belongs. For example $a_1a_2a_3 = aba$ encodes a cluster solution (parent) of 3 fMRI ICs; where the first and third fMRI ICs (chromosomes) belong to the same cluster *a* and the second fMRI IC belongs to cluster *b*. Also, the GAICA ensures that each of the initial parents represents all cluster indices.

After the initial parent population is randomly derived, in the second step of GAICA, each fMRI IC time series is subjected to a fitness function (F) (Equation 9-1) to measure the correlation distance between the ICs (*x*). The GAICA seeks to minimize the fitness function (F). Therefore selecting only the most fit to be parents for the next generation.

F = d_{rs}; **Equation 9-1**

$$d_{rs} = 1 - \frac{(x_r - \bar{x}_r)(x_s - \bar{x}_s)'}{[(x_r - \bar{x}_r)(x_r - \bar{x}_r)']^{\frac{1}{2}}[(x_s - \bar{x}_s)(x_s - \bar{x}_s)']^{\frac{1}{2}}};$$

$$\bar{x}_r = \frac{1}{n}\sum_j x_{rj}$$

$$\bar{x}_s = \frac{1}{n}\sum_j x_{sj}$$

After the fitness evaluation of each fMRI IC cluster according to the fitness function, we used the roulette wheel strategy (Equation 9-2) for selection of parents in the previous generation.

$$P(S_i) = \frac{F(S_i)}{\sum_{j=1}^{N} F(S_i)}$$ **Equation 9-2**

In Equation 9-2, probability *P of* each parent S_i is dependent on the fitness value $F(S_i)$. This allows for our criteria to select all the initial parents, then after the first generation the top 50% most fit of previous parents are chosen and the top 50% of the current generation's offspring move on to mate (crossover). Therefore only the most fit parents (cluster candidates) move on and crossover, and allows for keeping the population pool constant throughout.

The fifth step of GAICA is the crossover. For the crossover we choose uniform crossover criteria, because it was found that such a crossover methodology helps to yield better results especially with smaller populations [10]. Figure 9-3 shows our uniform crossover criteria with a mixing ratio of 0.5.

P1:	**a**	**b**	**c**	**a**
P2:	a	a	b	a
O1:	**a**	**b**	b	a
O2:	**c**	**a**	a	a

Figure 9-3 Uniform crossover with 0.5 mixing ratio

Here in we show a simplified example of uniform crossover with 0.5 mixing ratio, which was used in GAICA. In that, each parent (P1 and P2 respectively) passes on 50% of its chromosomes which are the representative letters to each of the two offspring (O1 and O2 respectively).

As stated earlier, the GAICA has a mutation rate of .01 where a number of parents are randomly selected and a random number of their chromosomes are randomly altered. This perturbation of the population's characteristics prevents evolutionary dead ends and convergence to local optima. Then the GAICA checks if the last generation is reached; if not, it will continue to the next generation, otherwise it will output the global optima cluster solution represented by a parent. GAICA was designed, coded, and implemented using MATLAB (The Mathworks, Inc.).

GAICA Parameters and input data	
Population size	12 parents
Number of clusters	8 clusters
Crossover type and rate	Uniform crossover, 0.5
Mutation type and rate	Random mutation, 0.01
Number of fMRI time series ICs per participant	16

Table 9-1 GAICA algorithm GA parameters and number of ICs for each participant (input data).

Local and Global Optimum Measurement

An estimated optima was determined through different runs of k-means analysis. Since k-means is more prone to local maxima convergence, we ran the k-means analysis using MATLAB (The Mathworks, Inc.) on the ICs 50 times to get an estimate of at least the local maxima. The convergence value is the average distance between all fMRI ICs in a cluster; across all apriori set number of clusters. We assumed that the lowest of these values was the "best" local optimum convergence value. This is in order to determine if the GAICA converges to a global optimum partition.

The convergence value from kmeans was set as the upper threshold for GAICA. We then ran GAICA for several generations to determine if it converges to a value lower than that of kmeans. This value had to be also consistently acquired in order to determine if GAICA converged to a global maxima or not. Also the intra-cluster fMRI signal intensity ICs had to show a close or transient relationship in order to provide concrete evidence that such a partition is the global optimum solution.

9.3 Results

Figures 9-4 – 9-9 show the left and right cortical activations for each respective participant. These were derived using GIFT [6] single participant ICA analysis. Also, in each figure is the signal intensity fluctuations derived from the BOLD response during the fMRI acquisition. Both participants' 1 and 3 show close signal intensity fluctuations and amplitudes for the bilateral cortical activation task. These participants showed extensive visual cortex activation related to each respective lateralized visuomotor task. On the other hand, the signal intensity fluctuation of participant 2 tends to vary from that of participant 1 and participant 3. As for participant 2, there is noticeably less bilateral visual cortex activation (Figure 9-6 – 9-7) compared to participants 1 and 3.

The results from the k-means iterative runs are provided in Figure 9-10 below. The convergence value was based on the average intra-cluster correlation distance across all clusters in a single run. The convergence values ranged from 0.75 to 0.55. The convergence values did not follow any specific

trajectory (Figure 9-10) and the runs were independent and randomly generated at different time points.

The implementation of GAICA to the ICs from the 3 participants resulted in an optimum partition (Figure 9-11 and Figure 9-12). GAICA consistently converged to 0.53 convergence value which is lower than the lowest convergence value obtained using the standard k-means approach. Figure 9-11 provides a close depiction of the average within cluster distance across all iterations (generations). It can be seen from Figure 9-11 that as the generations progress in the algorithm, the within-cluster distance decreases gradually with minor oscillations. At generation 321 the global optimum partition is obtained.

Figure 9-12 provides the global optimum partition after all required generations (iterations) of GAICA. Clusters A and B are evidentially task related. Specifically, cluster A is for the left visuomotor task, and Cluster B is for the right visuomotor task. Clusters C,D, and E are transiently task related, and clusters F,G, and H contain signals that are not task related (i.e. scanner noise, physiological noise).

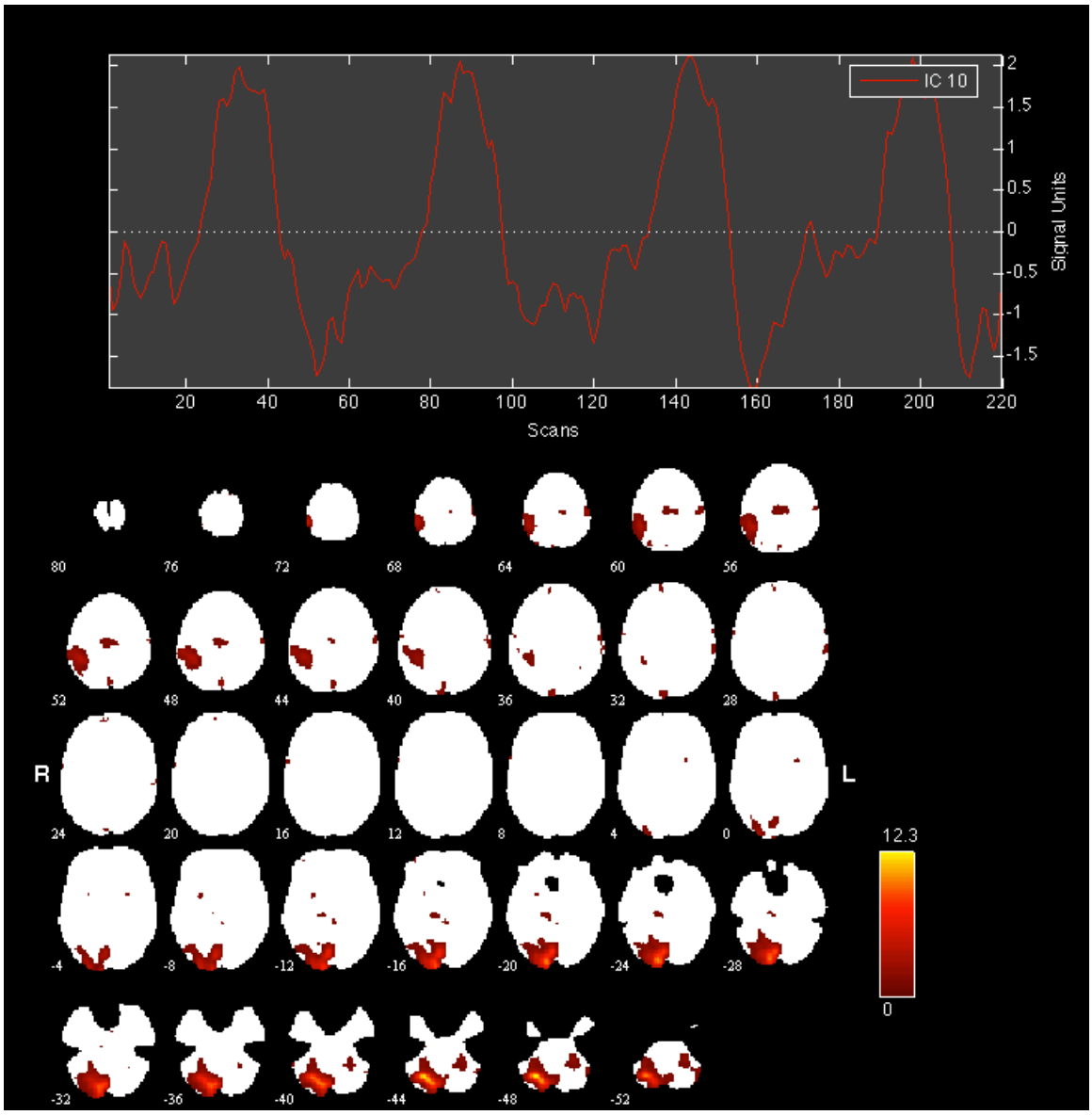

Figure 9-4 Activation map IC for left visuomotor task for participant #1. Significant activation is present (red, yellow) in the right visual and motor cortices. The first two rows show the right motor cortex activation, and the last two rows depict the right hemispheric visual cortex activation.

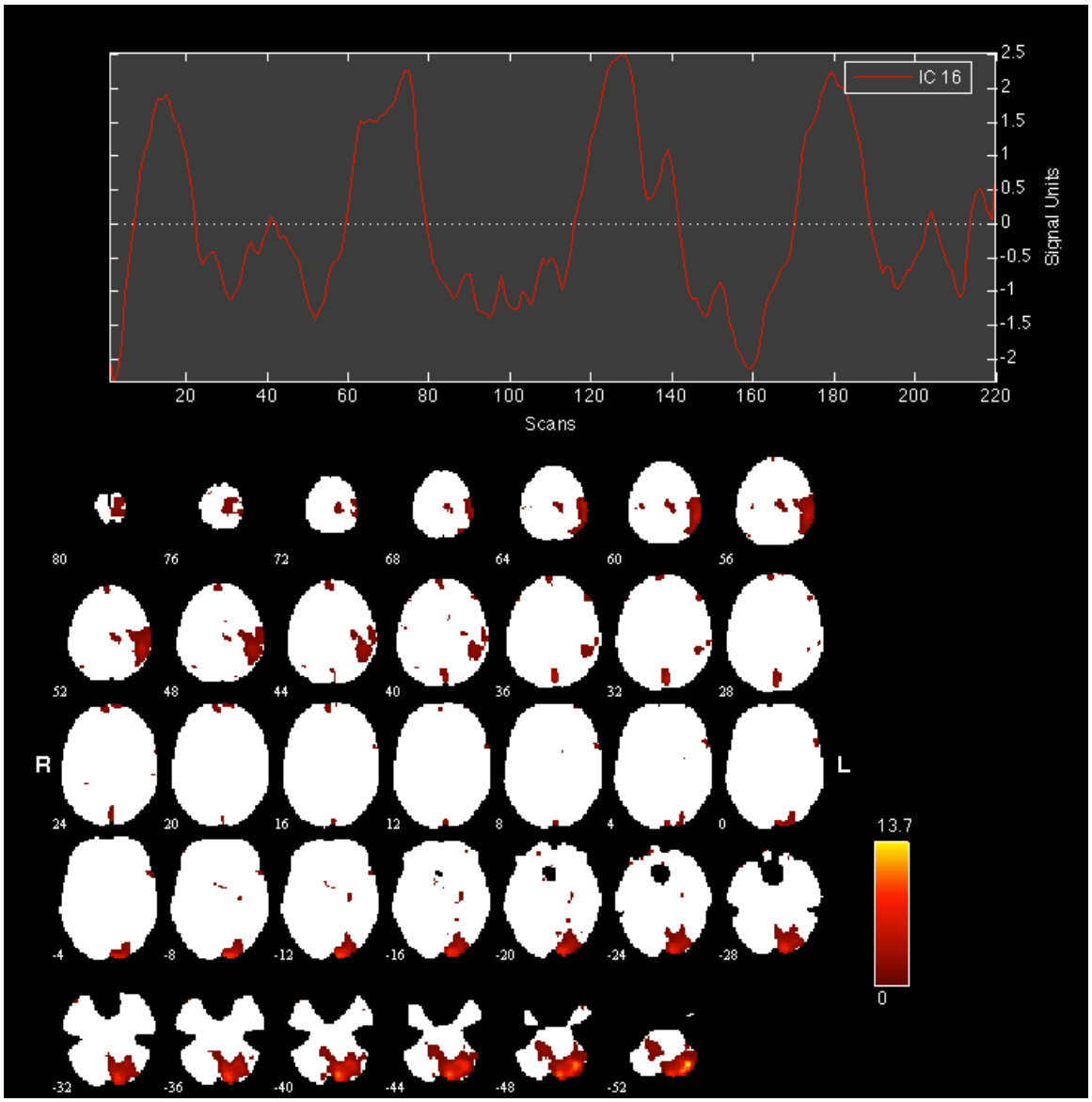

Figure 9-5 Activation map IC for right visuomotor task for participant #1. Significant activation is present (red, yellow) in the left visual and motor cortices. The first two rows show the left motor cortex activation, and the last two rows depict the left hemispheric visual cortex activation.

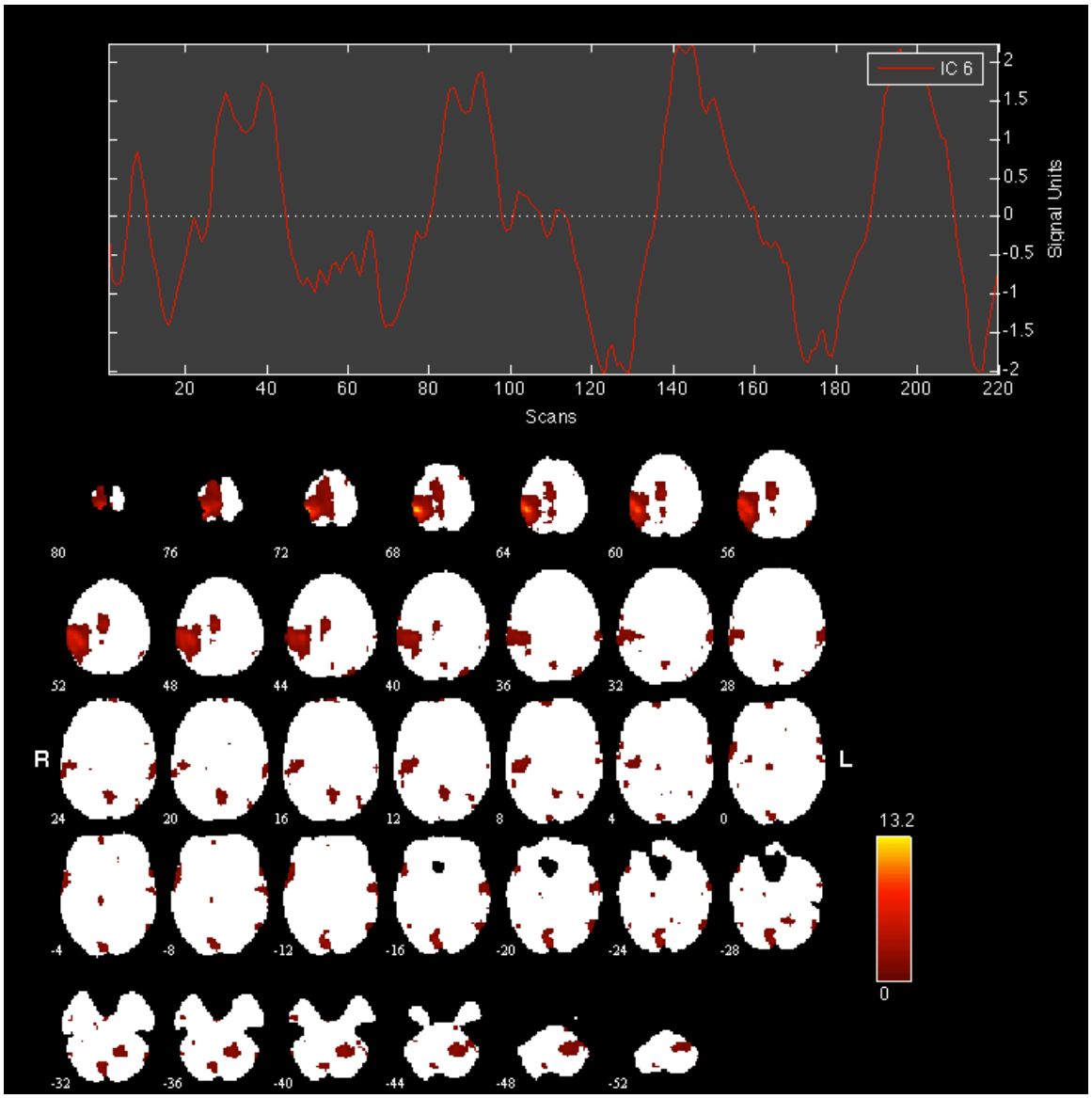

Figure 9-6 Activation map IC for left visuomotor task for participant #2. Significant activation is present (red, yellow) in the right visual and motor cortices. The first two rows show the right motor cortex activation, and the last two rows depict the right hemispheric visual cortex activation. Note that the visual cortex activation does not extend to much of the right visual cortex.

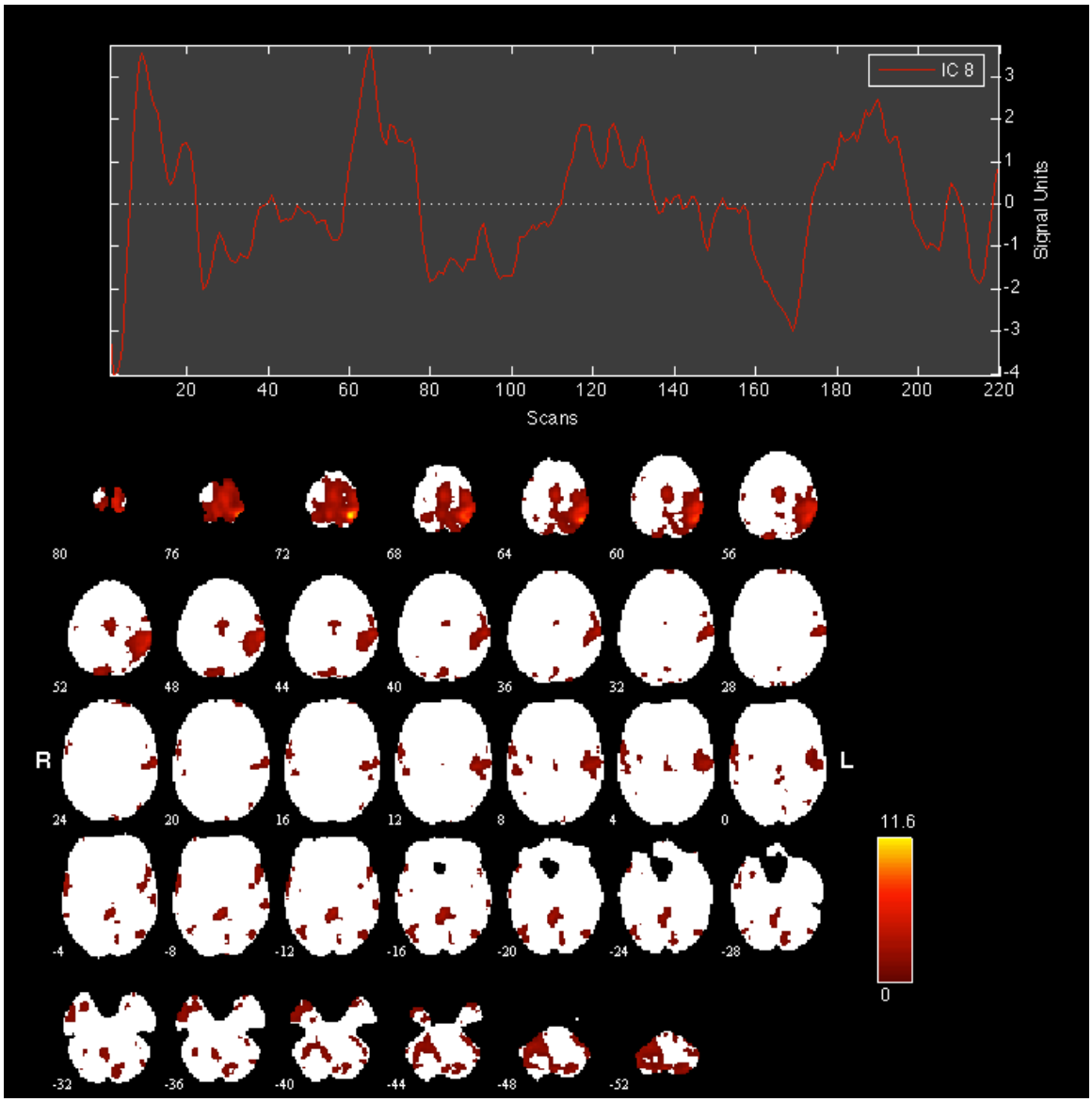

Figure 9-7 Activation map IC for right visuomotor task for participant #2. Significant activation is present (red, yellow) in the left visual and motor cortices. The first two rows show the left motor cortex activation, and the last two rows depict the left hemispheric visual cortex activation. Note that the visual cortex activation does not extend to much of the left visual cortex.

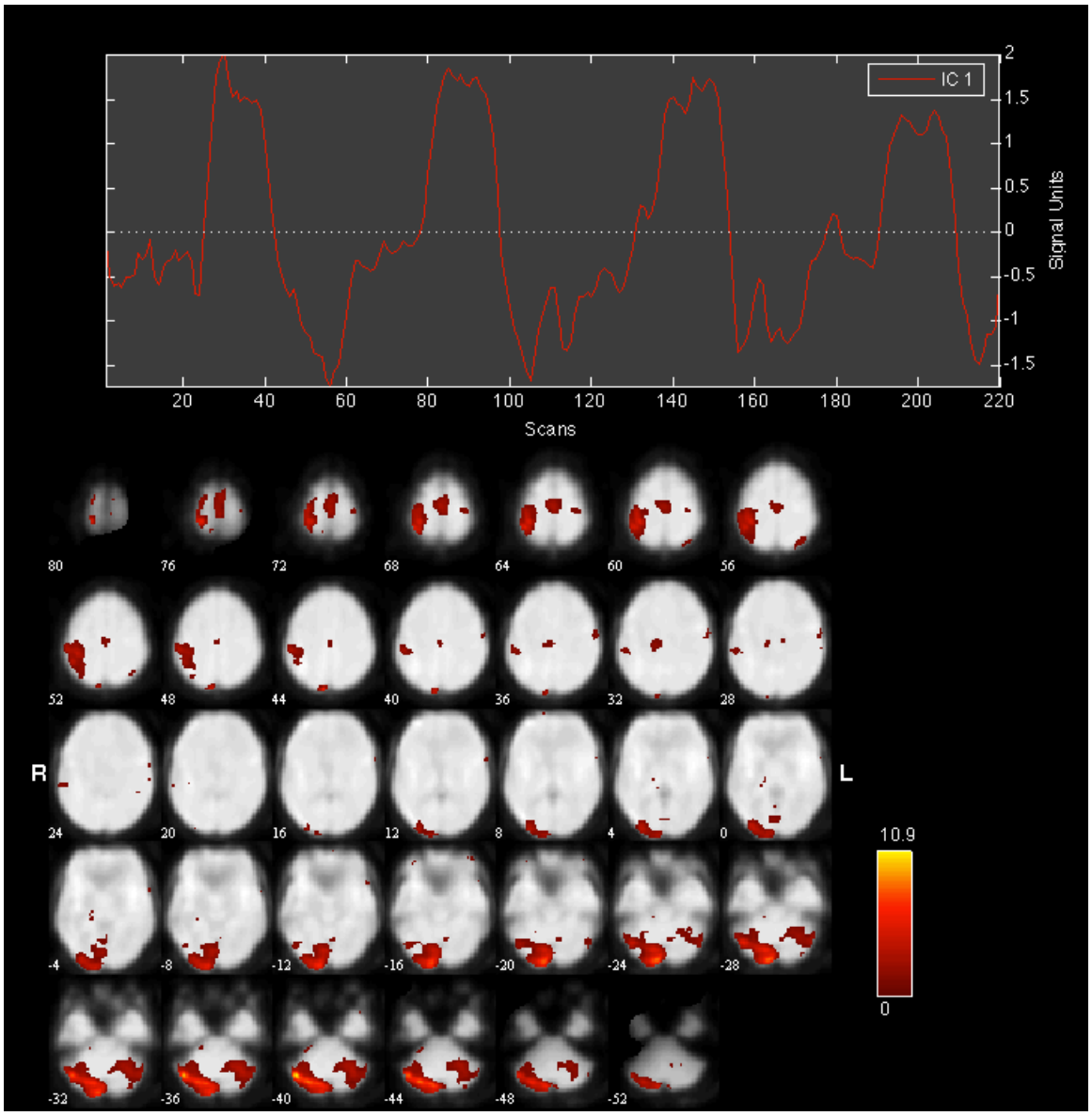

Figure 9-8 Activation map IC for left visuomotor task for participant #3. Significant activation is present (red, yellow) in the right visual and motor cortices. The first two rows show the right motor cortex activation, and the last two rows depict the right hemispheric visual cortex activation.

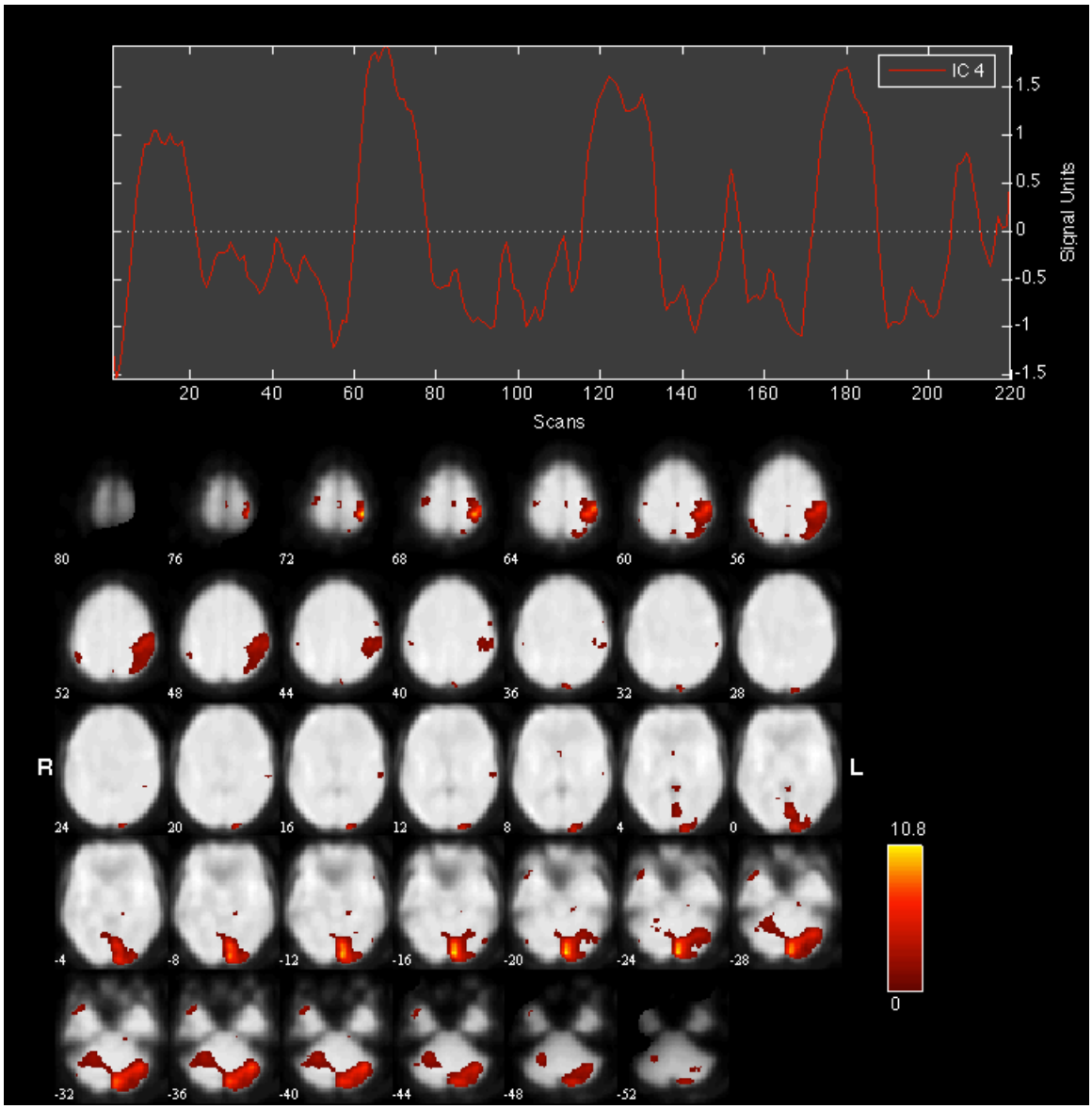

Figure 9-9 Activation map IC for right visuomotor task for participant #3. Significant activation is present (red, yellow) in the left visual and motor cortices. The first two rows show the left motor cortex activation, and the last two rows depict the left hemispheric visual cortex activation.

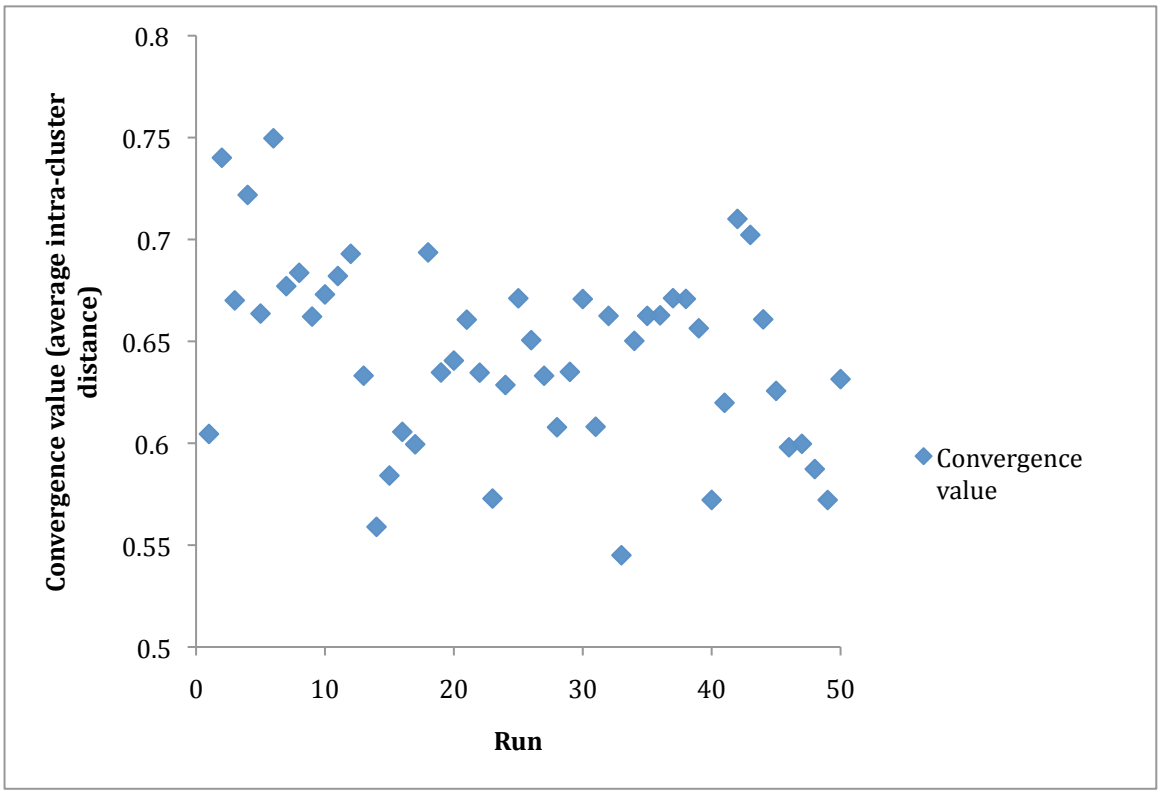

Figure 9-10 Scatter plot of convergence values of intra-cluster average for 50 runs of k-means analysis.

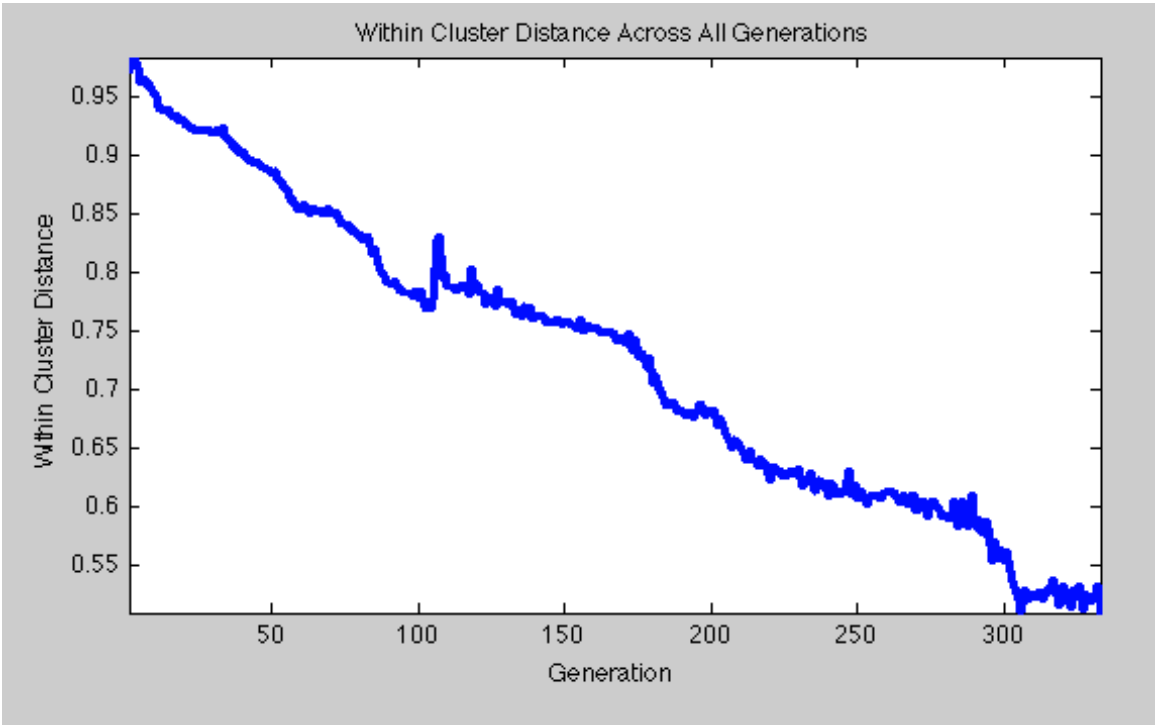

Figure 9-11 Intra-cluster average distance across all generations (iterations) of GAICA to converge to the global optimum convergence value.

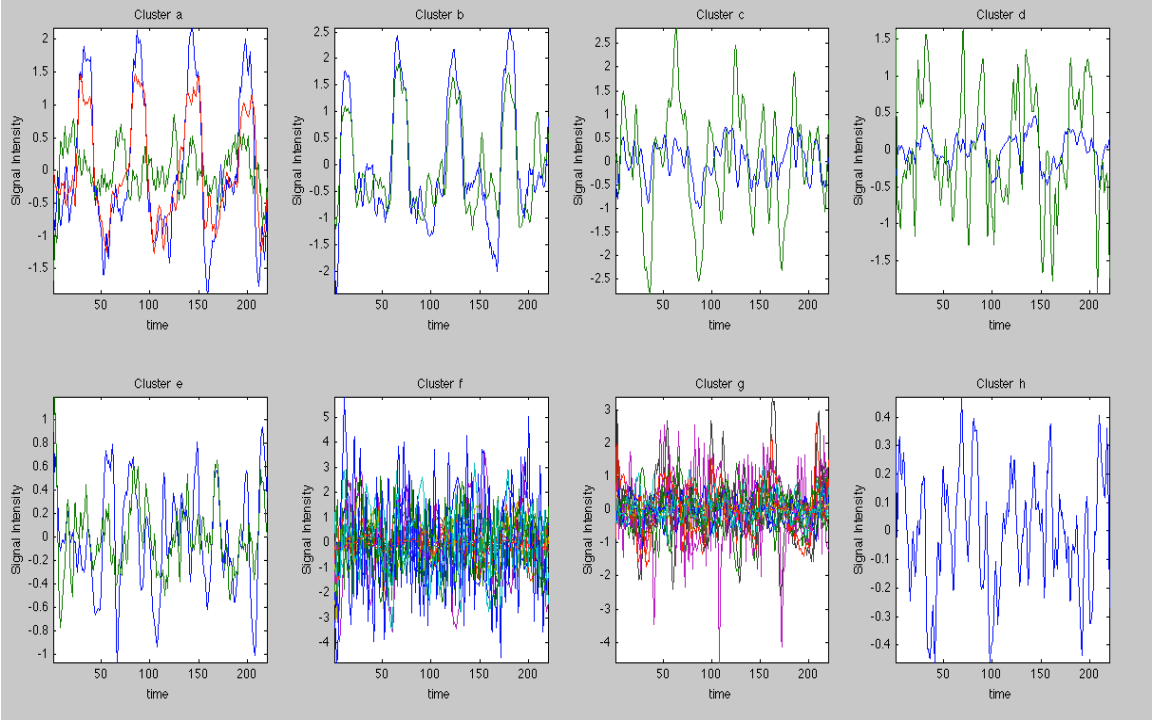

Figure 9-12 Global optimum partition of GAICA for the fMRI signal intensity ICs. Clusters are indexed alphabetically.

9.4 Discussion and Conclusions

A close analysis was conducted for the GAICA algorithm to provide evidence to global optimum convergence and ,thus, a global optimum partitioning of the fMRI signal intensity ICs. The purpose of this being; to provide a complimentary or supplementary technique towards group ICA fMRI data analysis. Therefore, I have designed, developed, and implemented GAICA using a genetic algorithm due to its robustness in converging to the global optima.

A standard k-means algorithm was designed for clustering and run 50 times. The purpose of these 50 runs is to provide evidence of different convergence values to be contrasted with GAICA, as well as to provide an upper threshold for GAICA convergence values. Figure 9-10 portrays the average intra-cluster distance (convergence value) obtained for each run, across all 50 runs of the k-means algorithm. There was no consistency among all runs. The convergence values ranged from 0.55 to 0.75. The convergence value of 0.55 was obtained only once across all 50 runs. Therefore if we assume this to be the global optima convergence value, this would mean that the k-means converged to a local optimum partition of the fMRI ICs 49/50 times, or 99% total local optima convergence. Again, this is assuming that 0.55 is the global optima generated by k-means algorithm.

In order to test whether or not GAICA provides global optimum partition for the fMRI signal intensity ICs, we allowed GAICA to run for several generations (iterations) until it reached convergence. Repeatedly, GAICA converged to a convergence value of 0.53, but varied in the number of generations it required to

obtain this convergence value. The number of generations ranged from 100 to 500 generations (iterations) to reach this optimum convergence value for partitioning of the fMRI time series. See Figure 9-11 for a depiction of the decrease in the intra-cluster average distance until the global optimum convergence values is reached at generation 321.

The convergence value obtained using GAICA is the global optima, since it was lower than the lowest convergence value from the k-means approach, and it was demonstrated to be acquired repeatedly in GAICA. This is aside from the fact that genetic algorithm computations have been shown to be robust for global optima convergence in different implementations [10-16].

The GAICA solution provided in Figure 9-12 provides a global optimum partition of the fMRI signal intensity time series (ICs) according to correlation distance between intra-cluster signals. This, therefore allows clustering for fMRI data without the hindrance of frequent local optimum solutions. Importantly, GAICA is able to partition data into task related (clusters a and b in Figure 9-12), transiently task related (clusters c,d, and e in Figure 9-12), and non-task related partitions (clusters f, g, and h in Figure 8-12).

As stated earlier, GAICA is based on a genetic algorithm (GA), and GAs are known to be computationally expensive [17]. For the current fMRI data and GAICA parameters, 100 generations would take approximately 3.5 minutes on a single processor. However, the issue of expensive computation can be resolved by parallelizing the GAICA algorithm code and running it on more than one processer. Current technology allow for more than one processor on a computer

and there are other schemes (i.e. cluster computers) that allow for several processors, and thus, faster computations.

Despite being computationally expensive, GAICA is able to provide a global optimum partition of the fMRI time series ICs and is less hindered by local optima, which the k-means is much more prone to. We have shown that GAICA may be used as a complimentary or supplementary approach for fMRI group ICA analysis. In that, it is able to provide a global optimized partitioning mechanism to study brain activations, and related fMRI signals may be clustered together. Furthermore, task-related, transiently task related, non-task related, and physiological and scanner noise can be clustered respectively. Therefore providing a robust mechanism for group ICA clustering of fMRI time series and an optimizated method to study brain activation.

Future Work

A few directions to develop on this work, may include a dedicated optimization algorithm to optimize the mutation rate based on the number of fMRI data series to be analyzed. Also, an optimization algorithm can be developed to choose the initial set of parents based on the size of the fMRI data set at hand. In both these directions, further developments need to be addressed regarding reducing computational time.

9.5 References

[1] M. J. McKeown and T. J. Sejnowski, "Independent component analysis of fMRI data: Examining the assumptions," *Hum. Brain Map.,* vol. 6, pp. 368-372, 1998.

[2] R. Baumgartner*, et al.*, "Quantification in Functional Magnetic Resonance Imaging: Fuzzy Clustering vs. Correlation Analysis," *Magnetic Resonance Imaging,* vol. 16, pp. 115-125, 1998.

[3] C. Goutte*, et al.*, "On Clustering fMRI Time Series," *NeuroImage,* vol. 9, pp. 298-310, 1999.

[4] J. H. Holland, *Adaptation in Natural and Artificial Systems*. Ann Arbor, 1975.

[5] V. D. Calhoun*, et al.*, "A method for comparing group fMRI data using independent component analysis: application to visual, motor and visuomotor tasks," *Magn Reson Imaging,* vol. 22, pp. 1181-1191, 2004.

[6] V. D. Calhoun. (2004). *Group ICA of fMRI Toolbox (GIFT)*. Available: http://icatb.sourceforge.net

[7] J. Talairach and T. P. , "A co-planar stereotaxic atlas of a human brain," *Stuttgart7 Thieme,* 1988.

[8] V. D. Calhoun*, et al.*, "A method for making group inferences from functional MRI data using independent component analysis," *Hum. Brain Map.,* vol. 14, pp. 140-151, 2001.

[9] L. Shi*, et al.*, "Unifying Genetic Algorithm and Clustering Method for Recognizing Activated fMRI Time Series," in *Advances in Machine Learning and Cybernetics*, ed: Springer Berlin / Heidelberg, 2006.

[10] L. J. Eshelman, "The chc adaptive search algorithm: How to have safe search when engaging in nontraditional genetic recombination," in *Foundations of Genetic Algorithms-1*, ed: Morgan Kauffman, 1991, pp. 265-283.

[11] D. E. Goldberg, *Genetic Algorithm in Search, Optimization and Machine Learning*. Boston: Addison-Wesley Longman Publishing Co, 1989.

[12] D. R. Jones and M. A. Beltramo, "Solving partitioning problems with genetic algorithms," in *Proc. 4th Int. Conf. Genetic Algorithms*, San Mateo, CA, 1991.

[13] A. H. Wright, "Genetic algorithms for real parameter optimization," in *Foundations of Genetic Algorithms* vol. G. Rawlins, ed., ed: Morgan Kaufmann, 1991.

[14] H. Mühlenbein and D. Schlierkamp-Voosen, "Predictive Models for the Breeder Genetic Algorithm: I. Continuous Parameter Optimization," *Evolutionary Computation,* vol. 1, pp. 25-49, 1993.

[15] L. D. Whitley, *Foundations of Genetic Algorithms 2*, 1993.

[16] M. Srinivas and L. M. Patnaik, "Genetic Algorithms: a survey," *Computer,* vol. 27, pp. 17-26, 1994.

[17] M. Mitchell, *An Introduction to Genetic Algorithms*. Cambridge,MA: MIT Press, 1996.

Appendix I

Stimuli letter strings and respective specifications

frequency	Real words without diacritics	Real words with diacritics	Quantization of words that are different	Word meaning with diacritics	transliteration	# of letters	# of syllables	# of diacritics	Non-words with no diacritics	Non-words with diacritics	Real words with diacritics	Quantization measure words vs. non-words
772.33	قانون	قانُون		law	ganoon	5	2	1	ناقون	ناقُون	قانُون	0
698.65	حديث	حَديث		topic	hadeeth	4	2	2	ثديح	ثَديح	حَديث	0
668.37	فريق	فَريق		team	fareeq	4	2	2	قديف	قَريف	فَريق	0
571.03	حقوق	حُقُوق		rights	hoqooq	4	2	2	قحوق	قُحُوق	حُقُوق	0
567.7	بيان	بَيان		formal statement	bayan	4	2	1	نباي	نَباي	بَيان	0
553.47	نائب	نائب		member	naib	4	2	1	بائن	بائن	نائب	0
551.99	لقاء	لقاء		meeting	liqa'	4	2	1	إلاق	إلاق	لقاء	0
541.34	أعضاء	أعْضاء		members	a'tha'	5	2	2	أضعاء	أضْعاء	أعْضاء	0
538.45	مناطق	مَناطق		areas	manatiq	5	3	2	طنامق	طنامق	مَناطق	0
533.12	إنسان	إنْسان		human	insan	5	2	2	سأنان	سأنان	إنْسان	0
519.51	ائرط	طائر		bird	ta'ir	4	2	1	راطئ	راطئ	طائر	0
519.41	مكان	مَكان		place	makan	4	2	1	نكام	نكام	مَكان	0
496.66	بطول	بُطُول		bottles	bottool	4	2	2	طلوب	طلُوب	بُطُول	0
469.44	أراضي	أراضي		lands	araathee	5	2	2	رائاضي	رَئاضي	أراضي	0
421.73	نتائج	نَتائج		results	natai'j	5	3	2	نئاتج	نَئاتج	نَتائج	0
414.17	نهاية	نهاية		an/the end	nihayah	5	2	2	منايۃ	منايَة	نهايَة	0
409.97	مكتب	مَكْتَب		office	maktab	4	2	3	كمتب	كَمْتَب	مَكْتَب	0
386.29	أسواق	أسْواق		markets	aswaq	5	2	2	سئواق	سَئْواق	أسْواق	0
357.49	إعلام	إعْلام		media	I'llam	5	2	2	مئلاع	مئلاع	إعْلام	0
338.16	أحزاب	أحْزاب		parties (as in political parties)	ahzab	5	2	2	حئزاب	حَئْزاب	أحْزاب	0
336.85	أسباب	أسْباب		reasons	asbab	5	2	2	أبساب	أبْساب	أسْباب	0

326.13	خليج	خَليج		gulf	khaleeij	4	2	2	لجيخ	لَجيخ	خَليج	0
308.35	ظروف	ظُرُوف		reasons/excuses	thoroof	4	2	2	رظوف	رُظوف	ظُرُوف	0
300.78	زعيم	زَعِيم		leader	zaeim	4	2	2	زميع	زَميع	زَعِيم	0
299.93	أمير	أمِير		amir	ameir	4	2	2	مأير	مَأير	أمِير	0
294.37	أهداف	أهْداف		goals	ahdaaf	5	2	2	هأداف	هَأداف	أهْداف	0
289.44	أنباء	أنْباء		news	anba'	5	2	2	نئباء	نَئباء	أنْباء	0
280.47	أهرام	أهْرام		pyramids	ahram	5	2	2	أرهام	أرْهام	أهْرام	0
277.38	إعلان	إعْلان		ad	I'laan	5	2	2	إنلاع	إنْلاع	إعْلان	0
271.36	توقيع	تَوْقِيع		signature	tawgee'	5	2	3	قوتيع	قَوْتِيع	تَوْقِيع	0
269.06	عضو	عُضْو	1 – (000) (010)	member	O'dho	3	2	2	ضعو	ضُعْو	عُضْو	0
268.04	فيلم	فِيلم	2 – (101) (011)	film	feilm	4	1	1	ليفم	ليفِم	فِيلم	0
267.15	أموال	أمْوال	3 – (010) (010)	money	amwaal	5	2	2	لئوام	لَئُوام	أمْوال	0
265.24	برلمان	بَرْلَمان		parliament	barlaman	6	3	3	مرلبان	مَرْلَبان	بَرْلَمان	0
258.08	سلاح	سِلاح		weapon	silah	4	2	1	حسال	حِسال	سِلاح	0
249.27	قائد	قائِد		leader	qaai'd	4	2	1	دائق	دائِق	قائِد	0
247.06	صندوق	صُنْدُوق	4- (000) (002)	box	sandook	5	2	3	ندصوق	نْدُصوُق	صُنْدُوق	0
243.88	مقر	مَقَرّ	5 – (000) (101)	gathering place	maqar	3	2	3	قيرم	قَيَرمَ	مَقَرّ	0.03
226.78	حياة	حَياة		life	hayat	4	2	1	تياح	تَياح	حَياة	0
225.1	شروط	شُرُوط	6 – (110) (000)	guidelines	shoroot	4	2	2	رشوط	رُشُوط	وطشُرُ	0
224.18	تأمين	تَأمِين	7 – (000) (111)	insurance	tai'meen	5	2	3	أنمين	أنْمِين	تَأمِين	0
222.44	أطفال	أطْفال	8 – (011) (000)	kids	atfaal	5	2	2	طأفل	طأفِل	أطْفال	0
222.41	أستاذ	أسْتاذ	9 – (010) (000)	teacher	ostaath	5	2	2	سأتاذ	سْأتاذ	أسْتاذ	0
221.62	شؤون	شُؤُون	10 – (001) (210)	affairs	sho'oon	4	2	2	نؤوش	نْؤُوش	شُؤُون	0
215.47	أصحاب	أصْحاب	11 – (110) (110)	friends	As-haab	5	2	2	صئحاب	صَئحاب	أصْحاب	0
GAP 14.1												
200.12	شعوب	شُعُوب		populations	sho'oob	4	2	2	بعوش	بُعُوش	شُعُوب	0
198.93	متر	مِتْر	2 – (101) (110)	meter	mitr	3	1	2	متير	مِتَيْر	مِتْر	0.1
198.37	أبناء	أبْناء		children	abnaa'	5	2	2	بنئاء	بَنَئْاء	أبْناء	0
197.49	ملف	مِلَفّ	5 – (000) (101)	file	milaf	3	2	3	لمف	لَمَفّ	مِلَفّ	0
195.38	مطار	مَطار		airport	mataar	4	2	1	رماط	رَماط	مَطار	0

194.82	تـَيـّار	تَيّار		current	taiyaar	4	2	2	ريات	رَيّات	تَيّار	0
190.98	شاعر	شاعِر		poet	shaai'r	4	2	1	راشع	راشِع	شاعِر	0
190.06	مصارف	مَصارف		banks	masaarif	5	3	2	صمارف	صَمارف	مَصارف	0
189.89	صحفي	صُحُفـيّ		journalist	sahafeei	4	3	4	حصفـي	حُصُفـيّ	صُحُفـيّ	0
189.53	مراكز	مَراكِز		centers	maraakiz	5	3	2	رماكز	رَماكِز	مَراكِز	0
181.94	قواعد	قَواعِد		basis (as in military basis)	qawaai'd	5	2	2	عواقد	عَواقِد	قَواعِد	0
177.1	مهرجان	مَهْرَجان		festival	mahrajaan	6	3	3	جمهران	جَمْهَران	مَهْرَجان	0
159.28	أصوات	أصْوات		sounds	aswaat	5	2	2	صىَوات	صَىَوات	أصْوات	0
158.82	علوم	عُلُوم		sciences	oloom	4	2	2	لعوم	لُعُوم	عُلُوم	0
152.28	جنود	جُنُود		soldiers	jonood	4	2	2	دنوج	دُنُوج	جُنُود	0
150.47	شارع	شارع		street	shaari'	4	2	1	راشع	راشِع	شارِع	0
149.39	كهرباء	كَهْرَباء		electricity	kahrabaai'	6	3	3	هكرباء	هَكْرَباء	كَهْرَباء	0
148.01	مدارس	مَدارِس	3 – (010) (000)	schools	madaaris	5	3	2	دمارس	دَمارِس	مَدارِس	0
147.61	مراحل	مَراحِل	6 – (110) (110)	stages (as in stages in a video game)	maraahil	5	3	2	رماحل	رَماحِل	مَراحِل	0
144.33	أسماء	أسْماء		names	asmaai'	5	2	3	سىَماء	سَىَماء	أسْماء	0
143.6	بنوك	بُنُوك		banks	bonook	4	2	2	كنوب	كُنُوب	بُنُوك	0
143.47	علاج	عِلاج		medicine	ilaaj	4	2	1	جلاع	جِلاع	عِلاج	0
141.37	جمهور	جُمْهُور	7 – (000) (111)	audience	jomhoor	5	2	3	مهجور	مُهْجُور	جُمْهُور	0
140.84	أحكام	أحْكام		laws	ahkaam	5	2	2	حىكام	حَىكام	أحْكام	0
140.38	شعار	شِعار		slogan	shia'aar	4	2	1	رشاع	رشاع	شِعار	0
140.22	روساء	رُوَساء		leaders	roa'saai'	5	2	2	أرسؤاء	أرَسؤاء	رُوَساء	0
135.32	جزيرة	جَزيرَة	8 – (011) (011)	island	jazeerah	5	3	3	زجيرة	زَجيرَة	جَزيرَة	0
134.59	لواء	لِواء		brigade	liwaai'	4	2	1	لاوء	لاوِء	لِواء	0
134.46	أفلام	أفـلام		films	aflaam	5	2	2	فىلام	فَىلام	أفـلام	0
132.72	كأس	كأس	1 – (000) (010)	cup	ka's	3	2	2	سىك	سَىك	كأس	0
131.14	طلاب	طلاب		students	tolaab	4	2	2	لباط	لُباط	طلاب	0
130.62	جماهير	جَماهير		audiences	jamaheer	6	3	2	مجاهير	مَجاهير	جَماهير	0
129.5	تعليق	تَعْليق	4 – (000) (002)	comment	tai'leeq	5	2	3	عتليق	عَتْليق	تَعْليق	0
99.22	شوارع	شَوارِع	9 – (010) (010)	streets	shawari'	5	3	2	رواشع	رَواشِع	شَوارِع	0

99.09	صواريخ	صَواريخ	11 – (110) (000)	rockets	sawareekh	6	3	2	رواصيخ	رَواصيخ	صَواريخ	0
98.1	وثايْق	وَثايْق		documents	wathaai'q	5	2	2	وئاثق	وَئاثق	وَثايْق	0
96.06	رأخبا	أخْبار		news	akhbaar	5	2	2	أبخار	أبْخار	أخْبار	0
95.9	بريد	بَريد		mail	bareed	4	2	2	رديب	رَديب	بَريد	0
93.01	صحراء	صَحْراء		desert	sahraa'	5	2	2	رصحاء	رَصْحاء	صَحْراء	0
92.88	أبحاث	أبْحاث		research (plural)	abhaath	5	2	2	بئحاث	بَئْحاث	أبْحاث	0
87.19	معاييِر	مَعاييِر		standards	ma'ayeer	6	3	2	رعاييم	رَعاييم	مَعاييِر	0
86.56	تكاليف	تَكاليف		expenses	takaleef	6	3	2	لكتاليف	لكَتاليف	تَكاليف	0
85.35	دمار	دَمار		destruction	damaar	4	2	1	ردام	رَدام	دَمار	0
84.75	مفكر	مُفَكِّر	10 – (001) (211)	thinker	mofakir	4	2	3	كفمر	كُفَمِّر	مُفَكِّر	0
84.36	ميثاق	مِيثاق		charter	meithaaq	5	2	1	ثيماق	ثيماق	مِيثاق	0
83.87	فنادق	فَنادِق		hotels	fanadig	5	2	2	نفادق	نَفادِق	فَنادِق	0
81.73	أجيال	أجْيال		generations	ajyal	5	2	2	لجياء	لَجيْاء	أجْيال	0
GAP 13.15												
68.58	رموز	رُمُوز		symbols	romooz	4	2	2	زروم	زُرُوم	رُمُوز	0
68.45	ديوان	دِيوان		"common gathering place" (Diwan)	Diwan	5	2	1	نيواد	نِيواد	دِيوان	0
68.45	رسول	رَسُول		messenger	rasool	4	2	2	رلوس	رَلُوس	رَسُول	0
68.38	رصاص	رَصاص		bullets	rasaas	4	2	1	صراص	صرَاص	رَصاص	0
67.69	امام	إمام		"Imam"	Imam	4	2	1	مماء	ميماء	إمام	0.03
67.63	قطار	قِطار		train	Qitaar	4	2	1	طقار	طِقار	قِطار	0
67.23	نجوم	نُجُوم		stars	nojoom	4	2	2	جنوم	جِنُوم	نُجُوم	0
67.2	ألوان	أَلْوان		colors	alwaan	5	2	2	نلواء	لْواءنَ	أَلْوان	0
66.84	عميد	عَميد		Dean	a'meed	4	2	2	دعيم	دَعيم	عَميد	0
66.61	أحلام	أحْلام		dreams	ahlaam	5	2	2	حئلام	حَئْلام	أحْلام	0
66.48	جوائز	جَوائز		awards	jawa'iz	5	3	2	أواجز	أواجز	جَوائز	0
64.47	صنادِيق	صَنادِيق	7 – (111) (111)	Funds	sanadeeq	6	3	2	نصاديق	نَصاديق	صَنادِيق	0
64.34	أصدقاء	أصْدِقاء		friends	asdiqaa'	6	3	3	قأصداء	قَأصداء	أصْدِقاء	0
64.14	ميزان	مِيزان		Balance (as in weight balance)	meizaan	5	2	1	زيمان	زيمان	مِيزان	0
63.45	وجوه	وُجُوه		faces	wojooh	4	2	2	وموج	وُمُوج	وُجُوه	0

63.22	عامل	عامِل		King	a'aahil	4	2	1	هاعِل	هاعِل	عامِل	0
62.86	اَلعاب	اَلْعاب		games	alaab	5	2	2	عىَلاب	عَىَّلاب	اَلْعاب	0
11.18	صخور	صُخُور		rocks	sokhoor	4	2	2	رخوص	رُخُوص	صُخُور	0
11.15	مِنتوج	مَنْتُوج		product	mantooj	5	2	3	نمتوج	نَمْتُوج	وجمَنْتُ	0
10.98	أبراج	أبْراج		towers	abraaj	5	2	2	بأراج	بَأراج	أبْراج	0
10.95	أرباب	أرْباب		Gods	arbaab	5	2	2	أبراب	أبْراب	أرْباب	0
10.85	أكاذيب	أكاذِيب	10 – (210) (211)	lies	akatheeb	6	3	2	أذاكيب	أذاكِيب	أكاذِيب	0
10.82	بريق	بَريق		shiny light	bareeq	4	2	2	ربيق	رَبيق	بَريق	0
10.78	دفاتر	دَفاتِر		notebooks	dafatir	5	3	2	فداتر	فَداتِر	دَفاتِر	0
10.75	أحفاد	أحْفاد		grandchildren	ahfaad	5	2	2	حىفاد	حَىْفاد	أحْفاد	0
10.68	عطور	عُطُور		perfumes	otoor	4	2	2	طعور	طُعُور	عُطُور	0
10.55	كنوز	كُنُوز	5 – (101) (101)	treasures	konoz	4	2	2	زنوك	زُنُوك	كُنُوز	0
10.52	مصباح	مِصْباح		lantern	misbaah	5	2	2	صمباح	صِمْباح	مِصْباح	0
10.49	مضمار	مِضْمار		Track	midhmaar	5	2	2	ضمرام	ضِمْرام	مِضْمار	0
10.49	زخارف	زَخارِف	3 – (010) (000)	decoration	zakharif	5	3	2	خزارف	خَزارِف	زَخارِف	0
1.32	تصاوير	تَصاوِير	11 – (110) (000)	images	tasaweer	6	3	2	تواصير	تَواصِير	تَصاوِير	0
1.32	أرحام	أرْحام		wombs	arhaam	5	2	2	أمحار	أمْحار	أرْحام	0
1.28	زفير	زَفير	6 – (000) (110)	exhalation	zafeir	4	2	2	فزير	فَزير	زَفير	0
1.28	كساء	كِساء		clothing	kisaa'	4	2	1	أكاس	أكاس	كِساء	0
1.28	قيظ	قَيْظ	1- (010) (010)	heat	qayth	3	1	2	ظيق	ظَيْق	قَيْظ	0
1.25	سياط	سِياط		whips	seyaat	4	2	1	ياط	ياط	سِياط	0
1.25	خفراء	خُفَراء		warders	khofaraa'	5	2	2	رفخاء	رُفَخاء	خُفَراء	0
1.25	قربان	قُرْبان		“animal sacrifice”	Qurban	5	2	2	نقراب	نُقَراب	قُرْبان	0
1.22	جحور	جُحُور	2 – (011) (110)	holes	johoor	4	2	2	رحوج	رُحُوج	جُحُور	0
1.22	سعير	سَعِير		fire	saa'eir	4	2	2	رعيس	رَعيس	سَعِير	0
1.22	أفاعي	أفاعِي		snakes	afai'ei	5	2	2	فىاعي	عِيفَىْا	أفاعِي	0
1.22	نفاىس	نَفاىِس	8 – (000) (011)	valuables	nafaai's	5	2	2	فناىس	فَناىِس	نَفاىِس	0
1.22	زعانف	زَعانِف	9 – (000) (010)	fins	za'aanif	5	2	2	عزانف	عَزانِف	زَعانِف	0
1.18	حيتان	حِيتان	4 – (002) (002)	whales	heetaan	5	2	1	تيحان	تِيحان	حِيتان	0
1.18	مسلخ	مَسْلَخ		butcher house	maslakh	4	2	3	سملخ	سَمْلَخ	مَسْلَخ	0

Frequency per million and associated words with and without diacritics. Quantization is provided for dissimilar stimuli with respect to number(#) of letters, syllables, and diacritics.

Note:

Quantization of words that are different:

The first number is the index of the words that are close but are not exactly the same in the orthographic similarity measure; The first 3 numbers in the parenthesis represent the difference between the parameters (# of letters, # of syllables, # of diacritics) of the indexed words across frequency levels (high,mid, low). The first parenthesis is for the difference between the current word and the higher/next lower word and the second parenthesis is for the next lower/lowest frequency level words. For example if we take the word O'dho (1 (000) (010)) The 1 is the index across frequencies (i.e. ka's for mid freq, qayth for low freq); the first number in the first category quantization (000) is 0 which represents that there is a difference of zero between the current word (O'dho) and the mid freq matched word (ka's) in the number of the letters, and the second number in the category quantization is for the difference in the number of syllables, and the third number is for the difference in the number of diacritics. The second category quantization is for the difference of the same index but between Odho (high freq.) and qayth (low freq.). This method of quantization is used for all words that are not exactly matched across frequencies in their number of letters, number of syllables, and number of diacritics. If a word does not have such indexing and quantization categories it suggests that this word has an exact match in these orthographic similarity parameters across different frequencies.

Appendix II

Mean and SD for All Participants of the Behavioral Study

Participant #	HFRWD	MFRWD	LFRWD	HFNWD	MFNWD	LFNWD	HFRWND	MFRWND	LFRWND	HFNWND	MFNWND	LFNWND	RWD	RWND	NWD	NWND	HF	MF	LF	*Mean*	*SD*
1	1.47	1.41	1.64	1.43	1.52	1.61	1.20	1.19	1.39	1.47	1.50	1.46	1.51	1.26	1.52	1.52	1.39	1.40	1.56	***1.44***	***0.12***
2	1.07	1.42	1.18	1.54	1.57	1.53	0.95	0.94	1.03	1.17	1.40	1.34	1.22	0.97	1.55	1.37	1.19	1.33	1.32	***1.27***	***0.21***
3	1.47	1.37	1.47	1.39	1.41	1.60	1.05	1.17	1.40	1.38	1.28	1.58	1.44	1.21	1.47	1.42	1.32	1.31	1.52	***1.38***	***0.14***
4	1.04	0.91	1.07	1.15	1.11	1.50	0.94	0.93	1.16	1.25	1.18	1.25	1.00	1.01	1.25	1.31	1.09	1.03	1.31	***1.13***	***0.15***
5	0.85	0.91	0.92	1.24	1.16	1.23	0.80	0.84	0.84	1.10	1.03	1.10	0.89	0.83	1.21	1.12	1.00	0.99	1.05	***1.00***	***0.15***
6	0.76	0.79	0.84	0.80	0.82	0.84	0.74	0.67	0.89	0.85	0.83	0.80	0.80	0.76	0.82	0.84	0.79	0.78	0.85	***0.80***	***0.05***
7	1.21	1.19	1.19	1.32	1.30	1.38	0.98	0.87	1.07	1.23	1.23	1.19	1.19	0.97	1.34	1.28	1.18	1.15	1.26	***1.19***	***0.13***
8	0.94	0.98	1.15	1.32	1.14	1.32	0.87	0.91	1.13	1.27	1.28	1.15	1.02	0.97	1.26	1.29	1.10	1.08	1.23	***1.13***	***0.15***
9	1.30	1.47	1.24	1.64	1.54	1.43	1.09	1.01	1.22	1.34	1.42	1.44	1.34	1.10	1.54	1.40	1.34	1.36	1.33	***1.34***	***0.16***
10	1.09	1.19	1.18	1.52	1.57	1.69	1.01	1.06	1.29	1.74	1.59	1.47	1.15	1.12	1.60	1.67	1.34	1.35	1.46	***1.37***	***0.24***
11	1.28	1.45	1.46	2.14	2.13	1.98	1.12	1.00	1.19	2.16	1.90	1.98	1.39	1.10	2.09	2.01	1.67	1.62	1.65	***1.65***	***0.40***
12	1.12	1.03	1.10	1.30	1.50	1.31	0.86	0.80	1.02	1.21	1.14	1.25	1.09	0.89	1.37	1.22	1.12	1.12	1.18	***1.14***	***0.18***
13	1.43	1.38	1.55	1.36	1.45	1.34	1.25	1.12	1.33	1.35	1.29	1.34	1.45	1.23	1.38	1.32	1.35	1.31	1.39	***1.35***	***0.09***
14	0.84	0.83	0.92	1.24	1.03	1.15	0.76	0.73	0.82	0.99	1.09	1.06	0.86	0.77	1.14	1.08	0.96	0.92	1.01	***0.96***	***0.15***
15	1.22	1.24	1.29	1.53	1.69	1.73	1.31	1.18	1.26	1.59	1.44	1.62	1.25	1.25	1.65	1.59	1.41	1.39	1.50	***1.43***	***0.18***

16	1.16	1.27	1.27	1.40	1.36	1.23	1.07	0.93	1.09	1.30	1.25	1.51	1.23	1.03	1.33	1.26	1.23	1.21	1.20	***1.23***	***0.13***
17	0.95	1.12	1.10	1.75	1.64	1.54	0.79	0.90	1.12	1.39	1.31	1.45	1.06	0.94	1.64	1.41	1.22	1.24	1.32	***1.26***	***0.27***
18	1.11	1.11	1.33	1.67	1.52	1.51	1.00	0.95	1.20	1.28	1.35	1.53	1.18	1.05	1.56	1.38	1.26	1.23	1.39	***1.29***	***0.20***
Mean	***1.13***	***1.17***	***1.22***	***1.43***	***1.41***	***1.44***	***0.99***	***0.96***	***1.14***	***1.34***	***1.31***	***1.36***	***1.17***	***1.03***	***1.43***	***1.36***	***1.22***	***1.21***	***1.31***	***1.24***	***0.15***
SD	***0.21***	***0.22***	***0.22***	***0.28***	***0.30***	***0.26***	***0.17***	***0.15***	***0.17***	***0.29***	***0.23***	***0.26***	***0.21***	***0.16***	***0.27***	***0.25***	***0.20***	***0.20***	***0.20***	***0.22***	***0.04***

Table 1 Mean reaction time (RT) in seconds per stimulus category, for each participant that participated in the behavioral study. The last two rows provide the mean and standard deviation (SD) respectively, per stimulus category. The last two columns list the mean and standard deviation respectively for RT, for each respective participant across all stimuli categories.

Participant #	HFRWD	MFRWD	LFRWD	HFNWD	MFNWD	LFNWD	HFRWND	MFRWND	LFRWND	HFNWND	MFNWND	LFNWND	RWD	RWND	NWD	NWND	HF	MF	LF	*Mean*	*SD*
1	43	44	43	44	44	44	44	45	43	45	44	44	43.3	44	44	44.3	44	44.3	43.5	***43.9***	***0.57***
2	45	44	43	42	39	43	45	45	44	43	41	44	44	44.7	41.3	42.7	43.8	42.3	43.5	***43.2***	***1.56***
3	41	45	39	45	45	42	44	45	40	44	44	42	41.7	43	44	43.3	43.5	44.8	40.8	***43***	***1.84***
4	44	45	38	43	42	42	45	44	39	42	42	42	42.3	42.7	42.3	42	43.5	43.3	40.3	***42.3***	***1.78***
5	45	44	43	45	40	40	45	45	43	44	39	43	44	44.3	41.7	42	44.8	42	42.3	***43***	***1.86***
6	43	44	38	44	44	43	45	44	35	44	42	43	41.7	41.3	43.7	43	44	43.5	39.8	***42.4***	***2.46***
7	44	44	42	44	42	40	44	44	43	44	43	43	43.3	43.7	42	43.3	44	43.3	42	***43.1***	***1.07***
8	44	44	42	45	43	42	44	45	42	43	44	44	43.3	43.7	43.3	43.7	44	44	42.5	***43.5***	***0.90***
9	43	43	41	40	44	41	43	44	41	42	43	43	42.3	42.7	41.7	42.7	42	43.5	41.5	***42.3***	***1.09***
10	45	45	41	42	38	42	44	44	42	44	42	44	43.7	43.3	40.7	43.3	43.8	42.3	42.3	***42.8***	***1.69***
11	45	45	44	38	40	41	45	45	43	38	42	38	44.7	44.3	39.7	39.3	41.5	43	41.5	***42***	***2.59***
12	41	44	41	44	39	42	44	44	42	45	40	35	42	43.3	41.7	40	43.5	41.8	40	***41.8***	***2.36***
13	43	42	36	45	45	45	43	44	37	45	44	45	40.3	41.3	45	44.7	44	43.8	40.8	***42.8***	***2.70***
14	45	42	41	41	43	43	45	45	41	43	41	44	42.7	43.7	42.3	42.7	43.5	42.8	42.3	***42.8***	***1.32***
15	44	44	42	42	42	43	41	45	41	44	44	44	43.3	42.3	42.3	44	42.8	43.8	42.5	***43***	***1.13***
16	42	45	38	44	45	43	42	45	38	45	41	40	41.7	41.7	44	42	43.3	44	39.8	***42.3***	***2.24***
17	45	45	42	39	41	43	45	45	43	42	41	45	44	44.3	41	42.7	42.8	43	43.3	***43***	***1.71***
18	45	45	40	43	43	43	45	45	43	42	43	42	43.3	44.3	43	42.3	43.8	44	42	***43.3***	***1.31***
Mean	***43.7***	***44.1***	***40.8***	***42.8***	***42.2***	***42.3***	***44.1***	***44.6***	***41.1***	***43.3***	***42.2***	***42.5***	***42.9***	***43.3***	***42.4***	***42.7***	***43.5***	***43.3***	***41.7***	***42.8***	***1.00***
SD	***1.4***	***1***	***2.2***	***2.1***	***2.2***	***1.3***	***1.2***	***0.5***	***2.4***	***1.7***	***1.5***	***2.5***	***1.1***	***1.1***	***1.4***	***1.3***	***0.8***	***0.8***	***1.2***	***1.5***	***0.58***

Table 2 Accuracy per stimulus category, for each participant that participated in the behavioral study (max accuracy score: 45). The last two rows provide the mean and standard deviation (SD) respectively, per stimulus category. The last two columns list the mean and standard deviation respectively for accuracy, for each respective participant across all stimuli categories.

Appendix III

Mean and SD for All Participants of the FMRI Behavioral Study

Participant#	HFRWD	LFRWD	HFNWD	LFNWD	HFRWND	LFRWND	HFNWND	LFNWND	RWD	RWND	NWD	NWND	HF	LF	*Mean*	*SD*
1	1.06	1.00	1.23	1.21	0.91	0.84	1.14	1.18	1.03	0.89	1.22	1.15	*1.08*	1.06	***1.07***	***0.13***
2	1.48	1.45	1.51	1.58	1.12	1.24	1.38	1.34	1.46	1.17	1.55	1.38	*1.37*	1.39	***1.39***	***0.13***
3	0.83	0.94	0.95	1.06	0.76	0.83	1.02	1.05	0.89	0.80	1.03	1.04	*0.90*	0.98	***0.93***	***0.10***
4	0.90	0.92	0.96	1.04	0.83	0.86	0.95	0.94	0.91	0.85	1.01	0.94	*0.91*	0.94	***0.93***	***0.06***
5	1.29	1.23	1.56	1.66	0.94	0.99	1.50	1.59	1.28	0.97	1.62	1.55	*1.33*	1.38	***1.35***	***0.25***
6	0.98	0.98	1.32	1.26	0.92	0.92	1.04	1.08	0.99	0.92	1.28	1.07	*1.06*	1.07	***1.06***	***0.13***
7	0.92	0.90	1.18	1.21	0.83	0.81	1.08	1.17	0.90	0.83	1.20	1.12	*1.00*	1.02	***1.01***	***0.15***
8	1.18	1.15	1.38	1.52	0.90	1.05	1.30	1.24	1.16	0.98	1.47	1.28	*1.20*	1.25	***1.22***	***0.17***
9	1.08	1.01	0.96	1.03	0.85	0.90	0.95	0.94	1.04	0.88	0.99	0.94	*0.95*	0.97	***0.96***	***0.06***
10	0.78	0.81	0.71	0.71	0.71	0.71	0.81	0.80	0.79	0.71	0.84	0.80	*0.78*	0.79	***0.77***	***0.05***
11	0.94	0.94	1.20	1.18	0.84	0.91	1.08	1.12	0.95	0.87	1.19	1.10	*1.02*	1.04	***1.03***	***0.12***
Mean	***1.04***	***1.03***	***1.18***	***1.22***	***0.87***	***0.91***	***1.11***	***1.13***	***1.04***	***0.90***	***1.22***	***1.12***	***1.05***	***1.08***	***1.06***	***0.11***
SD	***0.21***	***0.18***	***0.26***	***0.28***	***0.11***	***0.14***	***0.20***	***0.22***	***0.20***	***0.12***	***0.25***	***0.21***	***0.18***	***0.18***	***0.20***	***0.05***

Table 1 Mean reaction time (RT) in seconds per stimulus category, for each participant that underwent the fMRI study. The last two rows provide the mean and standard deviation (SD) respectively, per stimulus category. The last two columns list the mean and standard deviation respectively for RT, for each respective participant across all stimuli categories.

Participant #	HFRWD	LFRWD	HFNWD	LFNWD	HFRWND	LFRWND	HFNWND	LFNWND	RWD	RWND	NWD	NWND	HF	LF	*Mean*	*SD*
1	46	45	45	46	46	46	45	46	45.5	46	45.5	45.5	45.5	45.75	***45.63***	***0.40***
2	45	44	45	45	45	44	45	44	44.5	44.5	45	44.5	45	44.25	***44.63***	***0.42***
3	45	40	45	44	46	41	44	43	42.5	43.5	44.5	43.5	45	42	***43.5***	***1.68***
4	45	46	46	46	46	45	45	46	45.5	45.5	46	45.5	45.5	45.75	***45.63***	***0.40***
5	43	44	46	41	46	46	44	43	43.5	46	43.5	43.5	44.75	43.5	***44.13***	***1.48***
6	45	36	45	43	45	38	46	42	40.5	41.5	44	44	45.25	39.75	***42.5***	***3.02***
7	46	44	43	42	45	43	41	45	45	44	42.5	43	43.75	43.5	***43.63***	***1.35***
8	46	44	46	46	46	45	45	45	45	45.5	46	45	45.75	45	***45.38***	***0.61***
9	46	44	46	46	46	45	45	45	45	45.5	46	45	45.75	45	***45.38***	***0.61***
10	44	45	46	46	46	46	46	46	44.5	46	46	46	45.5	45.75	***45.63***	***0.66***
11	46	43	45	44	46	44	44	44	44.5	45	44.5	44	45.25	43.75	***44.5***	***0.86***
Mean	***45.18***	***43.18***	***45.27***	***44.45***	***45.73***	***43.91***	***44.55***	***44.45***	***44.18***	***44.82***	***44.86***	***44.5***	***45.18***	***44***	***44.59***	***0.66***
Std. Dev.	***0.98***	***2.82***	***0.9***	***1.81***	***0.47***	***2.47***	***1.37***	***1.37***	***1.5***	***1.38***	***1.19***	***0.97***	***0.57***	***1.84***	***1.4***	***0.66***

Table 2 Accuracy per stimulus category, for each participant that participated in the fMRI study (max accuracy score: 46). The last two rows provide the mean and standard deviation (SD) respectively, per stimulus category. The last two columns list the mean and standard deviation respectively for accuracy, for each respective participant across all stimuli categories.

Appendix IV

FMRI Activation Statistical Parametric Maps and Tables for Stimuli Comparisons of FMRI Study

RWD vs. FIXATION

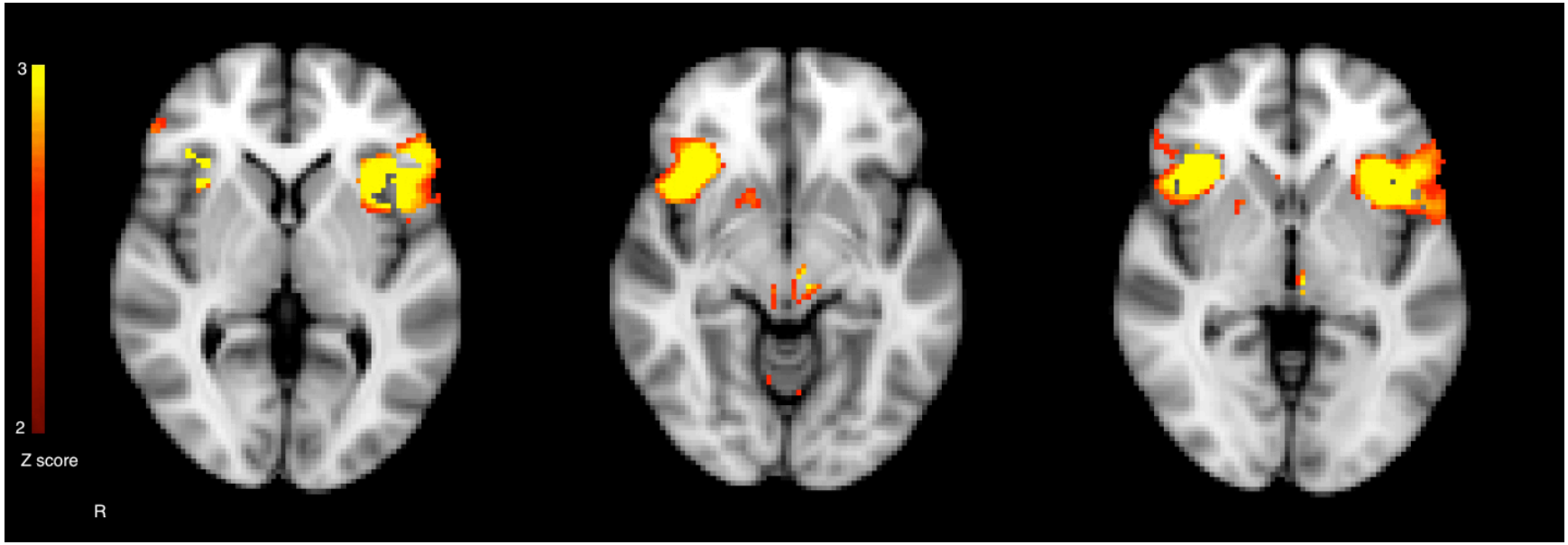

Figure 1 Statistical parametric activation map for brain regions associated with RWD > Fixation (yellow,red); Statistical results displayed are corrected and significant at $p < 0.001$.

RWD > Fixation Local Maxima (z>2.2)		
Brain Region	**Z – value**	**X,Y,Z**
Right Insular cortex	5.41	36,24,-2
Left Insular cortex (including Brodmann area 13)	4.88	-36,18,-2
Left Insular cortex	4.7	-42,16,0
Left Insular cortex (including Brodmann area 13)	4.69	-36,20,2
Left Brainstem	4.02	-4,-20,-12
Right Brainstem	3.71	4,-22,-12
Left cerebellum	3.2	-30,-66,-16
Right cerebellum	3.13	24,-78,-16
Right inferior frontal gyrus (including brodmann area 47)	3.0	46,22,-6
Left inferior frontal gyrus (including brodmann area 47)	3.01	-50,26,-2
Right dorsolateral prefrontal cortex (including Brodmann area 46)	2.34	50,40,2
Left superior temporal lobe (including Brodmann area 22)	2.33	-58,4,-2

Table 1 Details of the local maxima brain regions for RWD > Fixation (column 1) and their associated z- value (column 2), and x,y,and z MNI coordinates (column 3).

Fixation > RWND Local Maxima (z>2.2)		
Brain Region	**Z – value**	**X,Y,Z**
Right Parahippocampal gyrus (including brodmass area 19)	2.49	34,-40,-4
Right caudate	2.35	6,6,10

Table 2 Details of the local maxima brain regions for Fixation > RWND (column 1) and their associated z- value (column 2), and x,y,and z MNI coordinates (column 3).

RWND vs FIXATION

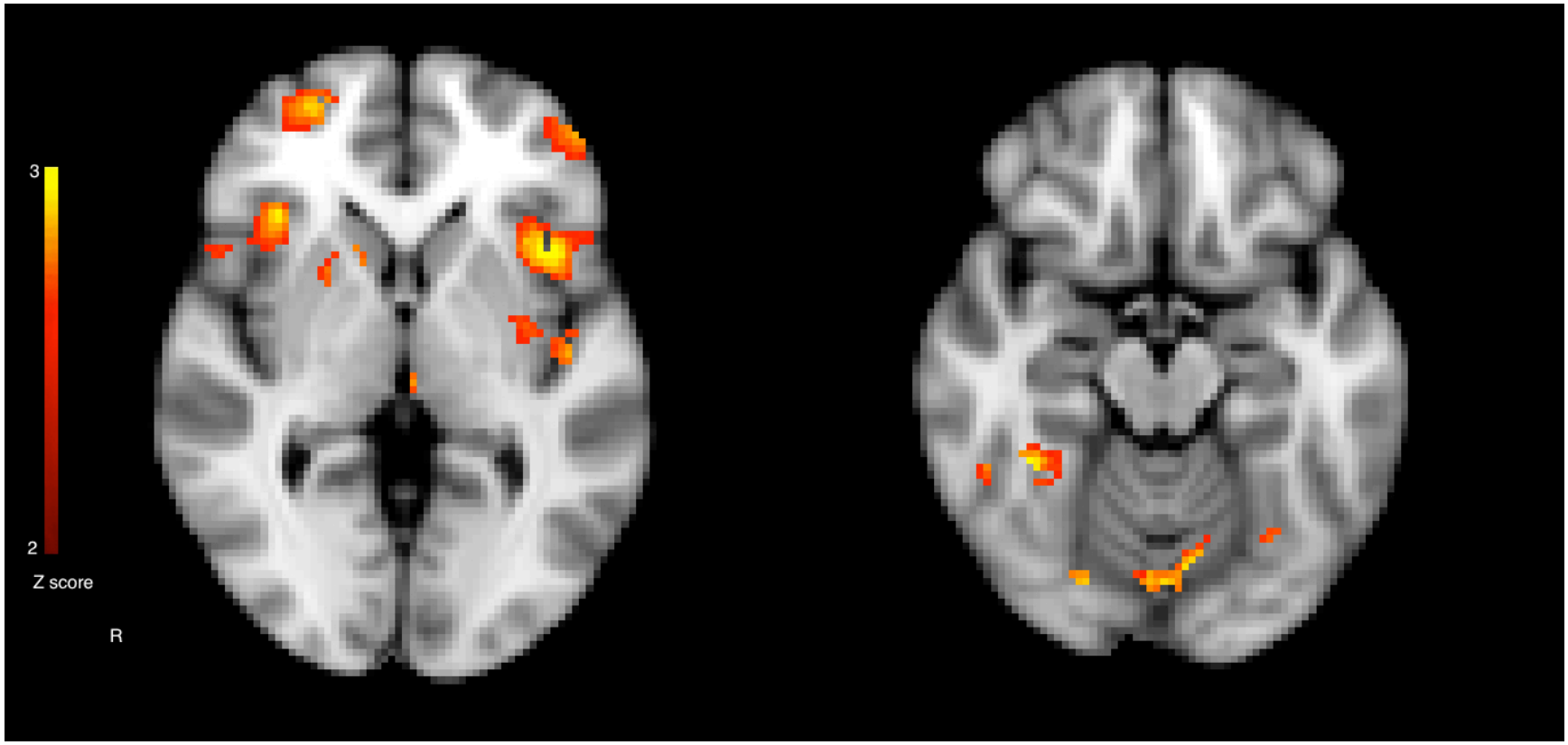

Figure 2 Statistical parametric activation map for brain regions associated with RWND > Fixation (yellow,red); Statistical results displayed are corrected and significant at $p < 0.001$.

RWND > FIXATION Local Maxima (z>2.2)		
Brain Region	**Z – value**	**X,Y,Z**
Left inferior frontal gyrus (including Brodmann area 45)	3.27	-44,14,4
Left insular cortex (including Brodmann area 13)	3.24	-42,14,0
Right caudate	3.21	12,12,-4
Left cerebellum	3.17	-6,-72,-10
Right fusiform gyrus (including Brodmass area 37)	3.16	38,-44,-16
Right cerebellum	3.14	18,-30,-14
Right inferior frontal gyrus (including Brodmann area 47)	2.98	44,36,-8
Right putamen	2.83	16,12,-8
Right parahippocampal gyrus (including Brodmann area 35)	2.74	24,-30,-8
Left inferior frontal gyrus	2.7	-46,46,2

Table 3 Details of the local maxima brain regions for RWND > Fixation (column 1) and their associated z- value (column 2), and x,y,and z MNI coordinates (column 3).

All clusters for Fixation>RWND have $z<1.73$

RWD vs. RWND

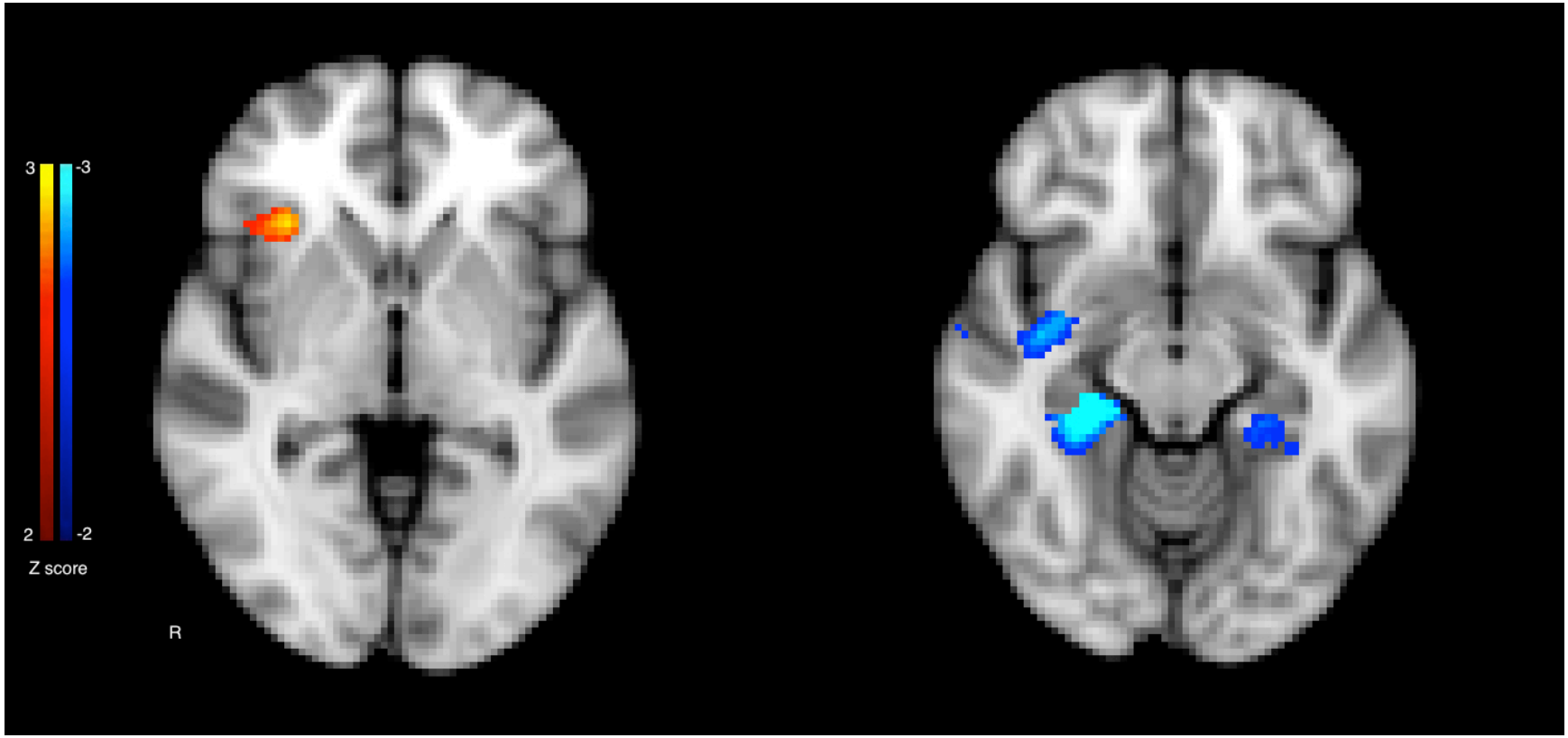

Figure 3 Statistical parametric activation map for brain regions associated with RWD > RWND (yellow,red), and RWND > RWD (blue,light blue); Statistical results displayed are corrected and significant at $p < 0.001$.

RWD > RWND Local Maxima (z>2.2)		
Brain Region	**Z – value**	**X,Y,Z**
Right insular cortex	2.99	32,26,2
Right insular cortex	2.9	32,24,-2

Table 4 Details of the local maxima brain regions for RWD > RWND (column 1) and their associated z- value (column 2), and x,y,and z MNI coordinates (column 3).

RWND > RWD Local Maxima (z>2.2)		
Brain Region	**Z – value**	**X,Y,Z**
Right parahippocampal gyrus (including Brodmann area 36)	3.88	26,-30,-14
Right parahippocampal gyrus	3.6	26,-32,-12
Right parahippocampal gyrus (including Brodmann area 36)	3.33	20,-30,-12
Right middle temporal lobe	2.78	40,-8,-12
Right parahippocampal gyrus	2.67	34,-4,-12
Right Hippocampus	2.6	32,-36,0
Left parahippocampal gyrus (including Brodmann area 36)	2.45	-24,-34,-12

Table 5 Details of the local maxima brain regions for RWND > RWD (column 1) and their associated z- value (column 2), and x,y,and z MNI coordinates (column 3).

NWD vs. FIXATION

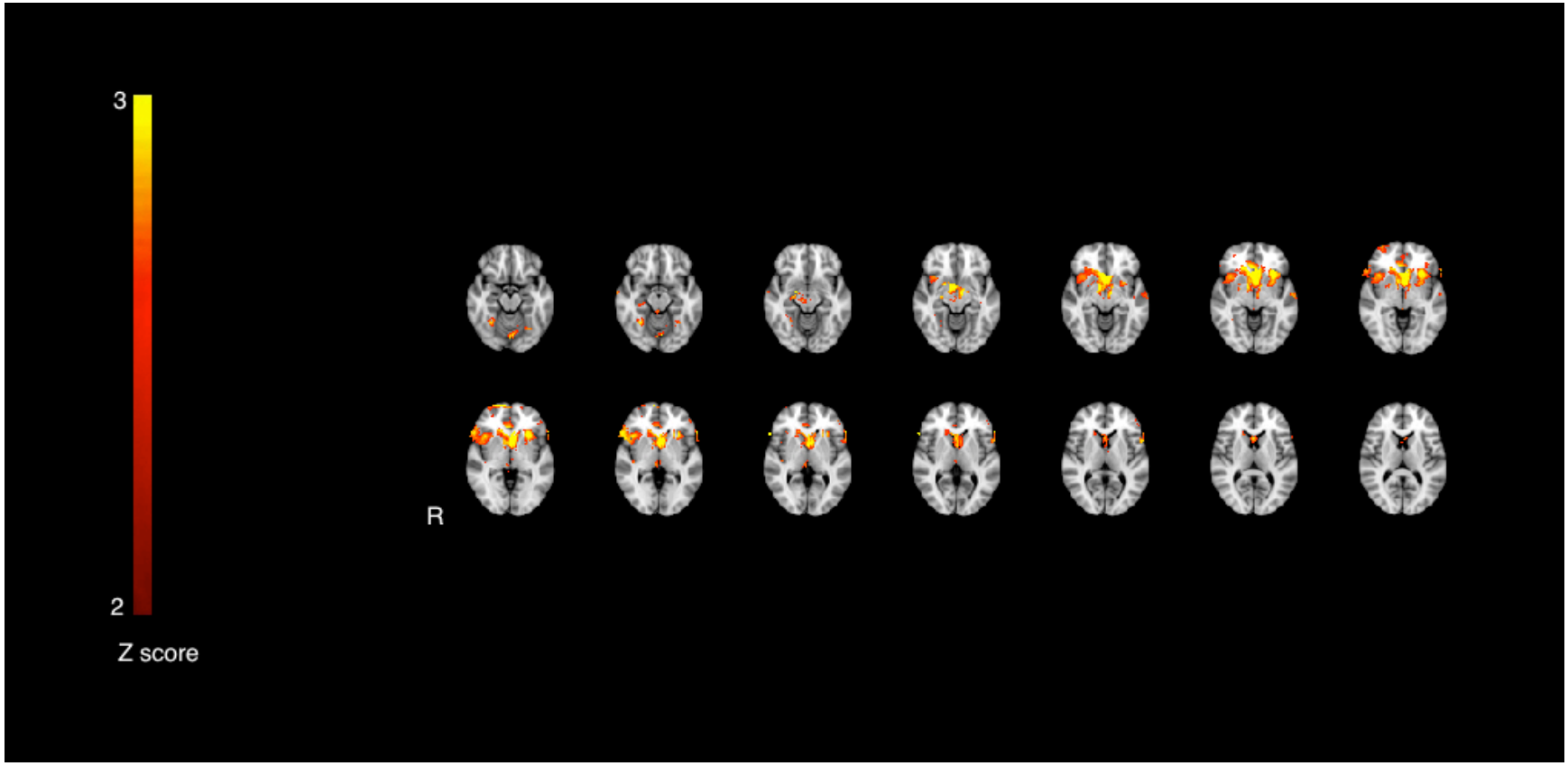

Figure 4 Statistical parametric activation map for brain regions associated with NWD > Fixation (yellow,red); Statistical results displayed are corrected and significant at $p < 0.001$.

NWD > FIXATION Local Maxima (z>2.2)		
Brain Region	**Z – value**	**X,Y,Z**
Left anterior cingulate cortex	5.09	0,24,-6
Left Caudate	5	-4,12,0
Left anterior cingulate cortex (including Brodmann area 25)	4.96	0,20,-8
Left anterior cingulated cortex (Brodmann area 25)	4.71	-2,16,-8
Right hypothalamus	4.07	8,0,-10
Right inferior frontal gyrus (Brodmann area 47)	3.76	54,22,0
Right medial frontal gyrus (Brodmann 10)	2.96	6,66,,0
Right cerebellum	2.83	30,-56,-16
Left putamen	2.87	-28,18,0
Left middle temporal gyrus	2.65	-62,-14,-6
Left cerebellum	2.55	-2,-76,-18

Table 6 Details of the local maxima brain regions for NWD > Fixation (column 1) and their associated z- value (column 2), and x,y,and z MNI coordinates (column 3).

All clusters for Fixation>NWD have z<1.6

NWND vs. FIXATION

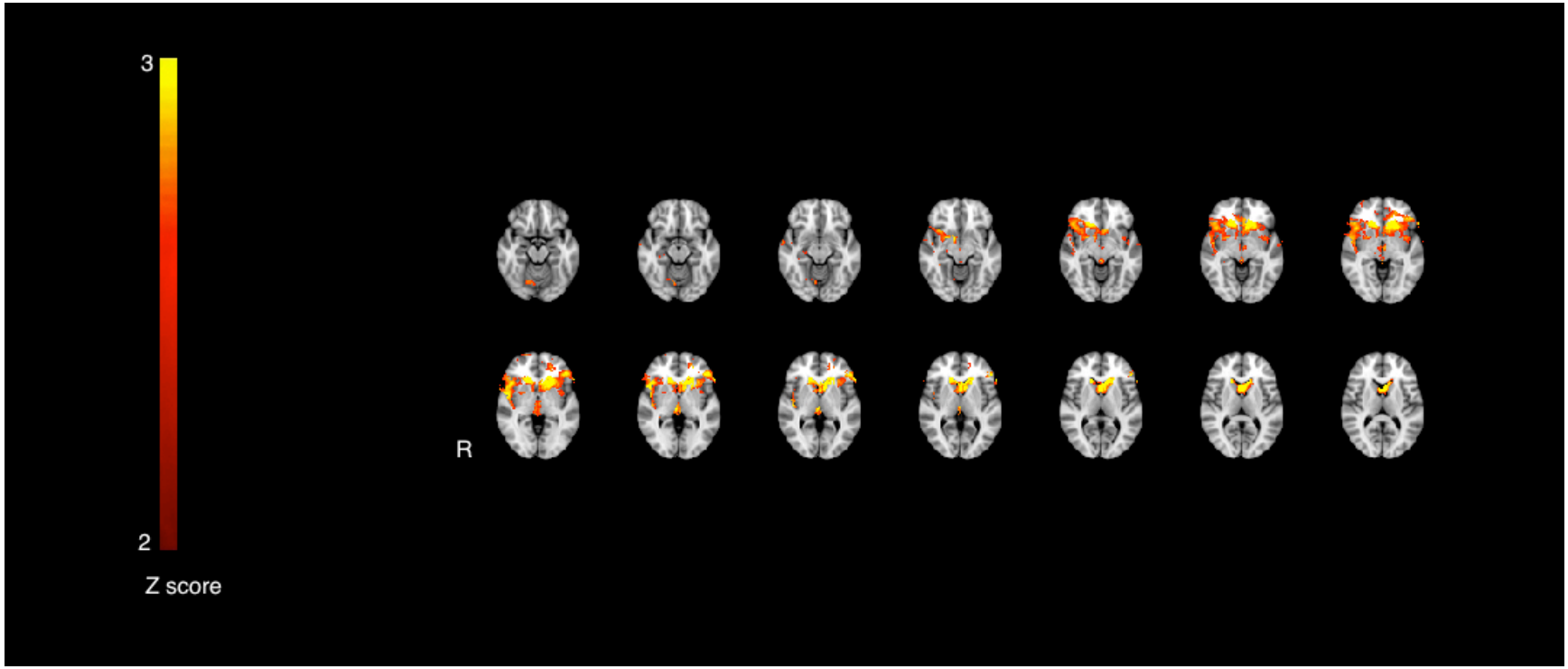

Figure 5 Statistical parametric activation map for brain regions associated with NWND > Fixation (yellow,red); Statistical results displayed are corrected and significant at $p < 0.001$.

NWND > FIXATION Local Maxima (z>2.2)		
Brain Region	**Z – value**	**X,Y,Z**
Right frontal lobe	5.23	18,30,-6
Right caudate	4.77	16,24,0
Left caudate	4.48	-20,26,2
Left anterior cingulated cortex	4.29	-12,32,-6
Left caudate	4.22	-10,24,0
Left putamen	4.15	-20,18,0
Left inferior frontal gyrus	3.25	-50,36,0
Left inferior frontal gyrus (Brodmann area 45)	2.8	-52,36,2
Right inferior frontal gyrus (including Brodmann area 47)	2.76	48,28,-8
Right cerebellum	2.41	14,-70,-16

Table 7 Details of the local maxima brain regions for NWND > Fixation (column 1) and their associated z- value (column 2), and x,y,and z MNI coordinates (column 3).

FIXATION > NWND Local Maxima (z>2.2)		
Brain Region	**Z – value**	**X,Y,Z**
Right fusiform gyrus	2.35	50,-48,-16

Table 8 Details of the local maxima brain regions for Fixation > NWND (column 1) and their associated z- value (column 2), and x,y,and z MNI coordinates (column 3).

NWD vs. NWND

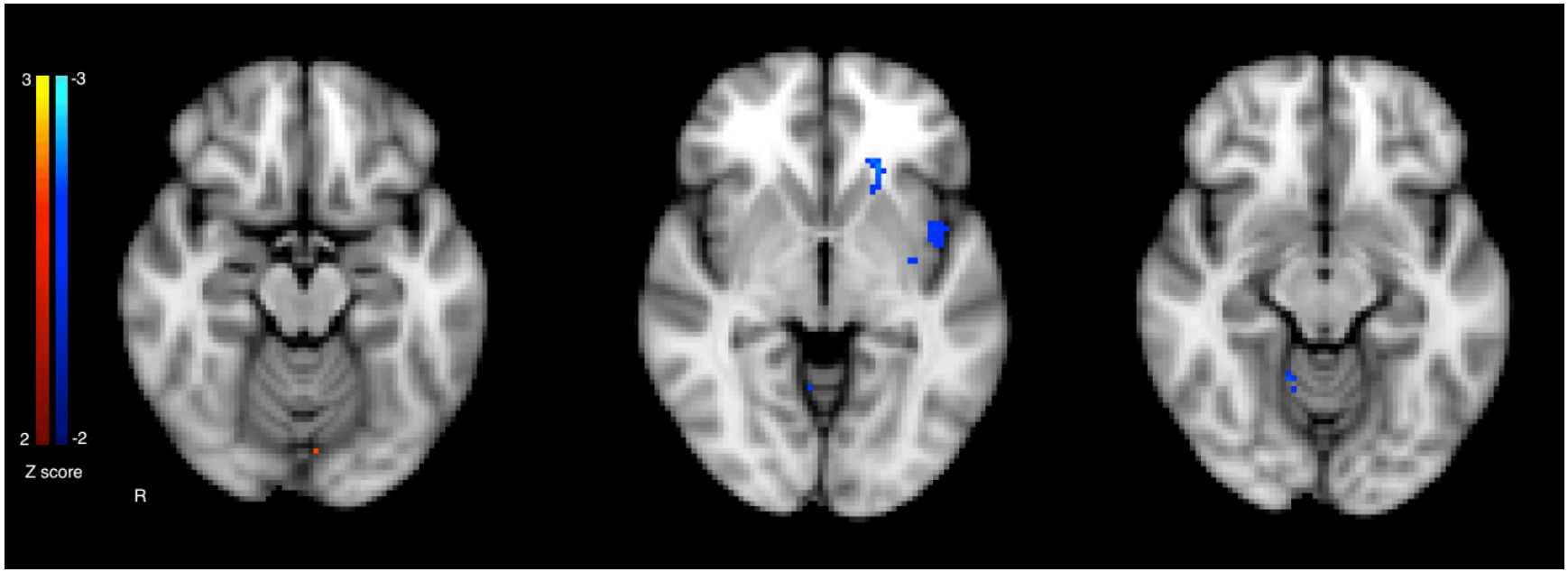

Figure 6 Statistical parametric activation map for brain regions associated with NWD > NWND (yellow,red), and NWND > NWD (blue,light blue); Statistical results displayed are corrected and significant at $p < 0.001$.

NWD > NWND Local Maxima (z>2.2)		
Brain Region	**Z – value**	**X,Y,Z**
Left occipital lobe	2.27	-4,-80,-16

Table 9 Details of the local maxima brain regions for NWD > NWND (column 1) and their associated z- value (column 2), and x,y,and z MNI coordinates (column 3).

NWND > NWD Local Maxima (z>2.2)		
Brain Region	**Z – value**	**X,Y,Z**
Left caudate	2.68	-18,22,0
Right cerebellum	2.32	14,-52,-12
Right cerebellum	2.32	8,-56,-8
Left insular cortex (including Brodmann area 13)	2.31	-42,4,-2
Left insular cortex	2.23	-42,4,-4

Table 10 Details of the local maxima brain regions for NWND > NWD (column 1) and their associated z- value (column 2), and x,y,and z MNI coordinates (column 3).

RWD vs. NWD

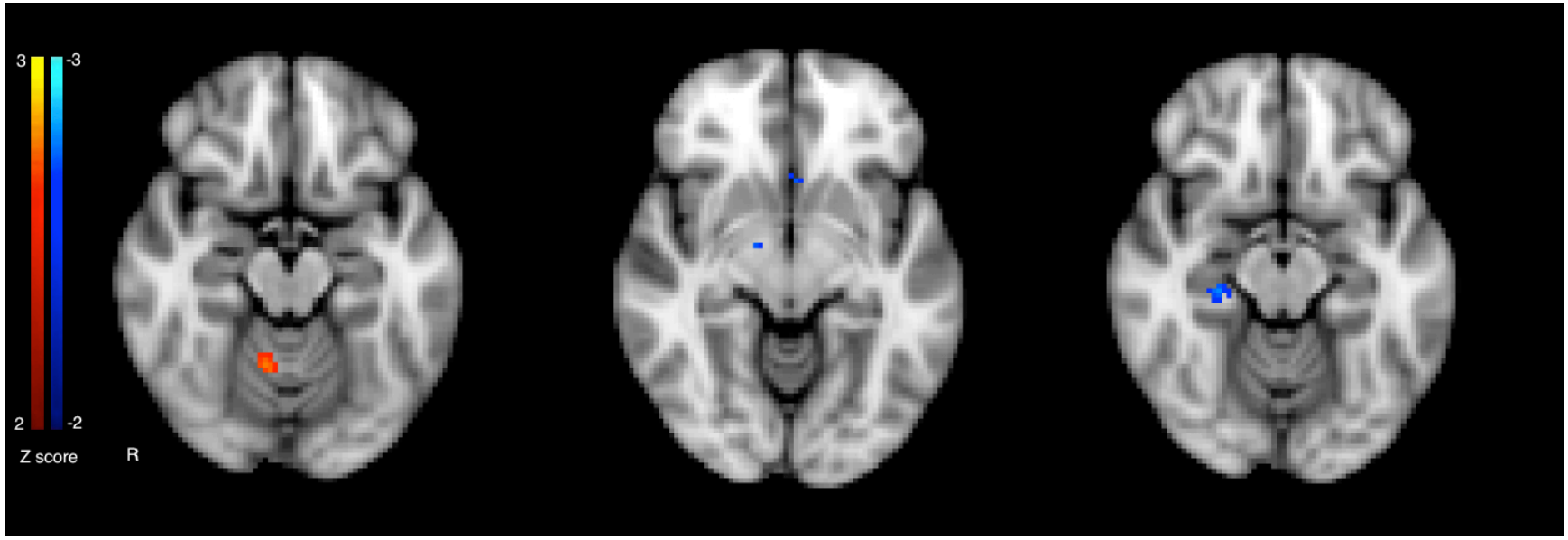

Figure 7 Statistical parametric activation map for brain regions associated with RWD > NWD (yellow,red), and NWD > RWD (blue,light blue); Statistical results displayed are corrected and significant at $p < 0.001$.

RWD > NWD Local Maxima (z>2.2)		
Brain Region	**Z – value**	**X,Y,Z**
Right cerebellum	2.48	8,-56,-14

Table 11 Details of the local maxima brain regions for RWD > NWD (column 1) and their associated z- value (column 2), and x,y,and z MNI coordinates (column 3).

NWD > RWD Local Maxima (z>2.2)		
Brain Region	**Z – value**	**X,Y,Z**
Right parahippocampal gyrus (Brodmann area 28)	2.79	20,-12,-12
Right brainstem	2.6	16,-10,-12
Right brainstem	2.3	14,-8,-8
Right parahippocampal gyrus (Brodmann area 35)	2.53	26,-26,-14
Left anterior cingulate	2.51	0,26,-6
Left anterior cingulated (Brodmann area 25)	2.34	-2,18,-8

Table 12 Details of the local maxima brain regions for NWD > RWD (column 1) and their associated z- value (column 2), and x,y,and z MNI coordinates (column 3).

HFRWD vs. FIX

HFRWD > FIXATION Local Maxima (z>2.2)		
Brain Region	**Z – value**	**X,Y,Z**
Right insular cortex	4.36	36,24,0
Right insular cortex (Brodmann area 13)	4.19	44,16,-4
Right insular cortex	4.08	42,22,-2
Left insular cortex	3.92	-38,16,-2
Left claustrum	3.75	-34,18,2
Right inferior frontal gyrus (Brodmann area 47)	3.61	38,22,-6
Right inferior frontal gyrus (including Brodmann area 45)	3.26	54,30,0
Left insular cortex (Brodmann area 13)	3.1	-40,14,-6
Right Brainstem	2.61	
Right cerebellum	2.4	24,-76,-16
Right caudate	2.4	8,20,2

Table 13 Details of the local maxima brain regions for HFRWD > Fixation (column 1) and their associated z- value (column 2), and x,y,and z MNI coordinates (column 3).

Fixation > HFRWD Local Maxima (z>2.2)		
Brain Region	**Z – value**	**X,Y,Z**
Right parahippocampal gyrus (Brodmann area 35)	2.27	28,-26,-14
Left fusiform gyrus (Brodmann area 37)	2.23	-34,-42,-10

Table 14 Details of the local maxima brain regions for Fixation >HFRWD (column 1) and their associated z- value (column 2), and x,y,and z MNI coordinates (column 3).

LFRWD VS. FIXATION

LFRWD > FIXATION Local Maxima (z>2.2)		
Brain Region	**Z – value**	**X,Y,Z**
Left brainstem	3.3	-4,-22,-2
Right cerebellum	3.24	32,-52,-16
Right cerebellum	3.23	30,-56,-16
Left anterior cingulated cortex (including Brodmann area 24)	3.17	-2,36,4
Left Brainstem	3.04	-2,-26,-12
Right infrerior frontal cortex(including Brodmann area 47)	2.9	46,20,-8
Left insular cortex(including Brodmann area 13)	2.84	-40,10,0
Left superior temporal gyrus	2.6	-58,0,0
Right insular cortex(Brodmann area 13)	2.3	34,22,-4

Table 15 Details of the local maxima brain regions for LFRWD >fixation (column 1) and their associated z- value (column 2), and x,y,and z MNI coordinates (column 3).

FIXATION > LFRWD Local Maxima (z>2.2)		
Brain Region	**Z – value**	**X,Y,Z**
Left frontal lobe	2.9	-30,50,-2

Table 16 Details of the local maxima brain regions for fixation > LFRWD (column 1) and their associated z- value (column 2), and x,y,and z MNI coordinates (column 3).

HFRWD VS. LFRWD

HFRWD > LFRWD Local Maxima (z>2.2)		
Brain Region	**Z – value**	**X,Y,Z**
Left frontal lobe	3	-38,44,2
Right insular cortex (Brodmann area 13)	2.92	48,16,0
Right inferior frontal gyrus (including Brodmann area 47)	2.88	48,14,-4

Table 17 Details of the local maxima brain regions for HFRWD > LFRWD (column 1) and their associated z- value (column 2), and x,y,and z MNI coordinates (column 3).

LFRWD > HFRWD Local Maxima (z>2.2)		
Brain Region	**Z – value**	**X,Y,Z**
Left parahippocampal gyrus	2.54	-26,-44,-14

Table 18 Details of the local maxima brain regions for LFRWD > HFRWD (column 1) and their associated z- value (column 2), and x,y,and z MNI coordinates (column 3).

HFRWND VS. FIXATION

HFRWND > FIXATION Local Maxima (z>2.2)		
Brain Region	**Z – value**	**X,Y,Z**
Right anterior cingulate (Brodmann area 32)	3.64	10,46,2
Right putamen	3.38	18,16,-4
Left caudate	3.09	-10,20,6
Right superior temporal gyrus (Brodmann area 38)	3.07	56,6,-10
Left parahippocampal gyrus	2.83	-30,-14,-10
Right parahippocampal gyrus (including Brodmann area 35)	2.65	22,-30,-10
Left putamen	2.35	-16,12,-8
Left insular cortex (Brodmann area 13)	2.35	-44,-4,22

Table 19 Details of the local maxima brain regions for HFRWND > Fixation (column 1) and their associated z- value (column 2), and x,y,and z MNI coordinates (column 3).

All clusters for Fixation < HFRWND have z < 1.97

LFRWND VS. FIXATION

LFRWND > FIXATION Local Maxima (z>2.2)		
Brain Region	**Z – value**	**X,Y,Z**
Right middle frontal gyrus	3.2	40,60,0
Right superior frontal gyrus (Brodmann area 10)	2.81	28,58,0
Left middle frontal gyrus	2.77	-30,63,6
Left cerebellum	2.5	-8,-72,-16
Right superior temporal (including Brodmann area 22)	2.38	52,-20,-6
Right cerebellum	2.33	4,-60,-8

Table 20 Details of the local maxima brain regions for LFRWND > Fixation (column 1) and their associated z- value (column 2), and x,y,and z MNI coordinates (column 3).

All clusters for Fixation < LFRWND have z < 2.0

HFRWND VS. LFRWND

HFRWND > LFRWND Local Maxima (z>2.2)		
Brain Region	**Z – value**	**X,Y,Z**
Right putamen	2.83	24,18,-4
Left frontal lobe(including inferior frontal gyrus)	2.66	-30,40,-4
Right putamen	2.4	24,14,-6
Right anterior cingulated(Brodmann area 32)	2.4	14,46,4
Left insular cortex(Brodmann area 13)	2.4	-50,10,2
Right superior temporal gyrus(including Brodmann area 38)	2.4	56,8,-10
Right parahippocampal gyrus (Brodmann area 35)	2.3	24,-16,-12

Table 21 Details of the local maxima brain regions for HFRWND > LFRWND (column 1) and their associated z- value (column 2), and x,y,and z MNI coordinates (column 3).

LFRWND > HFRWND Local Maxima (z>2.2)		
Left cerebellum	2.3	-4,-62,-8

Table 22 Details of the local maxima brain regions for LFRWND > HFRWND (column 1) and their associated z- value (column 2), and x,y,and z MNI coordinates (column 3).

HFRWD VS. HFRWND

HFRWD > HFRWND Local Maxima (z>2.2)		
Brain Region	**Z – value**	**X,Y,Z**
Left insular cortex	2.54	-30,24,-2
Right insular cortex	2.39	36,28,0
Right inferior frontal gyrus(including Brodmann area 47)	2.3	40,24,-4

Table 23 Details of the local maxima brain regions for HFRWD > HFRWND (column 1) and their associated z- value (column 2), and x,y,and z MNI coordinates (column 3).

HFRWND > HFRWD Local Maxima (z>2.2)		
Brain Region	**Z – value**	**X,Y,Z**
Right parahippocampal gyrus	3.27	24,-30,-14
Right anterior cingulated cortex	3.07	12,42,-6
Right putamen	2.59	20,18,-6
Left anterior cingulate cortex	2.48	-8,38,-2

Table 24 Details of the local maxima brain regions for HFRWND > HFRWD (column 1) and their associated z- value (column 2), and x,y,and z MNI coordinates (column 3).

LFRWD VS. LFRWND

LFRWD > LFRWND Local Maxima (z>2.2)		
Brain Region	**Z – value**	**X,Y,Z**
Right insular cortex	2.61	30,26,-6

Table 25 Details of the local maxima brain regions for LFRWD > LFRWND (column 1) and their associated z- value (column 2), and x,y,and z MNI coordinates (column 3).

LFRWND > LFRWD Local Maxima (z>2.2)		
Brain Region	**Z – value**	**X,Y,Z**
Left cerebellum	2.9	-10,-62,-12
Right parahippocampal gyrus(including Brodmann area 36)	2.78	30,-34,-14
Right inferior temporal gyrus(including Brodmann area 21)	2.63	60,-10,-14
Right insula	2.59	-42,-14,2
Left middle frontal gyrus(including Brodmann area 10)	2.58	-22,60,6
Right putamen	2.44	34,-4,-6

Table 26 Details of the local maxima brain regions for LFRWND > LFRWD (column 1) and their associated z- value (column 2), and x,y,and z MNI coordinates (column 3).

HF VS. FIX

HF > FIXATION Local Maxima (z>2.2)		
Brain Region	**Z – value**	**X,Y,Z**
Right insular cortex	6.73	38,22,0
Left insular cortex	6.65	-38,20,2
Inferior frontal gyrus(including Brodmann area 47)	4.96	-52,30,,0
Left brainstem	3.07	-2,-30,-6
Right medial occipito-temporal gyrus	3.11	32,-56,-16
Left cerebellum	3.05	-12,-76,-18
Right cerebellum	2.91	18,-70,-16
Left putamen	2.84	-22,8,-6
Right fusiform gyrus (Brodmann area 37)	2.8	50,-60,-18
Right putamen	2.42	22,10,-6

Table 27 Details of the local maxima brain regions for HF > fixation (column 1) and their associated z- value (column 2), and x,y,and z MNI coordinates (column 3).

FIXATION > HF Local Maxima (z>2.2)		
Brain Region	**Z – value**	**X,Y,Z**
Right anterior cingulated cortex (Brodmann area 32)	2.877	12,52,-4

Table 28 Details of the local maxima brain regions for fixation > HF (column 1) and their associated z- value (column 2), and x,y,and z MNI coordinates (column 3).

LF VS FIXATION

LF > FIXATION Local Maxima (z>2.2)		
Brain Region	**Z – value**	**X,Y,Z**
Right insular cortex	6.66	42,20,-2
Right medial occipito-temporal gyrus	5.47	34,-52,-16
Left cerebellum	4.45	-2,-76,-16
Right putamen	4.05	20,4,-4
Right cerebellum	3.7	24,-80,-20
Right brainstem	3.8	8,-20,,-12
Left insular cortex	3.3	-30,18,-4
Left putamen	3.26	-22,4,-4
Left brainstem	3.14	-2,-22,-4
Right inferior frontal gyrus (including Brodmann area 47)	3.09	48,36,-4
Left inferior frontal gyrus (including brodmann area 45,47)	2.6	-50,34,2
Right inferior temporal gyrus	2.6	50,-46,-16

Table 29 Details of the local maxima brain regions for LF > fixation (column 1) and their associated z- value (column 2), and x,y,and z MNI coordinates (column 3).

FIXATION > LF Local Maxima (z>2.2)		
Brain Region	**Z – value**	**X,Y,Z**
Right brainstem	2.71	2,-8,-10
Right superior temporal gyrus (including Brodmann area 21)	2.46	52,-4,-6
Left superior frontal gyrus	2.3	-20,48,-4

Table 30 Details of the local maxima brain regions for fixation > LF (column 1) and their associated z- value (column 2), and x,y,and z MNI coordinates (column 3).

HF vs. LF

HF > LF Local Maxima (z>2.2)		
Brain Region	**Z – value**	**X,Y,Z**
Right middle temporal gyrus (including Brodmann area 21)	2.68	54,2,-12
Right fusiform gyrus	2.59	40,-40,-16
Left middle frontal gyrus	2.58	-28,40,-4
Right parahippocampal gyrus (Brodmann area 37)	2.55	36,-38,-10

Table 31 Details of the local maxima brain regions for HF > LF (column 1) and their associated z- value (column 2), and x,y,and z MNI coordinates (column 3).

LF > HF Local Maxima (z>2.2)		
Brain Region	**Z – value**	**X,Y,Z**
Right putamen	2.52	24,-2,-6

Table 32 Details of the local maxima brain regions for LF > HF (column 1) and their associated z- value (column 2), and x,y,and z MNI coordinates (column 3).

Appendix V

Organization of Human Brain Mapping Abstract

Genetic Algorithm Clustering Technique for fMRI Data Analysis: A New fMRI Group ICA Algorithm

In recent years, a number of methodologies have been developed and implemented for analysis of group fMRI data. Among these methodologies is independent component analysis (ICA). Since ICA is a data driven analysis method, and because of its minimal assumptions, it has proven to be a very powerful data analysis methodology for single subject and group fMRI data[1]. Current group ICA analysis methods rely on hierarchical, K-means, and/or fuzzy logic approaches[2]. Such methods are known to be affected by local optimums and are more prone to converging to local optimum results, and thus may provide suboptimal solutions [3]. On the other hand, genetic algorithms are well suited for converging to the global optimum(s) and are not hindered by local optimum(s) [4]. Also, with regards to group ICA analysis of fMRI data, a genetic algorithm (GA) will ultimately converge to a global optimum and can provide a deterministic partition or clustering of fMRI time series leading to an optimum group activation map. Therefore we have designed developed a genetic algorithm based clustering technique for group ICA fMRI data analysis we called GAICA.

Our developed algorithm (GAICA) was used to provide group ICA analysis using visuomotor fMRI data from and with permission of the Medical Imaging Analysis Laboratory at the University of New Mexico[5]. After doing single subject ICA analysis for all 3 subjects' data using GIFT[6], GAICA was implemented for Group ICA analysis. Through the iteration of the GAICA to minimize the correlation distance by GA means, the fMRI time series from each subject were clustered into apriori set number of clusters. Therefore the fMRI time series from all subjects were partitioned in a global optimum partition according to the correlation distance between them. This allowed for correlated and or similar fMRI time series to belong to the same cluster, which in turn provides only a few clusters containing task-related fMRI times series (Figure 1). Also, the GAICA provided a partition for group ICA analysis of similar fMRI time series whether they are task related or not.

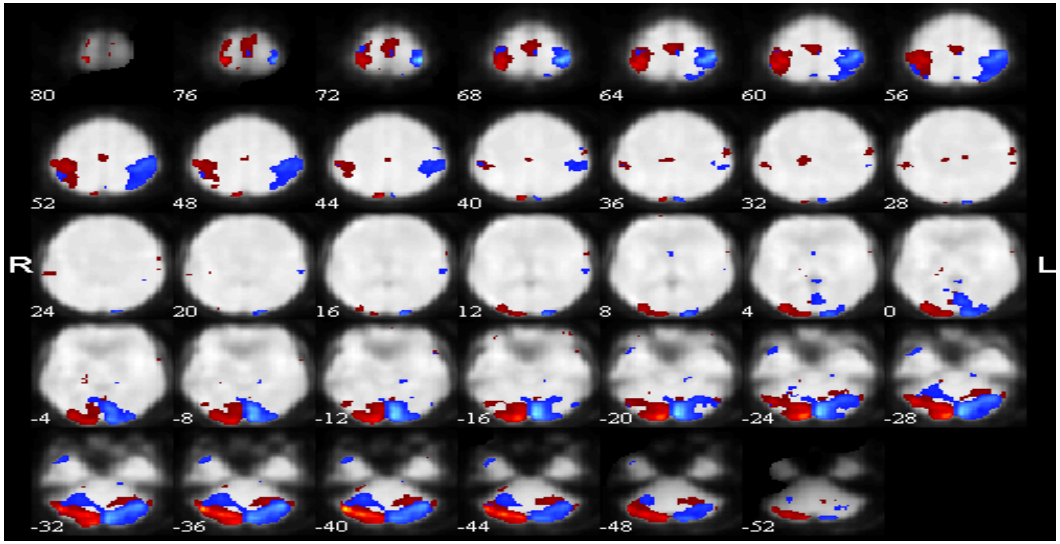

Figure 1 Task related activation that have been clustered in to two clusters resembling left and right hemispherical activations related to the visuomotor task. These maps were derived from fMRI time-series from two cluster outputs of GAICA.

Although ICA has been vastly developed and implemented for single subject analysis, a few approaches for group ICA analysis of fMRI data have been developed and implemented. However such group ICA approaches are more prone to local optimum convergence, thus, making it more likely to have less then optimum group ICA results. In this work we have proposed an algorithm that converges to a global optimum solution that can be used as a complementary or a supplementary technique for group ICA analysis of fMRI data.

References

[1] M. J. McKeown and T. J. Sejnowski, "Independent component analysis of fMRI data: Examining the assumptions," *Hum. Brain Map.,* vol. 6, pp. 368-372, 1998.

[2] R. Baumgartner*, et al.*, "Quantification in Functional Magnetic Resonance Imaging: Fuzzy Clustering vs. Correlation Analysis," *Magnetic Resonance Imaging,* vol. 16, pp. 115-125, 1998.

[3] C. Goutte*, et al.*, "On Clustering fMRI Time Series," *NeuroImage,* vol. 9, pp. 298-310, 1999.

[4] J. H. Holland, *Adaptation in Natural and Artificial Systems*. Ann Arbor, 1975.

[5] V. D. Calhoun*, et al.*, "A method for comparing group fMRI data using independent component analysis: application to visual, motor and visuomotor tasks," *Magn Reson Imaging,* vol. 22, pp. 1181-1191, 2004.

[6] V. D. Calhoun. (2004). *Group ICA of fMRI Toolbox (GIFT)*. Available: http://icatb.sourceforge.net

Genetic Algorithm Clustering Technique for fMRI Data Analysis: A New fMRI Group ICA Algorithm

Ali K. Bourisly^*, Wei Huang, Yanping Sun*, Mitchell Albert***

^Department of Biomedical Engineering, Worcester Polytechnic Institute

*Advanced MRI Center, Department of Radiology, University of Massachusetts Medical School

**Center for Comparative Neuroimaging, Department of Psychiatry, University of Massachusetts Medical School

Seeking a Global Optimum Solution

In recent years, a number of methodologies have been developed and implemented for analysis of group fMRI data. Among these methodologies is independent component analysis (ICA). Since ICA is a data driven analysis method, and because of its minimal assumptions, it has proven to be a very powerful data analysis methodology for single subject and group fMRI data. **Current group ICA analysis methods rely on hierarchical, K-means, and/ or fuzzy logic approaches. Such methods are known to be affected by local optimums and are more prone to converging to local optimum results, and thus often may provide suboptimal solutions** . On the other hand, **genetic algorithms are well suited for converging to the global optimum(s)** and are much less hindered by local optimums. Also, with regards to group ICA analysis of fMRI data, a genetic algorithm (GA) will ultimately converge to a global optimum and can provide a deterministic partition or clustering of fMRI time series leading to an optimum group activation map. **Therefore we have designed and developed a genetic algorithm-based clustering technique for group ICA fMRI data analysis, which we called GAICA.**

Independent Component Analysis (ICA)

ICA assumes the relationship and linear mixing as:

$X = AS$;
X: *Observed signal*
a: *Mixing matrix*
S : *Original signal*

$$X_1 = a_{11}S_1 + a_{12}S_2 + \ldots + a_{1p}S_p$$
$$X_2 = a_{21}S_1 + a_{22}S_2 + \ldots + a_{2p}S_p$$
$$\vdots$$
$$X_p = a_{p0}S_1 + a_{p2}S_2 + \ldots + a_{pp}S_p$$

X is the observed signal collected from the sensors, and ICA assumes that the original signal of interest S is linearly mixed using a mixing matrix a . Therefore, the task for ICA is to retrieve the original signals S without knowing the mixing matrix A.

$u = WX$

u: Independent components (recovered signals)
W: Unmixing matrix
X: source signals

ICA retrieves the original signal of interest by defining an unmixing matrix W .The reason for an unmixing matrix (W) is that we do not know the mixing matrix in order to recover the original signals of interest. Therefore u is an estimate of S in the sense that each component S appears in any component u with a scalar factor.

Experimental fMRI data and Single Subject ICA Analysis

The fMRI data was obtained from the ICA GIFT project database, with permission from Medical Imaging Analysis Laboratory, University of New Mexico. The fMRI data was from three right-handed male subjects with normal vision. **The stimuli was a visuomotor paradigm**. This fMRI data was acquired on a 1.5T Philips Medical Systems' MRI. An Echo planar sequence was used to acquire the functional images (64x64 matrix; flip angle = 90°; TR = 1000 ms; TE = 39 ms; FOV=24 cm; slice thickness, 5 mm; 18 slices) each with a 3 minute 40-s period for a total of 220 time points.

The model illustration below shows single subject fMRI ICA blind source separation. In that it assumes that the observed signals (X) are linearly mixed fMRI source signals (S) using an unknown mixing matrix (A). The ICA algorithm goes an iterative optimization feedback mechanism to recover the original fMRI source signals (u) utilizing an unmixing matrix (W)

GAICA Framework for Global Optimum Clustering of fMRI Group Data

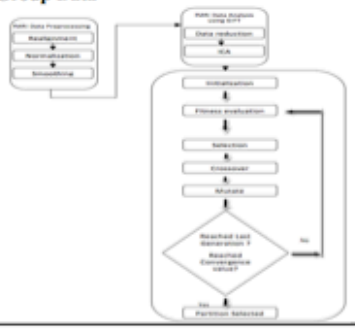

Fitness function

$$F = d_{rs}; \quad d_{rs} = 1 - \frac{(x_r - \bar{x}_r)(x_s - \bar{x}_s)'}{\sqrt{[(x_r - \bar{x}_r)(x_r - \bar{x}_r)']^2}\sqrt{[(x_s - \bar{x}_s)(x_s - \bar{x}_s)']^2}}$$

$$\bar{x}_r = \frac{1}{n}\sum_j x_{rj}$$

$$\bar{x}_s = \frac{1}{n}\sum_j x_{sj}$$

Probability Function for Parent Selection

$$P(S_i) = \frac{F(S_i)}{\sum_{j=1}^{N} F(S_i)}$$

Results

The **global optimum partition** with mean intra-cluster **distance of <0.53** was obtained after **321 generations**. The partition allowed for global optimum clustering of group fMRI data. A part of the clusters contained task-related and transiently task related fMRI signal fluctuations.

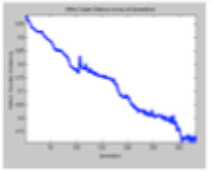

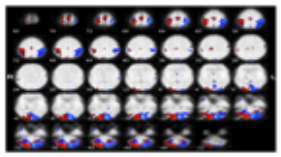

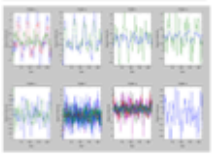

Conclusion

Although ICA has been vastly developed and implemented for single subject analysis, a few approaches for group ICA analysis of fMRI data have been developed and implemented. However such group ICA approaches are more prone to local optimum convergence, thus, making it more likely to have less than optimum group ICA results. In this work we have proposed an algorithm that converges to a global optimum solution that can be used as a complementary or a supplementary technique for group ICA analysis of fMRI data.

References

[1] M. J. McKeown and T. J. Sejnowski, "Independent component analysis of fMRI data: Examining the assumptions," *Hum. Brain Map.*, vol. 6, pp. 368-372, 1998.

[2] R. Baumgartner, *et al.*, "Quantification in Functional Magnetic Resonance Imaging: Fuzzy Clustering vs. Correlation Analysis," *Magnetic Resonance Imaging*, vol. 16, pp. 115-125, 1998.

[3] C. Goutte, *et al.*, "On Clustering fMRI Time Series," *NeuroImage*, vol. 9, pp. 298-310, 1999.

[4] H. Holland, *Adaptation in Natural and Artificial Systems*. Ann Arbor, 1975.

[5] V. D. Calhoun, *et al.*, "A method for comparing group fMRI data using independent component analysis: application to visual, motor and visuomotor tasks," *Magn Reson Imaging*, vol. 22, pp. 1181-1191, 2004.

[6] V. D. Calhoun, (2004). *Group ICA of fMRI Toolbox (GIFT)*. Available: http://icatb.sourceforge.net

[7] V. Calhoun and T. Adali, (2008) Unmixing fMRI with Independent Component Analysis: Using ICA to characterize high dimensional fMRI Data in a Concise Manner. *IEEE Engineering in Medicine and Biology*.

Appendix VI

Arabic Alphabet

خ	ح	ج	ث	ت	ب	ا
kha	haa	jiim	thaa	taa	baa	alif
ص	ش	س	ز	ر	ذ	د
saad	shiin	siin	zaay	raa	thaal	daal
ق	ف	غ	ع	ظ	ط	ض
qaaf	faa	ghayn	ayn	thaa	taa	daad
ي	و	ه	ن	م	ل	ك
yaa	waaw	ha	nuun	miim	laam	kaaf

Appendix VII

Summary Table of Studies of Diacritics in Arabic and Hebrew

Author(s)	Year of study	Reading skill level	Reading stage	Reading task	Facilitate RW Acc?	Facilitate RW Speed?	L1
Koriat	1985	Skilled	Adult	Words		Yes	Hebrew
Navon &Shimron	1981	Skilled	Adult	Words		Yes	Hebrew
Ravid	1996	Developing	1st grade	Sentences	Yes *		Hebrew
Ravid	1996	Developing	4th grade	Sentences	No **		Hebrew
Ravid & Schlesinger	2001	Skilled	11th grade	Words	Yes		Hebrew
Ravid & Schlesinger	2001	Skilled	Adult	Words	Yes		Hebrew
Ravid & Schlesinger	2001	Developing	5th	Words	No		Hebrew
Ravid & Schlesinger	2001	Developing	7th	Words	No		Hebrew
Ravid & Schlesinger	2001	Developing	9th	Words	No		Hebrew
Abu-Rabia	1996	Skilled	10th grade	Paragraphs	Yes		Arabic
Abu-Rabia	1996	Skilled	10th grade	Words	Yes		Arabic
Abu-Rabia	1996	Skilled	10th grade	Sentences	Yes		Arabic
Abu-Rabia	1996	Poor	10th grade	Paragraphs	Yes		Arabic
Abu-Rabia	1996	Poor	10th grade	Words	Yes		Arabic
Abu-Rabia	1996	Poor	10th grade	Sentences	Yes		Arabic
Abu-Rabia	1997	Skilled	10th grade	Words	Yes		Arabic
Abu-Rabia	1997	Poor	10th grade	Words	Yes		Arabic
Abu-Rabia	1997	Skilled	10th grade	Sentences	Yes		Arabic
Abu-Rabia	1997	Poor	10th grade	Sentences	Yes		Arabic
Abu-Rabia	1997	Skilled	10th grade	Paragraphs	Yes		Arabic
Abu-Rabia	1997	Poor	10th grade	Paragraphs	Yes		Arabic
Abu-Rabia	1998	Skilled	11th grade	Paragraphs	Yes		Arabic
Abu-Rabia	1998	Poor	11th grade	Paragraphs	Yes		Arabic
Abu-Rabia	2001	Skilled	Adult	Words	Yes		Arabic
Abu-Rabia	2001	Skilled	Adult	Paragraphs	Yes		Arabic

Table 1 Summary of studies of diacritics in Arabic and Hebrew. Author(s) : Author(s) of the study; Year of study: The year the study was published; Reading skill level: Reading skill level of participants (skilled, developing, poor); Reading stage: Adult or grade-level; Reading task: single word reading vs. contextual (paragraph, sentences) reading; Facilitate RW Acc?: Do the results of the respective study show a facilitative role for diacritics on real word (RW) accuracy (Acc)?; Facilitate RW Speed?: Do the results of the respective study show a facilitative role for diacritics on real word(RW) recognition speed?; L1: First language of participants.

* Performance compared to 4th graders.

** Performance compared to 1st graders.